Thermodynamics and Mechanisms of Lead Softening

by

Sadegh Firoozi

Department of Mining, Metals and Materials Engineering

McGill University, Montreal, Canada

September 2005

A thesis submitted to the Office of Graduate and Postdoctoral Studies in partial fulfillment of the requirements for the degree of Doctor of Philosophy

Your file Votre référence
ISBN: 978-0-494-25144-7
Our file Notre référence
ISBN: 978-0-494-25144-7

The aim of science is to seek the simplest explanation of complex facts. We are apt to fall into the error of thinking that the facts are simple because simplicity is the goal of our quest. The guiding motto in the life of every natural philosopher should be "***Seek simplicity and distrust it***".

Alfred North Whitehead (1861-1947) English mathematician and philosopher

ABSTRACT

Visualization and quantitative oxidation kinetic experiments on 100 g samples of Pb-As at 600 °C; thermal analysis and phase-equilibrium measurements of Pb-PbO-As_2O_3 samples under argon over the temperature range of 420 °C to 875 °C; computational thermodynamic solution modeling; and phase diagram and equilibrium calculations using FACT*Sage*™ were performed to elaborate the poorly documented thermodynamics of the slags in the lead softening stage in the pyrometallurgical refining of lead. In the softening stage, the minor element impurities: arsenic, antimony and tin are removed from lead bullion by oxidation and are transferred to a skimmable oxide slag phase.

It was found that optimizing an ionic molten oxide solution model that was conceptualized to contain Pb^{2+} and O^{2-} with AsO_4^{3-} and AsO_3^{3-} ions, or with SbO_4^{3-} and SbO_3^{3-} ions in the respective PbO rich regions of the Pb-As-O and the Pb-Sb-O systems, was able to accurately reproduce the measured and published thermodynamic data. It was also found that the subsystems in the PbO-As_2O_3-As_2O_5 and PbO-Sb_2O_3-Sb_2O_5 systems showed small deviation from the ideal ionic solution model and small magnitude excess Gibbs energy parameters were sufficient to fit the predicted liquidus curves to the experimental measurements.

Arsenic in the +3 and +5 oxidation states was measured in the PbO rich region of the Pb-As-O liquid solution in the temperature range of 420 °C to 875 °C. The variability in the ratio of trivalent arsenic to the total arsenic content, as well as the complex variation of arsenic distribution between metal and oxide phases found strong interaction between the lead, arsenic and oxygen atoms at the 3PbO to 1As_2O_3 molar ratio thus suggesting a short range ordering corresponding to the formation of AsO_3^{3-} groupings, and indicating that the $Pb_3(AsO_3)_2$(l) species was likely to be present in the PbO rich region of the Pb-As-O system and contributing to an understanding of the Pb-As-O liquid oxide structure. Also, two new compounds ($Pb_3(AsO_3)_2$(s), Pb_2AsO_4(s)) were identified in the Pb-PbO-As_2O_3 quenched samples via wavelength-dispersive spectrometry using the electron microprobe.

The present work has application in commercial oxygen partial lead softening (OPLS), as *uniquely* practiced at Teck Cominco Ltd., British Columbia. There, pure oxygen gas is injected into the bath of impure bullion through a number of submerged lances in order to oxidize only part of the arsenic, antimony and tin into a slag phase. For such an operating practice, it was concluded from the visualization and quantitative oxidation experiments that the formation of solid oxides as the product of oxidation produced a physical barrier to the progress of oxidation and resulted in the commercially observed, highly-problematic, process initiation issues. When the product was liquid, there was much less of a barrier to rapid oxygen mass transfer to the minor element impurities and the softening reactions were easy to initiate. Such a change in the physical state of the products of oxidation was correlated to the optimized ternary Pb-As-O and Pb-Sb-O phase diagrams.

A current point of interest in partial lead softening is to increase the arsenic content of the slag phase. Arsenic distribution between lead bullion and slag calculated by the optimized solution model of the Pb-As-O system suggests that this can be achieved in a counter-current contacting of the slag and bullion.

RÉSUMÉ

Le présent travail de recherche vise à étudier la thermodynamique des scories obtenues lors de l'affinage du bouillon de plomb. Parmi les travaux complétés, on retrouve des expériences de visualisation et d'oxydation quantitatives sur des échantillons de 100 g de Pb-As à 600 °C, des mesures d'analyses thermiques et d'équilibre de phase d'échantillons Pb-PbO-As_2O_3 entre les températures 420 °C à 875 °C sous une atmosphère d'argon, de la modélisation de solution thermodynamique et des calculs de diagramme de phase et d'équilibre à l'aide de FACTSage™. L'affinage du plomb à l'oxygène est l'une des étapes dans le raffinage pyrométallurgique du bouillon primaire pendant laquelle les impuretés mineures telles que l'arsenic, l'antimoine et l'étain sont enlevées du bouillon par oxydation et transférées dans la phase de scories d'oxydes. Cette dernière est ensuite écrémée de la surface du bain.

Un modèle de solution d'oxyde ionique à l'état fondu a été conçu pour évaluer les ions Pb^{2+} et O^{2-} avec AsO_4^{3-} et AsO_3^{3-}, ou avec SbO_4^{3-} et SbO_3^{3-} pour la région riche en PbO dans les systèmes Pb-As-O et Pb-Sb-O respectivement. En optimisant ce modèle, il a été prouvé que l'on pouvait précisément reproduire les données thermodynamiques qui ont été mesurées pour ce travail ou qui sont disponibles dans les travaux publiés par d'autres chercheurs. Il a aussi été trouvé que les sous-systèmes dans les systèmes de PbO-As_2O_3-As_2O_5 et PbO-Sb_2O_3-Sb_2O_5 présentent seulement une petite déviation du modèle de solution ionique idéal et que des paramètres de petite magnitude pour l'énergie d'excès de Gibbs étaient suffisants pour adapter les courbes de liquidus prédites aux mesures expérimentales.

L'arsenic dans les états d'oxydation +3 et +5 a été mesuré dans la région riche en PbO de la solution liquide Pb-As-O entre les températures des 420°C à 875 °C. La variabilité dans la proportion d'arsenic trivalent au contenu d'arsenic total, ainsi que la variation complexe de la distribution d'arsenic entre les phases de métal et oxyde ont montré une interaction forte entre les atomes de plomb, d'arsenic et d'oxygène avec un ratio molaire de 3PbO:1As_2O_3. Ceci suggère un arrangement d'ordre court qui correspond à la formation de groupements et indique que l'espèce $Pb_3(AsO_3)_2$(l) pourrait être présente

dans la région riche en PbO du système Pb-As-O. Cette conclusion contribue à une meilleure compréhension de la structure d'oxyde liquide de cette région. Aussi, deux nouveaux composés, $Pb_3(AsO_3)_2(s)$ et $Pb_2AsO_4(s)$, ont été identifiés dans les échantillons trempés de Pb-PbO-As_2O_3 via la spectrométrie dispersive de longueur d'ondes à l'aide de la microsonde d'électrons.

Le travail présent a une application dans l'affinage partiel du plomb à l'aide d'oxygène, il est actuellement utilisé au niveau commercial uniquement par Teck Cominco Ltd., en Colombie Britannique. Dans leur procédé, le gaz d'oxygène pur est injecté dans le bouillon de plomb impur par plusieurs lances submergées afin d'oxyder et d'enlever dans une phase de scories une partie de l'arsenic, l'antimoine et l'étain. Dans la pratique commerciale, l'initiation des réactions d'oxydation peut être parfois extrêmement problématique. Des expériences de visualisation et d'oxydation quantitatives ont révélé que lorsque les produits d'oxydation étaient solides, ils créaient une barrière forte au processus d'oxydation. Cependant, lorsque les produits d'oxydation étaient liquides, il y avait moins d'obstacle au transfert d'oxygène rapide aux impuretés mineures et il était alors facile de lancer les réactions d'oxydation. Ce changement de l'état physique des produits de l'oxydation a été corrélé aux diagrammes de phase des systèmes ternaires Pb-As-O et Pb-Sb-O originaux et ceux optimisés récemment.

L'augmentation de la teneur en arsenic des scories est actuellement un sujet d'intérêt pour l'affinage du plomb. Un modèle thermodynamique du système Pb-As-O suggère que cela puisse être réalisé par le contre- courant contactant les scories et le bouillon.

ACKNOWLEDGEMENTS

I would like to express my sincerest appreciation to my supervisor, Professor Ralph Harris for his guidance and support throughout my studies in McGill. His positive view and his confidence in my abilities provided me the courage to explore and learn new areas of metallurgical engineering.

The financial assistance of the Natural Sciences and Engineering Research Council of Canada (NSERC) and Teck Cominco Ltd. are gratefully acknowledged. Thanks are due to Dr. Greg Richards at Teck Cominco for his continuous support throughout my study and also to Yemi Oyediran at Teck Cominco for his technical support.

I would like to extend my greatest thanks to Dr. Pascal Coursol who graciously offered his expertise in thermodynamic modeling and experimental procedures. The teachings of Professor Arthur Pelton in CRCT École Polytechnique have been a great asset and instructive to understand the thermodynamic modeling. Scientific discussions with Professor Bert Wraith are greatly appreciated.

I am grateful to Monique Riendeau for her assistance in the use of analytical instruments of the Department, to Ed Siliauskas for providing technical support in ICP analysis, to Glenna Keating for conducting the AAS and HG-AAS and to Alan Gagnon for constructing an apparatus for gas injection experiments. Utmost thanks to Lang Shi for his skilful assistance and great care he showed during the long EPMA sessions. I am thankful to Dr. Florence Paray for editing the French abstract of my thesis. My grateful thanks go to the administrative staff of the Department, Barbara Hanely, Nikki Middlemiss and Linda Chernabrow who always assisted me and patiently answered all my questions.

Special thanks to our group members, Ka Wing Ng for his assistance throughout the research, John Roumeliotis for his helpful advices that improved my presentation skills, Graeme Goodall for proofreading my thesis, Sina Kashani-Nejad for his friendship and his help in early stages of my research, Javad Khosravi for his friendship and help and finally to Daryl Vineberg for our enjoyable collaboration on the lead softening research.

This would not have been possible without the love and support from my family, Soraya, Shahpar, Nima, Mani and Sherry. Special thanks to my mother who encouraged me to continue my education and provided me financial support in every step of the way. Dedicated to Kati for all she is!

TABLE OF CONTENTS

LIST OF FIGURES

LIST OF TABLES

NOMENCLATURE

Symbol	Designation	Unit
A	atomic weight	kg
a_i	activity of component *i*	unitless
C_p	heat capacity	$J\ K^{-1}$
F	force	$kg\ m\ s^{-2}$
G_i^0	standard Gibbs energy of *i*	J
g_i^0	standard molar Gibbs energy of *i*	$J\ mol^{-1}$
g^E	excess molar Gibbs energy	$J\ mol^{-1}$
g_i^E	excess partial molar Gibbs energy of *i*	$J\ mol^{-1}$
ΔG^0	standard Gibbs energy change	J
Δg_f^0	standard molar Gibbs energy of fusion	$J\ mol^{-1}$
H_i^0	standard enthalpy of *i*	J
ΔH^0	standard enthalpy change	J
Δh_f^0	standard molar enthalpy of fusion	$J\ mol^{-1}$
m	mass	kg
n_i	number of moles of constituent *i*	mol
R	gas constant	$J\ mol^{-1}\ K^{-1}$
S_i^0	standard entropy of *i*	$J\ K^{-1}$
t	time	s
T	temperature	K
T_f	temperature of fusion	K
Y_i	site fraction of *i*	unitless
V	volume	m^3
X_i	mole fraction of *i*	unitless

$\omega_{A\text{-}B}$	excess interaction parameter in A-B solution	J mol^{-1}
γ_i	activity coefficient of component *i*	unitless
γ_i^0	limiting activity coefficient of component *i*	unitless
v	number of moles of foreign particles contributed by a mole of solute	unitless
ρ	density	kg m^{-3}

CHAPTER 1. INTRODUCTION

1.1 Scope

The present project deals with one component of the pyrometallurgical refining of commercially produced primary lead bullion. In particular, it examines the thermodynamics of the oxide products formed during the partial softening that is carried out with pure oxygen gas by Teck Cominco in Trail, British Colombia. In the softening of lead, arsenic, antimony and tin are partially or almost completely removed from the lead bullion. Because arsenic and antimony render lead hard in its solid state, this process is named "softening".

The present study follows a laboratory scale qualitative investigation of the oxide formation during lead softening carried out by D. Vineberg [1]. This previous work established the need to further determine the thermodynamics of the system in order to explain the observed complexity and the variability of the phases that were seemed to form during exposure of lead bullion to oxygen gas during softening.

In this introductory chapter, the refining of lead bullion and the commercial process of lead softening are presented for the background information of the reader. Teck Cominco's partial lead softening operation is then described in detail. The general operational problems confronting Teck Cominco's oxygen partial lead softening process (OPLS) along with the specific focus of this thesis objective complete the chapter.

1.2 Lead Refining

Primary lead is mainly produced by smelting concentrate in either the conventional sinter machine blast furnace process or by newer processes such as QSL[i], Kivcet and Ausmelt [2]. The product of the smelting process is a crude lead, commonly known as "lead bullion", which exits the smelting vessel in the temperature range of 850-1250 °C [2], depending on the smelting process. At these temperatures, lead has considerable

[i] Queneau-Schuhmann-Lurgi process.

solubility for impurities entrained from either the concentrate or recycled materials. The main impurities in lead bullion are Cu, Zn, Sb, As, Sn, Bi, Te, Ag, Au and S [3]. Depending on the smelting process and composition of the feed material, crude lead has variable amounts of these impurities, with totals between 1 and 6 wt% [2] but levels as high as 10 wt% have also been reported [4]. In order for the lead to have applications, these impurities need to be removed in the lead refining process that follows the smelting process.

Lead bullion is refined either by the conventional stepwise pyrometallurgical route, or by electrolytic refining. In 1990, the electrolytic refining capacity of the world's lead industry was about 1.25 million tonnes per annum, which was about half of the pyrometallurgical refining capacity [5]. In 2000, it was reported [2] that pyrometallurgical refining accounted for about 90% of the lead refining capacity with Teck Cominco contributing about one third of this total.

Figure 1 shows the typical steps in the pyrometallurgical refining of lead [3]. Regardless of the refining technique, the first step is copper drossing, in which lead bullion is cooled to near the melting point of lead. At this temperature and depending on the impurity levels of the lead bullion, the solubility of copper in lead decreases to 0.02-0.07 wt% Cu and subsequently copper is rejected as copper compounds into a dross phase. The main components of the so called copper dross are sulfides, arsenides and antimonides of copper. Further removal of copper is possible through addition of sulfur and the formation of a matte phase in a process called sulfur drossing.

In the second step, softening, Sb, As and Sn, each with a more negative standard Gibbs energy of oxidation than lead, are removed from the lead bullion via preferential oxidation. This process is explained in detail in the next section.

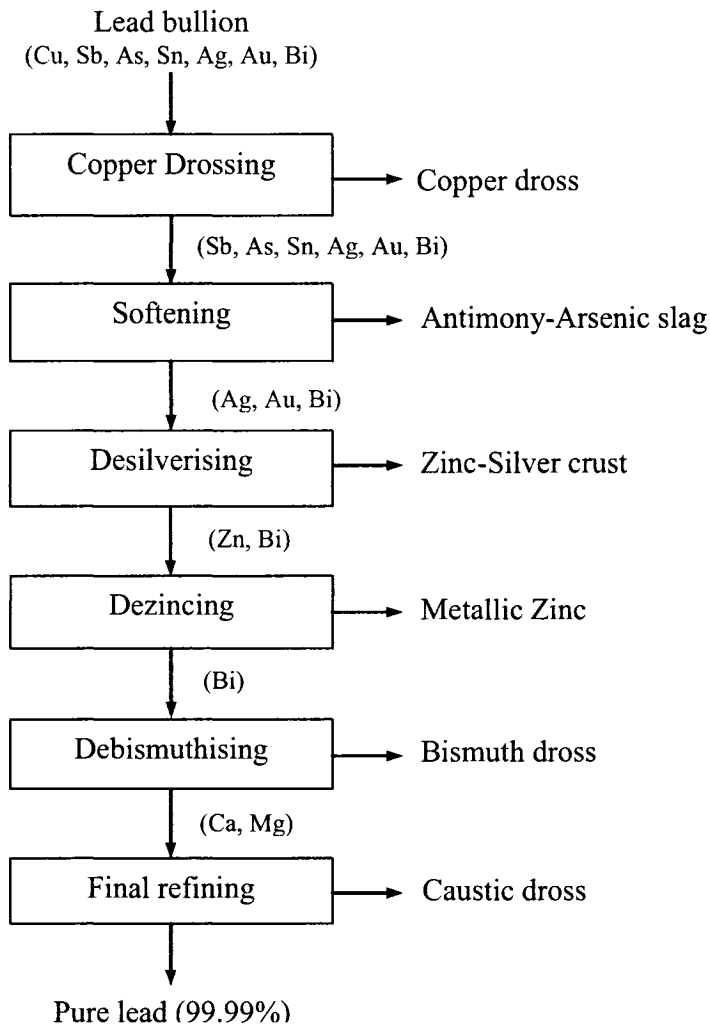

Figure 1 – Flowchart of pyrometallurgical refining of lead [3].

In conventional pyro-refining of lead bullion, the impurities remaining in the lead after the softening process are mainly silver, gold and bismuth. They are more noble than lead and cannot be removed by selective reaction with oxygen, sulfur or chlorine [3]. Thus, the softened lead is treated with zinc to precipitate silver in a form of silver-zinc intermetallic compound. During the desilverizing process, 0.5 to 0.6 wt% zinc dissolves in the lead, which is subsequently removed by vacuum treatment. Vacuum treatment takes advantage of the higher vapor pressure of the zinc relative to the lead and zinc's high positive deviation from ideal behavior in liquid lead, and allows simple recovery of the excess zinc to be used in the next refining batch. After the dezincing process, bismuth is removed from lead by the Kroll-Betterton process, which uses calcium and magnesium

to precipitate bismuth as an intermetallic compound, $CaMg_2Bi_2$. The final step uses caustic soda and/or sodium nitrate to oxidize the remaining trace impurities that are more easily oxidized than lead [3].

By contrast, electrolytic refining employs the Betts process in which all impurities remaining after copper drossing are simultaneously removed in one electrolytic refining step. This single step electrolytic refining minimizes lead and other gas emission and can produce lead with very low bismuth levels (less than 10ppm) [6]. The high cost of electricity is a significant factor for this process and therefore the choice of refining process is based on the degree of bismuth removal required, cost of electricity, efficiency and cost of by-product removal, and recovery [2, 7].

It is not necessary to remove the arsenic and antimony prior to Betts electrolytic refining, however the refining process practiced at Teck Cominco ltd. employs a partial softening prior to electrolytic refining to adjust the arsenic and antimony levels and recover some of the antimony to a slag phase. The details of the partial lead softening process, which form the basis for the industrial background of the current research, are discussed in the next section.

1.3 Lead Softening

Several methods are currently practiced for lead softening. The Harris process is a low-temperature (450 °C) softening process, in which a strong oxidizing agent, such as sodium nitrate, oxidizes the impurities and converts them to sodium salts, such as Na_3AsO_4. The salts are subsequently absorbed into a caustic soda slag [3]. The Harris process has the capability of removing arsenic and tin preferentially over the removal of antimony. This is especially advantageous if tin is present in economically viable amounts [5]. The main disadvantages of the Harris process are the high capital and large operating costs [8].

The more common softening processes use air, or oxygen enriched air, or oxygen as the oxidizing agent and operate at higher temperatures than Harris process, between 470 and 750 °C [2]. Other oxidizing agents such as caustic soda are sometimes added to enhance the impurity removal and decrease lead losses to the slag phase. This process can be

carried out in a reverberatory furnace or in kettles and can be operated as either a batch or a continuous process. The batch process has the advantage of better control on the degree of impurity removal as well as the handling of bullion of varying composition. However, the batch process requires large kettles that need to be kept at high temperature and results in higher energy consumption. On the other hand, the continuous process has higher production output from smaller vessels, but cannot easily handle varying bullion composition [6].

1.3.1 Lead Softening Chemistry

Several complex oxidation reactions may occur during the refining of lead with oxygen. The following simple reactions (Reactions 11 to 4 [9, 10]) may be used to represent the overall reactions that occur during softening. These reactions indicate that lead, which is the main element in the bullion, reacts with the oxygen and forms PbO according to Reaction 1. Subsequently, PbO reacts with the arsenic, antimony and tin, according to Reactions 2 to 4, to form the oxides of these species. The mixture of the oxide phases commonly referred to as the slag is found to consist mainly of PbO combined with oxides of arsenic, antimony and tin. The slag is skimmed from the softening vessel and treated for its lead and antimony values as a lead-antimony alloy [2, 11].

$$Pb_{(l\text{-bullion})} + 0.5\ O_{2\,(g)} \rightarrow PbO_{(slag)} \quad (1)$$

$$3\ PbO_{(slag)} + 2\ As_{(l\text{-bullion})} \rightarrow As_2O_{3\,(slag)} + 3\ Pb_{(l\text{-bullion})} \quad (2)$$

$$3\ PbO_{(slag)} + 2\ Sb_{(l\text{-bullion})} \rightarrow Sb_2O_{3\,(slag)} + 3\ Pb_{(l\text{-bullion})} \quad (3)$$

$$2\ PbO_{(slag)} + Sn_{(l\text{-bullion})} \rightarrow SnO_{2\,(slag)} + 2\ Pb_{(l\text{-bullion})} \quad (4)$$

1.4 Teck Cominco Operations

In the Betts electrolytic refining of lead, as practiced by Teck Cominco, the anode impurities, which are mainly antimony, arsenic, copper, silver, bismuth and gold, remain on the surface of the anode and form an adhering layer of porous slime. To ensure that the slime remains on the surface of the anode, an optimum amount of 1.5 to 2.0 wt% total antimony and arsenic are required in the anode. These impurities form a network

structure that holds the slime to the anode for the subsequent removal from the cell and treatment [11].

Until 1986, Teck Cominco's arsenic and antimony levels were below the level required to optimize the system and consequently high antimony and arsenic bearing materials from their silver refiner were recycled to the operation [12]. After 1986, the levels of antimony and arsenic were able to exceed the required amount due to an increase in the impurity levels in the Sullivan mine, which generated feed for the Teck Cominco smelter, and also because of the treatment of larger amount of silver-gold bearing lead concentrate in the lead smelting operation, a partial lead softening vessel was commissioned in 1986 to adjust the arsenic and antimony to the desired level when required. After reviewing the available methods for lead softening, Teck Cominco decided to employ partial lead softening using pure oxygen [7, 12].

The first partial softener vessel had a 20-tonne capacity and was made from a blast furnace pre-hearth, with six oxygen lances capable of injecting up to 20 Nm^3/h of 98 % technical oxygen into the lead. Because of the exothermic oxidation reactions, the temperature of the lead bullion increased during the softening. The temperature of the bath was maintained at about 620°C by pumping new lead bullion at 450 °C. A top mounted natural gas burner directed onto the surface of the slag to maintain a fluid slag at temperature of about 700 °C [12, 13].

Since the initial conception in 1986, the design of the softener vessel and the softening circuit has been modified on numerous occasions. In the late 1990's, the softening circuit was substantially modified as part of the modernization of the Teck Cominco lead refining circuit, and start up of the Kivcet process [14].

Figure 2 is a simplified[i] refining circuit in Teck Cominco operation [1]. Typically, every 3 hours, a batch of 60 tonnes of lead bullion from the Kivcet smelter flows into the Continuous Drossing Furnace (CDF) at 850-950 °C. In the CDF, lead bullion is cooled to

[i] A more complete description of the refining circuit is available in D. Vineberg M. Eng. Thesis [1].

400 °C to reduce the copper content to 0.05-0.06 wt% after which it is pumped into Pot #2.

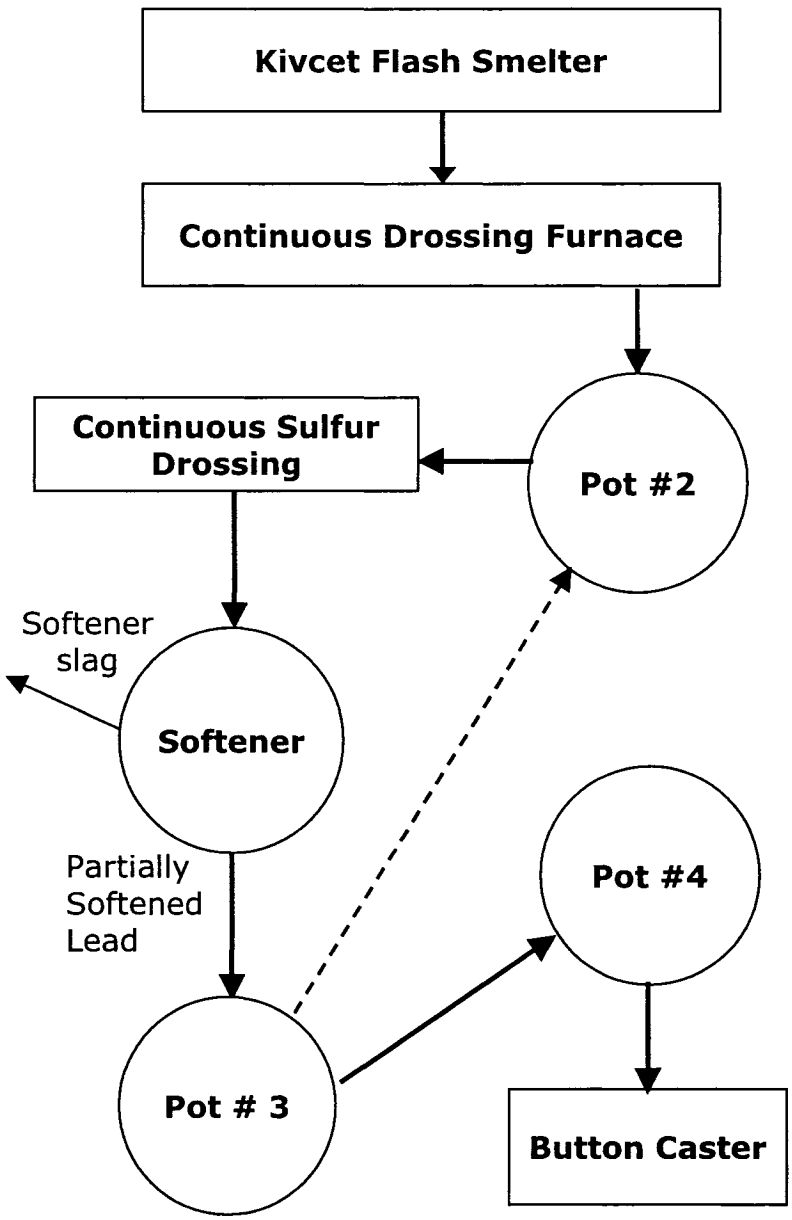

Figure 2 – Teck Cominco's schematic refining circuit flowchart [1] (parts of the circuit are omitted for simplification).

The lead bullion is then transferred to Continuous Sulphur Drossing (CSD) where the bullion temperature is lowered to just above the melting point of the lead (~ 330 °C), and solid sulphur prills are added. With the combined effect of sulphur addition and the reduction of temperature, the copper content of the lead is reduced to less than 0.005 wt%

by precipitation, and copper is drossed in form of a matte. If the tin content of the bullion is sufficiently high, then a de-tinning process via chloride addition and oxygen injection may be performed in the CSD vessel [15].

After sulfur drossing, the lead bullion is transferred to the softener vessel. Softening is dependant upon the antimony and arsenic content of the bullion. If the antimony and arsenic content are within the target range, then softener remains idle and the lead bullion passes through the softener without any refining. Once the arsenic and antimony exceeds the upper limit of the target range, the softener is operated and some of the As and Sb are oxidized via the injection of pure oxygen into the softener vessel. Since early 2004, the softener has been in continuous operation because of high impurity level.

The relatively low density molten oxide product from the reaction of the injected oxygen, lead, antimony, arsenic, and tin rises and accumulates at the top of the vessel where it is periodically skimmed. From the softener, lead is transferred to Pot #3 and then to Pot #4, from where it goes to the button casters for anode casting.

A recycling circuit exists from Pot #3 to Pot #2. The lead is re-circulated to Pot #2 until the composition of the lead at the softener exit is near to or below, the lower end of the target range at which time lead is directed to Pot #4 for casting.

If the new lead from the Kivcet furnace has very high impurity contents, then the softener runs for a greater period of time, thereby producing lead with low arsenic and antimony levels. By mixing new lead with the softened bullion in Pot #2, the variations in the Kivcet product are dampened. Table 1 shows the 2004 assay with minimum, maximum and average composition of the softener feed, partially softened lead, and the softener slag[i] [15]. Since early 2004, Teck Cominco has been treating concentrates with higher arsenic content, and it is expected that the level of arsenic will remain high in the future [16]. The details of the partial lead softener operation are explained in the next section.

[i] Because the slag is not regularly assayed, the reported values may not be a good representation of the range of compositions that may occur.

Table 1 – Average, minimum and maximum composition of the softener feed, partially softened bullion and 3 samples of softener slag in year 2004 [15].

	Sb (wt %)	As (wt %)	Sn (wt %)	Pb (wt %)
	Average max–min	Average max–min	Average max–min	Average max–min
Softener feed	1.55 2.65-1.03	0.65 1.14-0.30	0.09 0.28-0.001	rem.
Softener output	1.2 2.38-0.40	0.34 0.75-0.05	0.003 0.072-0.001	rem.
Softener slag	10.7 11.9-9.4	10.3 11.9-9.2	1.4 3.5-0.28	62.7 66-60

1.4.1 Oxygen Partial Lead Softening Practice

Teck Cominco's current partial lead softening vessel, schematically depicted in Figure 3, is 3 m high, 2.5 m internal diameter and has a 200 tonne capacity [15]. The softener pot is partially segmented by a submerged, open-ended inner steel ring, in which four oxygen lances are immersed. The outer pot is brick walled. Oxygen lances are closed at the submerged end and have four, 5 mm holes through the sides of the lance tip to allow the passage of oxygen into the bullion. Total oxygen flow to the vessel is maintained between 50 and 120 Nm^3/hr. A gas burner within the inner ring directed onto the top of the melt keeps the slag fluid [1, 15]. During oxygen injection, slag accumulates on the surface of the bath and is taped from the furnace through slag launders at approximately 10 tonnes per 24 hours of operation [1]. The softened lead is pumped from the bottom of the outer pot, through a riser, and exits from the top of the furnace [15].

The softening reactions are confined to the inner ring, which also serves to localize the heat generated to protect the pot. The softener works either in batch mode or continuously with a lead flow rate of 40 tonnes per hour, which is double the nominal production due to the re-circulation of lead in the refining circuit.

Lead bullion at a temperature of around 400 °C is pumped into the inner ring below the melt surface, and after mixing with the lead bullion, the melt is stabilized at about 620 °C. The softening operation starts once oxygen is injected into the melt and thereafter no

additional heat is required. After the operation starts, the burners are decreased to 10% capacity to maintain a fluid slag on top of the vessel.

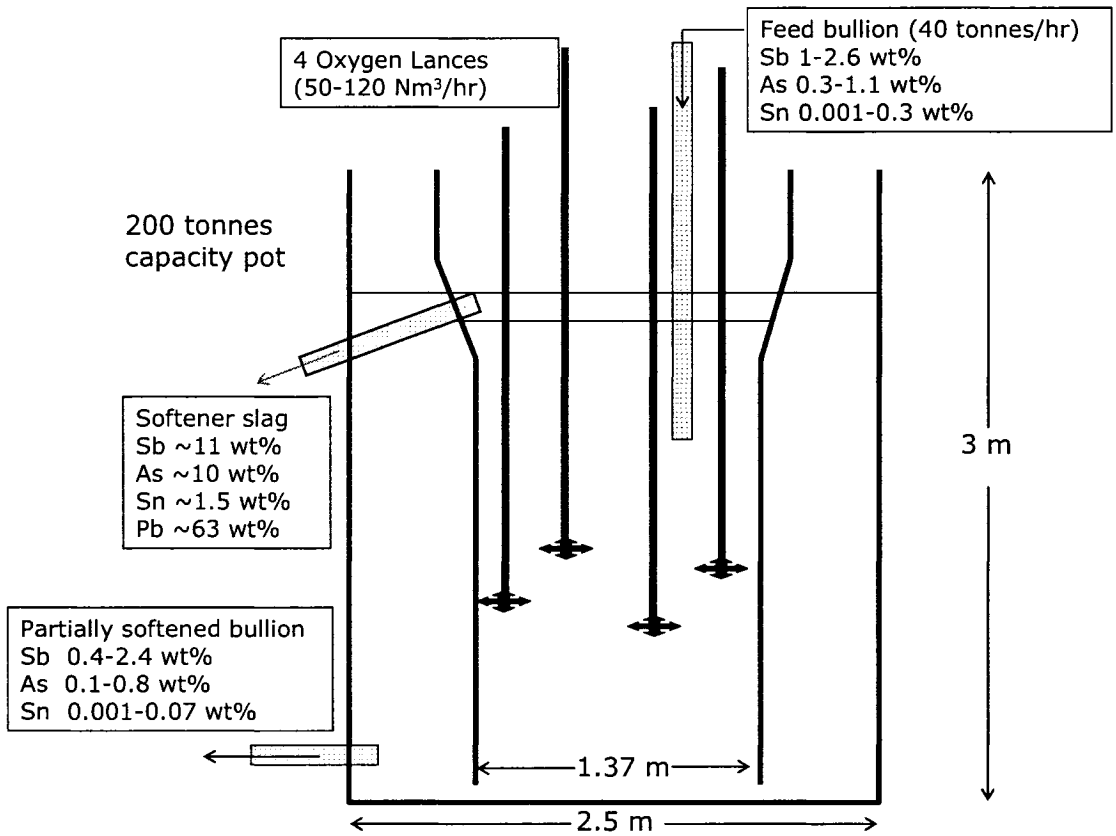

Figure 3 – Schematic figure of the oxygen partial softener vessel [15].

Temperature is monitored by means of a thermocouple deep in the center of the inner ring at an angle through the "feed-wall" to protect it from contact with the slag. The oxidation reactions that occur during the softening are exothermic and cooling is a more important issue because superheating shortens the life of the oxygen lances, softener vessel, thus lowering the productivity. The temperature during softening is controlled primarily by changing the flow rate of oxygen and incoming cold bullion. Due to the low heat transfer coefficient of lead and poor mixing of the melt, the temperature inside the bath is not uniform, with the lower portion of the bath near 550 °C and the upper portion as high as 700 °C. If the temperature of the melt as measured by the thermocouple exceeds 670 °C, oxygen is automatically switched off to protect the inner ring and the lances [15].

To start the softening reactions, the lances are initially positioned at a shallow depth inside the inner ring, where lead is hotter than the rest of the bath due to the top surface heating. After the start of the oxygen flow to the lances, an absence of gas bubbles break-up at the surface of the melt is an indication that the softening reactions have successfully started, and all of the oxygen is being consumed rapidly inside the bath. Thereafter the lances are gradually lowered to an operational depth of one meter below the melt surface [15].

Teck Cominco is unique in its use of pure oxygen for softening without the addition of other oxidizing reagents such as NaOH. The reason for not using additional reagents was to facilitate the processing of the softener slag for recovery of lead and antimony [16]. The use of pure oxygen also has the important advantage of minimal fume production due to the absence of unreacted nitrogen flowing through the melt, compared with the use of air. The result is that the Teck Cominco process is far more hygienic and less environmentally damaging, compared with regular air or oxygen enriched-air softening. The challenges of operating and controlling this process, which has been the motivation for conducting this study, are described in the next section.

1.4.2 Industrial Challenges

The initiation of the softening reaction has recently been coined as "ignition" [17] and in order for ignition to happen, the melt should be brought to a "critical temperature". The ignition temperature was reported to be near 620 °C in practice at Teck Cominco [6, 12, 15]. Teck Cominco has reported that ignition is difficult and unpredictable since the composition of the softener feed is constantly changing and the effects of process variables are not clearly understood. A similar ignition temperature (630 °C) was reported for the BHAS lead smelter at Port Pirie which uses oxygen softening combined with the addition of caustic soda [18]. Although the oxidation reactions of arsenic, antimony, and tin are thermodynamically favorable at temperatures below the ignition temperature, the rate of the reaction was reported to be low [18]. In practice, low rates of softening are associated with the observation of un-reacted oxygen bubbles collapsing at the surface of the melt.

Furthermore, with the increased arsenic level of the smelter feed mentioned above, there is a greater need for process control, which is currently heavily reliant upon operator experience. At the moment a current goal is to increase the arsenic content of the softener slag, to reduce lead losses to the slag phase. The softener vessel has been frequently modified and improved since it was first commissioned in 1989, and despite the efforts by the operating team of Teck Cominco the extent of progress has been frustratingly limited. This delay is due to a lack of fundamental studies on the process thermodynamics as well as on the dynamics of oxygen injection into the impure lead.

Teck Cominco's desire to find a solution to the ignition problem, and to devise a process control strategy for the softening operation, has been the incentive for conducting this research.

1.5 Research Objectives

The observations and measurements of the rate of oxygen uptake to the stagnant lead bullion by Vineberg [1] showed that the physical state of the lead oxide changed the rate of oxygen uptake. The present preliminary observations and quantitative kinetic studies of the oxidation of lead-arsenic melts, presented in Appendix 1, also found that with changing local oxygen potential, the form of the local oxide phase was altered and contributed to the formation of a physical barrier for the oxygen transfer into the melt.

The primary objective of this research was to provide the necessary thermodynamic knowledge needed to describe the complex industrial and laboratory observations.

Phase diagrams demonstrate the equilibrium phases present within a system at any composition and temperature. As part of the present objective, this research aimed to construct a set of phase diagrams describing the softener slag in order to relate the form of the oxides at the gas/liquid interface, to the presence of a physical barrier for the oxygen transfer into the melt. A combination of laboratory experiments and thermodynamic modeling was used to achieve this goal.

Moreover, the combination of experiments and thermodynamic modeling in conjunction with the available thermochemical software programs may also be used to determine the equilibrium conditions and element distribution between oxide and metallic phases of the softening practice. This provides a powerful tool to devise a control strategy in the industrial softening operation and allows Teck Cominco to begin knowledge based optimization of the refining technology. This research intends to generate part of the necessary thermodynamic data, and took the first step toward providing the thermodynamic models required for these purposes.

Some satisfaction was also gained from fulfilling the present objectives as they address the challenges expressed by the father of the lead refining, T.R.A. Davey in 1980 [3] as "*the physical chemistry of softening has not been fully examined, largely because there is small possibility of significant improvement by optimizing operations. The thermodynamic data on the metal oxides are uncertain, and sound activity data on oxide systems do not exist*".

CHAPTER 2. LITERATURE SURVEY

2.1 Scope

This chapter reviews the prominent published works on the thermodynamics of systems that relate to lead softening. The focus is on the thermodynamics of the lead-arsenic and lead-antimony oxide systems. The lead-tin oxide system is outside the scope of this study and is not included in this review.

Section 2.2 briefly reviews the metallic Pb-As-Sb system to provide the background information needed to calculate the equilibrium between metal and oxide phases. Section 2.3 investigates the lead-arsenic oxide system in the composition ranges of lead softening and Section 2.4 considers the lead-antimony oxide system in the same composition range. The derivative thermodynamic studies on lead softening are presented in Section 2.5. The chapter ends with concluding remarks on the values and shortcomings of the published works.

2.2 Pb-As-Sb Metallic Systems

Pb-As system:

Much work has been devoted to the measurement of the phase diagram and component activities in the Pb-As system.

McClincy [19] measured the activity of arsenic in dilute Pb-As alloys at 703 °C and reported ideal behavior of arsenic in dilute lead solutions. Itagaki [20] measured the activity of arsenic in lead between 464 and 582 °C and reported a "slight" positive deviation from Raoultian behavior for arsenic. Gokcen [21] and Rannikko et al. [22] separately reviewed the published data on thermodynamic properties of lead arsenic alloys and assessed the excess Gibbs energy and activity coefficient of components in Pb-As system. Rannikko et al. reported Equation 5 for the limiting Raoultian activity coefficient of arsenic in lead alloys as a function of temperature.

$$\ln \gamma_{As}^{0} = -0.325 + \frac{444.17}{T} \quad (5)$$

Pb-Sb system:

The thermodynamics of the lead-antimony system have been the subject of studies since the late 19 century [23]. Seltz and DeWitt [24] measured the activities of the components in liquid Pb-Sb alloys at 748 K by the electromotive force (emf) method. They reported a "slight" negative deviation from Raoult's law for both lead and antimony.

Moser et al. [25] measured the activities of the components in Pb-Sb alloys by the emf method between temperatures of 750 and 940 K and assessed the integral and partial thermodynamic properties of the system. Equation 6 expresses the Raoultian activity coefficient of Sb in liquid lead.

$$\ln \gamma_{Sb} = -\left(\frac{101}{T} + 0.063\right)\left[(1 - X_{Pb})^{1.83} - 2.205(1 - X_{Pb})^{0.83} + 1.205\right] \quad (6)$$

Moser et al. [25] also measured the liquidus temperatures via cooling curve measurements and constructed a Pb-Sb phase diagram based on the assessed values of thermodynamic properties. They also compared the results with their thermal analysis measurements as well as previous works of other researchers.

Taskinen and Teppo [26] critically assessed the published thermodynamic properties of Pb-Sb alloys between 673 and 1073 K. They obtained an internally consistent set of excess Gibbs energy functions by simultaneous least square analysis of all the available thermodynamic data of the Pb-Sb system.

Pb-As-Sb-O metallic system:

Taskinen [27-29] measured the activity coefficient of dissolved oxygen in lead-arsenic and lead-antimony melts and formulated the first order interaction coefficient of arsenic and antimony on oxygen in liquid lead.

Dessureault and Pelton [30] used all available thermodynamic data related to lead bullion to optimize a solution model of lead bullion that contained As, Sb (amongst other impurities such as Sn, Bi, Zn) by a modified quasichemical model. Their model was valid over the range of 300 °C and 1200 °C and compositions above 80 at% Pb. The liquid Pb alloy solution database of the FACT*Sage*™ thermochemical software program [31] that was based on the Dessureault and Pelton's [30] model includes As, Sb and O as the impurities in lead and was used in this research to determine the activity of the components in metallic phase.

2.3 Pb-As-O System

The main studies on this system in the past have focused on the arsenic distribution between metal and oxide phases and phase diagrams for the PbO-As_2O_5 and PbO-As_2O_3 systems. The more descriptive and complete work of Gelach et al [32] is reviewed here before the prior works of Pelzel [33] and Zunkel and Larson [34], on the same system, because the author wishes to use it as the point of reference for further discussion of the literature.

Gerlach et al. [32, 35] studied the lead-arsenic-oxygen and the lead-antimony-oxygen systems, extensively. They constructed a phase diagram for PbO-As_2O_5 and performed thermal analysis on the PbO-As_2O_3 system in inert and oxidative atmospheres. They were able to prepare several pure compounds of $nPbO:1As_2O_5$ (with n = 8, 4, 3 and 2) and generated X-ray diffraction patterns for these compounds. The liquidus temperatures in the PbO-As_2O_5 system measured by Gerlach et al. [32] were in good agreement with the only previous study on this system by Amadori [36] (Figure 4).

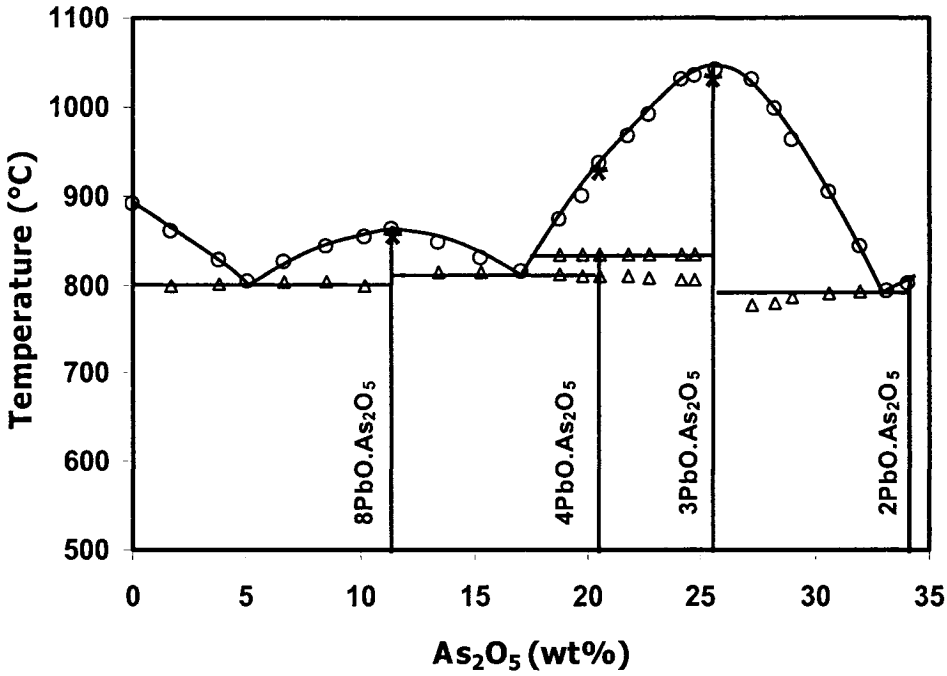

Figure 4 – PbO rich side of the PbO-As_2O_5 system; ○ liquidus and △ secondary thermal arrests from Amadori's [36] and * from Gerlach et al.)

Gerlach et al. observed separation of metallic lead from the PbO-As_2O_3 mixtures between 5 and 18 wt% As_2O_3 that were heated under inert atmosphere. They explained this phenomenon with the oxidation of As_2O_3 to As_2O_5 by PbO and proposed the following redox reaction:

$$2\ PbO + As_2O_3 = 2\ Pb + As_2O_5 \tag{7}$$

$$K_{eq} = 6 \times 10^{-23} \text{ at } 298\ K \text{ (FACT}\textit{Sage}^{TM}\text{ [31])} \tag{8}$$

They measured the amount of separated lead and reported that less than one third of the stoichiometric amount possible from Equation 7 was separated. The K_{eq} for this reaction is extremely low as shown by Equation 8. Given the fact that the activity of lead is close to one, the activity of As_2O_5 would need to be extremely low in order to satisfy the calculated equilibrium constant in Equation 8. As the result, it is doubtful that the separation of lead occurs according to Reaction 7, and there needs to be an alternative reaction to explain this observation.

Gerlach et al. explained that because of the partial oxidation of As_2O_3 to As_2O_5, it was not possible to construct the PbO-As_2O_3 quasi-binary phase diagram. They plotted the measured liquidus temperatures on a phase diagram based on the initial As_2O_3 content in the mixture (Figure 5). Gerlach et al. stated that the phase diagram was very close to PbO-As_2O_5 phase diagram up to 12 wt% As_2O_3, when As_2O_3 was converted to As_2O_5.

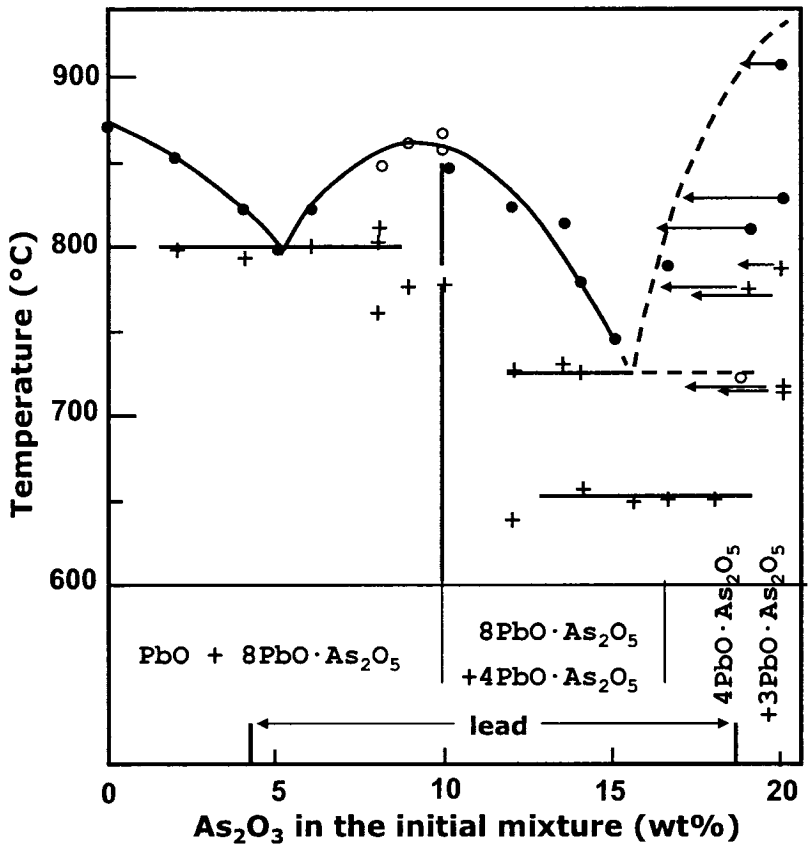

Figure 5 – (Upper portion) thermal arrests in PbO-As_2O_3 mixture, (lower portion) composition of the solidified samples (after Gerlach et al. [32]).

Gerlach et al. also reported low melting temperatures during heating of samples with more than about 0.23 wt% As_2O_3 (e.g., 510 °C for 0.23 wt% As_2O_3). However, they observed that with continued heating, lead separation occurred and the melting temperature during cooling was substantially higher than that measured during heating. They did not explain the observation and drew a dashed line for the liquidus curve above 15 wt% As_2O_3 because of the uncertainly. Figure 5 shows the change in the composition of the samples due to the evaporation of As_2O_3. It could be proposed that the separation of lead occurred after the evaporation of As_2O_3 which would shift the redox reaction

equilibrium to favor formation of Pb and As_2O_5 compounds in the new, post evaporation, composition.

Gerlach et al. also tried to detect the formation of new arsenate compounds for the mixtures that were heated at low temperature (between 250 and 400 °C), where lead separation was not observed. Unfortunately, they were not successful in drawing any conclusions because of an abundance of reflections in the X-ray diffraction patterns. [31]

Prior to Gerlach et al. Pelzel [33] conducted the first study of the PbO-As_2O_3 phase diagram. He measured the liquidus temperature of five PbO-As_2O_3 mixtures and showed a substantial decrease in PbO liquidus temperature with the addition of As_2O_3. Pelzel did not report any separation of lead during his experiments. Pelzel suggested the existence of two previously unreported solid compounds in the PbO-As_2O_3 phase diagram: $3PbO{\cdot}As_2O_3$[i] and $2PbO{\cdot}As_2O_3$[ii] (Figure 6), even though, he was not able to detect them. Pelzel also reported formation of a glass above 30 wt% As_2O_3.

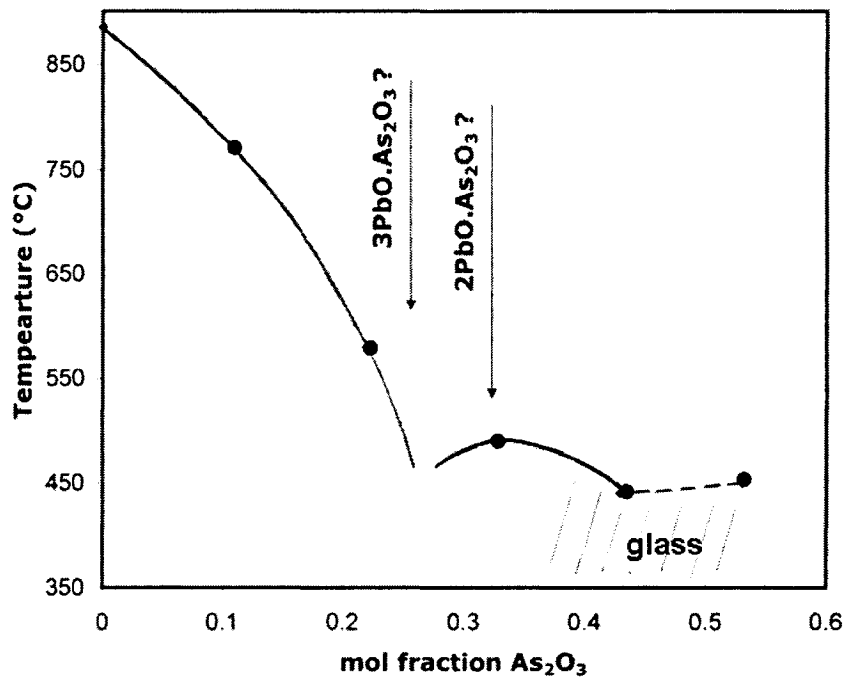

Figure 6 – Liquidus curve in PbO side of PbO- As_2O_3 phase diagram; • measured liquidus temperatures (redrawn after Pelzel [33]).

[i] In the thesis, $3PbO.As_2O_3$ was presented as $Pb_3(AsO_3)_2$.
[ii] In the thesis, $2PbO.As_2O_3$ was presented as $Pb_2As_2O_5$.

Liquidus temperatures reported by Pelzel for samples with either 10 or 20 wt % As_2O_3 were roughly 760 °C and 570 °C respectively, which are noticeably lower than later measured by Gerlach et al. [32] (860 °C and 905 °C respectively). In their analysis, Gerlach et al. attributed this large difference to the absence of lead separation and the absence of oxidation of As_2O_3 into a higher oxidation state with higher liquidus temperature in Pelzel's work. Gerlach et al. suggested that the raw material used by Pelzel might have been damp and the moisture might have stabilized the As_2O_3 beyond its melting temperature.

Zunkel and Larson also studied the PbO-As_2O_3 and PbO-Sb_2O_3 systems extensively [34, 37] prior to Gerlach et al. They equilibrated PbO-As_2O_3 melts with metallic lead and measured the arsenic distribution between the two phases over the range from 650 to 750 °C. They also measured the liquidus and solidus temperatures in PbO-As_2O_3 melts by thermal analysis. Similar to Pelzel [33], they did not report oxidation of As_2O_3 to a higher oxidation state. However, the analytical method they used[i] could not detect the arsenic in different oxidation states; hence, if any pentavalent arsenic did exist in their oxide samples, it could not be differentiated from the trivalent arsenic.

Zunkel and Larson constructed a PbO-As_2O_3 phase diagram (Figure 7). They showed a solid solubility of ~ 5 mol% As_2O_3 in PbO at 700 °C. Zunkel and Larson determined the solid solubility by plotting the arsenic wt% in alloy versus arsenic content in oxide phase. They argued that in the two phase region (i.e. liquid oxide/solid oxide), the arsenic content at equilibrium with the oxide would be constant. In the one phase region (i.e. liquid oxide or solid oxide) the arsenic content in the metallic phase would change with a change in oxide phase. They distinguished three different regions in the isotherms (Figure 8[ii]): 1) At low As_2O_3 content, arsenic content in lead increased with an increase in the As_2O_3 in the oxide phase; 2) at medium As_2O_3 content, arsenic content in lead phase remained constant with an increase in the As_2O_3 in the oxide phase and 3) at high As_2O_3 content, the behavior was similar to the first region. However, close examination of the results (Figure 8) does not find a consistent presence of these three regions in the

[i] ASTM E46-56, a $KBrO_3$ titration method, is the standard method for analysis of lead and tin solders.
[ii] Reproduced from the original data that was collected from Zunkel and Larson [34].

isotherms. At 750 °C, it can be seen that only one behavior, increasing arsenic content in lead with increasing As_2O_3 in the oxide phase, was observed. The arsenic distribution later measured by Gerlach et al. [32] at 800 °C showed only two regions (Figure 9).

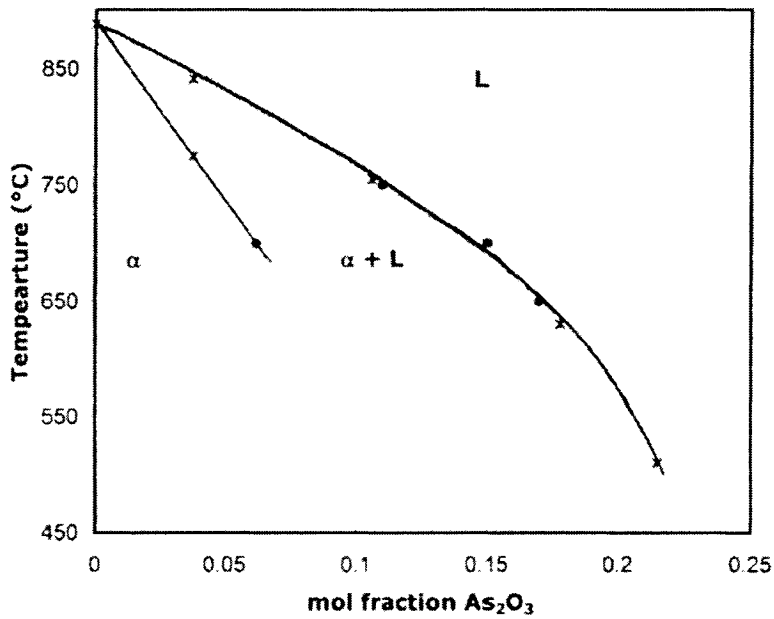

Figure 7 – PbO-As_2O_3 phase diagram redrawn after Zunkel and Larson [34], • from thermal analysis, ∗ from oxide-metal equilibria.

Zunkel and Larson postulated that the observation of the first region was proof of the As_2O_3 solution in solid PbO, but solubility of As_2O_3 in solid PbO was not reported by any other researchers who studied the system. Using the same methods in the PbO-Sb_2O_3 system, Zunkel and Larson reported a solubility of 5.6 mol% Sb_2O_3 in solid PbO [37]. This has also not been observed by any other researchers who studied the system. Consequently, in order to resolve these inconsistencies further studies were performed here to determine As_2O_3 solid solution in PbO from direct observation by wavelength dispersive X-Ray spectrometry (Section 5.2.3).

Zunkel and Larson used a graphical method to establish the liquidus composition at the known equilibration temperature. Their method (presented in Appendix 2) was applied to Zunkel and Larson's experimental values with an assumption of no solid solubility. On average, a shift of 2 mol% higher As_2O_3 was calculated for the liquidus composition at known temperature and the revised values were used in this research.

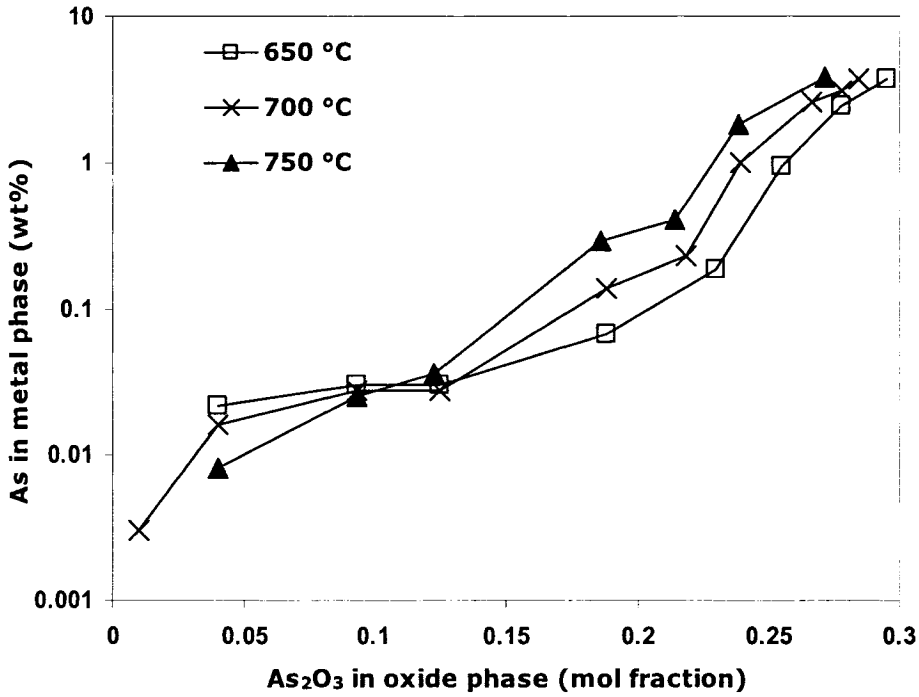

Figure 8 – Equilibrium arsenic contents of Pb-As alloys in contact with PbO As_2O_3 oxides between 650 and 750 °C (experimental values from Zunkel and Larson [34]).

Zunkel and Larson showed (Figure 8) that the arsenic content in the metal phase increased with increasing temperature between 650 °C and 750 °C in the single-phase liquid slag region. The arsenic distribution measured by Zunkel and Larson showed a substantial difference to that measured by Gerlach et al. at 800 °C (Figure 9). The large difference between the results of Zunkel and Larson and Gerlach et al. cannot be explained by experimental variations alone, if the 50 °C difference in their experiment temperatures was insignificant enough to have no appreciable effect on the arsenic distribution.

The only other report on the distribution of the arsenic between oxide and metal phase was by Pelzel [38]. Pelzel studied the dynamic oxidation of Pb-As alloys with different initial compositions and analyzed the composition of metal and slag phases during the course of oxidation. Because of the dynamic nature of Pelzel's test, it cannot be directly compared to the equilibrium studies of Zunkel and Larson and Gerlach et al. Figure 9 shows that at high As_2O_3 content, Pelzel's result was a reasonable extension of Gerlach et

al.'s results. At 15 mol% As_2O_3 Pelzel's data was close to the results of Zunkel and Larson and at 8 mol% As_2O_3, Pelzel's data lay significantly higher than the other two results.

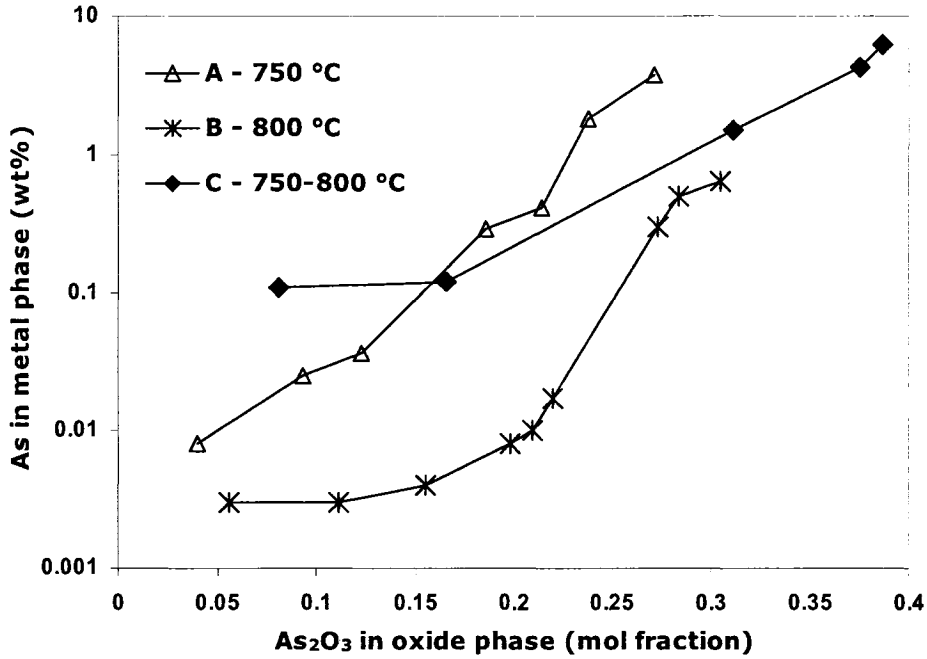

Figure 9 – Equilibrium arsenic contents of Pb-As alloys in contact with PbO As_2O_3 oxides between 750 and 800 °C (A from Zunkel and Larson [34]; B from Gerlach et al. [32] and C from Pelzel [38]).

Returning to the pentavalent PbO-As_2O_5 system, Kasenov et al. [39, 40], constructed the phase diagram for PbO-As_2O_5 over the entire composition range by thermal analysis (Figure 10). Their measurements were in good agreement with the work of Gerlach et al. [32] and Amadori [36], who studied the PbO rich region of the PbO-As_2O_5 binary (Figure 4). The eutectic composition between PbO-$Pb_8As_2O_{13}$ and $Pb_8As_2O_{13}$-$Pb_3(AsO_4)_2$ that was reported by Kasenov et al. [39] (7 mol% As_2O_5 at 780 °C and 18 mol% at 790 °C) was slightly lower than that measured by Amadori (5 mol% at 802 °C and 16.5 mol% at 815 °C).

The published derivative studies on Pb-As-O (and Pb-Sb-O systems), based on the original works of the researchers, are presented in Section 2.5 after a review of the Pb-Sb-O system.

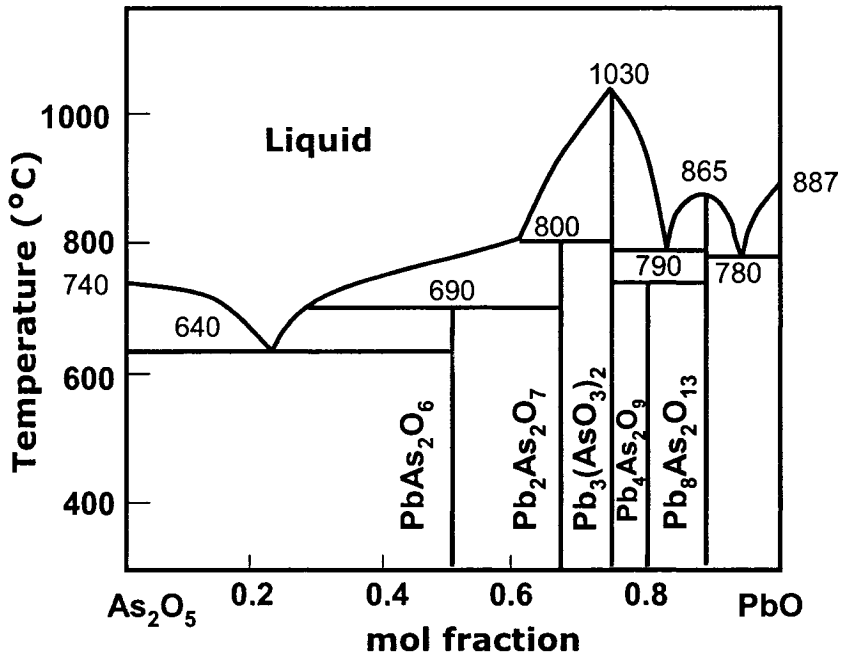

Figure 10 – PbO-As_2O_5 phase diagram (After Kasenov et al. [39])

2.4 Pb-Sb-O System

Maier and Hincke [41] conducted the first extensive study on the PbO-Sb_2O_3 system. They measured the liquidus and eutectic temperatures over the entire range of composition. Similar to the PbO-As_2O_3 system, the PbO-Sb_2O_3 system at compositions above 70 % PbO showed lead separation and oxidation of Sb_2O_3 to higher oxidation states. At these compositions, Maier and Hincke stated that "*no great accuracy may be claimed for the melting points in this region, since the composition of the melt was changing continuously*". They explained this phenomenon via the redox Reactions 9 and 11:

$$PbO + Sb_2O_3 = Pb + Sb_2O_4^{i} \quad (9)$$

$$K_{eq} = 5 \times 10^{-27} \text{ at } 298 \text{ K (FACTSage™ [31])} \quad (10)$$

$$2\ PbO + Sb_2O_3 = 2\ Pb + Sb_2O_5 \quad (11)$$

[i] Sb_2O_4 is a form of antimony oxide, where antimony is believed to be a mixture of +3 and +5 oxidation state.

$$K_{eq} = 7 \times 10^{-6} \text{ at } 298 \text{ K (FACT}Sage\text{™ [31])} \quad (12)$$

Similar to the PbO-As_2O_3 system, the equilibrium constants for these reactions were small and given that lead activity is close to unity, the activity of Sb_2O_4 and Sb_2O_5 in Reactions 9 and 11 would need to be extremely low in order to satisfy Equations 10 and 12, respectively. Therefore, it is doubtful that the separation of lead occurred according to Reactions 9 and 11 and there needs to be an alternative reaction suggested in order to explain the observation.

Maier and Hincke [41] also measured the vapor pressure of Sb_2O_3 over solid and liquid PbO-Sb_2O_3 mixtures at 539 and 697 °C. At 697 °C, when the sample was mainly liquid, they observed relatively high Sb_2O_3 vapor pressures (from 135 to 1700 kPa) at Sb_2O_3 contents more than the composition of the observed PbO·Sb_2O_3 compound. At lower Sb_2O_3 contents, the vapor pressure of Sb_2O_3 fell off rapidly (less than 135 Pa). Maier and Hincke stated that at compositions with Sb_2O_3 higher than the composition of PbO·Sb_2O_3: "*apparently there is a solution of Sb_2O_3 in the compound of this composition: PbO·Sb_2O_3*" [41].

Maier and Hincke [41] were only able to detect the solid compound PbO·Sb_2O_3[i] in this binary system and could not confirm the presence of a previously noted compound having the composition of $Pb_3(SbO_3)_2$ [42].

Hennig and Kohlmeyer [43] constructed the PbO-Sb_2O_3, PbO-Sb_2O_4 and PbO-Sb_2O_5 phase diagrams by thermal analysis. Figure 11 shows a ternary space view of a portion of PbO-Sb_2O_3-Sb_2O_5 phase diagram constructed by Hennig and Kohlmeyer. They confirmed the formation of the PbO·Sb_2O_3 compound and the shape of the liquidus curve presented by Maier and Hincke in the PbO-Sb_2O_3 binary [41], although they reported considerably higher liquidus temperatures (Figure 12).

[i] In this study, PbO·Sb_2O_3 is presented as $PbSb_2O_4$

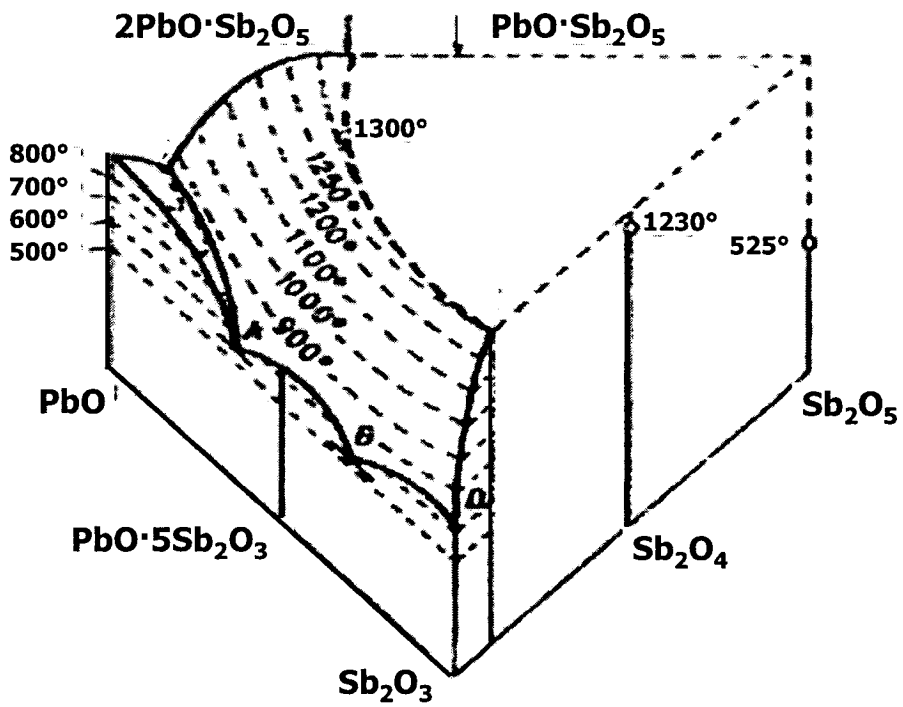

Figure 11 – Ternary space view of liquidus surfaces of PbO-Sb_2O_3-Sb_2O_5 system (after Hennig and Kohlmeyer [43]).

Hennig and Kohlmeyer [43] found a new compound in the PbO-Sb_2O_5 binary with a composition of $2PbO{\cdot}Sb_2O_5$ and explained the separation of lead from the PbO-Sb_2O_3 mixtures via the redox Reaction 13:

$$PbO{\cdot}Sb_2O_3 + 3\ PbO = 2PbO{\cdot}Sb_2O_5 + 2\ Pb \qquad (13)$$

The Gibbs energy of formation of $2PbO{\cdot}Sb_2O_5$ and $PbO{\cdot}Sb_2O_3$ are not known, hence Gibbs energies of the reaction were not reported.

Barthel [44] studied the PbO-Sb_2O_3-Sb_2O_5 phase diagrams by thermal analysis and also determined the antimony distribution between Pb-Sb alloy and PbO-Sb_2O_3 oxide phases. Barthel's results for the liquidus temperatures of the PbO-Sb_2O_3 system were in good agreement with Maier and Hincke (Figure 12). Barthel reported two other solid compounds in this region, namely $5PbO{\cdot}Sb_2O_3$[i] and $3PbO{\cdot}Sb_2O_3$[ii].

[i] In this study, $5PbO.Sb_2O_3$ was presented as $Pb_5Sb_2O_8$

[ii] In this study, $3PbO.Sb_2O_3$ was presented as $Pb_3(SbO_3)_2$

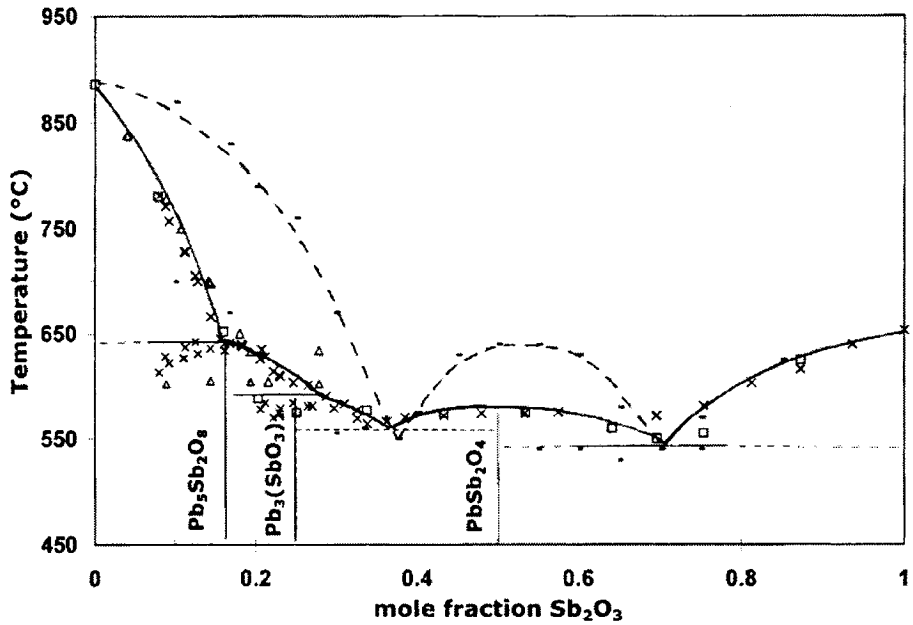

Figure 12 – PbO-Sb_2O_3 phase diagram; × from Barthel [44], △ from Zunkel and Larson [37], □ from Maier and Hincke [41] (solid line) and - from Henning and Kohlmeyer [43] (dash line).

Zunkel and Larson [34, 37] studied the Pb-PbO-Sb_2O_3 system by thermal analysis and equilibration of metal and oxide samples. As for the Pb-PbO-As_2O_3, they did not report separation of Pb from heated PbO-Sb_2O_3 mixtures. Using their method, explained in Section 2.3, they found a maximum of 5.6 mol% Sb_2O_3 in solid PbO at 604 °C. This has not been confirmed by other independent research. The liquidus temperatures measured by thermal analysis and determined by equilibrium experiments were in good agreement with the values of Maier and Hincke [41]. McClincy and Larson [45] continued Zunkel and Larson's work and measured the vapor pressure of $Sb_4O_{6(g)}$ by the inert gas saturation method and calculated the activity of Sb_2O_3 between 650 °C and 750 °C to a maximum of 50 mol% Sb_2O_3 in PbO-Sb_2O_3 melts. For Sb_2O_3, they reported a high negative deviation from Raoult's law. This was confirmed by Sugimoto et al. [46] who measured the activity of Sb_2O_3 in PbO-Sb_2O_3 melts at 750 °C by the emf method over the entire range of composition. The activity of PbO was then calculated by applying the Gibbs-Duhem equation.

Itoh et al. [47] equilibrated Pb-Sb alloys with PbO-Sb_2O_3 melts at 900 °C and 950 °C and measured the antimony distribution in the metallic and oxide phases. They applied Gibbs-Duhem equations to the elements in the metal and oxide phases. At equilibrium, the activities of the components in both phases have identical values. Hence with negligible solubility of oxygen in lead and the known activity of antimony in lead, they were able to calculate the equilibrium oxygen partial pressure. They validated their calculation by measuring the oxygen partial pressure by the emf method at two selected compositions. Thereafter they calculated the activity of Sb_2O_3 in the liquid melt by using the Gibbs energy of formation of Sb_2O_3 and the calculated oxygen partial pressure. Their results (Figure 13) were in good agreement with Sugimoto et al. [46].

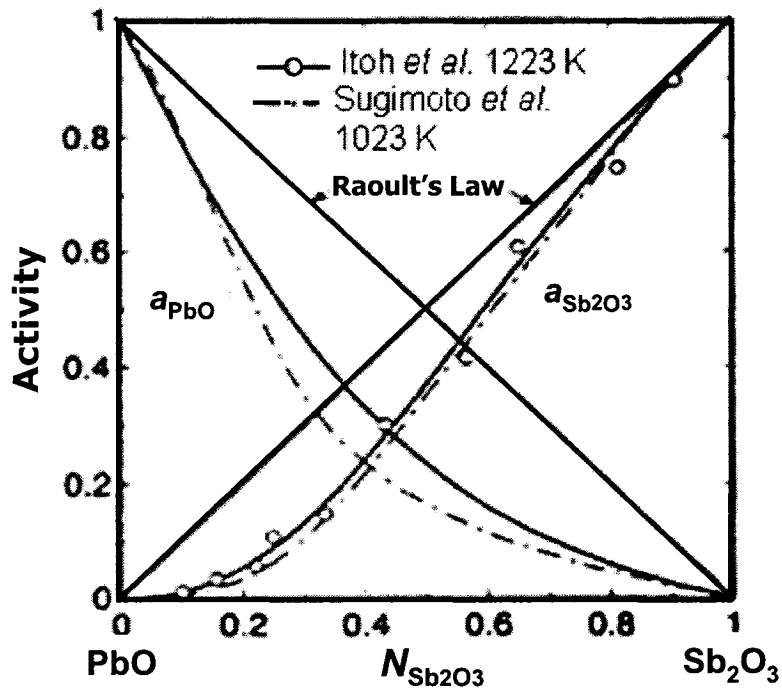

Figure 13 – Sb_2O_3 and PbO activities in PbO-Sb_2O_3 melts at 750 °C and 950 °C (after Itoh et al. [47]).

Itoh et al. [47] also used a regular solution model to evaluate the activity coefficient of $SbO_{1.5}$ in the PbO-$SbO_{1.5}$ pseudo-binary by the least square method. The result is shown in Equation 14:

$$\log \gamma_{SbO_{1.5}} = -0.351\ (1 - X_{SbO_{1.5}})^2 \qquad (14)$$

Using Equation 14, Itoh estimated the activity coefficient at infinite dilution in PbO "$\gamma^0_{SbO1.5}$", to be 0.45 at 950 °C. Using the regular solution model, $\gamma^0_{Sb_2O_3}$ was estimated here using the least squares method from the values reported by Sugimoto et al. [46] at 750 °C and from Itoh et al. [47] at 950 °C. It was calculated to be 0.10 and 0.13 respectively. These values indicated significant negative deviation from Raoult's law.

Several researchers measured antimony distribution between metal and oxide phases at temperatures between 650 °C and 950 °C (Figure 14) with considerable variation between their findings. Zunkel and Larson [37] showed that the antimony content of the metal phase increased with increasing temperature over the entire experimental composition range, but they disagreed with the measurements of Itoh et al. [47] at compositions up to 40 mol % Sb_2O_3 and Pelzel [33] over the entire experimental composition range. In fact, Pelzel results showed that antimony content of the metal phase decreased with increasing temperature.

Results from Barthel [44] at 800 °C, Zunkel and Larson [37] between 650 °C and 750 °C and Pelzel [33] at 750 °C and 800 °C, showed low antimony levels in the metal phase (< 0.2 wt%) up to 20 mol% Sb_2O_3 in the oxide phase. Thereafter a rapid increase in antimony content in the metal phase was observed with increasing Sb_2O_3 in the oxide phase. This trend was not clear in results of Itoh et al. [47]. Wong et al. [48] who studied the solubility of oxygen in Pb-Sb melts, conducted equilibration and quenching experiments of metallic lead-antimony alloys at equilibrium with the oxide phase over the entire composition range at 900 °C. Their results showed low antimony content in lead alloy (~ 0.1 wt%) up to 40 mol% Sb_2O_3 in the oxide phase. Above this level of Sb_2O_3, a rapid increase in the antimony was observed. At low Sb_2O_3 contents in the oxide phase, their results were close to the results of Zunkel and Larson [37] and substantially lower than the results of Itoh et al.[47].

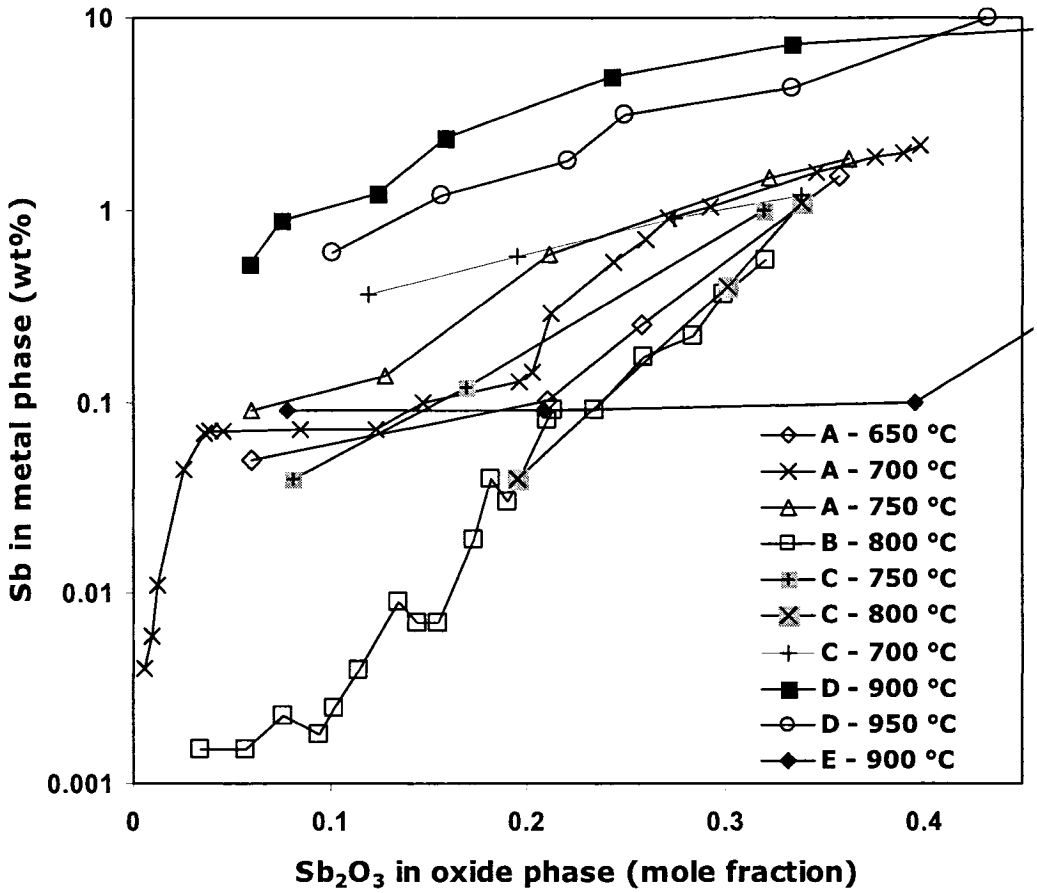

Figure 14 – Antimony distribution between metal and oxide phases; A: from Zunkel and Larson [37], B: from Barthel [44], C: from Pelzel [33], D: from Itoh et al. [47]and E from Wong et al.[48].

Gerlach et al. [35] studied the Pb-Sb-O system by thermal analysis in inert and oxidative atmospheres. They found the formation of a previously unreported $PbO\text{-}Sb_2O_3$ compound, $5PbO{\cdot}Sb_2O_3$ ($Pb_5Sb_2O_8$). By XRD analysis of the heated $PbO\text{-}Sb_2O_3$ mixtures, they observed the separation of lead and the coexistence of oxides of lead-trivalent antimony and lead-pentavalent antimony (e.g. $PbO + 5PbO{\cdot}Sb_2O_3 + 3PbO{\cdot}Sb_2O_5$ + Pb). However, according to the Gibbs phase rule, at constant temperature and pressure, the presence of 4 condensed phases is not possible in a 3-component system. The presence of 4 phases was presumably due to dynamic cooling and changes in the equilibrium conditions during cooling.

Gelach et al. also measured the liquidus temperatures in the $PbO\text{-}Sb_2O_5$ binary system (Figure 15) and their results closely matched the results of Hennig and Kohlmeyer [43].

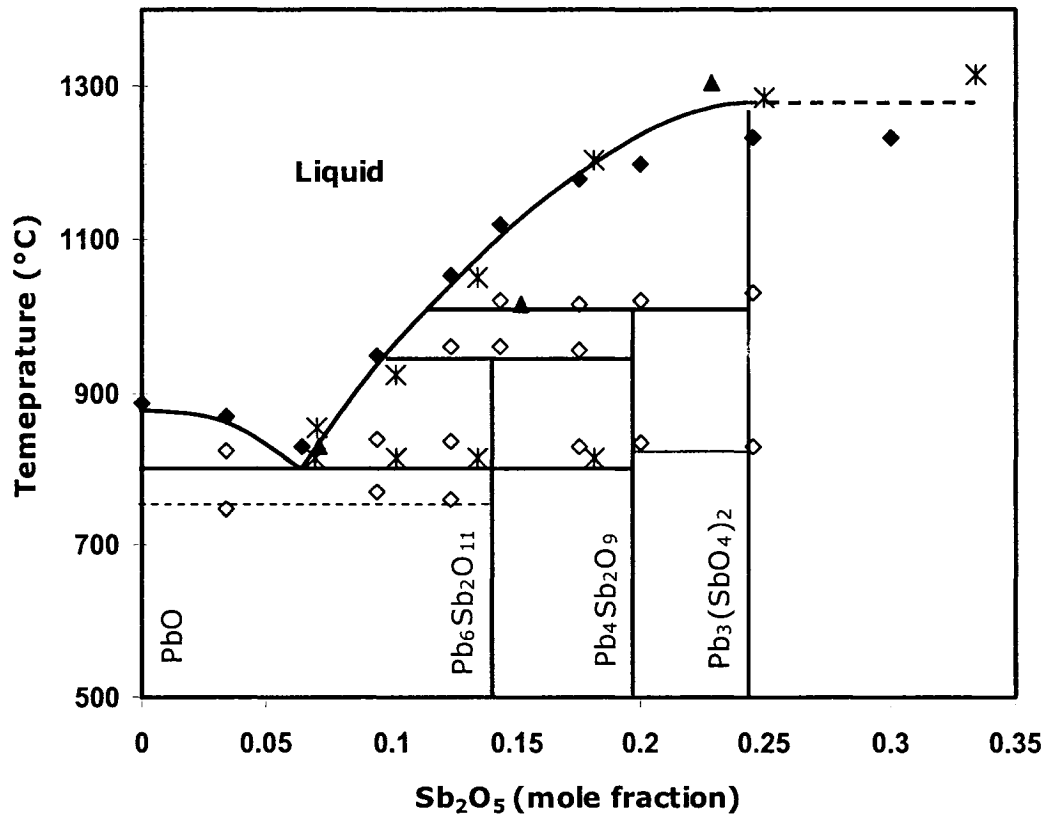

Figure 15 – PbO-Sb_2O_5 phase diagram; ▲ from Grlach et al. [35], ∗ from Hennig and Kohlmeyer [43], ◆ and ◇ from Bush and Venevtsev [49].

Gerlach et al. [35] observed the oxidation of PbO-Sb_2O_3 mixtures heated in air, to mixtures of PbO and Sb_2O_5, Sb_2O_4 oxides. Urazov and Speranskaya [50] observed the same oxidation behavior by thermal analysis of PbO-Sb_2O_3 mixtures between 420 °C and 720 °C. Bush and Venevtsev [49] constructed the phase diagram of PbO-Sb_2O_3 under air and also reported the oxidation of Sb_2O_3 to Sb_2O_5. They found two new compounds of lead oxide with pentavalent antimony oxide ($Pb_4Sb_2O_9$ and $Pb_6Sb_2O_{11}$). Bush and Venevtsev [49] reported that with the oxidation of PbO-Sb_2O_3 mixtures with a ratio close to 3:1, a non-stoichiometric compound, $Pb_{3+x}Sb_2O_{8+x}$ was formed and had a homogeneity region of 23-30 mol% Sb_2O_3. Similar observations were reported by Urazov and Speranskaya [50].

The PbO-Sb_2O_3 phase diagram constructed by Bush and Venevtsev was in fact a PbO-Sb_2O_5 phase diagram with the X-axis being the initial Sb_2O_3. In Figure 15, the PbO-

Sb_2O_3 phase diagram that was constructed by Bush and Venevtsev is converted to a PbO-Sb_2O_5 phase diagram and uses the values reported by Hennig and Kohlmeyer [43] and Gerlach et al. [35].

The thermodynamic data above was used in a number of derivative studies, either to model the lead softening process or to calculate the equilibrium in softening practice, which is explained in the following Section.

2.5 Derivative Thermodynamic Studies of Lead Softening

Paulin et al. [9, 51, 52] studied the Pb-Sb-O, Pb-As-O and Pb-Sn-O systems from the published thermodynamic data. They used the Sb_2O_3 vapor pressure over PbO-Sb_2O_3 melts measured by Maier and Hinke [41] and calculated the activity of Sb_2O_3. Using the known standard Gibbs energy for Equation 3, they calculated the activity of PbO. Paulin et al. stated that in softening of lead-antimony melts with oxygen-enriched air, the products were mainly PbO and $Pb_5Sb_2O_8$, which are both solid below 640 °C. With these assumptions, Paulin et al. [52] calculated the activity of Sb_2O_3 in the skim phase to be 0.002 for a skim with less than 20 wt% Sb_2O_3. Subsequently, they predicted an antimony content of 0.007 wt% at about 600 °C. They were able to confirm this in industrial trials where a value of 0.008 wt% Sb was measured in one batch at 600 °C. They stated that in a reverberatory softening at 700 °C with about 30 wt % Sb in the slag phase, 0.05 wt% Sb would be the limit of antimony removal by oxidation.

For the Pb-As-O system, Paulin [9] stated that a liquid slag is probably favored due to the low melting point of As_2O_3. Because of lack of thermodynamic data for the Pb-As-O system, Paulin was unable to make equilibrium calculations.

Kapusta [6] assumed that the following equations were representative of the oxygen softening process and wrote a Gibbs energy minimization routine to predict the equilibrium conditions in softening practice.

$$\tfrac{1}{2}\, O_{2(g)} = O_{(Bullion)} \qquad (15)$$

$$Pb_{(l)} + \tfrac{1}{2}\, O_{2(g)} = PbO_{(slag)} \qquad (16)$$

$$Sb_{(l)} + \tfrac{3}{4}\, O_{2(g)} = SbO_{1.5(Slag)} \quad (17)$$

$$As_{(l)} + \tfrac{3}{4}\, O_{2(g)} = AsO_{1.5(slag)} \quad (18)$$

Kapusta used the activity values measured by Sugimoto [46] for $PbO\text{-}Sb_2O_3$ (discussed in the previous section) and the unpublished work of Chaskar[i] to estimate the activity of PbO in the $PbO\text{-}SbO_{1.5}\text{-}AsO_{1.5}$ melts. Kapusta collected industrial data on the compositions of bullion and slag from the Teck Cominco operation in Trail, B.C. and fitted the activity coefficients of $SbO_{1.5}$ and $AsO_{1.5}$ values to achieve the same distribution of arsenic and antimony between slag and bullion phases. In this way, he was able to report a value for the activity coefficient that was independent of composition and would reproduce that particular slag composition. Kapusta validated the model by comparing the equilibrium constant calculated by the standard Gibbs energy of Reactions 2 and 3 with the values calculated by the fitted model and found good agreement. Kapusta stated that laboratory tests are required to develop a better model of the slag thermo-chemistry and to verify that the thermodynamic model applies to softening at high impurity levels.

In a more recent study, Friedrich et al. [53] examined the equilibria in Pb-As-Sb-O melts related to lead softening. They explained and used a triangulation method to construct the phase boundaries in the Pb-As-O and Pb-Sb-O systems and considered all the reported solid oxide compounds. Because of the reported oxidation of trivalent arsenic to pentavalent arsenic [32], they stated that the $PbO\text{-}As_2O_3$ quasi-binary did not exist and described the lead separation by oxidation of As_2O_3 to one of the many mixed oxides of Pb-As-O such as shown by Equation 19:

$$5\ PbO + As_2O_3 = 2\ Pb + 3PbO{\cdot}As_2O_5 \quad (19)$$

Friedrich et al. explained the distribution of arsenic between metal and oxide phase by oxidation of arsenic to one of the many mixed oxides of Pb-As-O, for example Equation 20:

$$8\ PbO + 2\ As = 5\ Pb + 3PbO{\cdot}As_2O_5 \quad (20)$$

[i] This work was reported by Kapusta in private communication has not been published. Consequently there was no information available to be included in this research.

Friedrich et al. used the thermochemical software FACT*Sage*™ [31] to calculate the equilibria between the metal and oxide phases. They took into account only the PbO and $3PbO{\cdot}As_2O_5$ compounds because only the thermodynamic data for these two compounds were available to them. They also took into account the presence of a liquid oxide phase by using the "slag" solution database that is part of the FACT*Sage*™ software. However, the slag database is optimized for SiO_2-rich slags in the composition region of fayalite slags. Friedrich et al.'s compositions and temperatures were extrapolated outside the suggested range[i]. Despite these short-comings, they performed equilibrium calculations using the database and reported the arsenic distribution between metal and slag phase between 350 °C and 800 °C. They made no comparisons between the calculated and measured values.

For the Pb-Sb-O system, Friedrich et al. used the same method and considered the formation of different mixed oxides of Pb-Sb (see Section 3.2.1). Because of the reported stable compounds of trivalent antimony, they assumed multiple possible reactions of oxides of both trivalent and pentavalent antimony, for example Equations 21 or 22

$$6\ PbO + 2\ Sb = 3\ Pb + 3PbO{\cdot}Sb_2O_3 \qquad (21)$$

$$5\ Pb + 2\ Sb + 5\ O_2 = 2\ PbO + 3PbO{\cdot}Sb_2O_5 \qquad (22)$$

However, no thermodynamic data for the mixed Pb-Sb oxides were available to them and they used only the PbO, Sb_2O_3, Sb_2O_4 and Sb_2O_5 compounds in their calculations. For the liquid phase, they assumed the formation of pure liquid oxide phases since there was no Pb-Sb-O solution data available in FACT*Sage*™. They performed the equilibrium calculations using FACT*Sage*™ and reported the antimony distribution between the metal and slag phase, again no comparison was made between the calculations and the laboratory or industrial results.

Friedrich et al.'s calculations predicted the formation of solid PbO for a mixture of PbO with 40 mol% Sb_2O_3 at 800 °C, contradicting the published work stating that the mixture

[i] FACT-SLAG [31] solution database suggested the applicable composition range for As_2O_3 to be less than 10 wt%; For temperatures above 460 °C thermodynamic properties were extrapolated from 460 °C.

should be liquid at 550 °C [35, 43]. Because Friedrich et al. assumed that there was no liquid oxide solution phase for this system, it is doubtful that the equilibrium calculations resulted in accurate answers.

2.6 Summary

The three main studies on the PbO-As_2O_3 system focused on the distribution of arsenic between metal and oxide phases and the construction of phase diagrams by thermal analysis. The equilibrium arsenic distributions between the metal and oxide phases as well as the liquidus temperatures of the PbO-As_2O_3 mixtures were not in good agreement amongst the reports. There were no quantitative measurements of the arsenic oxidation state in the oxide phases and two of the reports considered only the presence of trivalent arsenic.

The two available phase diagrams for the PbO-As_2O_5 are consistent. Previous attempts to construct a thermodynamic model for lead softening or predict the equilibrium conditions based on available thermodynamic data suffered from a lack of sufficient and reliable data or used models that were not valid for the softening conditions.

Several studies focused on the measurement of the phase diagram, antimony distributions and Sb_2O_3 vapor pressures for the PbO-Sb_2O_3 binary. The reported phase diagrams were in reasonable agreement with the exception of Henning and Kohlmeyer [43]. Although there was disagreement between reports for the antimony distribution in metal and oxide phases an "optimized" thermodynamic model of the system developed here should be able to resolve the discrepancies.

Conclusions:

Because of the shortcomings of the available data for the Pb-As-O system, it was decided here to conduct complementary experiments that quantitatively measured arsenic in the oxide phase under different oxidation states. It was believed that enough thermodynamic data was available for the Pb-Sb-O system to study the thermodynamics of this system without further experimental measurements.

It was decided to use thermodynamic modeling in addition to the experimental studies as a powerful tool to develop an understanding of the observations in terms of thermodynamics. In this way all the published thermodynamic data and new data from this study were used to obtain an "optimized" model for this system. The next chapter introduces the "thermodynamic modeling" and "optimization" techniques and explains the reasons for using the thermodynamic modeling. It also describes the basis for the thermodynamic model that was suggested here for the softening slag in detail.

CHAPTER 3. THERMODYNAMIC MODELING AND OPTIMIZATION

3.1 Scope

To help explain the ignition phenomena observed in industrial practice, the past and present laboratory observations, and the complexity from the findings of the qualitative kinetic studies (see Appendix 1 and Vineberg [1]), knowledge of the thermodynamics of the Pb-As-Sb-Sn-O system in the composition range of lead softening was deemed necessary. Unfortunately, the available thermodynamic data and phase diagrams were limited and there were considerable discrepancies amongst those that did exist. As a first step toward gaining the required understanding of the thermodynamics of the softening process, a thermodynamic solution model of the Pb-As-O and Pb-Sb-O systems in the composition range of lead softening practice was constructed as described below.

In Section 3.2, the concept of thermodynamic modeling, optimization and calculation of the phase diagram and phase equilibria from the model is explained. Schematic ternary composition triangles of Pb-As-O and Pb-Sb-O systems are drawn in order to show the region of study and the associated compounds. In Section 3.3, the structure of the liquid phases in the Pb-As-O and Pb-Sb-O system is defined. Subsequently in Section 3.4, the liquid solution model for the Pb-As-O and Pb-Sb-O systems in the compositional ranges of lead softening are defined and the method to estimate and assess the parameters in the model from the thermodynamic data is explained.

3.2 Thermodynamic Modeling

A thermodynamic model is a set of equations for Gibbs energy that describes all of the phases in a system as a function of composition, temperature and pressure[i]. For elements and pure compounds, Gibbs energy is a function of temperature only. For a pure compound, Gibbs energy may be written as:

[i] Total pressure is usually constant for metallurgical systems and is not included in the equations.

$$G_i^0 = H_i^0 - TS_i^0 \tag{23}$$

where G_i^0, H_i^0 and S_i^0 are standard Gibbs energy, enthalpy and entropy of *i*, respectively, and T is the absolute temperature. H_i^0 and S_i^0 are both a function of temperature and may be written as:

$$H_i^0 = A + \int_{298.15}^{T} C_p \, dT \tag{24}$$

$$S_i^0 = B + \int_{298.15}^{T} \frac{C_p}{T} dT \tag{25}$$

C_P, the heat capacity at constant pressure, may be expressed as a function of temperature as follows:

$$C_p = a + bT + cT^{-2} \tag{26}$$

In Equations 24 to 26, A, B, a, b and c are parameters in the Gibbs energy function (Equation 23) that need to be defined for each pure compound in the system.

For the solution phase, Gibbs energy as a function of temperature and composition may be written as:

$$g = \sum_i X_i \, g_i^0 + \mathrm{R}T \sum_i X_i \ln X_i + g^{\mathrm{E}} \tag{27}$$

where g is the molar Gibbs energy of solution, X_i is the mole fraction of the pure component (or the end member) *i* in the solution, g_i^0 is the standard molar Gibbs energy of the pure component *i* (which is a function of temperature as it was described for the pure compounds) and g^{E} is the molar excess Gibbs energy of mixing. As an example, g^{E} for a regular binary solution of A and B may be written as:

$$g^{\mathrm{E}} = X_{\mathrm{A}} \, X_{\mathrm{B}} \, (\omega - \eta T) \tag{28}$$

where ω and η are parameters that would be optimized in a regular solution model.

With the increased sophistication of the technology of numerical methods and computer software that are now available, and using the thermodynamic laws and principles that inter-relate the thermodynamic properties of the phases in the system, it is now possible to simultaneously use all of the available and relevant thermodynamic data (e.g. activity, phase diagrams, heat of mixing) in order to obtain the optimum set of equations that best describes the system. In this way, paraphrasing from A.D. Pelton [54], "the derived equations are rendered self-consistent and consistent with the thermodynamic principles and thus all of the thermodynamic properties and phase diagrams can be back-calculated. Moreover, discrepancies between different sets of experimental data can often be resolved but more importantly, using proper interpolation and extrapolation techniques, it is possible to predict the properties of complex multi-component systems, using only data from binary systems and data, if any is available, from the higher order systems". The use of these new tools greatly reduces the number of experiments required to obtain the thermodynamic properties of a multi-component system.

Optimization:

The simultaneous evaluation of all the available thermodynamic data to obtain the parameters in the set of Gibbs energy equations, i.e., thermodynamic model, is generally termed thermodynamic "optimization". Since the Gibbs energy equations (e.g. Equation 27) in the model are all linear, it is possible to include all the thermodynamic data in one simultaneous linear optimization technique (e.g. least square optimization).

In this research, a commercially available optimizing program, which is a module in the FACT*Sage*™ [31] thermochemical software, was employed. However, where it was possible to use thermodynamic principles to obtain the parameters in the model, the optimizing program was not used as is shown in the later chapters.

Calculation of phase equilibria and phase diagram

The Gibbs energy minimization method was used to calculate the phase equilibria and the phase diagram from the optimized thermodynamic model. For this purpose, a general

Gibbs energy minimization program (FACT*Sage*™ [31]) was employed to perform such calculations. The Gibbs energy minimization algorithm is outside the scope of this study but the basic principle is well explained by A.D. Pelton in "Thermodynamics and Phase Diagrams of Materials" [54].

Despite the power of this approach for quantifying the thermodynamic behavior of a system, one should always be cautious of using an optimized model because the thermodynamic experimental data can only report if a "suggested" thermodynamic model of a system is possible or not, i.e., it fits the data. This does not necessarily mean that the suggested model is fundamentally correct[i] and if it is the exclusive model for that system. The reason for this potential error is that it may be possible to fit all the available data into an incorrect model and reproduce the original data by back-calculation of the properties from the model. However, once this model is applied to predict the properties of higher degree systems, serious disagreement between the predictions and real behavior may arise.

3.2.1 Background

The Pb-As-Sb-Sn-O system is comprised of pure components, compounds and solution phases. The thermodynamic properties of metallic lead solutions with arsenic, antimony, tin and oxygen as impurities were previously measured by several authors [25, 27-29, 55-61] and an optimized solution model of the molten lead alloy has already been constructed [30] and is commercially available [31]. The current study extends the models by focusing on the liquid oxide solution and solid oxide compounds of lead, arsenic, and antimony[ii].

Figure 16 and Figure 17 show the ternary composition triangles of Pb-As-O and Pb-Sb-O, the two important subsystems in lead softening. The softener slag is rich in PbO and the region of interest in each of these ternaries may be shown with smaller ternaries within the complete systems, which are shown with numbers 1, 4 and 9 and 1, 4 and 10 for Pb-As-O and Pb-Sb-O systems, respectively. The softener slag is in contact with metallic

[i] By "fundamentally correct", it is meant that the basis for the model reflects the real behavior, for example presence of ionic species with an ionic model.

[ii] Tin oxides were outside the scope of this research.

lead and equilibrium between the slag and metallic phases was assumed in interpreting the observations.

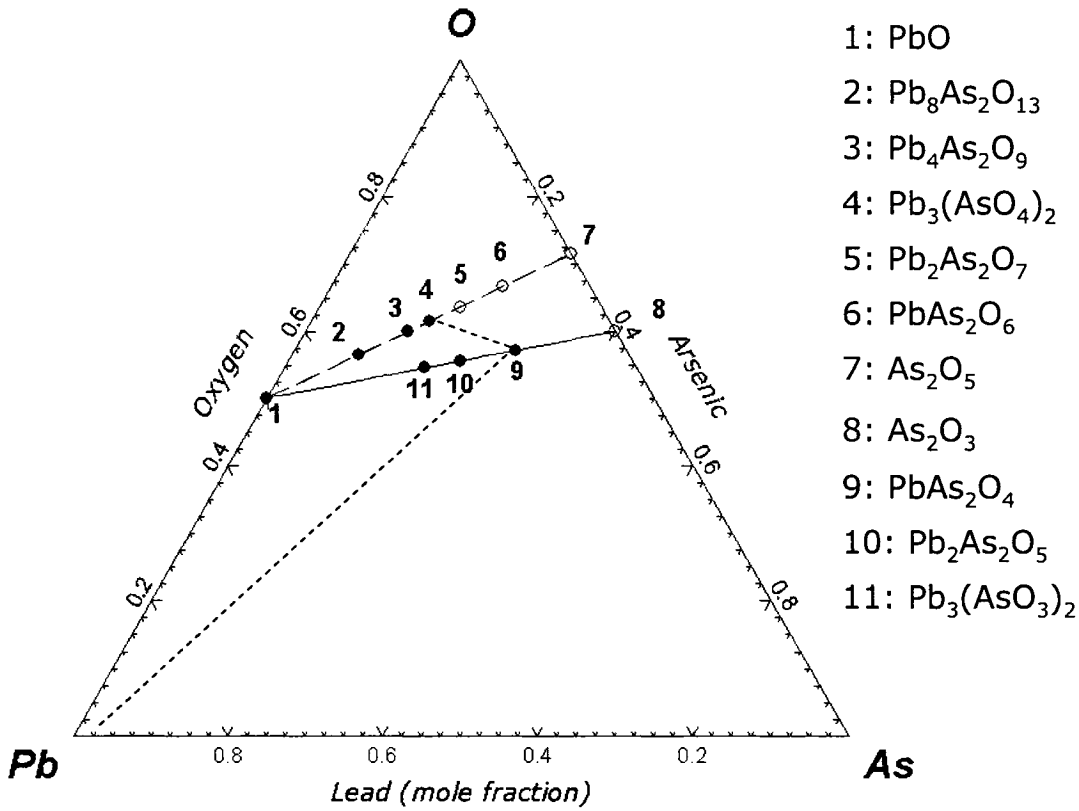

Figure 16 – Compounds in the Pb-As-O composition triangle; region between 1, 4 and 9 at equilibrium with metallic lead, is the important region for the lead softening. Compounds marked with • were part of the model and ○ were not included in the model (graph generated with FACT*Sage*™ [31]).

The compounds in the corners of each smaller ternary are the end members of the solution model for that system and each of these smaller ternaries are comprised of three pseudo-binaries. The thermodynamic properties of these compounds are introduced in the Chapter 5 and Chapter 6.

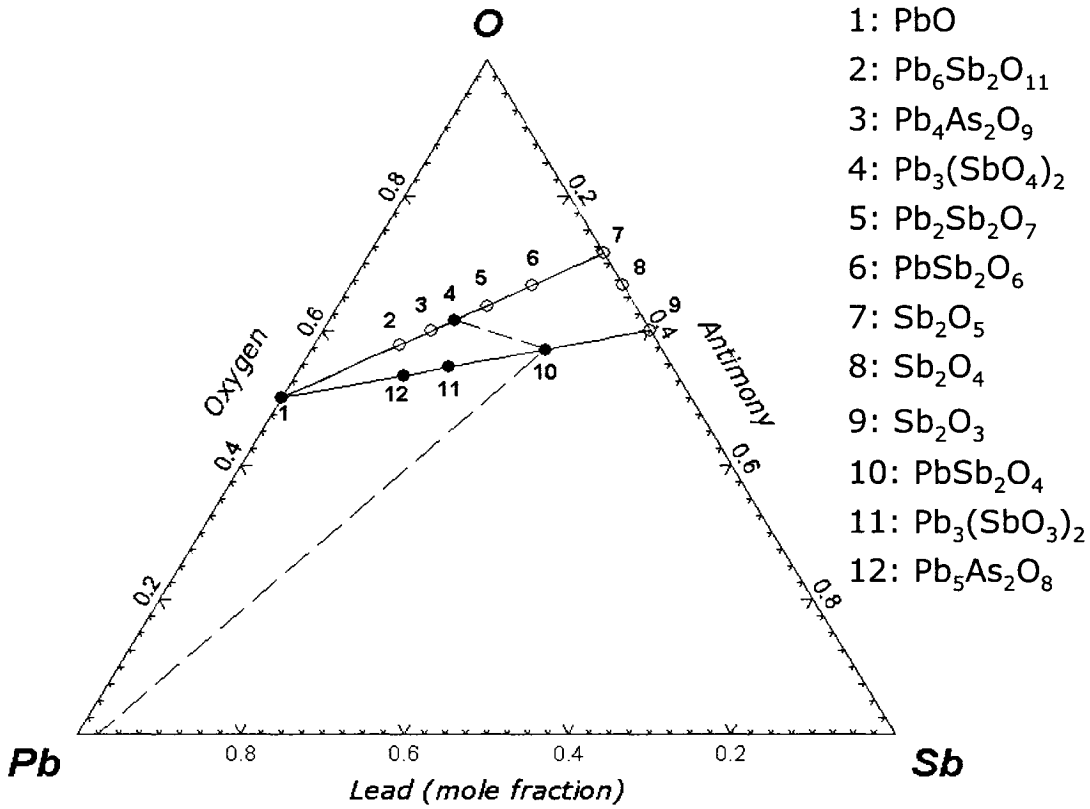

Figure 17 – Compounds in the Pb-Sb-O composition triangle; region between 1, 4 and 10 at equilibrium with metallic lead, is the important region for the lead softening. Compounds marked with • were part of the model and ○ were not included in the model (graph generated with FACT*Sage*™ [31]).

3.3 Structure of Liquid in the Pb-As and Pb-Sb Oxide Systems

Pure molten lead oxide is an ionic liquid and is believed to exist in a completely dissociated form due to the large value of specific conductivity [62, 63]. PbO forms Pb^{2+} and O^{2-} ions[i] according to Equation 29:

$$PbO \rightarrow Pb^{2+} + O^{2-} \qquad (29)$$

Being a completely ionic melt, the above equation is moved almost completely to the right hand side [63].

[i] An oxygen ion donor is commonly referred to as a "base" and oxygen ion acceptor as an "acid" [64]. Thereby, in this work the PbO rich solution that is mainly dissociated into Pb^{2+} and O^{2-} is sometimes referred to as a Basic slag.

On the other hand, As_2O_3 is a strong *network former* that forms a corner sharing AsO_3 pyramidal unit [65-67]. Sb_2O_3 is also a network former [68], which in a style similar to As_2O_3 forms SbO_3 pyramidal structure. Some refer to Sb_2O_3 as *conditional network former* that needs certain amount of other species such as As_2O_3 to form a network structure [65, 69].

In general PbO is known to be a *network modifier*. In the presence of a network former such as As_2O_3, Pb^{2+} and O^{2-} ions break up the As-O-As bonds in the network structure (normally the O^{2-} ions break the local symmetry while Pb^{2+} ions occupy interstitial positions) [66, 70]. Subsequently, based on the composition of the PbO-As_2O_3-Sb_2O_3 melts, an ionic melt or a network structured melt may form and some consideration of the real behavior is required to choose the correct description for the range of composition of interest.

Nassau et al. [65, 66] studied the glass[i] forming region in PbO-As_2O_3-Sb_2O_3 melts and reported that no glass was formed for 75% PbO – 25% As_2O_3 mixtures and only traces of glass were observed for a composition of 46% PbO – 30% As_2O_3 – 23% Sb_2O_3. Also, Pelzel [33] reported formation of glass in PbO-As_2O_3 mixtures once As_2O_3 exceeded 30 mol%. Similarly, Heaton and Moore [67] who studied the glass forming ability of heavy metals, reported that once the molar ratio of PbO:As_2O_3 exceeded 2:1, no glass was formed. As a result, it was assumed that the structure of the softener slag, which is rich in PbO, was ionic because the arsenic and antimony oxide composition were below these values.

Arsenic and antimony have been reported to be present in the +3 and +5 oxidation states [71-74]. In fact, the redox reaction between As^{3+} and As^{5+} is used industrially to clarify glass, whereby As^{3+} reacts with dissolved oxygen and removes fine oxygen bubbles by forming As^{5+} [75, 76]. Kojo et al. [77] determined the oxidation state of As and Sb in a sodium carbonate slag in copper refining. They reported that depending on the partial pressure of oxygen, Sb was in either the +5 or +3 oxidation state and As was in +5 oxidation state in the range of their experiments.

[i] A network structure is sometimes commonly referred to as glass structure.

There have been a number of studies on the structure of the pentavalent arsenic in liquid oxide system. Konijnendijk and Buster [71, 78] detected the presence of As^{5+} by Raman spectrometry in the glass oxide phase to be in the form of AsO_4^{3-} complex ions, and showed As^{5+} is not present as As_2O_5. This was later confirmed by Verweij [79] by Raman spectrometry of an arsenic-containing potassium silicate glass.

Reddy et al. [80, 81] depicted the pentavalent arsenic and antimony species as AsO_4^{3-} and SbO_4^{3-} ions and constructed a solution model for the arsenate capacity of copper slag. The authors claimed that, in the basic region, the anions were randomly mixed and there was little deviation from ideal behavior. Coursol [82] and Coursol et al. [83] optimized a solution model for an As and Sb containing alkalai sulfate slag for refining anode copper. They stated that arsenic and antimony in their range of interest were present in the +5 oxidation state and formed AsO_4^{3-} and SbO_4^{3-} anions, respectively. As a result, it was assumed that the present work for arsenic and antimony in the +5 oxidation state exist as AsO_4^{3-} and SbO_4^{3-} complex anions and that they form $Pb_3(AsO_4)_2$ and $Pb_3(SbO_4)_2$, respectively.

It is known that trivalent arsenic and antimony form AsO_3 and SbO_3 pyramidal networks in acidic melts [72, 84] however there were no reports of the structure of these elements in basic melts. Masayasu et al. [72] suggested that for basic melts of $CaO\text{-}Fe_2O_3$, the arsenic redox reaction happens between AsO_4^{5-} and AsO_4^{3-} complex ions as shown in Equation 30, however AsO_4^{5-} is not a common arsenic ion.

$$AsO_4^{5-} + \tfrac{1}{2} O_2 = AsO_4^{3-} + O^{2-} \qquad (30)$$

Sometimes it is assumed that they remain as As_2O_3 and Sb_2O_3 in the liquid oxide, [34] but an examination of the limiting slope of the PbO liquidus in the $PbO\text{-}As_2O_3$ and $PbO\text{-}Sb_2O_3$ pseudo-binaries invalidated this assumption for these two systems in the basic region. The reason for this invalidation is that all solvents obey Raoult's law at the $X_{solvent} \rightarrow 1$ limit, i.e., the limiting slope of the liquidus line is inversely proportional to

the number, ν, of unit particles (e.g., atoms, ions, molecules, etc.) of solute added to the solvent upon dissolution of the species [54]. This relation is shown in Equation 31:

$$\lim_{X_{PbO \to 1}} = \frac{dX^{L}_{PbO}}{dT} = \frac{\Delta h^{0}_{f(PbO)}}{\nu R (T_{f(PbO)})^{2}} \tag{31}$$

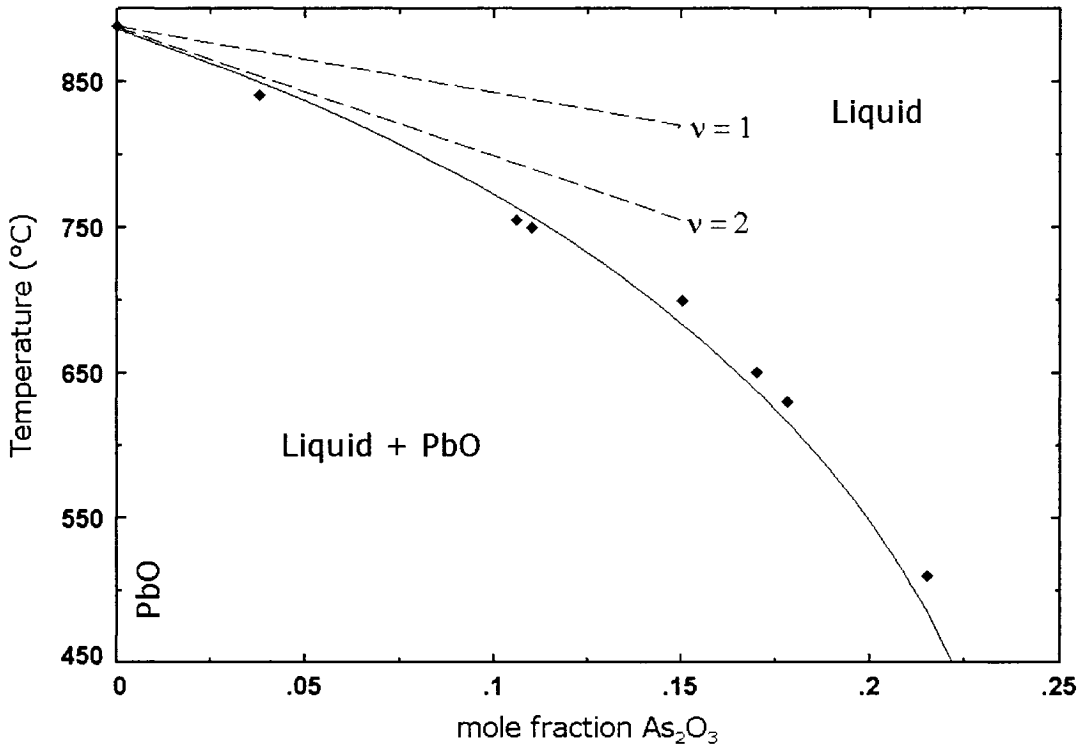

Figure 18 – Limiting slope lines with ν = 1 and ν = 2 are compared with the PbO liquidus curve in PbO-As_2O_3 phase diagram (◆ Zunkel and Larson [34]); (graph generated with FACT*Sage*™ [31]).

Here, $\Delta h^{0}_{f(PbO)}$ and $T_{f\ (PbO)}$ are the standard heat of fusion and melting point of PbO, respectively. Figure 18 shows the PbO liquidus curve for the PbO-As_2O_3 binary [34]. Two lines have been drawn at $X_{PbO} \rightarrow 1$ for the addition of one (ν = 1) or two (ν = 2) particles. It can be seen that the slope of the line for ν = 2, i.e. when As_2O_3 dissociates into two particles, agrees more closely with the slope of the tangent to the liquidus than the slope for the line for ν = 1, i.e. when As_2O_3 does not dissociate. The PbO liquidus in the Sb_2O_3-PbO binary [37, 41, 44] (Figure 19) exhibits similar behavior. Thus, it can be

assumed that both As_2O_3 and Sb_2O_3 do not remain, as monomeric As_2O_3 and Sb_2O_3 species in the molten liquid and possibly dissociate into ions.

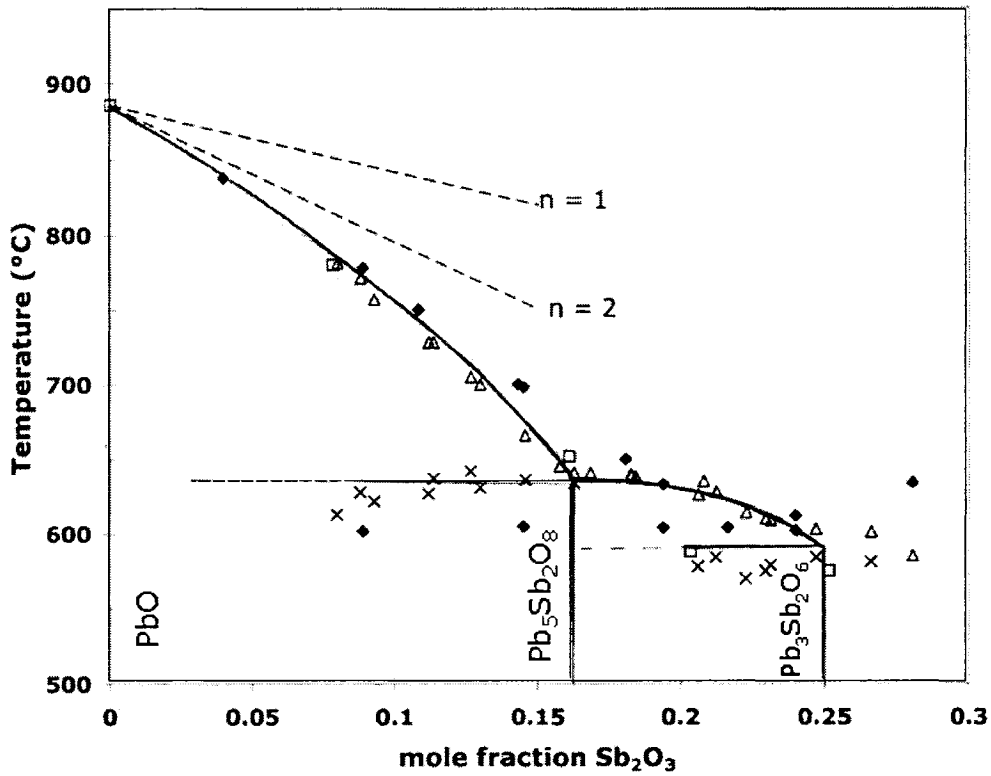

Figure 19 – Limiting slope lines with ν = 1 and ν = 2 are compared with the PbO liquidus curve in PbO-Sb_2O_3 phase diagram. ♦ from Zunkel and Larson [37] □ from Maier and Hincke [41] , × and △ from Bartherl [44].

$(AsO_3)^{3-}$ and $(SbO_3)^{3-}$ are two common complex anions of As^{3+} and Sb^{3+}, respectively and their presence is reported in aqueous systems [85-88]. In fact, $(AsO_3)^{3-}$ belongs to an anionic group that forms $(As_2O_5)^{4-}$ polymeric clusters [89], as do $(SiO_4)^{4-}$ form $(Si_2O_7)^{6-}$ in silicates [90]. Pelzel [33] measured the liquidus temperature in PbO-As_2O_3 system and observed a sharp decrease in the PbO liquidus with additions of As_2O_3 up to the composition corresponding to 3PbO:1As_2O_3 ($Pb_3(AsO_3)_2$). The sharp minimum in the liquidus at 3PbO:1As_2O_3 is an indication of short range ordering that corresponds to the formation of $(AsO_3)^{3-}$ groupings. As the result, $(AsO_3)^{3-}$ was chosen to represent the +3 oxidation state of arsenic in lead oxide melts. $(SbO_3)^{3-}$ was chosen to represent the +3 oxidation state of Sb because of its structural similarity to the arsenic trioxide.

There is also some indication that at higher concentration of trivalent arsenic and antimony, $PbO{\cdot}As_2O_3$[i] and $PbO{\cdot}Sb_2O_3$ compounds would form in the liquid phase. These compounds correspond to the formation of $(AsO_2)^{1-}$ and $(SbO_2)^{1-}$ groupings[ii] in the liquid oxide. For antimony this was postulated by Maier and Hincke [41], which was explained in Section 2.4. For trivalent arsenic oxide, Heaton and Moore [67] experiment indicates the formation of $PbO{\cdot}As_2O_3$(l) in the liquid oxide phase. Heaton and Moore melted mixtures of PbO/As_2O_3 with a molar ratio between 1:9 and 3:1 at 600 °C with no protection for evaporation. They observed that glasses made from mixtures, which initially contained high proportions of As_2O_3 (i.e., 9:1 to 1:1 ratio) the final composition tended towards PbO/As_2O_3 ratio of 1:1 due to evaporation. This observation indicates that at compositions with more than 50 mol % As_2O_3 in $PbO\text{-}As_2O_3$ mixtures, some of the arsenic exists in the form of As_2O_3, which has a high vapor pressure at 600 °C (0.49 atm at 600 °C [31]) and in an open system at 600 °C, would quickly evaporate. In addition, it indicates that a stable $PbO{\cdot}As_2O_3$ compound existes in the liquid phase. As a result, $PbO{\cdot}As_2O_3$ and $PbO{\cdot}Sb_2O_3$ species were assumed to represent the structure of the $PbO\text{-}As_2O_3$ and $PbO\text{-}Sb_2O_3$ melts at relatively higher As_2O_3 and Sb_2O_3 content, respectively.

3.4 Thermodynamic Model of the Solution (an Ionic Model)

An ionic sublattice solution model was adopted for the description of the PbO rich liquid phase because of the ionic properties of the PbO rich softener slag explained above. The liquid solution was assumed to consist of O^{2-}, $(AsO_4)^{3-}$ and $(AsO_3)^{3-}$ anions for the Pb-As-O system and O^{2-}, $(SbO_4)^{3-}$ and $(SbO_3)^{3-}$ anions for the Pb-Sb-O system occupying the anionic sites and only Pb^{2+} cations occupying the cationic sites in both systems. The components in the liquid phase were taken as PbO, $Pb_3(AsO_3)_2$ $Pb_3(AsO_4)_2$, in the Pb-As-O system and PbO, $Pb_3(SbO_3)_2$ $Pb_3(SbO_4)_2$ in the Pb-Sb-O system.

---

[i] In solid form, $PbO{\cdot}As_2O_3$ (or $PbAs_2O_4$) is formed by polymerization of AsO_3 pyramids, which are corner connected [91].

[ii] AsO_2^{1-} and SbO_2^{1-} are the other anionic oxides of the trivalent arsenic and antimony [87, 92]. In a potassium silicate glass Verweij [79] reported presence of As^{3+} as $(AsO_2^{1-})\infty$ chains. AsO_2^{1-} and SbO_2^{1-} have been also detected by gas phase IR spectrometry, forming gaseous $MAsO_2$ and $MSbO_2$ molecules with M being an alkali metal [93].

The initial assumption of the molten ionic solution model is the ideal Temkin model [94]. In the Temkin model, the number of sites in each sublattice is equal to the number of ions in that sublattice [83] with anions surrounded only by cations and vise versa [95]. The entropy change is due to random mixing of ions in their respective sites.

Using the Temkin definition of ionic liquids, the ideal activities of the compounds in the $PbO\text{-}Pb_3(AsO_4)_2$ binary, which is a portion of $PbO\text{-}As_2O_5$ binary, were represented as Equations 32 and 33. In order to simplify the mathematical equations, the compounds in the solution were represented by unit anionic number (i.e. $Pb_{1.5}AsO_4$, instead of $Pb_3(AsO_4)_2$). Similar equations were used to represent all the other binaries in the system.

$$a_{PbO}^{ideal} = Y_{Pb^{2+}} . Y_{O^{2-}} = 1.\frac{n_{O^{2-}}}{n_{O^{2-}} + n_{AsO_4^{3-}}}$$

$$= \frac{n_{PbO} - 3n_{As_2O_5}}{n_{PbO} - 3n_{As_2O_5} + 2n_{As_2O_5}} = \frac{X_{PbO} - 3X_{As_2O_5}}{X_{PbO} - X_{As_2O_5}} \qquad (32)$$

$$a_{Pb_{1.5}AsO_4}^{ideal} = Y_{Pb^{2+}}^{1.5} . Y_{AsO_4^{3-}} = 1.\frac{n_{AsO_4^{3-}}}{n_{O^{2-}} + n_{AsO_4^{3-}}}$$

$$= \frac{2n_{As_2O_5}}{n_{PbO} - 3n_{As_2O_5} + 2n_{As_2O_5}} = \frac{2X_{As_2O_5}}{X_{PbO} - X_{As_2O_5}} \qquad (33)$$

Here, Y_i is the site fraction of i ion in the $PbO\text{-}Pb_{1.5}AsO_4$ binary; and X is the mole fraction in the $PbO\text{-}As_2O_5$ binary.

Deviation from ideal (Temkin) ionic behavior was accommodated with a regular solution type parameter for the excess Gibbs energy term. Equation 34 may be written for the g^E terms for the $PbO\text{-}Pb_{1.5}AsO_4$ binary. Similar equations were used for the other binaries in the system.

$$g_{PbO\text{-}Pb_{1.5}AsO_4}^{E} = \omega_1 . X_{PbO} . X_{Pb_{1.5}AsO_4} \qquad (34)$$

Here ω_1 is the parameter of the ionic solution model that is obtained via optimization. If this ionic solution model parameter has a small value and is independent of composition, then the model is mathematically identical to a regular solution of PbO and $Pb_{1.5}AsO_4$ with ω_1 equal to the regular solution parameter. In a similar way to a regular solution, partial Gibbs energy and activity coefficients for $Pb_{1.5}AsO_4$ and PbO were defined as shown in Equations 35 and 36. Similar equations were used for the other binaries in the system.

$$g^{E}_{Pb_{1.5}AsO_4} = R.T.\ln\gamma_{Pb_{1.5}AsO_4} = \omega_1.(X_{PbO})^2 \tag{35}$$

$$g^{E}_{PbO} = R.T.\ln\gamma_{PbO} = \omega_1.(X_{Pb_{1.5}AsO_4})^2 \tag{36}$$

The molar Gibbs energy of the PbO-$Pb_{1.5}AsO_4$ binary solution was modeled by Equation 37.

$$g = \left(X_{PbO}\cdot g^{0}_{PbO} + X_{Pb_{1.5}AsO_4} g^{0}_{Pb_{1.5}AsO_4}\right) +$$

$$RT\left(X_{PbO}\ln X_{PbO} + X_{Pb_{1.5}AsO_4}\ln X_{Pb_{1.5}AsO_4}\right) + g^{E}_{PbO\text{-}Pb_{1.5}AsO_4} \tag{37}$$

Only binary parameters were defined to describe the ionic interaction in the solution. For interpolation of the binaries to the ternaries, the Kohler symmetric approximation [96] was used.

Calculating the model parameters from experimental phase diagram measurements:

Phase diagrams are a source of thermodynamic data. Along the liquidus curves, e.g. the PbO liquidus in Figure 18, the PbO chemical potential is equal in both the solid and liquid phases, that is $g^{l}_{PbO} = g^{s}_{PbO}$. As described by Pelton [54], if we subtract the Gibbs energy of fusion for PbO, $\Delta g^{0}_{f(PbO)} = (g^{0(l)}_{PbO} - g^{0(s)}_{PbO})$, from both sides and rearrange this equation, we get:

$$\left(g^{l}_{PbO} - g^{0(l)}_{PbO}\right) - \left(g^{(s)}_{PbO} - g^{0(s)}_{PbO}\right) = -\left(g^{0(l)}_{PbO} - g^{0(s)}_{PbO}\right) \tag{38}$$

With $\Delta g_{PbO} = g_{PbO} - g^0_{PbO} = RT \ln a_{PbO}$, Equation 38 may be written as:

$$RT\left(\ln a^{l}_{PbO} - \ln a^{s}_{PbO}\right) = -\Delta g^0_{f(PbO)} \qquad (39$$

where $\ln a^{l}_{PbO}$ and $\ln a^{s}_{PbO}$ are the activity of PbO in the respective liquid and solid phases. $\Delta g^0_{f(PbO)}$ is given by $\Delta g^0_{f(PbO)} = \Delta h^0_{f(PbO)} - T\,\Delta s^0_{f(PbO)}$, where $\Delta h^0_{f(PbO)}$ and $\Delta s^0_{f(PbO)}$ are standard enthalpy and entropy of fusion of PbO. At the equilibrium melting temperature of pure PbO ($T = T^0_{f(PbO)}$), $\Delta g^0_{f(PbO)} = 0$; hence $\Delta h^0_{f(PbO)} = T^0_{f(PbO)} \cdot \Delta s^0_{f(PbO)}$. Subsequently Equation 39 transforms to:

$$\ln a^{l}_{PbO} - \ln a^{s}_{PbO} = -\frac{\Delta h^0_{f(PbO)}}{RT}\left(1 - \frac{T}{T^0_{f(PbO)}}\right) \qquad (40)$$

where T is a temperature on the PbO liquidus curve. Assuming negligible solid solubility of the second component in the system in PbO, Equation 40 simplifies to:

$$\ln a^{l}_{PbO} = -\frac{\Delta h^0_{f(PbO)}}{RT}\left(1 - \frac{T}{T^0_{f(PbO)}}\right) \qquad (41)$$

Equation 41 may also be written for all other components in the system and with a defined liquidus curve and heat of fusion, the activity of that component along the liquidus curve may be calculated. With the known heat of fusion of PbO, via Equation 41, the activity of PbO in the binary systems such as PbO-$Pb_3(AsO_4)_2$ may be calculated and thereafter the activity coefficient of PbO maybe determined. Using Equation 36, the activity coefficient of PbO is related to the excess Gibbs energy in binary PbO-$Pb_3(AsO_4)_2$ and ω_1 is calculated.

Alternatively, if the activity of a component in the solution is known at the liquidus point and using an equation similar to Equation 41 for that component, the standard heat of fusion for that compound may be calculated. Application of these procedures and

equations to determine the parameters of the present ionic solution model is shown in the Results Sections.

3.5 Summary

The need for a fundamental understanding of the thermodynamics of lead softening was described. Additionally, thermodynamic modeling as a powerful tool to describe all of the thermodynamic properties of the system in a single set of self-consistent Gibbs energy equations was introduced.

Based on the anticipated structure of the softening slag, an ionic solution model was suggested to describe the PbO rich region of the Pb-As-O and Pb-Sb-O systems and the mathematical equations that relate phase diagram data to the parameters of the model were presented.

It was evident from the review of the literature that there was a need to collect thermodynamic data that were more reliable in order to perform the optimization of the model. The lack of sufficient useful information and discrepancy amongst those that existed was higher for the Pb-As-O system, so experimental studies were planned to extend the available data by measuring the liquidus temperatures in $PbO\text{-}As_2O_3\text{-}As_2O_5$ ternary, and measuring the arsenic distribution between metal and oxide phases in the ranges of interest for lead softening. For the Pb-Sb-O system, there was enough information to perform the primary optimization. The experimental methodology is explained in the next chapter.

CHAPTER 4. EXPERIMENTAL METHODOLOGY

4.1 Scope

A number of experimental activities were undertaken in the course of the present study. At first, experiments aimed at visualizing the oxidation of pure lead and lead-arsenic melts via top jetting and submerged injection of pure oxygen were carried out. Simultaneous recording of the weight changes and temperature change during the visualization experiments was also explored (Section 4.2)[i].

After these studies, the focus of effort shifted to the measurement of temperature vs. composition phase transformations via the Differential Thermal Analysis (DTA) technique, and to the phase equilibrium measurements in the PbO rich region of the Pb-As-O system. The quantitative measurements were then used in conjunction with state-of-the-art software for computational optimization of a thermodynamic model for the oxide phase in the Pb-As-O system in the region of interest. The resulting optimized parameters were used to compute the phase diagrams for the Pb-As-O system in the region of interest for lead softening.

The present chapter deals with the experimental methods directed at obtaining the experimental data required to optimize the parameters of the thermodynamic model. The first part presents the sample preparation for, and methodology of, DTA (Section 4.3), and the Equilibration-Quenching experiments (Section 4.4). The equilibration experiments were used to determine the phase transformation temperatures, i.e., the liquidus and eutectic temperatures, and the resulting solid compounds that formed in the Pb-As-O system at the compositions of interest to partial lead softening.

The second part presents the quantitative analytical methods (Electron Probe Micro Analysis and Wet Chemical Analytical methods) that were employed to measure the composition of the resulting phases in the DTA and Equilibrium-Quenching experiments.

---

[i] The results of the visualization work were not the central findings of the thesis, thus the description of the effort and the associated results are included in Appendix -1.

The present study represents an initial step towards developing a complete thermodynamic solution model for Pb-As-Sb-Sn-O and was necessary because there were only limited data for the Pb-As-O system. Because data that are more reliable exist for the Pb-Sb-O system, no measurements were required in order to incorporate Sb-Pb-oxides into the liquid oxide solution model. Measurements in the Pb-Sn-O system were also unnecessary because the addition of Sn oxide to the liquid oxide solution model was outside the scope of the present work.

Part I: Thermodynamic Measurements and Preliminary Qualitative Kinetic Studies

4.2 Observation of the Melt/Gas Interface and Laboratory Model of the Softener

In order to understand the mechanism of the oxide formation during softening, a laboratory scale hot model of the softener was designed and constructed such that the melt was suspended from a balance to facilitate instantaneous mass measurements. Pure oxygen gas could be either impinged on the surface or injected below the melt surface. Visual observations and video recording of the melt surface was done with the oxygen impinging on the melt surface. Weight and temperature changes were measured while oxygen was being injected into the melt. Since this part of the research served to give a better understanding of the ignition problem and was not the main focus of this study, the details of the experiments, together with the results, discussion and conclusions are presented in Appendix 1.

4.3 Differential Thermal Analysis (DTA)

Differential thermal analysis is a well-established method used to construct phase diagrams. Several reference books and journals explain the principles of this methods [97-99]. DTA was used to measure the liquidus and eutectic temperatures of the Pb-As-O system in the region of interest.

In particular, the preparation of the samples to achieve a non-reacting, uniform and non-volatile mixture for thermal analysis is presented below and is followed by the experimental procedures that were used in this study. Finally, this Section ends with a description of a separate experiment done to prepare samples to measure the composition of the liquid oxide phase in the DTA experiments.

4.3.1 Sample Preparation

Binary mixtures of PbO-massicot[i], with 2.9 to 31 weight percent of As_2O_3-arsenolite[ii], were mixed and ground in a mortar.

Initial DTA measurements for these mixtures of pure PbO and As_2O_3 showed exothermic reactions between 250 °C and 360 °C[iii]. Moreover, excessive evaporation of As_2O_3[iv] (up to 20 wt % of the As_2O_3) was observed during the heating. These two phenomena interfered with the measurement of the phase transformations in the sample and therefore it was not possible to interpret the result of the measurements. As the result, a non-reacting, non-evaporating and preferably uniform sample was required. A heat treatment procedure was devised to prepare appropriate samples for DTA. This heat treatment, commonly referred to as "synthesis" hereinafter, was performed by keeping the samples at a temperature above the range in which PbO and As_2O_3 react for an extended time and in a closed environment to prevent evaporation.

The pure mixtures were first placed in silver tubing[v] that had been welded closed at one end and were lightly compacted to increase the contact area between the particles of the mixture. The other end of the tubing was then flattened in a way to have the minimum amount of air trapped inside the tube. The capsule (Figure 20, left) was sealed by welding using a self-designed carbon electrode arc welder.

---

i 99.999% purity PbO-massicot purchased from Alfa Aesar.

ii 99.95% purity As_2O_3-arsenolite, purchased from Alfa Aesar.

iii The reaction between PbO and As_2O_3 that resulted, formation of pentavalent arsenic compounds and separation of metallic lead was explained in Section 2.3.

iv The only commercially available allotrope of As_2O_3 is arsenolite, which is the metastable allotrope of As_2O_3 above -45 °C. This allotrope has a very high vapor pressure (vapor pressure of As_2O_3-arsenolite is 0.26 atm at 312°C [31], which is even higher than the vapor pressure of liquid As_2O_3 (vapor pressure of $As_2O_{3(l)}$ = 0.06 atm at 312 °C [31]).

v 3 cm long, 6mm OD, 0.2 mm wall thickness.

The welder used a 600 Watt DC power supply with the voltage adjusted to 14.5 Volts. A 0.3 cm diameter carbon electrode with a sharpened tip was used as the electrode. With this setup, it was possible to form an arc with enough power to melt only the tip of the tubes without heating the entire sample.

Figure 20 – Silver capsules prepared for preparation of DTA samples.

The capsules were placed in a copper powder bed in a horizontal electric resistance furnace under an argon atmosphere. Copper powder was used to lower the availability of oxygen inside the furnace that would penetrate into the capsules if the capsule welding had any microscopic pores. Heating the samples in the sealed capsule prevented the evaporation of As_2O_3–arsenolite. It was then possible to prepare samples with predetermined and known arsenic content. It is important to note that changes in the sample composition due to evaporation, in principle, did not invalidate the result of thermal analysis, because the composition of the samples was determined after the synthesis process. However, in practice, it is preferable to have the least amount of change in composition as possible.

In the synthesis procedure, samples were heated to 390 °C and held for over 24 hours with weights taken before and after heating. No weight gain was observed in any of the capsules, however, if the welding was not performed properly, a weight loss (> 0.5%) was observed and a new sample was prepared for that composition. After the first heating, samples were pulverized and mixed in a mortar before being re-encapsulated the same

way. The sample was then heated again for 24 hours at 390 °C. The second heating was performed to ensure homogeneity. The synthesized samples were analyzed by X-ray powder diffraction with CuKα radiation to determine any new compounds that may have formed during synthesis.

4.3.2 Experimental

Apparatus:

A NETZSCH[i] STA 409 PC simultaneous DTA-TGA[ii] instrument in the Brockhouse Institute for Materials Research at McMaster University and a SETARAM[iii] Labsys, simultaneous TGA-DSC[iv]-DTA instrument in the Department of Mining, Metals and Materials Engineering of McGill University were used for thermal analysis experiments.

Procedure

About 200-300 mg of the synthesized sample was placed in a 100 µl alumina crucible and positioned very close to a reference sample, which was an identical, but empty, alumina crucible (Figure 21). The sample and the reference were subjected to the same heating and cooling cycles at rates of 10 °C/min under an argon atmosphere. The thermal cycle was repeated once the sample was cooled to ~ 200 °C to ensure the repeatability of the measured temperatures.

Two thermocouples attached to the bottom of the crucibles measured the temperatures of the sample and the reference sample. The measured temperature was automatically transferred to a computer that recorded the temperatures and calculated difference between the two thermocouples.

When exothermic or endothermic transformations occurred in the sample, the temperature of the sample increased faster or slower than the reference sample. Accordingly, a

---

i NETZSCH is a trademark of NETZSCH Instrument Ltd., Germany.
ii TGA is the acronym for Thermo Gravimetric Analysis
iii SETARAM is a trademark of SETARAM instrument Ltd. France
iv DSC is the acronym for Differential Scanning Calorimetry.

sudden change in the temperature difference curve would be observed. Figure 22 shows the cooling curve of a sample with an initial composition of PbO – 2.9 wt% As_2O_3.

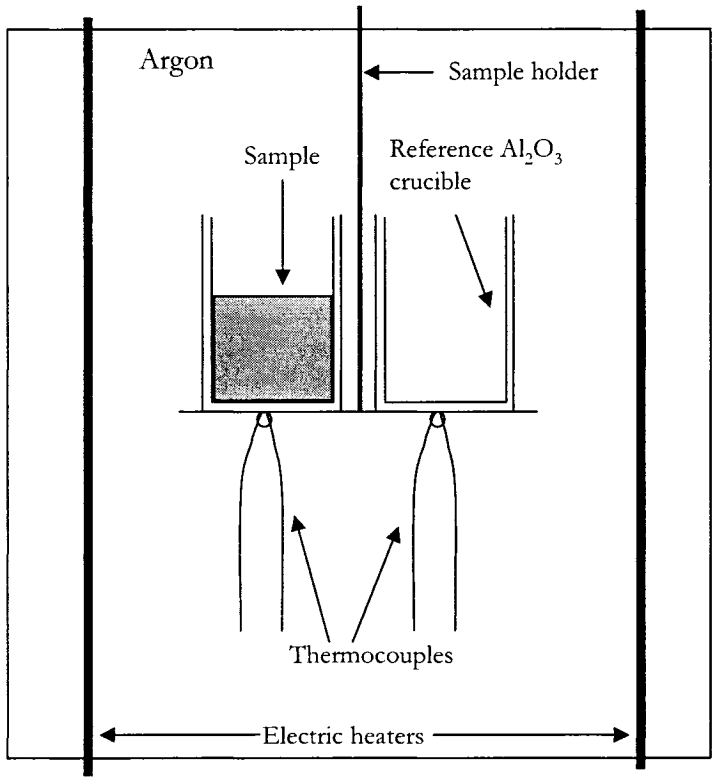

Figure 21 – Schematic figure of the differential thermal analyzer

In order to determine the exact transformation temperature, the first derivative of the temperature difference curve was calculated and the onset temperature was taken as the temperature of phase transformation as it is shown in the lower curve of Figure 22. In this example, the first exothermic phase transformation measured at 823 °C was the liquidus temperature and the second exothermic phase transformation measured at 773 °C was the eutectic temperature.

Cooling curves were used to determine the liquidus temperatures and secondary thermal arrests or eutectic temperatures. With an increase in the As_2O_3 of the mixtures, the oxide phase became glassier, increasing the under-cooling. Hence the accuracy of the liquidus temperatures measured via the cooling curve was not good at higher As concentration. For these samples both heating and cooling curves in two consecutive cycles were used to determine the liquidus temperature.

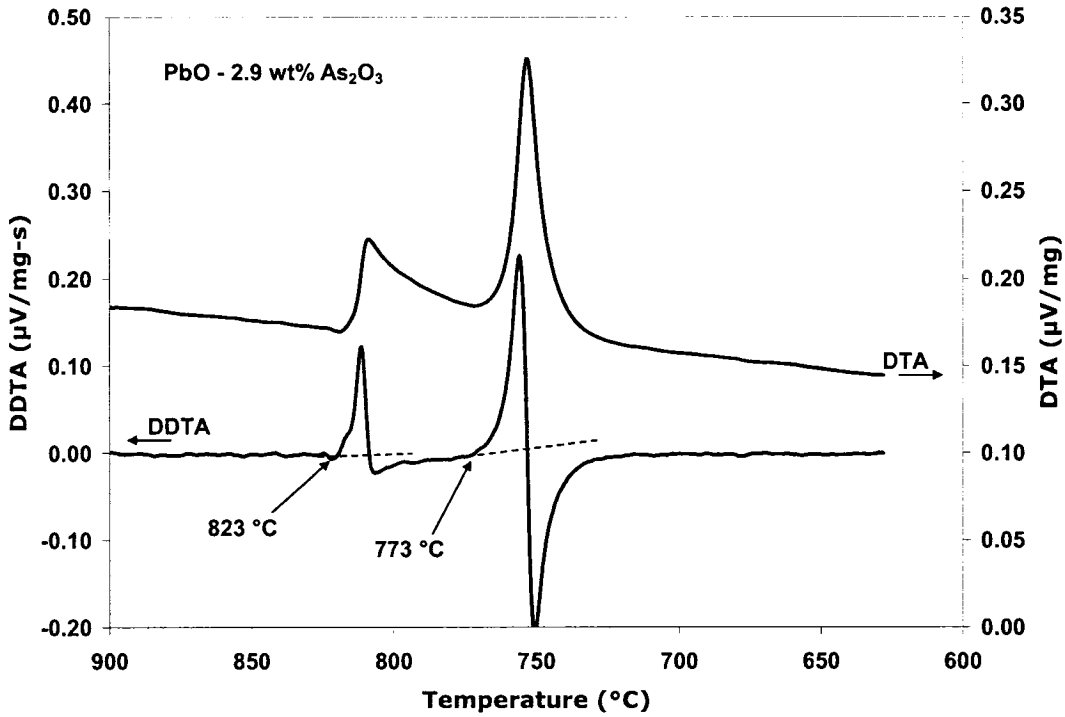

Figure 22 – DTA cooling curve (upper curve) and first derivative of DTA curve (DDTA – lower curve) of a sample with initial composition of PbO – 2.9 wt% As_2O_3. The onset temperatures from the DDTA curves, 823 and 773 °C, are the liquidus and eutectic temperatures respectively.

Determining the sample composition

Reactions between PbO and As_2O_3 resulted in the formation of pentavalent arsenic compounds and the separation of metallic lead. As a result, the composition of the oxide sample under investigation was different from the initial raw mixtures. Hence, it was necessary to determine the composition of the solidifying liquid, which was essential for constructing the phase diagram. Samples with the same composition as the solidifying liquid in the DTA experiments had to be prepared and their composition had to be determined by quantitative analytical methods. The experimental setup that was used to prepare these samples was similar to the Equilibration and Quenching experiments (Figure 24), which are described in detail in the next section.

In order to prepare these new set of samples, about 250 mg of the same synthesized mixtures that were used for the thermal analysis experiments were placed in identical alumina crucibles that were used in DTA tests and heated under argon atmosphere to

about 50 °C above the melting point of the mixtures based on the temperatures that were already determined by the differential thermal analysis. Samples were then cooled to slightly above (~ 10 °C) their respective liquidus temperatures and then quenched in iced water in order to preserve the composition of the liquid oxide phase. The composition of the liquid at this condition was taken as the composition of the solidifying liquid in the thermal analysis. The analytical method used to measure the composition of the quenched liquid is described in Section 4.5.

Prior to using alumina crucibles, the synthesized powder was placed in either silver[i] (Figure 20, right) or platinum[ii] capsules and subjected to the heat treatment as described for alumina crucibles. Results showed there was considerable dissolution of platinum in the metallic lead phase at elevated temperatures[iii], thereby lowering the activity of lead in the metallic phase. As a result, the samples were not representative of the samples that were used in DTA tests in alumina crucibles. However, the chemical analyses of these samples were collected and were compared against the samples in alumina crucibles as described in the next chapter.

To measure the liquidus points, it is preferable to use an isothermal experiment rather than a dynamic test such as DTA. In this way, it is possible to obtain data for the thermodynamic equilibrium between different phases in the system. The next section explains the equilibration-quenching experiments that were done at a constant temperature.

4.4 Equilibration and Quenching

In the equilibration and quenching experiments, samples were kept at the desired temperature for a long enough time to reach equilibrium and then rapidly quenched to maintain the composition of the liquid phase. The method of equilibrating and then quenching has been used by several researchers to study phase diagrams [100, 101]. This

---

[i] 1.5 cm length, 4 mm OD and 0.15 mm wall thickness silver tubes, for samples with a melting temperature lower than ~ 700 °C.

[ii] 1.2 cm length, 4 mm OD and 0.13 mm wall thickness platinum tubes, for samples with a melting temperature above ~ 700 °C

[iii] Lead dissolved up to 70 wt% of platinum at 810 °C; silver capsules were destroyed above ~ 750°C.

method is especially powerful once it is combined with new analytical methods such as electron probe micro analysis that makes it possible to individually measure the compositions of all the phases in one sample and has been used by a few researchers to study phase diagrams of complex multi-component system [82, 102-104].

Objective:

In the present study, the equilibration and quenching technique was used for two purposes:

1. To measure the composition of the liquidus where the solid oxide phase precipitates at the equilibration temperature.

2. To measure the composition of the equilibrium between a fully liquid oxide phase (Pb-As-O) and liquid metal phase (Pb-As).

4.4.1 Apparatus

A relatively simple setup was designed and constructed for this purpose, (Figure 24). A quartz tube (5 cm OD) was placed in a vertical electric resistance furnace. Two removable glass lids were used to close the top and the bottom of the quartz tube. Argon gas was passed through the tube from the top lid, in order to maintain a low oxygen atmosphere.

Crucibles:

The choice of the crucibles is critical in equilibrium-quenching experiments. The crucibles should preferably not react with the materials inside the crucible, and if the quenching is performed within the crucible, it should provide fast heat transfer to the sample inside. Initially platinum capsules were used but their use was discontinued because the platinum reacted with lead in the sample. The presence of lead was unavoidable even if no lead was added to the oxide mixture as explained above in Section 2.3. A stainless steel capsule was also tested at a temperature of about 800 °C. After the quenching, the inside surface of the stainless steel container was seen to be reactive to the

materials inside. Also the quenched oxide had an unusually dark black color that suggested presence of iron in the oxide phase. Stainless steel was not used again.

It was decided to use high alumina (99.8 % purity) crucibles and in order to reduce contamination of the samples by dissolution of alumina in the oxide phase, it was decided to use the minimum required time to achieve equilibrium between the oxide and metal phase (explained below). To ensure a fast quenching rate, 100 µl alumina crucibles with initial wall thickness of 0.5 mm were thinned to ~ 0.2 mm by careful manual grinding (Figure 23). If the quenching speed was not fast enough, the liquid phase would partially transform and its composition would change. In this case, measuring the composition of each phase in the sample is of no value and only bulk composition is measured.

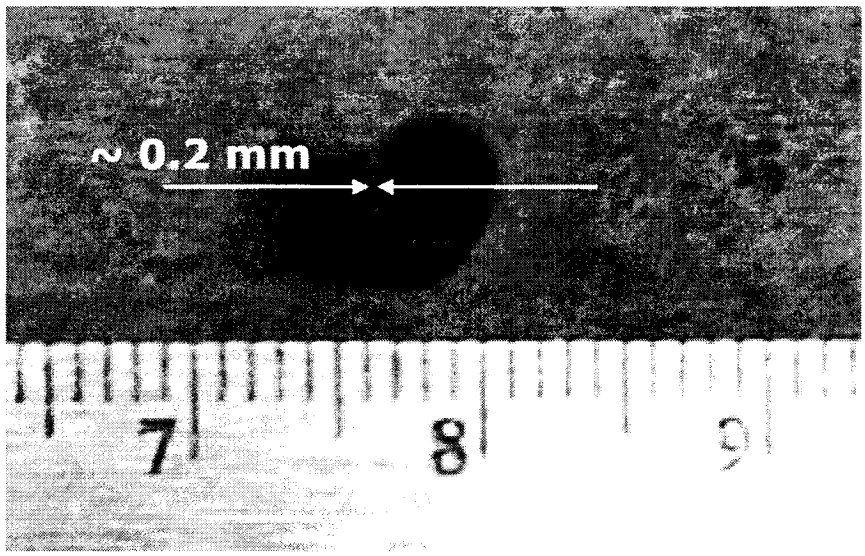

Figure 23 – 100-µL high alumina crucible with ~ 0.2 mm wall thickness that was used in equilibration experiments.

4.4.2 Procedure

Samples were prepared by weighing mixtures of PbO with 2.9 to 31 weight percent of As_2O_3. Samples were manually ground and mixed in a mortar. About 250 mg of this mixture and 100 mg of pure lead[i] were then placed in the thinned alumina crucible. An alumina cover was placed on top of the crucible and was tightly fixed in place with a platinum wire. The cover was used to reduce the evaporation of the arsenic compounds at

[i] 99.99 wt% purity, purchased from ESPI.

elevated temperature as well as to protect the sample during quenching against the ice water quenching medium.

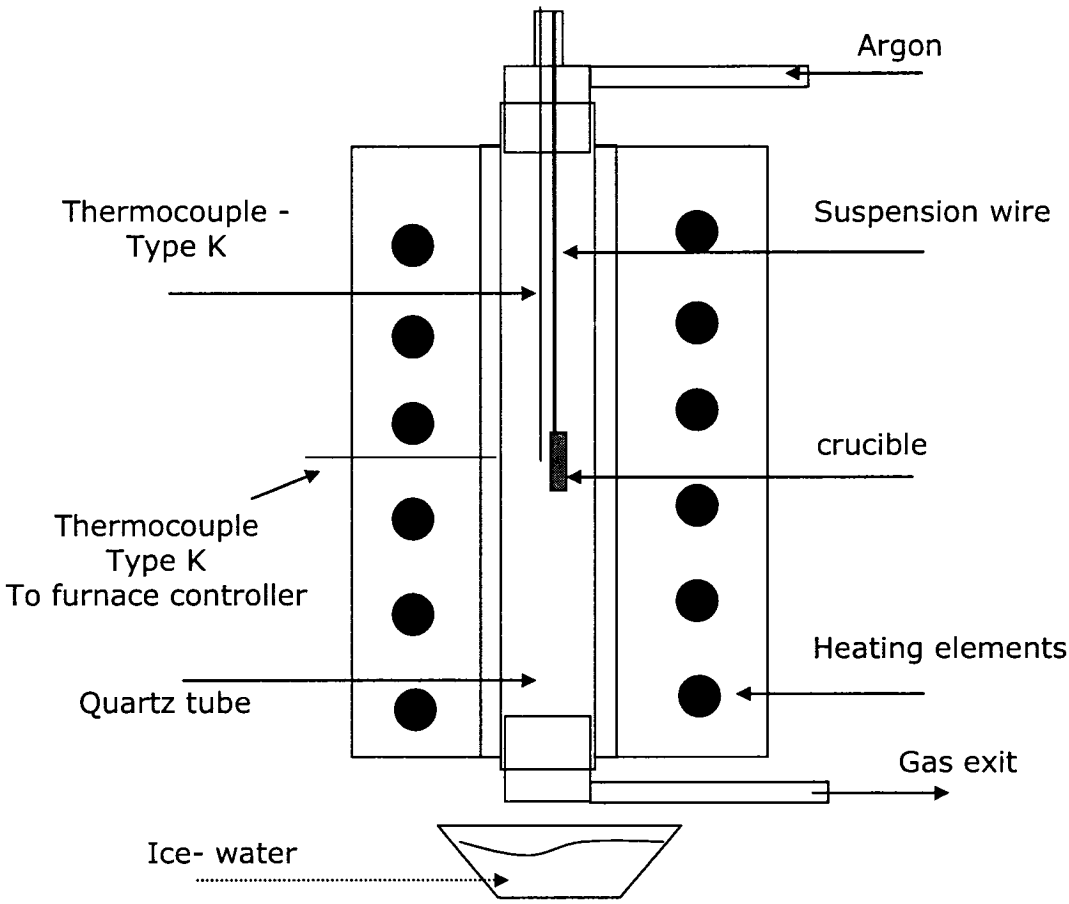

Figure 24 – Schematic figure of the setup used for equilibration and quenching experiments.

The covered crucible was suspended by a platinum wire in the middle of the furnace and a K type thermocouple was placed as close as possible to the crucible to measure the sample temperature. To ensure the accuracy of the thermocouple, one reference thermocouple was calibrated against the melting temperatures of lead, silver and sodium chloride and the thermocouple in use was periodically checked against the calibrated thermocouple. The ambient temperature where the temperature controller was mounted was stable at 23 ± 2 °C during the experimental campaign.

Samples were first heated to above their liquidus temperature and kept for ~ 10 minutes to ensure complete melting of the mixtures. Subsequently they were cooled to the desired

equilibration temperature and held at that temperature to achieve equilibrium. At the end of the holding time, the bottom cover of the quartz tube was opened, the platinum wire was quickly released and sample was quenched in the iced water. Crucibles were then crushed, the metal and oxide phase were separated and the chemical composition of all the phases in the sample were analyzed (explained in Part II of this chapter).

Determining the equilibration time:

Two identical samples were prepared and heated at the same temperature and conditions; one held for 2 hours and the other for 8 hours. At the end of holding, the samples were quenched in iced water. The difference in the composition of two samples for the oxide and the metal phase were within the error of the analysis. It was undesirable to keep the samples at elevated temperature for an extended time as the longer heating time increased the alumina contamination in the oxide phase. The holding time was chosen to be between 4 and 1.5 hours where shorter equilibration time was used for fully liquid samples and at higher temperatures and longer time was used for the solid-liquid samples and lower temperatures. Samples were equilibrated for about 24 hours when the equilibration temperatures were lower than 500 °C.

Part II - Quantitative Analytical Methods

4.5 Calculating the Composition of the Liquid Oxide Phase from Analytical Measurements

The mathematical calculations that relate the result of the chemical analysis to the components in the Pb-As-O (i.e. PbO, $Pb_3(AsO_4)_2$ and $Pb_3(AsO_3)_2$) solution model and to the phase diagram are described below.

Wet chemical analytical methods (Section 4.6) were used to measure the bulk composition of the homogenous oxide phase. This method provided a direct measure of the arsenic assay for different oxidation states. As^{3+} was measured by potassium bromide titration (Section 4.6.3) and the total arsenic was measured by either Induction Coupled

Plasma (ICP) or Atomic Absorption Spectrometry (AAS) (Section 4.6.2). As^{5+} was then determined by computing the difference in assays.

Equations 42 to 44 were used to calculate the number of moles of the elements in the liquid oxide as a function of As^{5+} and As^{3+} weight percentages.

$$n_{As} = \frac{\text{wt\% As}^{3+}}{A_{As}} + \frac{\text{wt\% As}^{5+}}{A_{As}} \tag{42}$$

$$n_{Pb} = \frac{100 A_{As} - \text{wt\% As}^{3+} (A_{As} + 1.5A_o) - \text{wt\% As}^{5+} (A_{As} + 2.5A_o)}{A_{As} (A_{Pb} + A_O)} \tag{43}$$

$$n_O = n_{Pb} + \frac{1.5\,\text{wt\% As}^{3+}}{A_{As}} + \frac{2.5\,\text{wt\% As}^{5+}}{A_{As}} \tag{44}$$

Here, A_{Pb}, A_{As} and A_O are the atomic weight of Pb, As and O, respectively.

Electron Probe Micro Analysis (Section 4.7) was used to measure the composition of the oxide phases in the quenched samples. EPMA has the capability of analyzing individually each of the oxide phases present in a quenched sample. The oxide phase might be either a homogeneous quenched liquid or a mixture of oxide compounds and quenched liquid oxide. EMPA measured the total Pb, As and O in the samples and also provided an indirect method to determine the arsenic assay at different valances by mass balance. With the known number of moles of elements measured by either EMPA or wet chemical analysis Equations 45 to 47 were used to calculate the number of moles of components in the liquid Pb-As-O phase (i.e. PbO, $Pb_3(AsO_4)_2$ and $Pb_3(AsO_3)_2$). Alternatively, compositions may be calculated in the $PbO\text{-}As_2O_3\text{-}As_2O_5$ ternary (equations are not written here).

$$n_{PbO} = n_{Pb} - 1.5 n_{As} \tag{45}$$

$$n_{Pb_3(AsO_4)_2} = 0.5 n_O - 0.5 n_{Pb} - 0.75 n_{As} \tag{46}$$

$$n_{Pb_3(AsO_3)_2} = 0.5 n_{Pb} - 0.5 n_O + 1.25 n_{As} \tag{47}$$

The composition of the solid compounds were determined based on the atomic proportion of the elements that were measured in the solid phase (or phases) of the sample under investigation. EPMA measurements of the homogeneous phases were compared to the results of the wet chemical analysis of the same samples to determine the reliability of this method. Table 15 in Appendix 3 shows this comparison for a number of homogeneous quenched liquid oxide phases. Good agreement was observed between the two different methods.

4.6 Wet Chemical Analytical Methods

Wet chemical analytical methods were used to measure the arsenic in metallic lead as well as arsenic and lead in the oxide phase.

4.6.1 Measuring the Arsenic in the Metallic Lead

The arsenic assay in the metallic phase was measured by the hydride-generation atomic absorption spectrometry technique as described by Nobbins and Ridge [105]. Between 50 and 100 mg of the metallic lead sample from the equilibrium-quenching experiments was dissolved in 20 to 40 cm^3 of hot concentrated nitric acid and diluted to 100 cm^3. The dissolved samples were then treated with potassium iodide and ascorbic acid to convert any arsenic present to As^{3+} and to form arsenic hydride. A commercial arsenic standard (Fisher Scientific) was used to calibrate the instrument and the total arsenic was then measured by hydride-generation AAS.

4.6.2 Measuring the Total Arsenic in the Oxide Phase

The total arsenic content in the oxide phase was measured by the Induction Coupled Plasma (ICP) and atomic absorption spectrometry (AAS). The AAS technique was used when the ICP instrument was out of order for an extended period time.

In preparation for analysis, an oxide sample was first ground in a mortar and any entrapped metallic lead was manually separated from the oxide. Three-molar hydrochloric acid was added to a measured mass (between 60 and 120 mg) of the metallic lead free oxide sample and stirred until completely dissolved. The hydrochloric acid that was used for digestion was purged with argon for 24 hours before digestion in order to

remove any dissolved oxygen and thereby prevent any oxidation of As^{3+} in the sample to As^{5+}. If some metallic lead was not removed prior to the digestion, it remained in solid form and was removed by filtration after the digestion. The separated metallic lead was weighed and subtracted from the initial oxide sample weight. A portion of this solution was used for measuring the total arsenic and lead via ICP and AAS, and the rest was used for measuring trivalent arsenic as explained in Section 4.6.3.

Commercially available standards for arsenic and lead (Fisher Scientific) were used to calibrate the ICP and AAS instruments.

4.6.3 Measuring Trivalent Arsenic by Potassium Bromide Titration

Trivalent arsenic in the samples was measured by a potassium bromide titration technique. Vogel [106] and Lafroukhi [107] explained the principle of this method. The reaction of trivalent arsenic and potassium bromide, Equation 48 [106], may be written as:

$$2KBrO_3 + 3As_2O_3 + 2HCl = 2KCl + 3As_2O_5 + 2HBr \qquad (48)$$

By measuring the volume of a solution of known concentration of potassium bromide, the equivalent amount of trivalent arsenic that was consumed during the titration could be determined.

In practice, a 200-ppm trivalent arsenic standard was prepared by dissolving 0.066 g As_2O_3 in 10 cm^3 of deionized water containing 0.2 g NaOH. The solution was acidified by the addition of 15 cm^3 of HCl and diluted to 250 cm^3. The trivalent arsenic standard was checked by both calibrated ICP and AAS instruments and was found to be within the error limits of the analysis. A 0.003 molar $KBrO_3$ solution was prepared by dissolving 0.2505 g of solid KBrO3[i] in deionized water. Potassium bromide molarity was then determined against the prepared arsenic standard. Methyl orange (0.1% solution) was used as the indicator for the end point of the titration.

[i] 99.8 wt%, Sigma Aldrich.

Procedure:

Twenty cm^3 of the arsenic solution was diluted to 50 cm^3 by adding 30 cm^3 of 1 molar HCl, and then 10 drops of methyl orange was added to the solution. Potassium bromide was added drop-wise at intervals of 3 to 6 seconds between the drops with constant stirring of the solution. Once the added potassium bromide consumed the trivalent arsenic, bromine was released and destroyed the indicator (i.e. the end point of titration was observed by discoloration of the methyl orange). A blank sample with the same matrix was titrated with the same method to correct for the matrix effect. Titration was repeated three times for each sample. The average standard deviation of the trivalent arsenic weight percentage from the mean of the three measurements was found to be 0.2 wt% As.

4.7 Electron Probe Micro Analysis (EPMA)

A JEOL[i] SuperProbe 8900 electron microprobe installed in the Department of Earth and Planetary Sciences of McGill University was used to measure the composition of each oxide phase in the quenched samples. The microprobe was able to measure the composition of distinct phases with a size greater than one micron in any sample. Such local assaying was not possible by other bulk analysis methods. The electron microprobe uses a wavelength-dispersive spectrometer (WDS) to measure the characteristic X-ray spectrum generated by the sample when the sample is exposed to the electron beam.

4.7.1 Procedure

A few pieces from the oxide phase from each quenched sample were randomly selected and separately cold mounted in epoxy resin. Surface quality of the samples affects the accuracy of the results in microprobe analysis and since samples with high PbO content were extremely soft, several polishing methods were tried to prepare an acceptable surface. No water could be used during the polishing, since some of the As^{5+} compounds have minor water solubility. Mounted samples were first dry polished using silicon carbide abrasive paper (120, 320, 600 and 1200 grit). Next, they were dry-polished with

[i] JEOL is the trademark of Japan Electron Optics Ltd., Tokyo, Japan.

alumina powder (5, 1 and 0.3 micron) and an optional final polishing was done using 0.1-micron diamond paste. Samples were then coated with a thin carbon layer to make the surface conductive before placing them inside the microprobe.

The beam current was set to 2.00e-8 Amp, with an acceleration voltage of 15 kV. The beam size was selected based on the size of the phases in the sample. Back-scattered electron images were used to observe the different phases present in the samples. For the quenched liquid phase, a beam size of 10, 5 or 3 microns was used, and for the solid phase, a beam size of 3 or 1 microns was used. Differentiation between quenched liquid and the solid phases was possible based on the shape, composition and trend in appearance or disappearance of a phase. This is explained with the following examples.

Figure 25 shows a sample with an initial composition of PbO – 3 wt% As_2O_3 quenched from 805 °C. The needle shape microstructure indicates the presence of a crystalline solid phase. Once this phase was assayed with the microprobe, the 1:1 atomic ratio between Pb and O that was observed with no arsenic indicated that this phase was solid PbO at the equilibration temperature.

Another method was to monitor the appearance of a phase in samples with the same initial compositions but quenched from different temperatures. Figure 26 and Figure 27 show samples with an initial composition of PbO - 23 wt% As_2O_3 quenched from 620 °C and 550 °C, respectively. It was known from DTA experiments that at 620 °C this sample was completely liquid and the back-scattered electron image showed the presence of a single homogeneous phase (Figure 26), thus it was concluded that this was the quenched liquid phase.

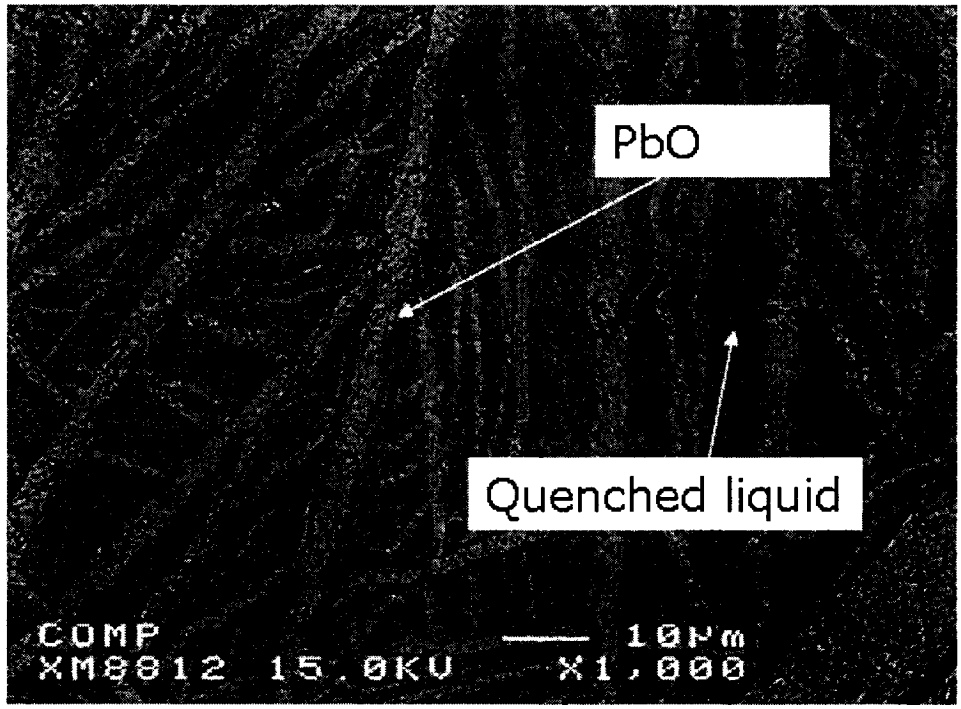

Figure 25 – A quenched liquid and needle shaped solid PbO were observed in the back-scattered image of a sample with initial composition of PbO - 3 wt% As_2O_3 quenched from 805 °C.

The sample quenched from 550 °C showed the appearance of a second phase with a lighter color (Figure 27). Also the matrix had a darker color, similar to the homogeneous phase in the previous sample. These two phases had distinct chemical compositions with the dark colored phase having a composition close to that of the quenched liquid phase in the previous sample quenched from 620 °C. Hence, it was determined that the darker phase was the quenched liquid and the newly appearing white colored phase was a solid phase. In this example, the composition of this solid was roughly Pb_2AsO_4[i]. This solid compound has never before been reported. Because the stoichiometric proportion for this compound did not match any known compound, differentiating between the liquid and solid phases would not have been possible based on the stoichiometric proportions of elements.

[i] Measured as $Pb_2AsO_{3.9}$

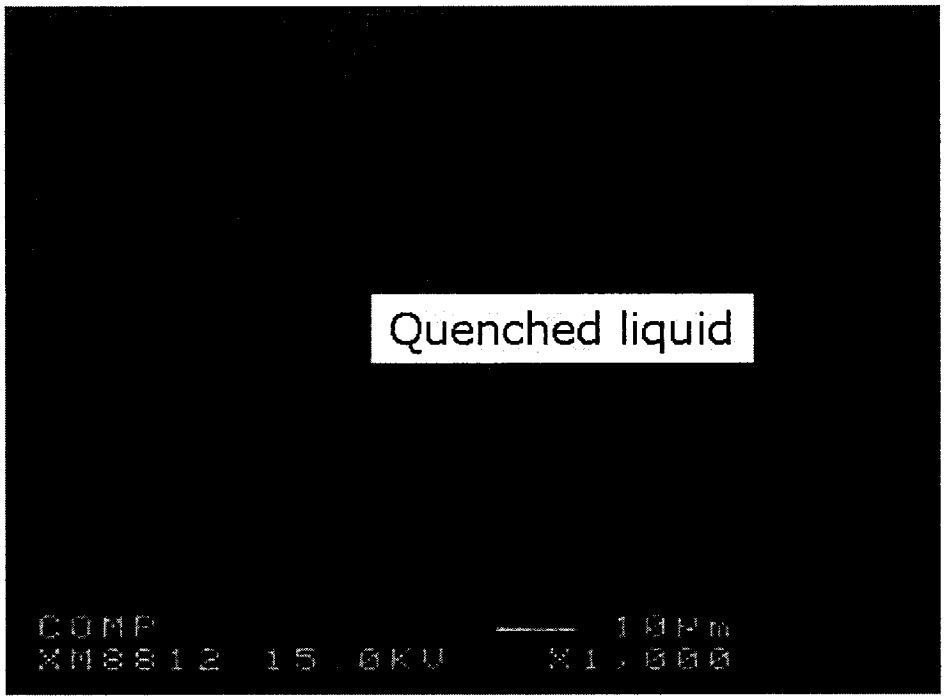

Figure 26 – A homogeneous quenched liquid was observed in the back-scattered image of a sample with initial composition of PbO - 23 wt% As_2O_3 quenched from 620 °C.

Aluminum was always detected in the liquid phase and was never observed in the solid compounds, thus in some instances the presence of aluminum was used to detect the presence of the quenched liquid. This was especially useful for samples that were quenched from temperatures below the eutectic temperature since two solid phases may be mistaken for one solid and one liquid phase.

The microprobe was calibrated with prepared standard samples (see next section) and then an average of 7 points from each phase was chosen for the measurement of Pb, As, O and Al[i]. The standard deviation of X_O, X_{Pb} and X_{As} from the mean of the measurements on any given sample was less than 0.005. A ZAF[ii] correction was applied to account for the matrix effects. The preparation and the choice of standards are explained in the next section.

---

i Aluminum was measured to quantify the dissolved alumina that came from the alumina crucible.

ii Certain factors, namely atomic number (Z), absorption (A) and fluorescence (F), related to the sample composition (called the matrix effect), can affect the X-ray spectrum produced in a microprobe analysis and have to be corrected for an accurate analysis. These matrix corrections are called ZAF corrections [108] and are applied automatically by the software program that is connected to the microprobe.

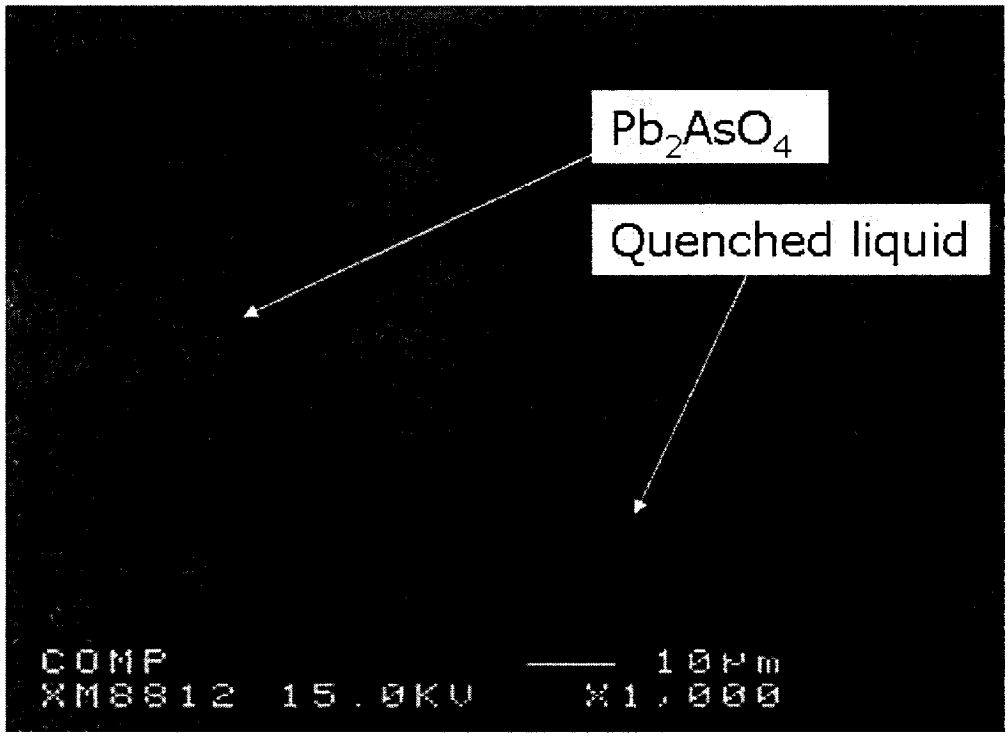

Figure 27 – A quenched liquid and a solid compound with a composition of Pb_2AsO_4 were observed in the back-scattered image of a sample with initial composition of PbO-23 wt% As_2O_3 quenched from 550 °C.

4.7.2 Preparation and Choice of Standards

In order to perform accurate measurements with the microprobe, standards need to have a chemical composition as close as possible to the phases under investigation. Since there was a wide range of liquid-solid compositions in the samples, it was necessary to prepare different standards with known compositions for each of the main elements in the system i.e. Pb, As and O. It is worth mentioning that if there was more than one appropriate standard to choose from, the choice was made based on the reliability of the standards. A standard that was seen to be more homogeneous[i] was taken as the more reliable standard.

A PbO standard was prepared by mixing 99.999% purity PbO (Alfa Aesar) and metallic lead. The mixture was heated to 920 °C in a platinum crucible under an inert atmosphere to melt the PbO and then it was slowly cooled inside the furnace to the room temperature. The presence of the metallic lead ensured that no other lead oxide beside PbO would form during the heat treatment. The PbO standard was used to measure lead and oxygen for

[i] A more homogeneous sample would have a smaller standard deviation in the measured composition.

samples with low arsenic (As less than about 5 %) and to measure only lead for samples with medium arsenic content (~ 5 < As < ~ 15 %).

A $Pb_8As_2O_{13}$ standard was prepared by mixing 8 moles of PbO with 1 mole of As_2O_5 (99.9 % purity, Alfa Aesar). Since As_2O_5 dissociates to As_2O_3 at $T > 600$ °C [109], the mixture was first heated in solid state in a closed silver tube at 400 °C in an air atmosphere. Subsequently the sample was melted in a platinum capsule under air atmosphere and slowly cooled to room temperature. The XRD analysis (see Figure 68 in Appendix 3) of the standard confirmed the formation of $Pb_8As_2O_{13}$. The XRD analysis showed no shift of the major peaks, indicating that there was no detectable solid solution. The XRD pattern also showed presence of small quantities of PbO that were observed in the back-scattered electron image of the standards. However, the presence of a second phase was not considered detrimental for the present purposes because points could be selected from the matrix without the interference of the second phase. The $Pb_8As_2O_{13}$ standard was used for arsenic analysis for samples with low arsenic content and for the arsenic and oxygen in samples with medium arsenic content.

A $Pb_2As_2O_5$ standard was used for measuring lead, arsenic and oxygen for samples with high arsenic content (As > ~ 15%). Paulmooreite with chemical composition of $Pb_2As_2O_5$ is a rare natural mineral with a known XRD pattern but there was no report that this compound had been synthetically produced. Nevertheless, to prepare this compound, the author mixed a proportion of 2 moles of PbO and 1 mole of As_2O_3 and then synthesized twice at 390 °C in sealed silver capsules as described in Section 4.3.1. The XRD analysis confirmed the formation of the $Pb_2As_2O_5$ compound, with no shift of the peaks, indicating that there was no detectable solid solution (see Figure 67 in Appendix 3). Similar to the synthesized $Pb_8As_2O_{13}$ standard, there was a small amount of a second phase observed in the back-scattered electron image, which did not interfere with the calibration (see Figure 65 in Appendix 3).

CHAPTER 5. CONTRIBUTION TO THE Pb-As-O SYSTEM

5.1 Scope

Contributions to the Pb-As-O system in the range of lead softening are presented in this chapter. Part I of this chapter presents and discusses the thermodynamic measurements whereas Part II presents and discusses the optimization of the model using the available data, starting with the subsystems and ending with the ternary system. The resulting predicted phase diagrams, predicted equilibria calculations and discussion of the results at the end of each part. Overall, conclusions of both parts are presented in Section 5.4.

5.2 Part I – Experimental

5.2.1 Differential Thermal Analysis

XRD analysis of the synthesized samples

Table 2 shows the XRD analysis results of the synthesized PbO-As_2O_3 mixtures that were used as the starting material for DTA experiments. The results are separated into two columns, one column containing the phases that were positively detected and the other column with partial matches. Generally, all of the samples showed numerous peaks in their XRD patterns that suggested presence of multiple oxides. In Samples B and C, with less that 7 wt% As_2O_3, a mixture of oxides (PbO and $Pb_8As_2O_{13}$) and metallic Pb were identified. All the major peaks were accounted for by the selected compounds. In Samples D and E, with between 8 and 10 wt% As_2O_3, only metallic Pb was positively detected while $Pb_4As_2O_9$ and $Pb_8As_2O_{13}$ were two compounds that were possibly present in the sample. These two compounds covered most of the major peaks in the samples, however some of the observed peaks showed a slight shift compared to the reference patterns.

In Sample G, with ~ 13 wt% As_2O_3, a mixture of oxides ($Pb_4As_2O_9$ and $Pb_8As_2O_{13}$) and metallic Pb were positively identified. All of the major peaks were accounted for by the selected compounds.

Table 2 – The XRD result of the synthesized PbO-As_2O_3 mixtures.

	Initial As_2O_3 Content (wt%)	Identified phases	Partial matches
B	4.2	Pb-PbO-$Pb_8As_2O_{13}$	none
C	6.9	Pb-PbO-$Pb_8As_2O_{13}$	none
D	8.1	Pb	$Pb_4As_2O_9$-$Pb_8As_2O_{13}$
E	10.0	Pb	$Pb_4As_2O_9$-$Pb_8As_2O_{13}$
G	12.9	Pb-$Pb_8As_2O_{13}$-$Pb_4As_2O_9$	none
I	18.1	Pb-$Pb_2As_2O_5$	$Pb_8As_2O_{13}$-$Pb_4As_2O_9$-$Pb_3As_2O_8$
J	22.8	Pb-$Pb_2As_2O_5$	$Pb_4As_2O_9$-$Pb_3As_2O_8$
K	30.7	$Pb_2As_2O_5$	none

In Sample I, with ~ 18 wt % As_2O_3, metallic Pb and $Pb_2As_2O_5$ were positively identified in the sample. The XRD reference patterns of $Pb_3As_2O_8$, $Pb_4As_2O_9$ and $Pb_8As_2O_{13}$ compounds partially matched Sample I. Many of the major peaks for the compounds were very close or overlapped each other and because of the abundance of the observed peaks and the possibility of a slight shift of the peaks, three compounds were reported as possible matches. Similarly in Sample J, with 22.8 wt% As_2O_3, metallic lead and $Pb_2As_2O_5$ were positively identified, while $Pb_4As_2O_9$ was also a close match even though a slight shift was observed compared with the standard pattern. The $Pb_3(AsO_4)_2$ reference pattern covered most of the remaining peaks in the sample however some of the primary peaks of the $Pb_3(AsO_4)_2$ standard were not observed in the sample. Because of the observed uncertainty for this sample, a separate sample with the same initial oxide mixture, but with the addition of metallic lead was synthesized. Excess lead was added to ensure that the entire sample was at equilibrium with metallic lead and it was not oxidized by the residual oxygen present in the capsule. A similar pattern was observed in the new

sample, i.e. Pb, $Pb_2As_2O_5$ and $Pb_4As_2O_9$ were present in the sample and $Pb_3(AsO_4)_2$ covered most of the remaining peaks in the sample, but some of the main peaks of the reference $Pb_3(AsO_4)_2$ pattern were still not found.

In Sample K, with ~ 31 wt% As_2O_3, only the $Pb_2As_2O_5$ compound was detected (Figure 67) and almost all of the major peaks in the sample were accounted for, thus suggesting the presence of a pure compound. As was mentioned in Section 4.7.2, a small amount of a second phase was observed in the back-scattered electron image of this compound. Because it was not detected in the XRD spectrum, it was concluded that the second phase was less than 5 wt% in the sample.

Thermal analysis:

Table 3 summarizes the results of the differential thermal analysis of the synthesized PbO-As_2O_3 mixtures. Figure 28, shows these results on a temperature-composition graph. It was not possible to demonstrate the thermal analysis result on a constant composition section (*isopleth*) of the Pb-As-O system because the composition of the samples did not lie in a single plane. As a result, the composition axis in Figure 28 was chosen as the summation of the trivalent and pentavalent arsenic oxide mole fractions.

Table 3 – Results of the DTA experiments. Compositions determined by the wet chemical analysis of the quenched samples.

	Initial As_2O_3 content (wt%)	Quenched liquid oxide composition (mole fraction)			Liquidus temperature (°C)	Second thermal arrest (°C)
		X_{PbO}	X_{As2O5}	X_{As2O3}		
A	2.9	0.966	0.021	0.013	832	773
B	4.2	0.948	0.036	0.016	818	767
C	6.9	0.924	0.048	0.028	796	-
D	8.1	0.902	0.067	0.031	809	-
E	10.0	0.882	0.072	0.046	803	628
F	11.2	0.888	0.044	0.067	802	669
G	12.9	0.840	0.057	0.103	780	595
H	15.3	0.817	0.054	0.130	695	640
I	18.1	0.782	0.035	0.184	672	-
J	22.8	0.750	0.008	0.243	590	463
K	30.7	0.675	0.004	0.321	462	390

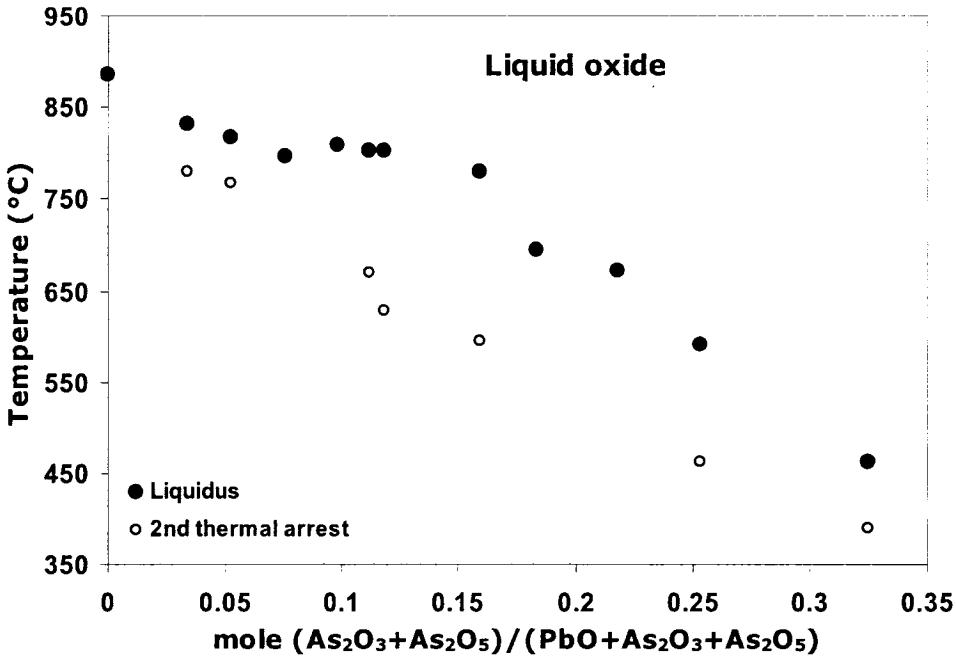

Figure 28 – Result of the thermal analysis shown on a composition temperature diagram.

Figure 29 shows the DTA results plotted on a section of the ternary composition triangle with PbO, As_2O_3 and As_2O_5 as the corners of the ternary system. The closed squares represent the composition of the quenched liquid oxide that was prepared in an alumina crucible to represent the composition of the solidifying liquid in the DTA experiments. Samples represented by open squares were prepared with the same starting materials in platinum or silver crucibles and are shown for comparison (samples with the same starting composition are connected).

The composition of the quenched liquid oxide phase (see Section 4.3.2 for the experimental procedure) was determined by the EMPA and wet analytical methods. Back-scattered electron images of the samples with less than 13 wt% As_2O_3 showed the presence of a second phase. Based on shape[i], it was determined that the second phase was precipitated during the quenching. As a result, for these sets of samples, EMPA results were not representative of the bulk composition. Thus, the reported composition

[i] Figure 70 in Appendix 3 shows the back-scattered electron image of the quenched liquid oxide of the sample with 6.9 wt% initial As_2O_3. The very thin layers of the PbO is a representative of a sample that is quenched from completely liquid state but below a critical cooling rate, required to prevent the precipitation of the solid compound.

of the oxide phase in Table 3 was based on wet analytical methods. In Table 15, Appendix 3, the EMPA results for the completely homogeneous samples (i.e. samples with more than 13 wt% As_2O_3) are compared against the wet analytical method.

Table 17 in Appendix 3 shows the composition of the quenched liquid that was prepared in platinum or silver capsules instead of alumina crucibles. For samples prepared in platinum capsules, the platinum content in metallic lead was found to be between 50 to 75 wt% Pt.

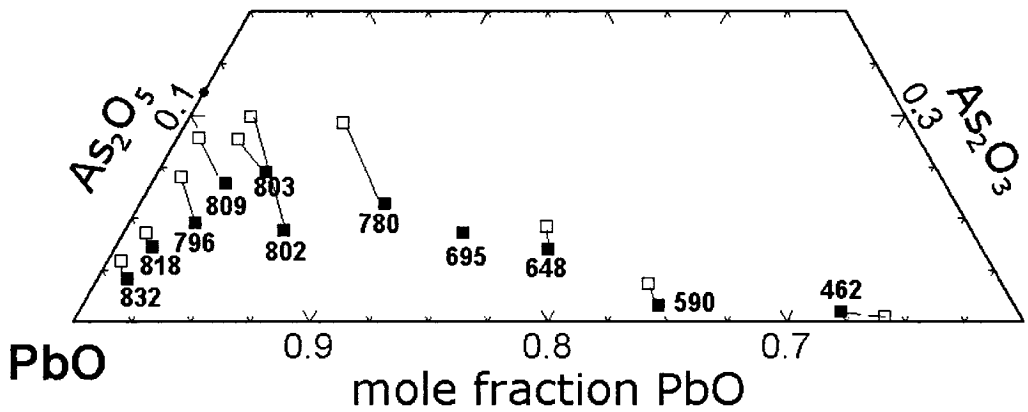

Figure 29 – Results of the DTA experiments shown in a section of the PbO-As_2O_3-As_2O_5 ternary system (temperatures in °C)[i]. ■ Samples quenched in alumina crucible, □ Samples quenched in platinum capsules (graph generated with FACT*Sage*™ [31]).

Beside the PbO-As_2O_3 mixtures above, a sample of Teck Cominco's softener slag was tested via DT-TG analysis under argon and air atmospheres separately. Table 4 shows the liquidus temperature and compositions of the tested softener slag[ii].

Thermogravimetric analysis of the Teck Cominco sample that was heated under air atmosphere showed a mass gain of about 4.1 wt% due to the oxidation of trivalent arsenic and antimony. The composition of the slag was measured by EMPA, which counted the

[i] Sample F, that was prepared in alumina crucible did not follow the pattern, which was observed in the composition of other prepared samples. As a result, Sample F was not used in the calculations of the thermodynamic model parameters

[ii] Sn was less than 0.5 wt%.

cations of each element, thus it was not possible to distinguish the oxidation state of arsenic and antimony elements[i].

Table 4 – Liquidus temperature of a Teck Cominco's softener slag under air and argon atmospheres.

Softener slag composition (wt%)				Liquidus under the air atmosphere (°C)	Liquidus under the argon atmosphere (°C)
Pb	As	Sb	O		
64.7	9.7	14.5	rem.	1003	501

5.2.2 Equilibration and Quenching

Based on the phases that were present, the quenched samples were divided into three groups.

Group 1 – Fully liquid oxide in equilibrium with metallic lead. A tie line may be drawn between the composition of the oxide and metal phase in these samples.

Group 2 – A mixture of solid and liquid oxide in equilibrium with the metallic lead. The composition of the liquidus point and the solid oxide at a known temperature were determined with these samples.

Group 3 – Completely solid oxide phase in equilibrium with metallic lead that could be used to estimate the end of solidification for a certain composition.

Table 5 for the Group 1 samples, shows the adjusted[ii] bulk equilibrium compositions of the quenched liquid oxide and metal phase for the samples that were quenched from temperatures where the oxide phase was fully liquid.

---

[i] For the Pb-As-O mixtures, as explained in 4.7, it became possible to determine the proportion of arsenic in different oxidation states by mass balance; however for a 4 component system that had two elements with varying oxidation states, mass balance could not determine the proportion of both elements at different oxidation states.

[ii] Adjusted to no alumina in the oxide phase.

Table 5 – Equilibrium composition of the quenched liquid oxide and metallic lead.

	Bulk composition of the oxide phase[i] (mole fraction)			Al in liquid oxide (wt%)	As in metallic lead (wt%)	Temperature (°C)
	PbO	As_2O_5	As_2O_3			
1	0.967	0.017	0.016	1.60	0.036	875
2	0.931	0.044	0.024	0.59	0.015	800
3	0.892	0.066	0.042	0.50	0.007	800
4	0.842	0.070	0.088	0.18	0.194	600
5	0.803	0.044	0.154	0.13	0.071	685
6	0.799	0.048	0.153	0.19	0.063	685
7	0.784	0.031	0.185	0.17	0.130	740
8	0.765	0.047	0.188	0.11	0.132	680
9	0.764	0.031	0.205	0.19	0.175	770
10	0.756	0.030	0.214	0.08	0.408	630
11	0.757	0.011	0.232	0.18	0.360	750
12	0.720	0.019	0.261	0.33	1.337	760
13	0.706	0.007	0.287	0.16	1.025	620
14	0.690	0.000	0.310	0.14	2.745	620
15	0.670	0.001	0.329	0.13	4.897	460

Figure 30 presents the results of Table 5 in a ternary composition triangle. Tie lines were drawn between the composition of the oxide phase confined to the PbO-As_2O_3-As_2O_5 triangle, and the metal phase in the Pb-As binary system. The dot near the middle of the PbO-As_2O_3 pseudo-binary shows the position of the $Pb_3(AsO_3)_2$ compound.

[i] Adjusted to no alumina in the oxide phase

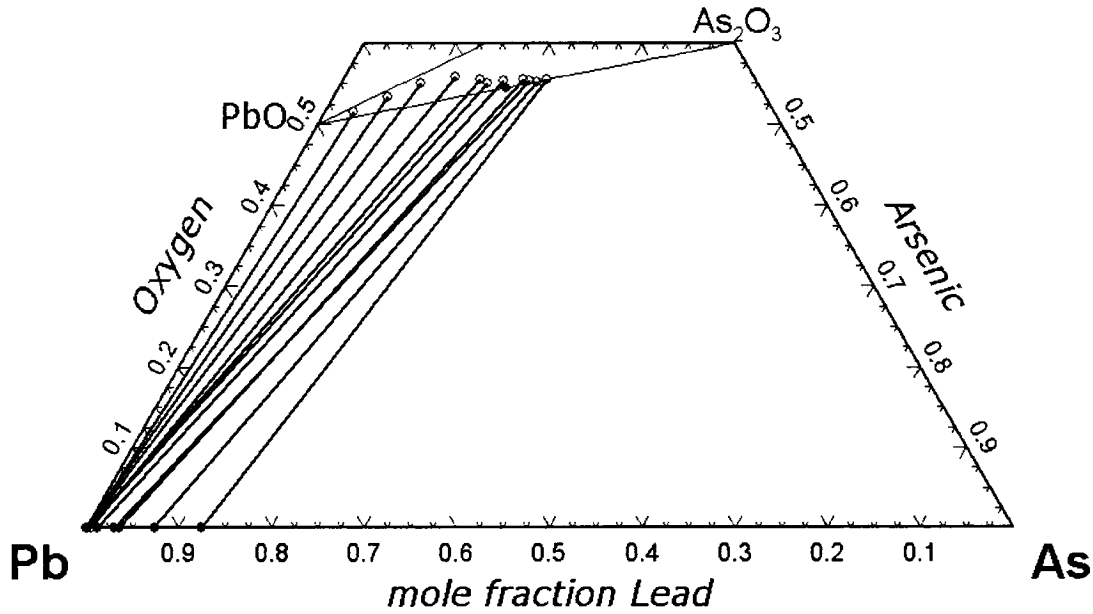

Figure 30 – Equilibrium composition of the oxide and metal phases located at the ends of the tie lines in the Pb-As-O ternary composition triangle (graph generated with FACT*Sage*™ [31]).

Table 6 for Groups 2 and 3 results shows the bulk equilibrium compositions of the quenched oxide and metal phases for the samples that were quenched from temperatures where the oxide phase was not completely liquid, liquid/solid oxide phases or solid/solid oxide phases[i].

Table 6 – Equilibrium bulk composition of the quenched oxide and metal phases.

	Bulk composition of the oxide phase (mole fraction)			As in metallic lead (wt%)	Equilibrium temperature (°C)
	PbO	As_2O_5	As_2O_3		
1	0.965	0.021	0.014	0.012	870
2	0.972	0.017	0.011	0.005	805
3	0.930	0.059	0.011	0.012	785
4	0.903	0.094	0.003	0.050	772
5	0.888	0.083	0.029	0.030	750
6	0.906	0.085	0.009	0.007	740
7	0.855	0.075	0.070	0.247	785
8	0.858	0.076	0.066	0.120	740
9	0.867	0.079	0.054	0.039	680
10	0.862	0.066	0.072	0.032	690

[i] The result of the multiphase samples was separated from the two phase samples because tie lines may be drawn only for the 2 phase regions.

11	0.837	0.094	0.069	0.007	670
12	0.741	0.022	0.237	0.327	550
13	0.892	0.072	0.036	0.005	800
14	0.667	0.020	0.313	2.532	420
15	0.722	0.025	0.252	0.366	440
16	0.741	0.032	0.227	0.313	420
17	0.755	0.021	0.224	0.284	420
18	0.931	0.048	0.021	0.015	800
19	0.938	0.056	0.006	0.001	740
20	0.814	0.082	0.105	0.206	630
21	0.825	0.092	0.083	0.301	735
22	0.829	0.090	0.081	0.400	590
23	0.837	0.093	0.070	0.296	630
24	0.838	0.099	0.063	0.224	630
25	0.857	0.092	0.051	0.120	600
26	0.892	0.077	0.031	0.095	600
27	0.893	0.089	0.019	0.272	550
28	0.898	0.071	0.031	0.264	740
29	0.914	0.079	0.007	0.012	630
30	0.937	0.056	0.007	0.013	805
31	0.940	0.057	0.004	0.071	770
32	0.973	0.026	0.001	0.000	770
33	0.924	0.076	0.001	0.007	750

Figure 31 shows the arsenic distribution between the oxide and metal phase for all samples in Table 5 and Table 6. Arsenic concentration in the metal phase is presented as a function of the total mole fraction of the As_2O_3 and As_2O_5 in the oxide phase. The equilibration temperature varied between 410 °C and 870 °C.

In Figure 32 the arsenic distribution in four separate sets of temperature ranges (800-805 °C, 740-770 °C, 600-630 °C and 420-450 °C) are aggregated in order to demonstrate the effect of temperature on the arsenic distribution between slag and metallic lead.

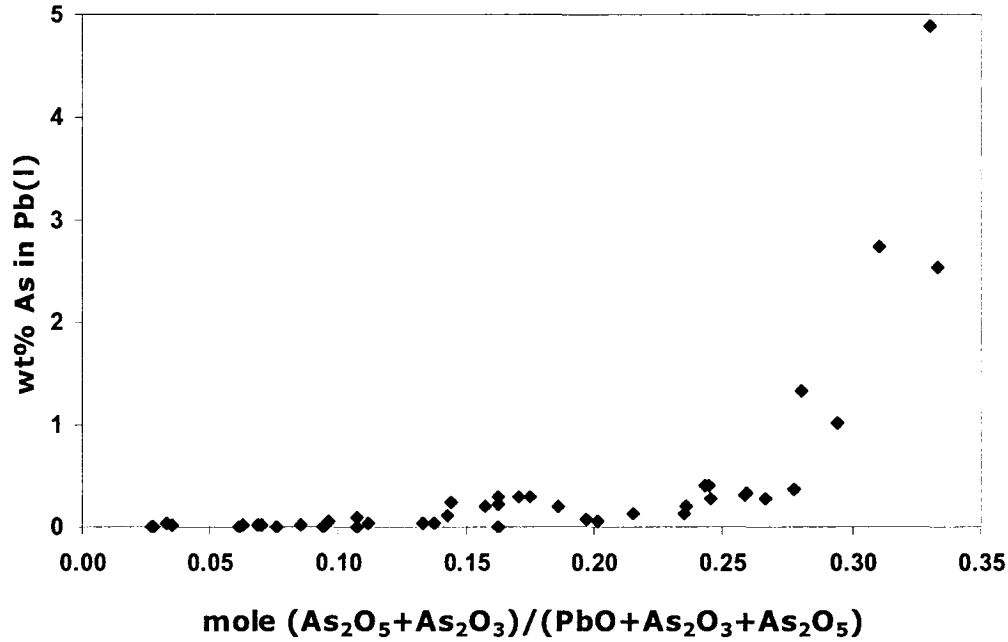

Figure 31 – Equilibrium arsenic distribution between metal and oxide phases at temperatures between 410 and 870 °C.

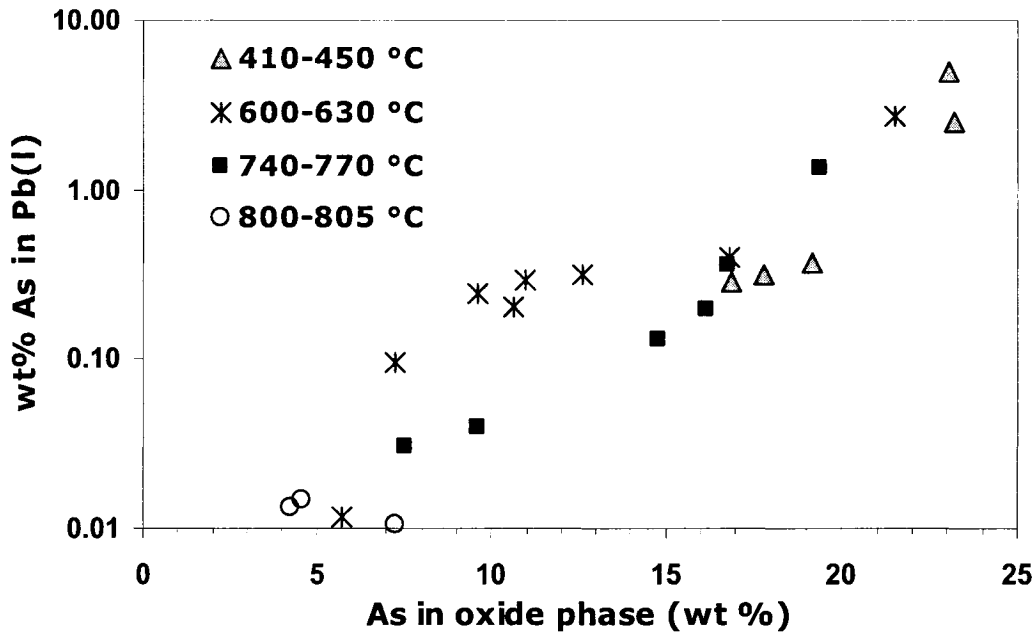

Figure 32 – Equilibrium arsenic distribution between metal and oxide phases at four different ranges of temperature.

The solid compounds that were observed in the quenched samples were PbO (Figure 26), $Pb_8As_2O_{13}$ (Figure 33), and two compounds with compositions close to $Pb_3(AsO_3)_2$

(Figure 34) and Pb_2AsO_4 (Figure 27). $Pb_3(AsO_3)_2$ and Pb_2AsO_4 have not been detected previously and the presence of these two solid compounds were claimed based on atomic proportions measured by EPMA (Table 7). A bigger sample, with a composition close to the sample where $Pb_3(AsO_3)_2$ was observed was prepared and equilibrated for over 24 hours at 410 °C then quenched to room temperature. Note that it was found not to be possible to prepare the pure form of this compound. In a back-scattered electron image of the bigger quenched sample two solid oxides $Pb_3(AsO_3)_2$ and Pb_2AsO_4, lead, and quenched liquid oxide were observed. The XRD diffraction pattern of the sample did not match any previously reported compound. Some of the standard peaks for $Pb_4As_2O_9$ and $Pb_3(AsO_4)_2$ matched with the sample peaks; however the complete pattern was not a match to the quenched sample.

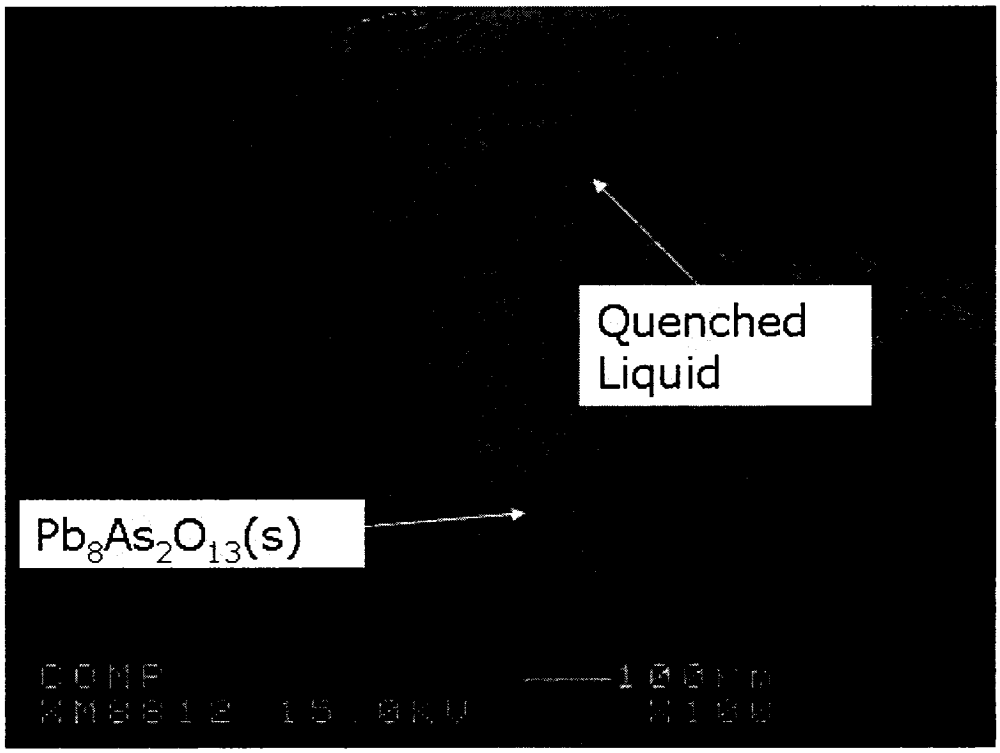

Figure 33 – Back-scattered electron image of Sample 10 in Table 6 and Table 8. $Pb_8As_2O_{13}(s)$ compound and the quenched liquid was observed.

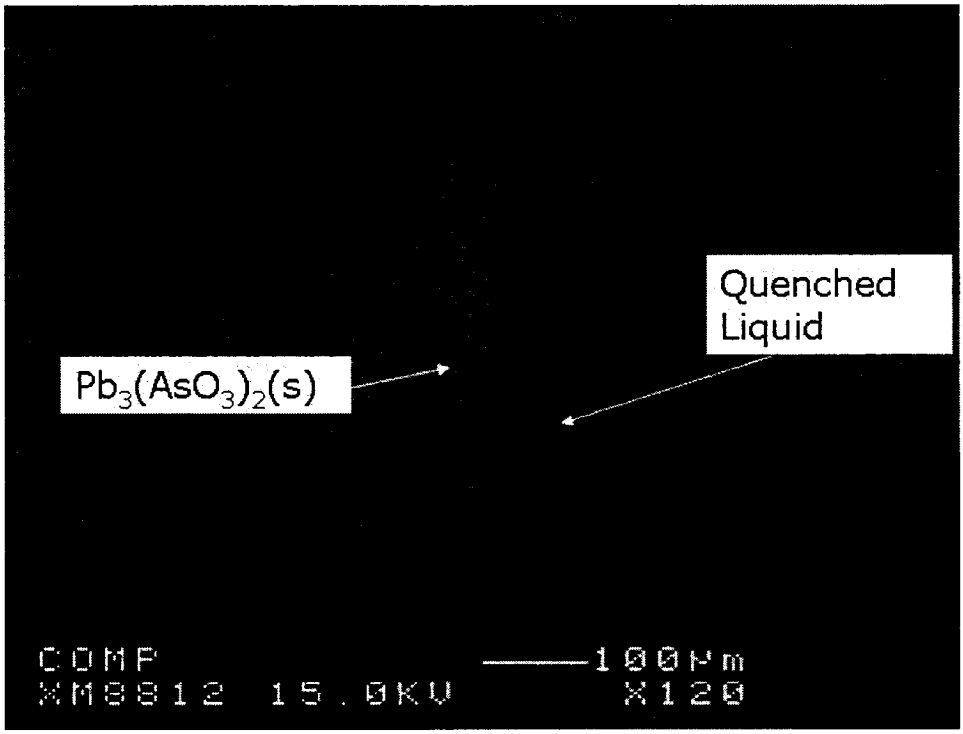

Figure 34 – Back-scattered electron image of Sample 1 in Table 7. $Pb_3(AsO_3)_2(s)$ compound and the quenched liquid oxide were observed.

Table 7 – Composition of the two Pb-As-O compounds that were found from EMPA.

	Weight percentage			Atomic percentage			Measured composition	Assumed composition
	Pb	As	O	Pb	As	O		
1	70.19	18.39	11.43	26.10	18.90	55.00	$Pb_{2.8}(AsO_{2.9})_2$	$Pb_3(AsO_3)_2$
2	75.83	13.45	11.31	29.27	14.40	56.32	$Pb_2AsO_{3.9}$	Pb_2AsO_4

Table 8 and Table 9 show the composition of the individual phases in the quenched samples that were measured by EPMA for the samples in Table 7 (Table 8 for the liquid/solid oxide mixtures and Table 9 the solid/solid oxide mixtures). Only samples that had a successful quench were included. The composition of the quenched liquid oxide was adjusted by subtracting the measured alumina in the liquid phase and then presented in the PbO-As_2O_3-As_2O_5 ternary system.

Table 8 – The compositions of the oxide phases (L + solid) that were measured by EPMA (sample numbers correspond to the samples in Table 6).

	Observed oxide Phases	Composition of the solid oxide (atomic fraction)			Composition of the quenched liquid oxide[i] (mole fraction)			Al in liquid phase
		O	As	Pb	PbO	As_2O_5	As_2O_3	(wt%)
1	L +PbO	0.499	-	0.501	0.965	0.026	0.009	0.80
2	L + PbO	0.492	-	0.507	0.950	0.027	0.023	1.04
3	L + PbO	0.507	-	0.491	0.936	0.054	0.010	0.70
5	L + $Pb_8As_2O_{13}$	0.563	0.088	0.349	0.831	0.066	0.103	0.33
6	L + $Pb_8As_2O_{13}$	0.565	0.088	0.347	0.792	0.076	0.132	0.35
7	L + $Pb_8As_2O_{13}$	0.569	0.087	0.344	0.849	0.064	0.087	0.32
8	L + $Pb_8As_2O_{13}$	0.563	0.089	0.348	0.826	0.068	0.106	0.28
9	L + $Pb_8As_2O_{13}$	0.563	0.087	0.349	0.802	0.057	0.142	0.15
10	L + $Pb_8As_2O_{13}$	0.562	0.087	0.350	0.808	0.062	0.131	0.28
11	L +$Pb_8As_2O_{13}$	0.560	0.087	0.354	0.780	0.038	0.183	0.23
22	L +$Pb_8As_2O_{13}$	0.561	0.087	0.352	0.746	0.028	0.225	0.43
23	L +$Pb_8As_2O_{13}$	0.559	0.088	0.353	0.759	0.029	0.212	0.34
24	L +$Pb_8As_2O_{13}$	0.561	0.088	0.352	0.759	0.018	0.223	0.31
25	L +$Pb_8As_2O_{13}$	0.561	0.087	0.351	0.743	0.014	0.243	0.34
12	L + Pb_2AsO_4	0.563	0.144	0.293	0.740	0.051	0.209	0.12
A[ii]	L + Pb_2AsO_4	0.556	0.146	0.297	0.734	0.056	0.210	0.21
14	L +$Pb_3(AsO_3)_2$	0.550	0.189	0.261	0.652	0.000	0.348	0.41
17[iii]	L +$Pb_3(AsO_3)_2$	0.554	0.186	0.260	0.657	0.000	0.343	0.94

Table 9 – The compositions of the oxide phases (solid/solid) that were measured by EPMA (sample numbers correspond to the samples in Table 6).

	Observed solid Phases	Composition of the first solid (atomic fraction)			Composition of the second solid (atomic fraction)		
		O	As	Pb	Pb	As	O
4	PbO + $Pb_8As_2O_{13}$	0.502	-	0.497	0.566	0.087	0.346
30	PbO + $Pb_8As_2O_{13}$	0.517	-	0.483	0.567	0.087	0.346
31	PbO + $Pb_8As_2O_{13}$	0.504	-	0.494	0.558	0.088	0.355
32	PbO + $Pb_8As_2O_{13}$	0.506	-	0.493	0.561	0.087	0.351
33	PbO + $Pb_8As_2O_{13}$	0.507	-	0.492	0.564	0.086	0.350
B[iv]	PbO + $Pb_8As_2O_{13}$	0.504	-	0.496	0.553	0.082	0.364

[i] Adjusted to no alumina in oxide phase

[ii] Equilibration temperature was 480 °C (not included in Table 6).

[iii] This sample was prepared in a bigger crucible (12 mm ID, 25 mm height) and most parts of the sample was quenched at a slow rate and multiple phases were observed at the parts that was quenched slowly. Only the regions that were close to the crucible walls were used for analysis.

[iv] PbO-4.5 wt% As_2O_3 mixture equilibrated in a platinum capsule at 675 °C and quenched. The second solid phase was close to $Pb_8As_2O_{13}$ (not included in Table 6).

Figure 35 shows the (As^{3+}/total As) ratio for the samples that were completely liquid at the equilibration temperature as a function of total arsenic in the oxide phase. The ratio is below 0.5 between 0 and 0.14 mole fraction (As_2O_3+As_2O_5). This value approached unity at 0.25 mole fraction of (As_2O_3+As_2O_5) and remained close to unity beyond this composition. Figure 69 in Appendix 3 shows the same results for all the samples (liquid oxide, liquid/solid and solid/solid oxide).

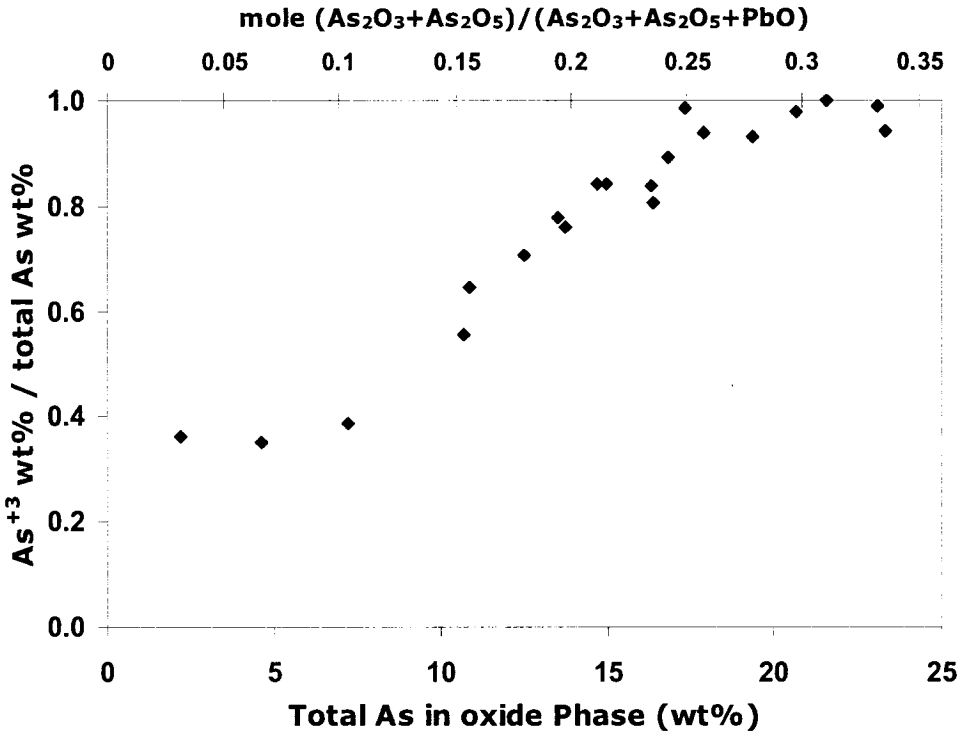

Figure 35 – Mass fraction of As^{3+} as a function of total arsenic in the oxide phase, at temperatures between 410 and 870 °C.

5.2.3 Discussion:

Sources of error in the measurements:

In thermal analysis, under-cooling can contribute a significant source of error. In the PbO-As_2O_3 mixtures, this problem was more pronounced at the higher As_2O_3 contents and it was impossible to quantify the amount of under-cooling in these samples. The heating curves were also examined to determine the liquidus temperatures. DTA results

were used together with the equilibration and quenching results and conclusions were drawn where the results in both experiments agreed.

In the equilibration-quenching experiments, the use of alumina crucibles was a source of error. The measured aluminum in the samples quenched at temperatures above 800 °C was significant (between 0.7 to 1 wt%) and adjusting the results to no aluminum, introduced an appreciable error into the liquidus points as follows.

The PbO-Al_2O_3 system has a eutectic transformation at 857 °C and 1.4 wt% Al_2O_3 (melting temperature of PbO being 887 °C). Subsequently, for the PbO primary field where a high amount of alumina was detected in the liquid phase, the measured liquidus temperatures could be up to 30 °C lower than what they would have been in the absence of alumina. The effect of alumina on the multi-component Pb-As-O was outside the scope of this study, and quantifying the exact effect on the results was not pursued. For other samples with a low amount of dissolved alumina (less than 0.2 wt% Al), it was believed that the effect of dissolved alumina was negligible.

A potential source of error in the quenching experiments was the quenching speed. A slow quenching speed could result in precipitation of solids out of liquid phase. Fortunately with the use of the microprobe, it was possible to observe these precipitates, and identify then based on their shape (thin flakes and sub-micron metallic lead globes) or by the number of phases observed in a sample. For example, if four phases were observed in a region of sample, it was evident that the quenching speed was slow and one or more phases precipitated at lower temperatures than the equilibration temperature[i]. These samples were not used to study the phase transformation, however the bulk composition of the samples was used to determine the arsenic distribution between oxide and metallic phases because the arsenic distribution between metal and oxide phases are less sensitive to the quenching speed.

[i] The Gibbs phase rule constrains a maximum three phases for a three component system (Pb-As-O) at a constant temperature and pressure.

Teck Cominco slag sample:

The EMPA was not capable of distinguishing the oxidation state of a multi-component sample with more than one multi-valance element (i.e., both arsenic and antimony may be at +3 and/or +5 oxidation state in the slag phase). In order to have quantitative values for the amount of arsenic and antimony in different oxidation states, it would have been necessary to conduct a wet chemical analysis[i] on the slag samples, however, since experiments on the multi-component (Pb-As-Sb-O) system was not the focus of the present research, such wet chemical analysis was not pursued.

The mass oxygen in Table 4 was calculated by difference (i.e., oxygen was assumed to be the only element present beside arsenic, antimony and lead), then the arsenic and antimony mass ratio showed that they would need to be almost completely in +3 oxidation state to complete the mass balance. Also, the weight gain (~ 4.1 %) measured with the thermo-gravimetric experiment was roughly equal to the oxygen required to oxidize all of the arsenic and antimony from the +3 oxidation state, to the +5 oxidation state. Hence, despite the explained deficiency of the analytical method, the combined results from the chemical analysis by EMPA and the thermo-gravimetric analysis of the slag samples suggested that the slag sample was consisted mainly[ii] of trivalent arsenic and antimony and that they were completely oxidized to pentavalent arsenic and antimony, respectively when heated in an air atmosphere.

The liquidus temperatures that were observed in argon vs. in air atmosphere were substantially different (~ 1000 °C in air vs. ~ 500 °C in argon). A validated phase diagram of the multi-component Pb-Sb-As-O system is not available but the available phase diagrams of Pb-As-O and Pb-Sb-O (see Sections 5.3.1, 5.3.2, 6.2 and 6.3) show substantially higher liquidus temperatures for the pentavalent arsenic and antimony systems compared to the trivalent arsenic and antimony systems. This observation also

---

[i] A modified titration method that was used for measuring the trivalent arsenic may be used to determine the trivalent arsenic and antimony in the slag system. Total arsenic and antimony may be measured with the conventional chemical analysis methods. Thereafter the pentavalent arsenic and antimony may be calculated by the difference of the total arsenic and antimony from the trivalent arsenic and antimony respectively.

[ii] Because of the uncertainty that was associated with the use of EPMA in assaying the slag sample, it was not possible to definitely determine the oxidation state of both arsenic and antimony.

provided evidence that for this slag sample, which was presumably at equilibrium with partially softened lead bullion, the arsenic and antimony were present in the trivalent oxidation state.

Synthesized samples and thermal analysis results:

The oxidation of As^{3+} to As^{5+} by PbO was confirmed by the XRD analysis of the synthesized samples. The formation of $Pb_8As_2O_{13}$ and metallic Pb that was observed in synthesized PbO-As_2O_3 mixtures with less than 7 wt% As_2O_3 showed that the redox reaction, Reaction 49, caused the oxidation of arsenic from the +3 oxidation state to +5 oxidation state.

$$10PbO + As_2O_3 = 2Pb + Pb_8As_2O_{13};\ \Delta G^0(298\ K) = -63.0\ kJ^{i} \qquad (49)$$

Based on the XRD results of the samples with an As_2O_3 assay between 7 and 23 wt%, the other redox reaction was:

$$6PbO + As_2O_3 = 2Pb + Pb_4As_2O_9;\ \Delta G^0(298\ K) = -60.7\ kJ^{i} \qquad (50)$$

The observation of $Pb_3(AsO_4)_2$ via XRD analysis was uncertain, hence Reaction 51 shown below, is suggested only as a possible reaction that could oxidize the As^{3+} to As^{5+} in the presence of PbO:

$$5PbO + As_2O_3 = 2Pb + Pb_3As_2O_8;\ \Delta G^0(298\ K) = -35.1\ kJ^{i} \qquad (51)$$

In Figure 29, a shift of composition towards more pentavalent arsenic was observed for the samples that were prepared in the platinum capsules. The reason for this shift was believed to be the dissolution of platinum in lead and the subsequent decrease of the activity of lead in the metal/oxide system. Lead has a high negative deviation from Raoultian behavior in Pt-Pb alloys (e.g., Raoultian activity of lead in a Pt-0.4 mole fraction Pb alloy is 0.093 at 1000 °C [110]). As a result, the activity of lead in the samples prepared in platinum capsules was approximately an order of magnitude less than the samples prepared in alumina crucibles (the Raoultian activity of lead was close to

[i] The standard Gibbs energy of this Reaction and Reactions 50 and 51 were calculated using the optimized PbO-As_2O_3-As_2O_5 thermodynamic model that is presented in Part II of this chapter.

unity in alumina capsules because the lead was almost pure). The lower activity of lead would result in the tendency of the redox reactions between trivalent and pentavalent arsenic (e.g., Reactions 49, 50 and 61) to proceed to the right. Such an effect was seen in Figure 29 as drift in the sample assay.

Arsenic solubility in solid PbO

The EPMA results showed that either zero, or a value below the detection limit, arsenic was present in solid PbO for the samples in Table 9 and Samples 1 to 3 in Table 8. Sample B in Table 9 was equilibrated at 680 °C, the temperature of the reported maximum of As_2O_3 in PbO(s) (Zunkel and Larson [34]). The measured arsenic content via EPMA was below the 0.1 wt% detection limit for arsenic. It was concluded that solubility of arsenic in PbO was less than 0.1 wt%, hence the reported ~ 5 wt% As_2O_3 dissolution in PbO(s) by Zunkel and Larson, which was not based on the direct measurement, is thought to be an error. This finding also casts doubt on the reported 5.6 wt% Sb_2O_3 dissolution in PbO(s) that was also reported by Zunkel and Larson based on the same indirect method that they used to report the dissolution of As_2O_3 in PbO.

$Pb_3(AsO_3)_2$(s) and Pb_2AsO_4(s) and $Pb_2As_2O_5$ compounds:

Two previously undetected compounds, $Pb_3(AsO_3)_2$ and Pb_2AsO_4 were observed with the electron microprobe analysis of the quenched samples. Unfortunately, it was not possible to prepare the pure form of $Pb_3(AsO_3)_2$ and Pb_2AsO_4.

For the first time, the $Pb_2As_2O_5$ compound was synthetically prepared and no secondary phase was detected in its XRD analysis. Thus, it was estimated that the sample was greater than 95% pure.

$Pb_3(AsO_3)_2$(s) is a compound in the PbO-As_2O_3 system. The formation of $Pb_3(AsO_3)_2$(s) was in agreement with Pelzel's [38] suggestion that a solid compound may exist at the 3:1, PbO:As_2O_3 molar ratio.

Thermal analysis of the 3:1 PbO:As_2O_3 mixture (Table 3) showed that this compound had an incongruent melting temperature of ~ 460 °C. This compound was detected in the

tests with pure lead and mixtures of PbO-0.33 and PbO-0.27 mole fraction As_2O_3 (Samples 14 and 17 in Table 8) that were heated to a fully liquid state (650 °C), then cooled and quenched from 420 °C. XRD analysis of Sample 17 showed the presence of a previously unreported compound. Because of the abundance of peaks and the failure to prepare the pure form of this compound, the XRD analysis is considered inconclusive.

XRD analysis of Sample K[i] in Table 2, with PbO-0.33 mole fraction As_2O_3 (same initial oxide mixture as Sample 14 in Table 8), showed only the presence of $Pb_2As_2O_5$. Thermal analysis of this sample showed a liquidus temperature of 462 °C and a second thermal arrest at ~ 390 °C. These analyses, and the observed $Pb_3(AsO_3)_2$ compound in the quenched sample at 420 °C, indicated that the $Pb_2As_2O_5$ compound had an incongruent melting temperature of ~ 390 °C. Such a finding followed from the logic that if the first thermal arrest at 462 °C was due to the congruent melting of $Pb_2As_2O_5$, then the compound $Pb_3(AsO_3)_2$, observed in Sample 14 at 420 °C, could not exist.

In practice, the Pb_2AsO_4 compound is a mixture of lead, oxygen and arsenic in +3 and +5 oxidation states. This compound may also be represented as $Pb_2(AsO_4)(AsO_3)O$, which includes all three anions that were present in the oxide system (i.e., $(AsO_4)^{3-}$, $(AsO_3)^{3-}$ and O^{2-}). The Pb_2AsO_4 compound was observed in two samples that were quenched from 550 °C and 480 °C (Sample 12 and Sample "A" in Table 8). However, it was not possible to estimate the melting temperature of this compound or to determine if this compound had congruent melting temperature.

Equilibration and quenching experiments:

The tie lines between the molten lead and liquid oxide in Figure 30 showed a clear change in behavior at 0.25 mole fraction As_2O_3 corresponding to the composition of $Pb_3(AsO_3)_2$). Between 0 and 0.25 mol fraction As_2O_3, the arsenic content in the metallic lead was very low, and arsenic was between 0.01 and 0.2 wt% with less than 0.24 mole fraction of As_2O_5+As_2O_3. The arsenic content in the metallic lead rapidly increased at As_2O_3 contents higher than 0.25 mol%, from 0.2 to 5 wt% arsenic with 0.24 to 0.33 mol % total (As_2O_5+As_2O_3) in the oxide phase. The same type of behavior was also observed in

[i] Synthesized at 390 °C in a silver capsule.

Figure 31 for the whole range of composition and temperatures, in which at ~ 0.25 mol fraction of total (As_2O_3 + As_2O_5), the arsenic content of the metallic lead suddenly increased.

The (As^{3+}/total As) ratio, shown in Figure 35, which was less than 0.5 up to ~ 0.12 mol fraction of total As_2O_5+As_2O_3 (i.e., pentavalent arsenic oxide was predominant) approached unity at 0.25 mol fraction of total As_2O_5 and As_2O_3, i.e., the arsenic was almost completely in +3 oxidation state, and it remained almost at unity at above 0.25 mole fraction As_2O_3. These two observations, arsenic distribution and ratio of arsenic trivalent to the total arsenic, suggest a strong interaction occurred between the Pb, As and O atoms at 0.25 mol fraction As_2O_3 and supported the proposed structural model for PbO-As_2O_3 system, since 0.25 mol fraction As_2O_3 corresponds to the formation of $Pb_3(AsO_3)_2$(l) in the liquid phase and the existence of Pb^{2+} and $(AsO_3)^{3-}$ ions.

The effect of temperature on the arsenic distribution was shown in Figure 32 in which the oxide phase was fully liquid or a mixture of liquid and solid phases. The results showed that at a high arsenic content in the oxide phase (~ 17 wt% As), where most of the samples were fully liquid, the arsenic in metallic lead increased with increasing temperature. This was in agreement with the findings of Zunkel and Larson [34] (Figure 8). At lower arsenic contents in the oxide phase (between 7 to 17 wt% As) this trend was reversed, whereby for the samples in the 600-630 °C temperature range, the arsenic content in the metallic phase remained almost constant, but for the 740-770 °C temperature range, the arsenic content constantly decreased. Zunkel and Larson reported a similar behavior; however they did not offer an explanation for their observation. Below this result is examined in conjunction with the phases that were seen to form at different composition and temperature ranges (Table 6, Table 8 and Table 9).

It was observed that when a mixture of liquid oxide and $Pb_8As_2O_{13}$(s) were present at a constant temperature, the arsenic in the metal phase remained constant at varying total arsenic in the oxide phase. Moreover, it was observed that for samples in the 600-630 °C temperature range, the formation of $Pb_8As_2O_{13}$ occurred at a higher total As content in the oxide phase (~17 wt %) relative to the 740-770 temperature range that occurred at ~ 14 wt%. From these observations, it can be seen that the constant arsenic content region in

the metallic phase occurred at higher arsenic content in the oxide phase at 600-630 °C temperature range relative to the 740-770 °C temperature range. The lower arsenic content at the higher temperature corresponded to the formation of $Pb_8As_2O_{13}$.

5.3 Part II – Thermodynamic Modeling

5.3.1 PbO-As_2O_5 System

Thermodynamic properties of the pure compounds:

Using the concept of the AsO_4^{3-} ion in the PbO-As_2O_5 system that was established in Section 3.3, the arsenic containing compounds up to 25 mol% As_2O_5 were considered with respect to the present model.

The properties of PbO, which was the common compound in all the pseudo-binaries, were taken from the FACT™ compound database of the FACT*Sage*™ [31] computer software (the original data source being Barin, *Thermochemical Data of Pure Substances* [111] and Barin et al., *Thermochemical Properties of Inorganic Substances* [112]). The other compounds in the region of interest were $Pb_8As_2O_{13}$, $Pb_4As_2O_9$ and $Pb_3(AsO_4)_2$.

$Pb_3(AsO_4)_2$ is an end member of the liquid solution model that was developed here. $Pb_3(AsO_4)_2$ has a congruent melting temperature of 1303 K. Thermodynamic properties of this compound are reported by Nekrasov et al. [113], Shashchanova et al. [114] and the compilation of Barin [115]. Nekrasov et al. used an empirical method [116] that predicts the thermodynamic properties of the double oxide compounds from the formation of simple oxides. Their estimate was close to Barin's (Figure 36). The calculated value of $G^0_{Pb_3(AsO_4)_2}$ from Shashchanova et al. was higher than Barin (Figure 36) at temperatures below 800 K. Above this temperature, values from Barin were inside the reported error by Shashchanova et al. Note that the uncertainties of measurement were only reported in Shashchanova et al.

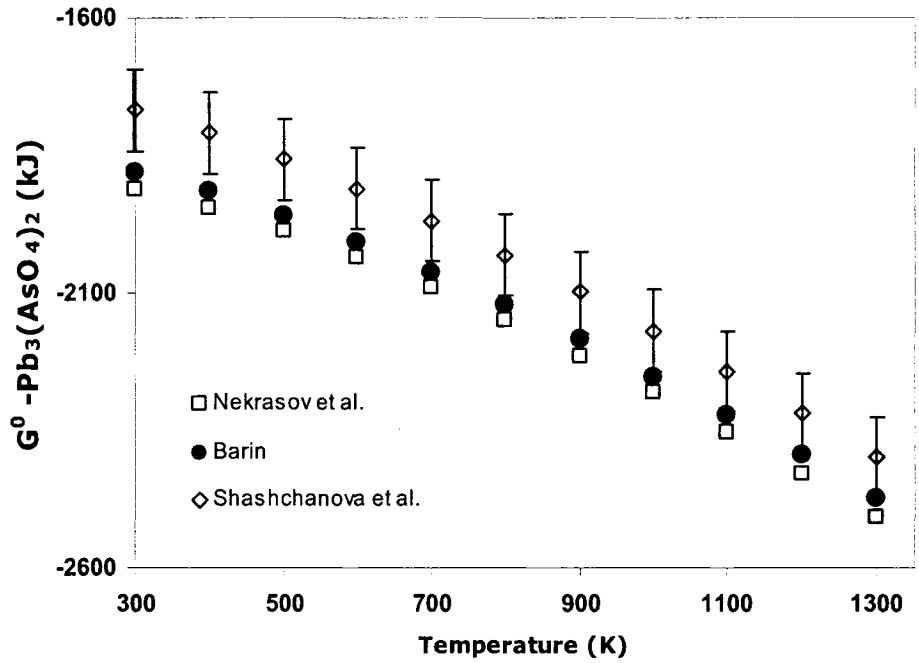

Figure 36 – Standard Gibbs energy of $Pb_3(AsO_4)_2$ compound calculated from thermodynamic properties reported from references (□ from [113] ◇ from [114]and • from [115]).

The compound $Pb_8As_2O_{13}$[i], has a congruent melting temperature of 865 °C [32, 39], and no thermodynamic properties have been reported for this compound. Initially, Equation 52, with the assumption of $\Delta G^0 = 0$[ii] was used to estimate the entropy and the heat capacity of $Pb_8As_2O_{13}$. The enthalpy of the reaction was estimated by an empirical method explained by Zhuang et al. [118]. In this method, the unknown enthalpy of formation for a double oxide is estimated using the known enthalpy of formation of a double oxide with the same constituent oxides. PbO and As_2O_5 are the constituent oxides of $Pb_8As_2O_{13}$ and $Pb_3(AsO_4)_2$. The measured enthalpy of formation for $Pb_3(AsO_4)_2$ [115] from 3PbO and $1As_2O_5$ was used to estimate the enthalpy of formation for $Pb_8As_2O_{13}$ from 8PbO and $1As_2O_5$. The standard enthalpy of formation of $Pb_8As_2O_{13}$ that was calculated with this method was -2932.5 kJ/mol.

$$5PbO_{(s)} + Pb_3(AsO_4)_{2\,(s)} = Pb_8As_2O_{13\,(s)} \qquad (52)$$

[i] This compound is also reported as $Pb_8O_5(AsO_4)_2$ based on its crystal structure [117]

[ii] Using $\Delta G^0 = 0$ for this equation means that the enthalpy, entropy and heat capacity of the new compound is equal to the summation of its composing compounds.

The thermodynamic properties of the compound $Pb_4As_2O_9$ had not previously been calculated. $Pb_4As_2O_9$ dissociates via a peritectoid reaction at 740 °C to $Pb_8As_2O_{13}$ and $Pb_3(AsO_4)_2$ [39] and does not affect the liquidus in the PbO-As_2O_5 system. The entropy and heat capacity of this compound was estimated using Equation 53 with the assumption of $\Delta G^0 = 0$

$$PbO_{(s)} + Pb_3(AsO_4)_{2\,(s)} = Pb_4As_2O_{9\,(s)} \qquad (53)$$

Using the same empirical method that was described for $Pb_8As_2O_{13}$, the enthalpy of formation of $Pb_4As_2O_9$ was estimated from the known enthalpy of formation of $Pb_3(AsO_4)_2$.

The thermodynamic properties of the compounds that are mentioned above are presented in Table 11.

Liquid solution:

The ionic model for the PbO-As_2O_5 liquid solution was introduced in Section 3.4. Because of the known value of the heat of fusion of PbO, the PbO liquidus curve in the PbO-As_2O_5 pseudo-binary was used to calculate the excess Gibbs energy parameter of the PbO-$Pb_{1.5}AsO_4$ pseudo-binary by Equation 34, in Section 3.4.

Equation 41 was the basis for calculating the excess parameter as it was described in Section 3.4. However in practice, the "Optimizer" module of the FACT*Sage*™ thermochemical program was used to determine this parameter. The excess Gibbs energy equation that was found to best-fit the liquidus curve in the PbO- $Pb_{1.5}AsO_4$ pseudo-binary is given in Equation 54:

$$g^E = -4950\, X_{PbO}^2 \cdot X_{Pb_{1.5}AsO_4} \qquad (54)$$

The standard Gibbs energy of $Pb_{1.5}AsO_4(l)$ was estimated by summing the Gibbs energy of melting for $Pb_3(AsO_4)_2(s)$ (or $Pb_{1.5}AsO_4$) and the standard Gibbs energy of solid $Pb_3(AsO_4)_2$ (Table 11). The Gibbs energy of melting was derived from the heat of melting of $Pb_{1.5}AsO_4$ that was estimated via Equation 55:

$$\ln a^{l}_{Pb_{1.5}AsO_4} = -\frac{\Delta h^{0}_{f(Pb_{1.5}AsO_4)}}{RT}\left(1-\frac{T}{T^{0}_{f(Pb_{1.5}AsO_4)}}\right) \qquad (55)$$

where T is the measured liquidus temperatures on the liquidus curve of the $Pb_{1.5}AsO_4$ as it was described in Section 3.4.

As an initial guess, the activity of $Pb_{1.5}AsO_4$ was taken as its mole fraction. The heat of melting that was calculated in this way was optimized using the OptiSage module of the FACT*Sage*™ [31]. OptiSage uses a similar method with the difference that it uses the activity of $Pb_{1.5}AsO_4$ to calculate the enthalpy of melting of $Pb_{1.5}AsO_4$ instead of using the mole fractions. In order to calculate the activity, OptiSage uses the excess Gibbs energy that was derived in Equation 54. The Gibbs energy of melting of $Pb_{1.5}AsO_4$ derived via the estimated heat of melting may be written as:

$$\Delta g^{0}_{f(Pb_{1.5}AsO_4)} = 33210 - 25.5T \text{ (J/mol)}; T_{f(Pb_{1.5}AsO_4)} = 1030(°C) \qquad (56)$$

Finally, the estimated values of the enthalpy of formation of $Pb_8As_2O_{13}$ and $Pb_4As_2O_9$ that were estimated in the previous section were slightly increased (17 kJ/mol for $Pb_8As_2O_{13}$ and 2 kJ/mol for $Pb_4As_2O_9$) to fit the calculated melting temperature of the $Pb_8As_2O_{13}$, and the peritectoid transformation of $Pb_4As_2O_9$, to the measured melting temperature and peritectoid transformation of these compounds respectively.

The defined solution model for PbO-$Pb_{1.5}AsO_4$, along with the solid compounds in Table 11, were used in the FACT*Sage*™ program to construct the pseudo-binary phase diagram for PbO-$Pb_{1.5}AsO_4$. The constructed diagram and the experimental values are shown in Figure 37.

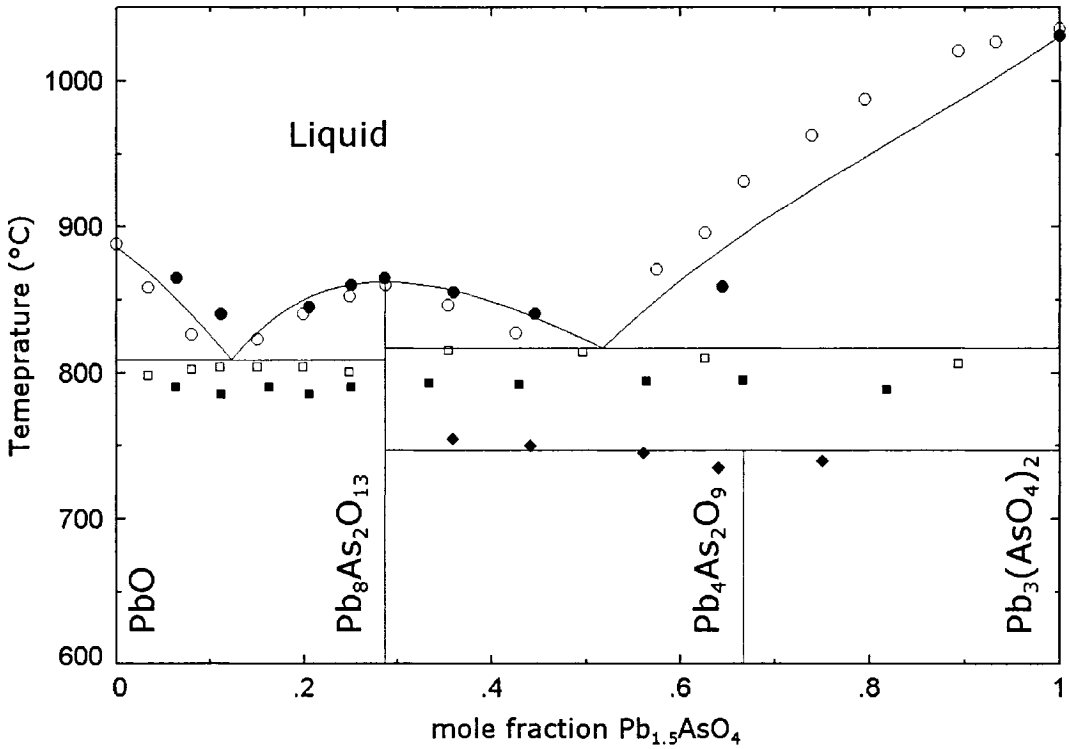

Figure 37 – Phase diagram for PbO-$Pb_{1.5}AsO_4$ calculated from the thermodynamic model. Experimental values, ● liquidus, ■ eutectic, ◆ peritectoid from Kasenov et al. [39], ○ liquidus, □ eutectic from Amadori [36] and Gerlach [32] (graph generated with FACT*Sage*™ [31]).

5.3.1.1 Discussion of the Present PbO-As_2O_5 Model

The calculated PbO-$Pb_{1.5}AsO_4$ pseudo-binary phase diagram, which is in the PbO rich Basic region of the PbO-As_2O_5 system, showed good agreement with the measured liquidus temperatures. The eutectic temperatures that were predicted with the model were slightly higher[i] than those reported by Kasenov et al. [39] and Amadori [36].

The assumption of ideality, i.e., no excess terms, showed reasonable agreement between the model calculations and the experiment (not shown). In fact, only one excess energy parameter with a relatively small value[ii] was enough to fit the model to the experimental values. Thereafter it can be concluded that the assumed ideal interaction and random distribution of the O^{2-} and $(AsO_4)^{3-}$ ions were a close approximation to reality, meaning

[i] Calculated eutectic between PbO-$Pb_8As_2O_{13}$ was 807 °C compared to 790 °C and 803 °C measured by Kasenov et al. [39] and Amadori [36] and calculated eutectic between $Pb_8As_2O_{13}$-$Pb_3(AsO_4)_2$ was 814 °C compared to 790 and 812 °C measured by Kasenov et al. [39] and Amadori [36], respectively.

[ii] From experience this value (-4.9 kJ) was considered to be a small value [119].

that the ionic structure of the liquid oxide with the Pb^{2+} cation and O^{2-} and $(AsO_4)^{3-}$ anions was reasonable and sufficiently sophisticated to represent the system. Nevertheless in reality, even in the ultra rich Basic PbO region of the solution, the structure of the oxide phase is more complex than described here and there is a possibility of the polymerization of the $(AsO_4)^{3-}$ in a form of $(As_2O_7)^{4-}$ or $(As_3O_{10})^{5-}$ [120]. However, in the current model the presence of any polymeric species was ignored.

The standard Gibbs energy of $Pb_3(AsO_4)_2(s)$ is an essential part of the model since the Gibbs energy of $Pb_3(AsO_4)_2(l)$ in the solution and all the other pentavalent arsenic solid oxides in this region were derived from this compound. Unfortunately, the error limits for the thermodynamic properties of $Pb_3(AsO_4)_2(s)$ that were used in this study were not reported by Barin [115], and an unknown error is thus associated with a main components of this system.

5.3.2 PbO-As_2O_3 System

Thermodynamic properties of the pure compounds:

The Pb-As-O compounds in the PbO-As_2O_3 binary system are $Pb_3(AsO_3)_2$, $Pb_2As_2O_5$ and $PbAs_2O_4$. Pelzel [33] measured the melting temperature of 2:1 and 1:1 molar ratios of PbO:As_2O_3 mixtures corresponding to the compositions of $Pb_2As_2O_5$ and $PbAs_2O_4$ compounds to be 480 °C and 450 °C (Figure 6), respectively.

The compound $Pb_3(AsO_3)_2$, which is an end member of the solution model, had not been reported prior to this study. As described in Section 5.2.3, $Pb_3(AsO_3)_2$ has an incongruent melting temperature of 463 °C.

The thermodynamic properties of these three compounds have not measured previously. Initially, Equations 57 to 59 with $\Delta G^0 = 0$ were used to estimate initial values for the Gibbs energies of these compounds.

$$3PbO_{(s)} + As_2O_{3\,(s)} = Pb_3(AsO_3)_{2\,(s)} \quad (57)$$

$$2PbO_{(s)} + As_2O_{3\,(s)} = Pb_2As_2O_{5\,(s)} \quad (58)$$

$$PbO_{(s)} + As_2O_{3\,(s)} = PbAs_2O_{4\,(s)} \quad (59)$$

Subsequently, the standard heats of formation of these compounds were changed during the optimization (see the following section) to obtain a match between the calculated melting temperatures and the measured melting temperatures. The thermodynamic properties for the solid compounds used in the current study are presented in Table 11.

Liquid solution:

The ionic solution model for the PbO-As_2O_3 was introduced in Section 3.4. In order to calculate the excess Gibbs energy for this binary system, the liquidus temperatures measured on the PbO liquidus curve from Zunkel and Larson [34], Pelzel [38] and the liquidus temperatures along the PbO liquidus surface on the ternary PbO-As_2O_3-As_2O_5 system (Table 5 and Table 8) from the current study were taken into account. The excess Gibbs energy parameter that was found via optimization using the OptiSage module of the FACT*Sage*™ software is given by Equation 60:

$$g^{E} = 1620\, X_{PbO}\, X_{Pb_{1.5}AsO_3} \quad (60)$$

The Redox reaction, Reaction 61, was used to calculate an initial value for the standard Gibbs energy of $Pb_{1.5}AsO_3$ (l).

$$PbO_{(l)} + Pb_{1.5}AsO_{3(l)} = Pb_{(l)} + Pb_{1.5}AsO_{4(l)} \quad (61)$$

$$K_{eq} = \frac{a_{Pb(l)}\, a_{Pb_{1.5}AsO_4(l)}}{a_{PbO(l)}\, a_{Pb_{1.5}AsO_3(l)}} \quad (62)$$

The equilibria between the molten lead and the liquid oxide measured in this study (Table 5) with a composition less than 0.25 mol fraction of initial As_2O_3, were used to calculate the equilibrium constant, Equation 62. The Raoultian activity of lead was taken as its mole fraction because the molten lead was almost pure at this composition range. The activity of PbO and $Pb_{1.5}AsO_3$ were estimated by their mole fractions and the activity of $Pb_{1.5}AsO_4$ was estimated from the optimized binary solution of PbO-$Pb_{1.5}AsO_4$ presented in the previous section.

With the known standard Gibbs energies of Pb(l), PbO(l) and $Pb_{1.5}AsO_4$(l), the standard Gibbs energy for the $Pb_{1.5}AsO_3$ in Reaction 61 was calculated. Figure 38 shows the PbO liquidus curve in the PbO-$Pb_{1.5}AsO_3$ system along with the experimental values of Zunkel and Larson [34] and Pelzel [38].

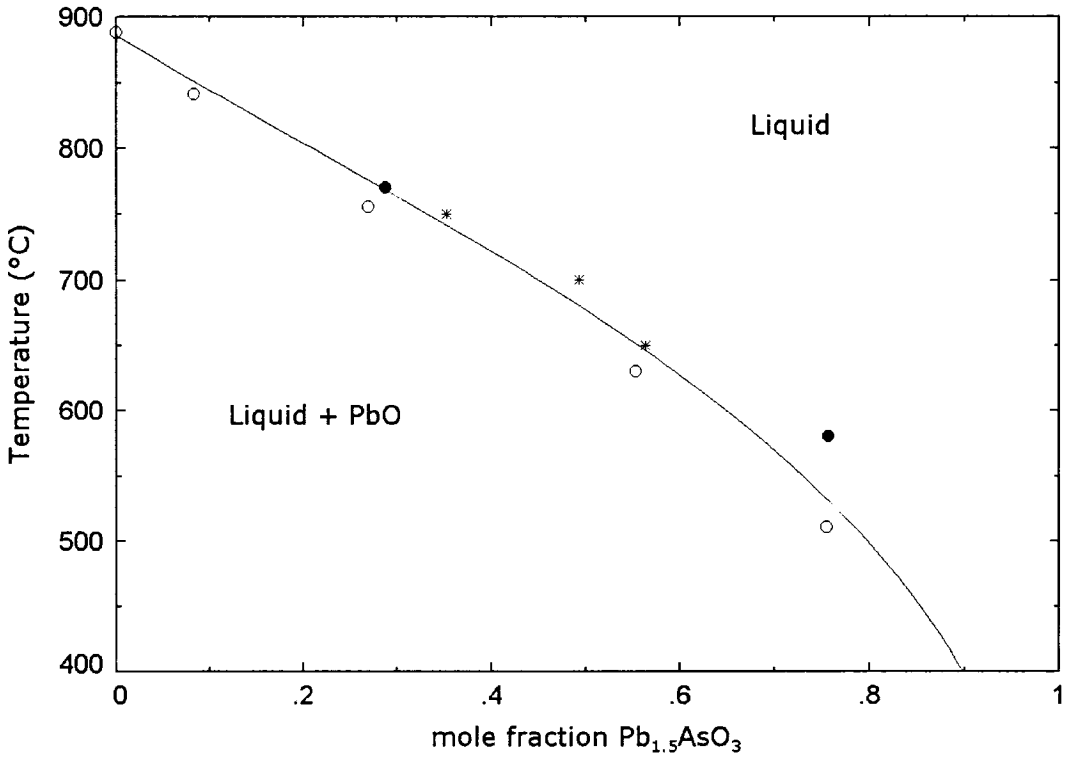

Figure 38 – PbO liquidus curve in PbO-$Pb_{1.5}AsO_3$ system. • from Pelzel [38], ○ thermal analysis and ✱ slag-metal equilibria from Zunkel and Larson [34] (graph generated with FACT*Sage*™ [31]).

The PbO-$Pb_3(AsO_3)_2$ model was not sufficiently accurate in its initial form to calculate the arsenic distribution between the metal and oxide phases in the range of interest because at the limit of the model the activity of PbO in the PbO-$Pb_{1.5}AsO_3$ system became zero; meaning metal/oxide equilibrium calculations were not possible. To overcome this deficiency, the current model was expanded by the addition of another species.

As explained in Section 3.3, the $PbO{\cdot}As_2O_{3(l)}$ (or $PbAs_2O_4$) compound was believed to exist in liquid PbO-As_2O_3 at relatively high As_2O_3 contents, hence the $PbAs_2O_4$ compound was introduced as a new component to the model to expand the composition

region of the model. Reaction 63 was used to estimate an initial value for the standard Gibbs energy of this compound.

$$1.5PbO_{(l)} + As_{(l)} = Pb_{(l)} + Pb_{0.5}AsO_{2(l)}^{i} \quad (63)$$

$$K_{eq} = \frac{a_{Pb(l)}\, a_{Pb_{0.5}AsO_2(l)}}{a_{PbO(l)}^{1.5} \cdot a_{As(l)}} \quad (64)$$

The equilibria between the liquid oxide and molten metallic lead that were measured at higher than 0.25 mol fraction As_2O_3 (data from Table 5 and Zunkel and Larson [34]), where the oxide phase consisted primarily of trivalent arsenic oxide, was used to calculate the equilibrium constant (Equation 64). The activities of Pb(l) and As(l) in the metallic phase were calculated using the Pb-liquid solution database of FACT*Sage*™ software. The activity of PbO(l) and $Pb_{0.5}AsO_2$(l) were estimated to be equal to their mole fractions. Subsequently, with the known standard Gibbs energies of PbO(l), Pb(l) and As(l), the initial estimate for the Gibbs energy of $PbAs_2O_4$(l) was measured.

The calculated values for the Gibbs energies of $Pb_{1.5}AsO_{3(l)}$ and $PbAs_2O_{4(l)}$ were modified during the optimization of the ternary PbO-As_2O_3-As_2O_5 system to fit the ternary experimental values (see the next section). Subsequently, the heats of formation of the solid compounds (i.e. $Pb_3(AsO_3)_2$, $Pb_2As_2O_5$ and $PbAs_2O_4$) which had been initially estimated through Equations 57 to 59, were modified in order to obtain a better match of the calculated melting temperatures of these compounds to the measured melting temperatures.

The phase diagram of the PbO-As_2O_3 system up to 0.5 mol fraction As_2O_3, predicted with the expanded solution model and experimental results from this study, Zunkel and Larson and Pelzel is shown in Figure 39. It is important to note that in this graph only the presence of arsenic in +3 oxidation state was taken into account.

[i] Similar to the $Pb_{1.5}AsO_3$, the compound $PbAs_2O_4$ was represented as $Pb_{0.5}AsO_2$ to unify the number of anions.

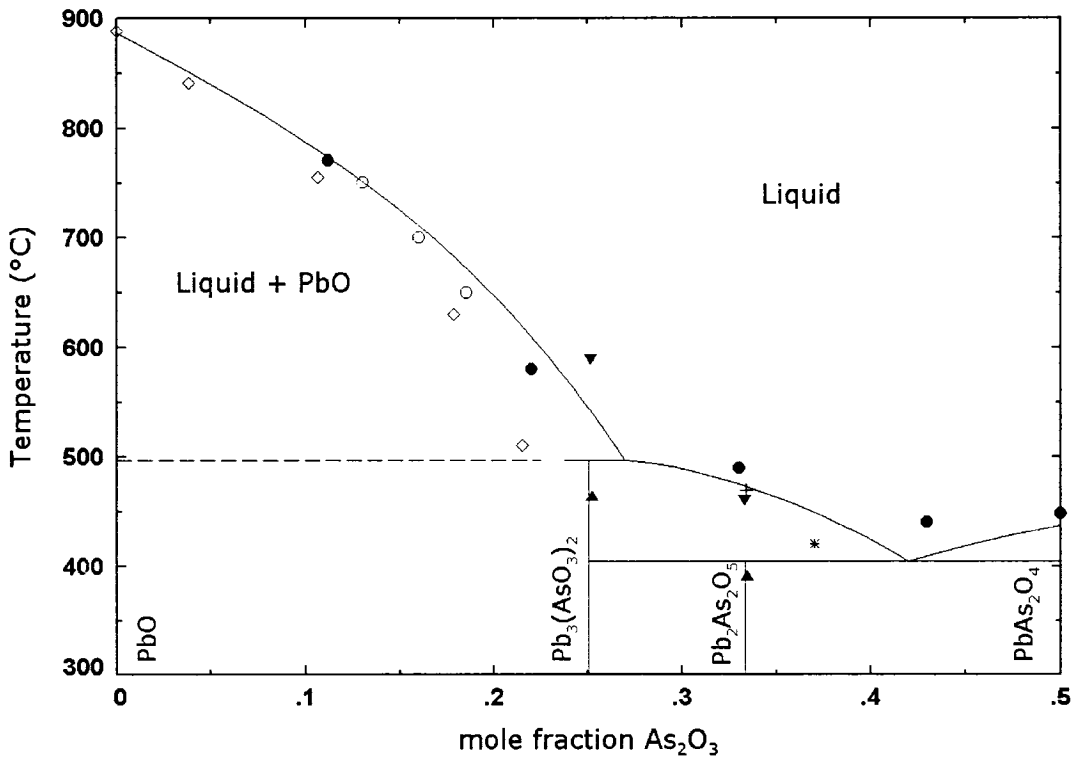

Figure 39 – PbO-As_2O_3 pseudo-binary phase diagram. • liquidus (Pelzel [38]), ◇ liquidus (Zunkel and Larson -thermal analysis [34]), ○ liquidus (Zunkel and Larson-equilibration), ✳ Liquidus (equilibrium between liquid and $Pb_3(AsO_3)_2$), ▼ liquidus (thermal analysis), ▲, second thermal arrest and + single liquid phase (graph generated with FACT*Sage*™ [31]).

The calculated distribution of the arsenic between the metal and oxide phases is presented in Section 5.3.3 where the PbO rich region of the ternary PbO-As_2O_3-As_2O_5 is described.

5.3.2.1 Discussion of the PbO-As_2O_3 System

The calculated liquidus of PbO in the PbO-$Pb_{1.5}AsO_3$ system showed good agreement with the experimental values. Only a single excess Gibbs parameter with a small value[i] was necessary to fit the model to the experimental values. In fact, when only the binary values were used for optimizing the excess parameter, the ideal assumption fitted the experimental values well. Hence, similar to the PbO-$Pb_{1.5}AsO_4$ system, it was concluded that in the Basic PbO rich region of the PbO-As_2O_3 system, the suggested Pb^{2+}, O^{2-} and $(AsO_3)^{3-}$ ionic structure was reasonable. This was in agreement with the conclusions of

[i] From the experience a value of 1620 J/mol for the regular type excess parameter was considered to be a low value [119].

the experimental results (Section 5.2.3) that $Pb_3(AsO_3)_2$ was forming in the liquid solution.

It was necessary to expand the range of composition in this system to higher As_2O_3 contents because the initial model was not applicable to equilibrium calculations between the metal and oxide phase in the region of interest for industrial softening and present experimental values. The expansion could have been accommodated using either the assumption of the formation of dimers of $(AsO_3)^{3-}$ in the form of $(As_2O_5)^{4-}$ ions or the formation of $(AsO_2)^{1-}$ groupings that corresponded to the $PbO{\cdot}As_2O_3$ species. It was decided to choose the latter, the inclusion of $PbO{\cdot}As_2O_3$ (or $PbAs_2O_4$), because of the formation of this compound in the liquid $PbO\text{-}As_2O_3$ suggested in Section 3.3. The calculated phase diagram of $PbO\text{-}As_2O_3$ up to 0.5 mol fraction of As_2O_3 (Figure 39) showed reasonable and sufficient agreement between the experimental results and the model predictions.

The assumption of ideal activity for the $PbAs_2O_4$ and no interaction with $Pb_3(AsO_3)_2$ in the solution was simplistic and in practice the structure of the liquid at high As_2O_3 is more complex than the structure assumed in this study. In order to consider polymerization and formation of new groupings that would allow extending the range of composition, a more advanced model (e.g. a modified quasichemical model[i] [121]) would be a better choice. If the quasichemical model was to be used for the $PbO\text{-}As_2O_3$ solution, short-range ordering, that here was defined by formation of $(AsO_3)^{3-}$ or $(AsO_2)^{1-}$ groupings, would be taken into account through a reaction among second nearest neighbor pairs:

$$(Pb\text{-}Pb)_{pair} + (As\text{-}As)_{pair} = 2\,(Pb\text{-}As)_{pair};\ \Delta g_{PbAs} \qquad (65)$$

where Δg_{PbAs}, the molar Gibbs energy of the Reaction 65, is the principal model parameter.

In a modified quasichemical model, Δg_{PbAs} is expanded as an empirical polynomial as a function of the pair fraction of As. This would allow for a change in the configurational entropy, without the need for introducing a new species into the system.

[i] The use of the modified quasi-chemical model was outside the scope of this work.

It is important to note that the solid compounds between 0 and 0.25 mol fraction As_2O_3 (Figure 39) are not shown in the graph and the peritectic reaction (L + PbO → $Pb_3(AsO_3)_2$) is shown with a dotted line. The reason is that in this range, pentavalent arsenic oxides exist in the PbO-As_2O_3 system.

The redox reactions that oxidized the As^{3+} to As^{5+} at As_2O_3 contents lower that 0.25 mole fraction were described in Section 5.2.3. Because of these reactions, the constant composition section (isopleth) of PbO-As_2O_3 is not a true pseudo-binary system. In the 0 to 0.25 mole fraction As_2O_3 range, trivalent arsenic compounds, pentavalent arsenic oxide (i.e., $Pb_8As_2O_{13}$ and $Pb_4As_2O_9$) and metallic lead exist together. This isopleth section has multiple transformations and so tie lines may not be drawn inside the isopleth. As a result, the PbO-As_2O_3 isopleth had little to teach us and was not drawn here[i]. Nevertheless, the shape of PbO liquidus curve did not change once the graph was presented as a pseudo-binary (i.e., no pentavalent arsenic oxide was taken into account for calculation of the phase diagram).

5.3.3 PbO-As_2O_5-As_2O_3 System and Its Application

For interpolation of the binaries to the ternaries, the Kohler symmetric approximation [96] was used with no ternary parameters. The parameters in PbO-As_2O_5 binary were fixed and the parameters in the PbO-As_2O_3 system were changed to fit the available ternary data to the model prediction. The excess Gibbs energy parameter in the PbO-As_2O_3 system was kept unchanged because it was assessed using ternary and binary data. The standard Gibbs energy of $Pb_{1.5}AsO_3$(l) and $PbAs_2O_4$(l) were changed (-12 kJ/mol and -6 kJ/mol, respectively) to match the measured liquidus points to the model prediction. The optimized values are presented in Table 10.

[i] With the use of computational thermodynamic software (e.g. FACT*Sage*™) the optimized model is capable of drawing this isopleth section.

Table 10 – Standard molar Gibbs energies of the components that were used in the liquid solution model.

i	g_i^0 (J/mol)
$Pb_3(AsO_4)_2$(l)	-1813532 + 1491.2 T -0.0327 T^2 + 1.5e6 T^{-1} -273 T ln T
$Pb_3(AsO_3)_2$(l)	-1340776 + 1615.2 T -0.01838 T^2 + 2.3e7 T^{-2} -789 $T^{-0.5}$ -295 T ln T
$PbAs_2O_4$(l)	-908230 + 1134.9 T -0.00613 T^2 + 7.6e6 T^{-2} -263 $T^{-0.5}$ -200 T ln T

Figure 40 shows the calculated liquidus projection of the PbO-$Pb_{1.5}AsO_3$-$Pb_{1.5}AsO_4$ along with the experimental values from the present work. The results of the thermal analysis show only the liquidus temperatures, although the equilibration and quenching results show both the position of the liquidus point, and the solid that was at equilibrium with that liquid.

Three primary fields were observed in the ternary system, i.e., $Pb_3(AsO_4)_2$, $Pb_8As_2O_{13}$ and PbO primary fields. The univariant valleys are drawn with thicker lines. No ternary eutectic was observed in the ternary system.

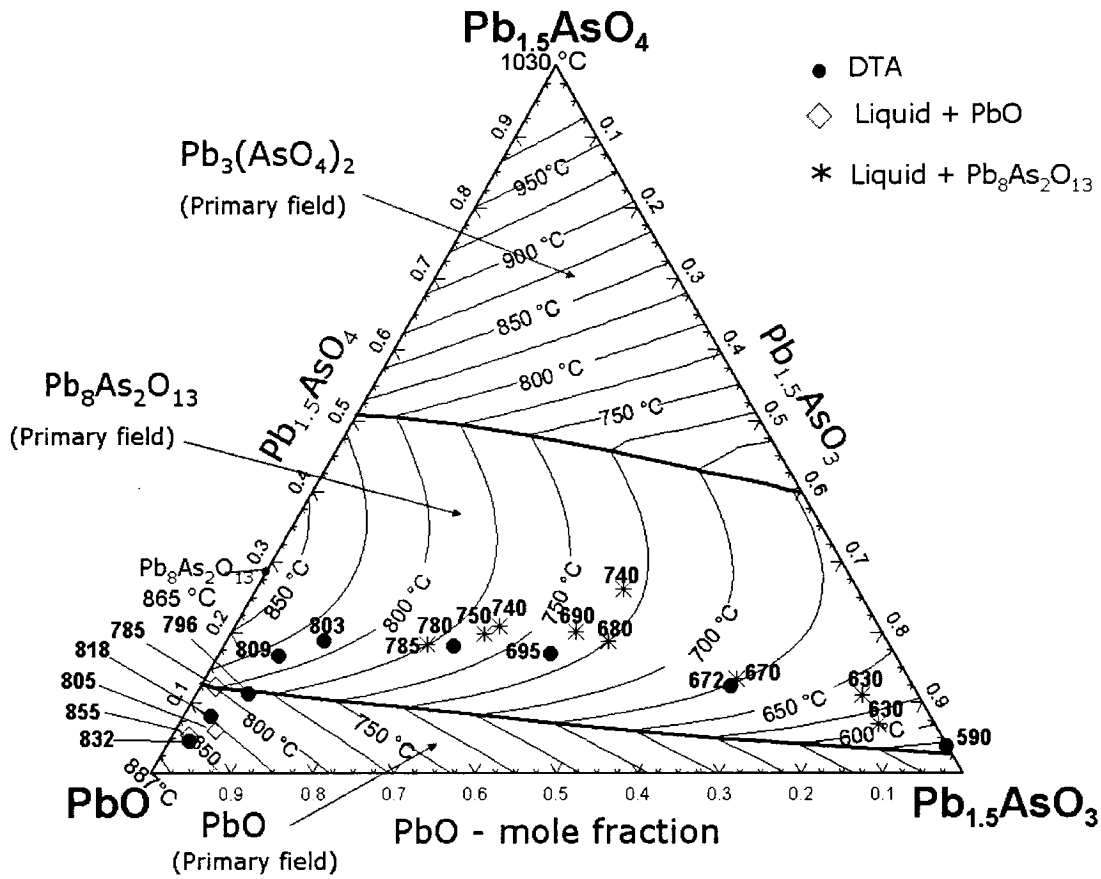

Figure 40 – Calculated projection of liquidus surfaces of the PbO-$Pb_{1.5}AsO_4$-$Pb_{1.5}AsO_3$ ternary system. Experimental values, • DTA, ✱ equilibration and quenching ($Pb_8As_2O_{13}$ primary field) and ◇ equilibration and quenching (PbO primary field).

Figure 41 shows the arsenic distribution predicted by the model between the molten lead and oxide phases along with the experimental values from Zunkel and Larson [34], Gerlach et al. [32], Pelzel [38] and the current study at temperature between 750 and 800 °C. Because only the current study quantitatively differentiated the different valances of arsenic in the oxide phase, the total atomic fraction of arsenic in the oxide was used in order to present all values in one graph.

Table 11 – Thermodynamic properties for one mole of the pure compounds (PbO from [31], $Pb_3(AsO_4)_2$ from [115] and the rest estimated in this work).

	ΔH^0_{298} (J)	S^0_{298} (J/K)	Cp (J/K)	Temperature range (K)
PbO (s)	-218062	68.7	$47.63 + 0.0122T - 4.554e7T^{-3} - 65.75T^{-0.5}$	298-1159
			65.00	1159-2000
PbO (l)	-192540	90.7	= Cp (PbO (s))	298-2000
$Pb_8As_2O_{13}$	-2915492	669.1	$520 + 0.103T - 328.8T^{-0.5} - 3.43e6\ T^{-2} + 1.77e\text{-}5\ T^2 -$	298-1159
			$598 + 0.067T - 3.08e6\ T^{-2}$	1159-1315
$Pb_4As_2O_9$	-2040295	357.3	$487 + 0.021T - 2726.8T^{-0.5} - 3.213e6T^{-2}$	298-1048
$Pb_3(AsO_4)_2$	-1785208	324.6	$208 + 0.0417T - 1.773e\text{-}5T^2 - 3.43e6\ T^{-2}$	298 – 600
			$273 + 0.066T - 6.03e\text{-}5T^2 - 3.08e6\ T^{-2}$	600-1315
$Pb_3(AsO_3)_2$	-1344081	312.0	$355 + 0.038T - 2045T^{-0.5} - 1.26e6\ T^{-2}$	298-607
			$388 - 0.020T - 2045T^{-0.5}$	607-866
$Pb_2As_2O_5$	-1117000	244.1	$158 + 0.137T - 131.5T^{-0.5} - 9.11e7T^{-3}$	298-663
$PbAs_2O_4$	-886278	179.7	$180 + 0.052T - 682T^{-0.5} - 1.26e6\ T^{-2}$	298-607
			$213 - 0.007T - 682T^{-0.5}$	607-866

At 800 °C, the model showed 2 distinct regions. At compositions above ~ 0.07 atomic fraction As, a single-phase liquid-oxide was observed and the arsenic content in the metallic phase increased with an increase in the arsenic in the liquid oxide phase. The increase in arsenic was gradual up to ~ 0.15 atm fraction arsenic in the oxide phase and then rapidly increased. At compositions lower than ~ 0.07 atomic fraction of As in the oxide phase, solid PbO was formed and the arsenic remained unchanged at 0.016 wt% in the metallic phase.

Figure 42 shows a subset of the same information as in Figure 41 up to 1 wt% arsenic in the metallic lead with the Y axis presented in logarithmic scale to better demonstrate the change in the arsenic content in the metallic lead at the low compositional range.

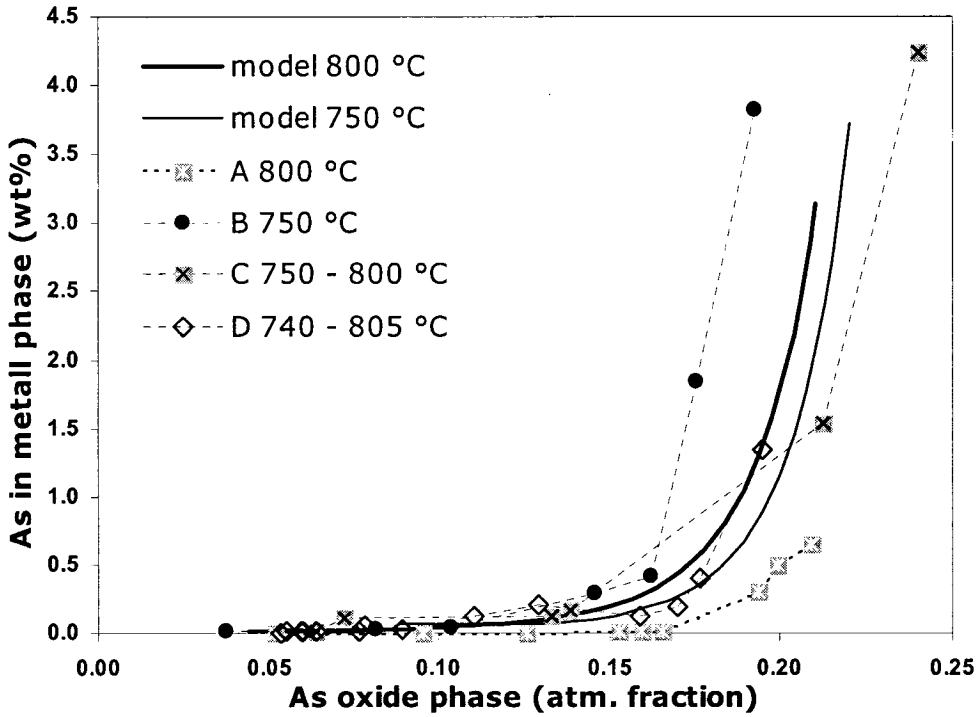

Figure 41 – Model predictions and experimental values of arsenic distribution between metal and oxide phases at 750 °C and 800 °C. A from Gerlach et al. [32], B from Zunkel and Larson [34], C from Pelzel [38] and D present work.

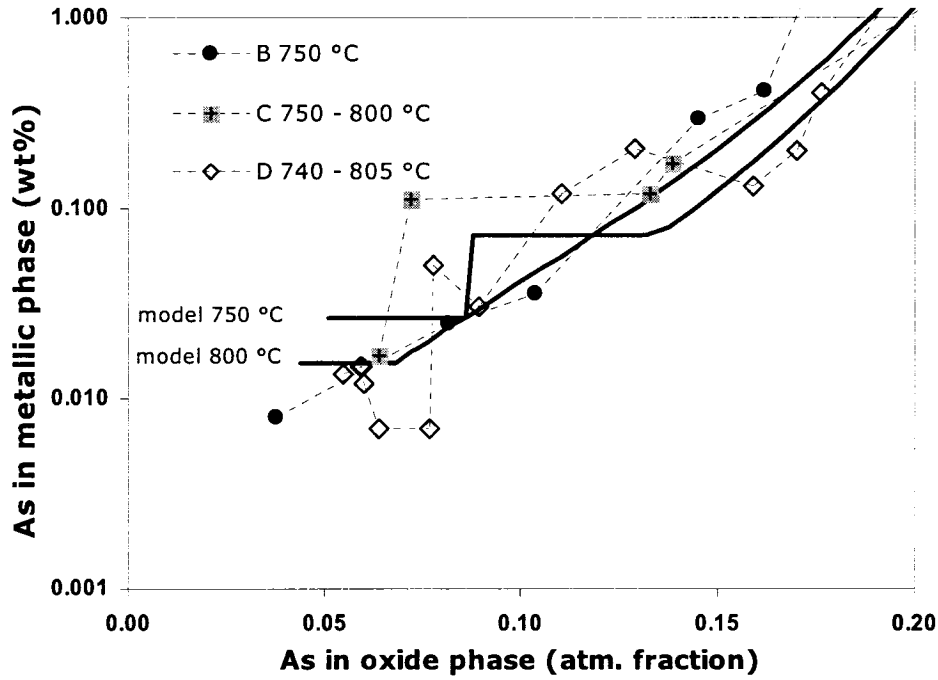

Figure 42 – Same as Figure 41 with Y axis in logarithmic scale for arsenic less than 1 wt% in metallic phase.

At 750 °C a third region was observed at compositions between 0.08 and 0.13 atomic fraction arsenic in the oxide phase. In this region, liquid oxide and the $Pb_8As_2O_{13}$ compound existed together. At ~ 0.13 atomic fraction arsenic, $Pb_8As_2O_{13}$ formed, and at ~ 0.08 atomic fraction arsenic, all the liquid oxide was consumed. These changes corresponded to the steps that were evident in both the predicted and measured values in Figure 42. At lower arsenic content, with formation of PbO(s), the arsenic concentration in the metallic lead remained constant at 0.025 wt%.

Figure 43 shows the arsenic distribution predicted by the model between the molten lead and oxide phases along with the experimental values from Zunkel and Larson [34] and the current study at temperatures between 450 and 650 °C. The three regions that were described above are again observed at both temperatures.

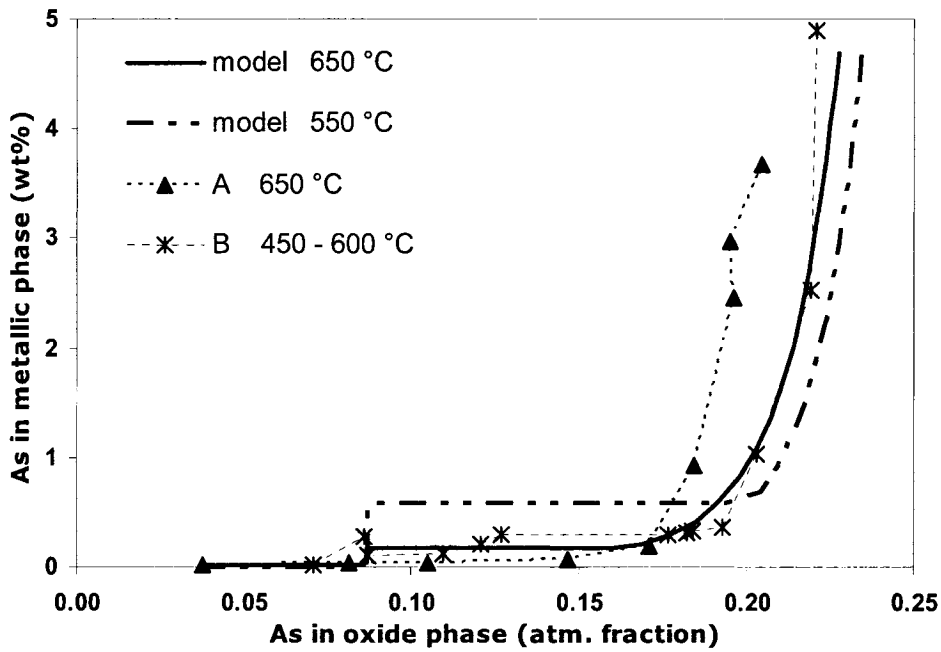

Figure 43 – Model predictions and experimental values of arsenic distribution between metal and oxide phases at temperatures between 450 °C and 650 °C. A from Zunkel and Larson [34], and B present work.

First region: a very low arsenic content in the metal (~ 0.01 wt%) at low arsenic in the slag phase (~ 0.08 atomic fractions As).

Second region, the stability field of $Pb_8As_2O_{13}$: arsenic was constant at 0.6 wt% in metallic lead with varying arsenic (0.08-0.17 atomic fraction) in the oxide phase at 650 °C and similarly arsenic concentration was constant at 0.2 wt% in metallic lead with varying arsenic values (0.08 to 0.2 atomic fraction) in the oxide phase at 450 °C.

The Third region: as arsenic values exceeded ~ 0.2 atomic fraction in the oxide phase the arsenic in metallic lead rapidly increased.

Figure 44 shows the predicted arsenic distributions at 600, 700 and 800 °C. Between 600 and 700 °C the three-region behavior that was previously discussed was observed, and for 800 °C the two-region behavior was observed. In the region where the oxide phase was fully liquid, the model showed that the arsenic in the metallic lead increased with an increase in temperature.

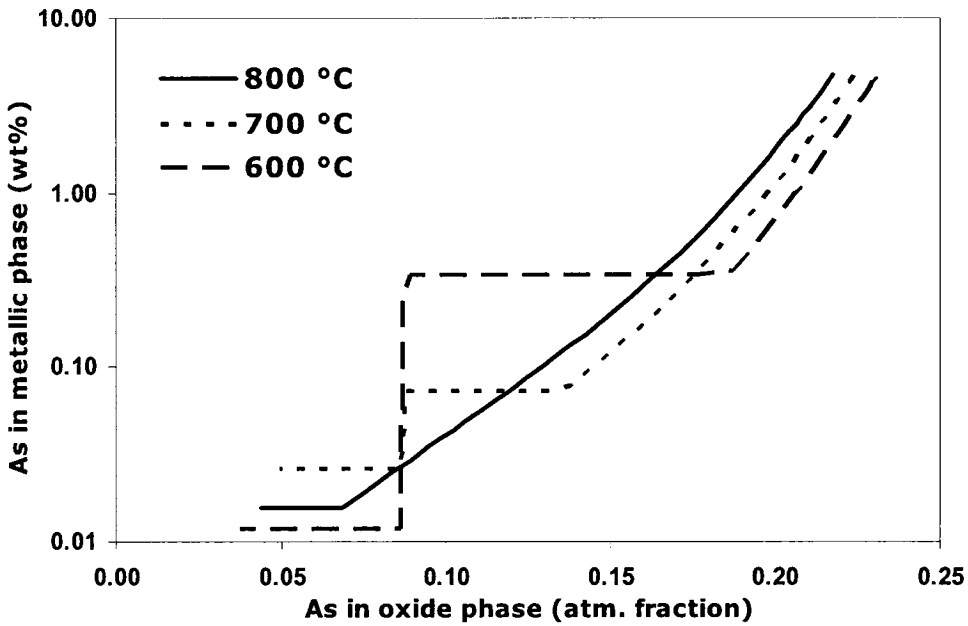

Figure 44 – Model calculation of the arsenic distribution between metal and oxide phases at 600, 700 and 800 °C.

5.3.3.1 Discussion

Reasonable agreement was observed between the model predictions and the experimental values for the liquidus temperatures and primary fields of the observed solids in the

ternary phase diagram of PbO-$Pb_{1.5}AsO_4$-$Pb_{1.5}AsO_3$,. The predicted liquidus temperatures in the PbO primary field were generally higher than the experimental values, and the average difference between the experimental measurements and the model calculations in the PbO primary field was 10 °C. The standard deviation of the difference between the measurements and model prediction was 13 °C[i].

The standard deviation of the difference between the measurements and model prediction was 21 °C in the $Pb_8As_2O_{13}$ primary field. The variation was more noticeable in the center region of the $Pb_8As_2O_{13}$ primary field, where Pb_2AsO_4(s) was observed in the quenched samples at temperatures below 550 °C. It is possible that the larger disparity in this region was due to the effect of Pb_2AsO_4(s) on the liquidus surface that was not included in the current model.

The behavior for the arsenic distribution between the oxide and metallic phase predicted by the model was close to the experimental values reported in the literature and to the results of the current study. One important feature was the flatness of the curve over a wide range of arsenic content in the oxide phase while another was a rapid increase in arsenic content in the metallic lead at arsenic compositions close to the $Pb_3(AsO_3)_2$ (or $3PbO{\cdot}As_2O_3$) and above. This trend was demonstrated in Figure 41 and Figure 43. In this region (i.e., high arsenic content in metallic phase) model predictions showed good agreement with both the results of the present study at the four studied temperature ranges and with results of Pelzel [38]. However the experimental results of Gerlach [32] showed an increase of arsenic in metallic lead at higher arsenic contents (~ 0.28 mol fraction As_2O_3) in the oxide phase, whereas a rapid increase happened at lower arsenic contents (~ 0.22 mol fraction As_2O_3) in Zunkel and Larson's experiments [34].

At lower As_2O_3 concentration, the results of Pelzel showed the same two-region behavior previously explained for equilibria at 800 °C, however the arsenic contents in the metallic phase were higher than the model prediction. Pelzel oxidized Pb-As alloy (~ 9 wt% As) and sampled both the lead and the oxide formed during the oxidation progress. As a

[i] In Section 5.2.3, it was explained that because of appreciable dissolution of alumina in this region (between 0.7 to 1 wt% Al), the liquidus temperatures were expected to be lower than what they would be without dissolution of alumina in PbO.

result, the arsenic content in metallic phase in his experiments would be equal to or greater than, the equilibrium arsenic content. In other words, if equilibrium was not attained in his experiments, the arsenic concentration in the metallic phase would be higher than the equilibrium values. Since Pelzel's experiments were dynamic rather than equilibrium experiments, the higher arsenic content is readily explained, and not a significant objection to the present work.

The results of Zunkel and Larson showed the same behavior and were in good agreement with the model prediction as shown in Figure 43 at 650 °C. Zunkel and Larson claimed to observe the three distinctive regions in their results at 650 °C (Section 5.2.3 discussed these three regions in detail).

In the 750-800 °C temperature region, the results of the current experimental study closely matched the model predictions as shown in Figure 41 and Figure 42. At the lower range of the experimental temperatures (420-600 °C), the three regions that were observed for the present study matched the predictions of the model. However, in the $Pb_8As_2O_{13}$ primary field (i.e., the second region), the model predicted 0.59 wt% arsenic in the metallic phase, which is higher than the average 0.35 wt% arsenic measured in this region.

The arsenic contents in the metallic lead in the Gerlach et al.'s experiments over the compositional range examined was all lower than the predictions of the model at 800 °C. It was not possible to determine the reason for the lower arsenic content measured by Gerlach et al.

The model predictions and experimental results showed that for partial softening of arsenic from metallic lead at a temperature of about 620 °C, as practiced by Teck Cominco, a high arsenic content in the oxide phase (i.e. lower loss of lead for the same arsenic removed) requires the arsenic content in the metallic phase to be above 0.2 wt% (i.e., 0.2 wt% is the onset of the rapid increase of arsenic in the metallic lead at 620 °C). Also, at lower temperature, this rapid increase occurs at a higher arsenic concentration in the oxide phase. This result suggests that a counter-current slag/bullion contacting

scenario, in which slag would be equilibrated with lead with higher arsenic content, would increase the ratio of the As to Pb contents of the slag.

The model was employed to explain the visual observations that were part of the study of the kinetics and mechanisms of lead softening conducted by the current author (Appendix 1) and by Vineberg [1]. Observations by Vineberg of the oxidation of a Pb 1 wt% As molten alloy under a low oxygen partial pressure at ~ 600 °C found the formation of a liquid oxide. This oxide remained liquid after excess oxygen was introduced onto the surface of the melt. However, with time and the progress of oxidation, a solid oxide started to form and eventually covered the entire surface of the melt.

The XRD spectrum of the accumulated solid oxides from that test showed the presence of $Pb_8As_2O_{13}$ and $Pb_4As_2O_9$. In the current author study of the mechanisms of softening, the formation of a liquid oxide was also observed on the surface of a Pb – 1 wt% As melt that was kept under a low oxygen content atmosphere at ~ 600 °C. With the jetting of the oxygen on the surface of the melt, a mixture of liquid and solid oxides appeared to form (Figure 56 and Figure 57). The solid oxides gradually covered the surface of the melt. With the cessation of the oxygen flow and a restarting of argon flow and the sample being kept under a low oxygen content atmosphere for some time, the liquid oxide formed again.

The observations above can be understood with reference to Figure 45, which shows an isothermal section of the Pb-As-O system at 600 °C. The points at the end of the dotted tie line show the composition of the metallic lead and oxide phase in the visual observation experiment presented in Section A.1.3 and in Vineberg's experiments. Figure 45 predicts the presence of a fully liquid slag phase at equilibrium with the Pb-1wt% As molten alloy at the start of the experiments in agreement with the visual observations. With the progress of oxidation, the arsenic content would decrease and solid $Pb_8As_2O_{13}$ would form. This conforms to the formation of a solid phase as observed in Vineberg's study and in the current study. The detected $Pb_8As_2O_{13}$ in Vineberg's result also confirmed the formation of this solid as predicted by the model.

Vineberg detected $Pb_4As_2O_9$ as well as $Pb_8As_2O_{13}$. Figure 45 shows that the stability region of $Pb_3(AsO_4)_2$ and $Pb_4As_2O_9$ are very close to that of $Pb_8As_2O_{13}$. If the surface of the oxide phase was at local equilibrium with oxygen in atmosphere, rather than with the metallic lead, the formation of either $Pb_4As_2O_9$ or $Pb_3(AsO_4)_2$ would be possible. Also, Vineberg allowed prolonged exposure of the samples (~ 60 minutes) to the high oxygen atmosphere, meaning it is reasonable that $Pb_4As_2O_9$ would form.

Formation of a fully liquid phase in the current study after stopping the oxygen jet showed that the composition of the entire molten bath was still within the fully liquid slag region, and that the formation of the solid $Pb_8As_2O_{13}$ had been a local phenomenon.

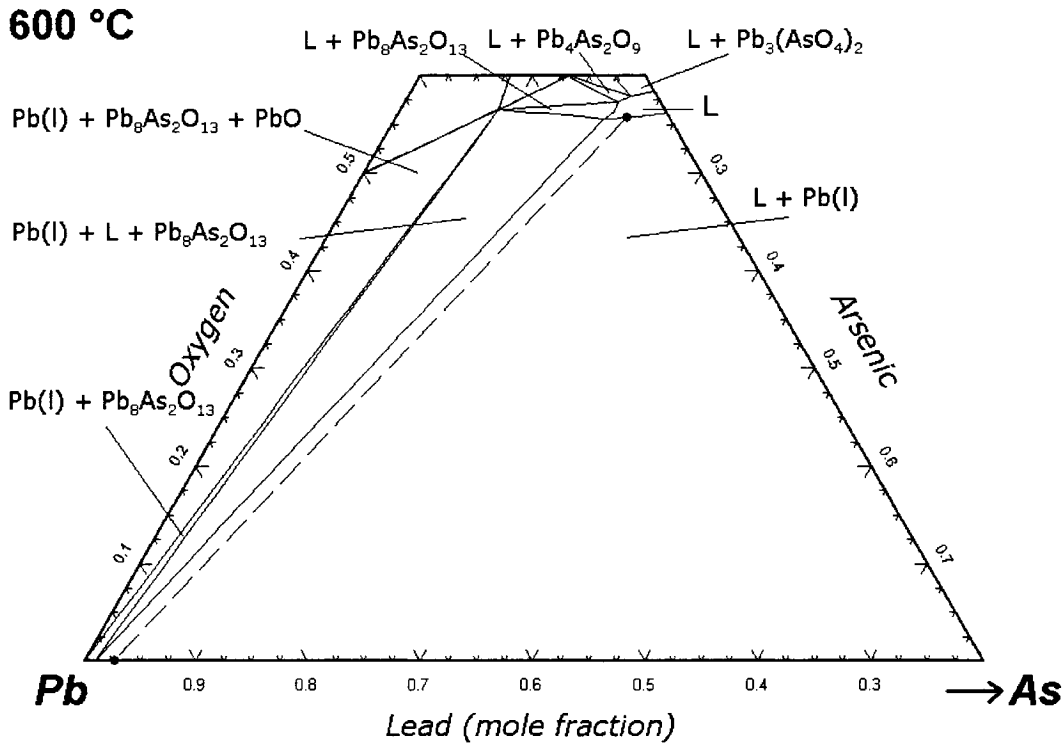

Figure 45 – Isothermal section of the Pb-As-O system at 600 °C. The points at the end of the dotted tie line shows the composition of the metallic lead and oxide phase in the visual observation experiment presented in Section A.1.3 and Vineberg's [1] experiments (figure generated with FACT*Sage*™ [31]).

Vineberg repeated his experiments at 500 °C and again observed a liquid phase on top of the Pb-1 wt% As molten alloy. Oxygen was then introduced on the surface of the melt, and after time and oxidation, the melt was again covered with a solid oxide layer. At 500

°C, the oxides covered the surface of the melt much faster than for the 600 °C experiments (75 s at 500 °C compared with 500 s at 600 °C).

This behavior can be understood with reference to Figure 46, which shows the isothermal section of the Pb-As-O system at 500 °C. The points at the end of the dotted tie line show the composition of the metallic lead and oxide phase in the Vineberg's experiment at 500 °C. It shows the presence of a fully liquid slag phase in equilibrium with the Pb-1wt% As molten alloy at the start of the experiments, which is in agreement with the visual observations. However, it can be seen that the tie line is very close to the $Pb_8As_2O_{13}$ formation line. Thus it is expected that with a slight change of composition, solid $Pb_8As_2O_{13}$ may form. In Vineberg's experiments this was interpreted as a shorter period of time needed to form a solid oxide layer.

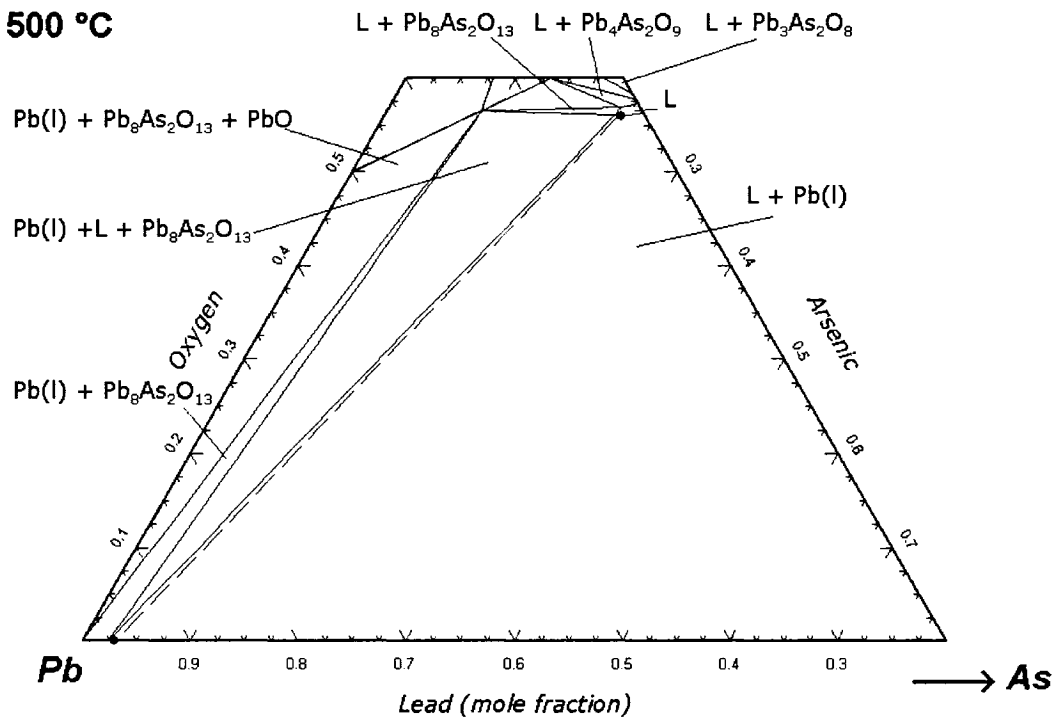

Figure 46 – Isothermal section of the Pb-As-O system at 500 °C. The points at the end of the dotted tie line shows the composition of the metallic lead and oxide phase in Vineberg's [1] experiments (figure generated with FACT*Sage*™ [31]).

Using XRD analysis Vineberg detected $Pb_8As_2O_{13}$, $Pb_4As_2O_9$ and $Pb_3(AsO_4)_2$ in the oxide layer accumulated on the surface of the melt at 500 °C. Similar to what was explained

above for the sample at 600 °C the formation of these solids was predicted based on the phase diagram and the long exposure to the oxygen atmosphere.

5.4 Conclusions

Thermal analysis and equilibration-and-quenching experiments were used to determine the liquidus, eutectic temperatures, and the formation of different oxide phases in the PbO-As_2O_3-As_2O_5 system. Two previously undetected compounds, $Pb_3(AsO_3)_2$, and Pb_2AsO_4 were identified by the electron microprobe analysis of the quenched samples. Change of arsenic distribution between the oxide and metallic phases, and the change of mass ratio of (As^{3+}/total As), suggested a strong tendency for formation of $Pb_3(AsO_3)_2$ ($3PbO{:}1As_2O_3$) in the liquid solution. Formation of $Pb_3(AsO_3)_2$(l) is in agreement with the assumed structure of liquid solution in the PbO-As_2O_3 system with AsO_3^{3-} anions.

The suggested ionic structure of a liquid oxide phase containing Pb^{2+}, O^{2-}, AsO_4^{3-} and AsO_3^{3-} ions was successfully used to reproduce the pseudo-binary phase diagrams and original experimental values in the ternary PbO-As_2O_3-As_2O_5 system. The small magnitude of the the excess Gibbs energy terms that were needed to fit the model to the experimental values were an indication that the assumption that arsenic forms AsO_4^{3-} and AsO_3^{3-} ions, for basic melts, was reasonable.

The model was expanded in the PbO-As_2O_3 system to predict the arsenic distribution in the range of interest. The predictions of the model were in agreement with the experimental results of the current study. The arsenic distribution between the metal and slag phases varied in different reports, but overall the model predictions were close to all but one of the reports. The expansion of the model was simplistic and the use of a more powerful model such as a modified quasichemical model was suggested. The model was able to explain some of the reported observations related to the softening of Pb-As alloys.

CHAPTER 6. CONTRIBUTION TO THE Pb-Sb-O SYSTEM

6.1 Scope

In this chapter, optimization of the thermodynamic model for the lead-antimony-oxygen system in the PbO rich region based on published thermodynamic data is presented, i.e. the PbO rich regions of the PbO-Sb_2O_5 and PbO-Sb_2O_3 pseudo-binaries are optimized and the ternary system is constructed by interpolation from these optimized binaries.

In each section below, the assumptions and the procedure to assess the parameters of the model are first described and then the calculated phase diagrams and the model's equilibrium predictions are presented. The optimization results are discussed and evaluated in each section and conclusions are drawn about the accuracy of the model in describing the various visual observations made to date.

6.2 PbO-Sb_2O_5 System

Thermodynamic properties of the pure compounds:

Using the model defined in Section 3.3, the compounds in the PbO-Sb_2O_5 system up to 25 mol% Sb_2O_5 were considered in the present model. Apart from PbO, the compounds that were reported to exist in this range of antimony oxide contents were $Pb_6Sb_2O_{11}$, $Pb_4Sb_2O_9$ and $Pb_3(SbO_4)_2$ [35, 49, 50, 122].

$Pb_3(SbO_4)_2$ is an end member of the solution model that was developed here. The congruent melting temperature was reported to be between 1240 and 1300 °C [35, 49]. Thermodynamic properties of this compound have not been measured. Nekrasov et al. [113] estimated the properties of this compound, by using an empirical method [116] to predict the heat of formation for double oxide compounds from simple oxides. In their method, if the electronegativity of the central cation on the Poling scale was greater than 1.9, then the heat of Reaction 66, ΔH_r^0, was estimated to be -29.2·M (kJ/mol), where M is the number of oxygen atoms in the double oxide.

$$3\ PbO + Sb_2O_5 = Pb_3(SbO_4)_2 \qquad (66)$$

Other published empirical methods [116, 118] were examined by the author. The other empirical methods required thermodynamic data on the $(SbO_4)^{3-}$ groupings or any other solid compounds in the $PbO\text{-}Sb_2O_5$ binary, but because of the lack of this thermodynamic data, it was not possible to use them. As a result, it was decided to use the method described by Nekrasov et al. [113]. The thermodynamic properties for $Pb_3(SbO_4)_2$(s) that were estimated by this method are presented in Table 12.

The thermodynamic properties of $Pb_6Sb_2O_{11}$ and $Pb_4Sb_2O_9$ were also previously unknown. $Pb_6Sb_2O_{11}$ and $Pb_4Sb_2O_9$ have incongruent melting temperatures at 970 °C and 1020 °C respectively [49]. Properties of these two solids did not effect the properties of the liquid solution and, because of the lack of any thermodynamic data for these compounds, they were not included in the current model.

Liquid solution:

The ionic model for the $PbO\text{-}Sb_2O_5$ pseudo-binary system was introduced in Section 3.4. Because PbO is the only component in the system that has a measured heat of melting, the PbO liquidus curve in the $PbO\text{-}Sb_2O_5$ system was used to calculate the excess Gibbs energy parameter of the $PbO\text{-}Pb_{1.5}SbO_4$ pseudo-binary in Equation67.

$$g = \left(X_{PbO} \cdot g^0_{PbO} + X_{Pb_{1.5}SbO_4}\ g^0_{Pb_{1.5}SbO_4}\right) +$$

$$RT\left(X_{PbO} \ln X_{PbO} + X_{Pb_{1.5}SbO_4} \ln X_{Pb_{1.5}SbO_4}\right) + \omega_{PbO\text{-}Pb_{1.5}SbO_4} \cdot X_{PbO} \cdot X_{Pb_{1.5}SbO_4} \qquad (67)$$

The mole fractions in Equation 67 are in the $PbO\text{-}Pb_{1.5}SbO_4$ system and related to the mole fractions in $PbO\text{-}Sb_2O_5$ system through Equations 68 and 69:

$$X_{PbO} = \frac{X'_{PbO} - 3X'_{Sb_2O_5}}{X'_{PbO} - X'_{Sb_2O_5}} \qquad (68)$$

$$X_{Pb_{1.5}SbO_4} = \frac{2X'_{Sb_2O_5}}{X'_{PbO} - X'_{Sb_2O_5}} \qquad (69)$$

where X' is the mole fraction in the $PbO\text{-}Sb_2O_5$ system and X and is the mole fraction in the $PbO\text{-}Pb_{1.5}SbO_4$ system.

Equation 41 was the basis for calculating the excess parameter as it was described in Section 3.4, however in practice, the "Optimizer" module of the FACT*Sage*™ thermochemical program was used to determine this parameter. The excess Gibbs energy parameter for the $PbO\text{-}Pb_{1.5}SbO_4$ was estimated to be 2350 J/mol[i].

The standard Gibbs energy of $Pb_{1.5}SbO_4(l)$ was estimated by summing the Gibbs energy of melting of $Pb_{1.5}SbO_4$ and the Gibbs energy of solid $Pb_{1.5}SbO_4$. The Gibbs energy of melting was derived from the heat of melting of $Pb_{1.5}SbO_4$ that was estimated via Equation 70:

$$\ln a^{l}_{Pb_{1.5}SbO_4} = -\frac{\Delta h^{0}_{f(Pb_{1.5}SbO_4)}}{RT}\left(1-\frac{T}{T^{0}_{f(Pb_{1.5}SbO_4)}}\right) \tag{70}$$

where T is the measured liquidus temperatures on the liquidus curve of the $Pb_{1.5}SbO_4$ as it was described in Section 3.4. The activity of $Pb_{1.5}SbO_4$ in Equation 70 was calculated using the activity coefficient of $Pb_{1.5}SbO_4$ that was related to the optimized excess Gibbs energy parameter of $PbO\text{-}Pb_{1.5}SbO_4$ via Equation 71:

$$R.T.\ln \gamma_{Pb_{1.5}SbO_4} = 2350\ (X_{PbO})^2 \text{ J/mol} \tag{71}$$

Thereafter the Gibbs energy of melting of this compound that was derived via the estimated heat of melting may be written as:

$$\Delta g^{0}_{f(Pb_{1.5}SbO_4)} = 50866 - 32.73T \text{ J/mol} \tag{72}$$

The defined solution model of $PbO\text{-}Pb_{1.5}SbO_4$ along with the defined solid compounds, were used in the FACT*Sage*™ program to construct the pseudo-binary phase diagram for

[i] From experience this is considered a small value [119].

$PbO\text{-}Pb_{1.5}SbO_4$. The constructed diagram and the experimental values are shown in Figure 47.

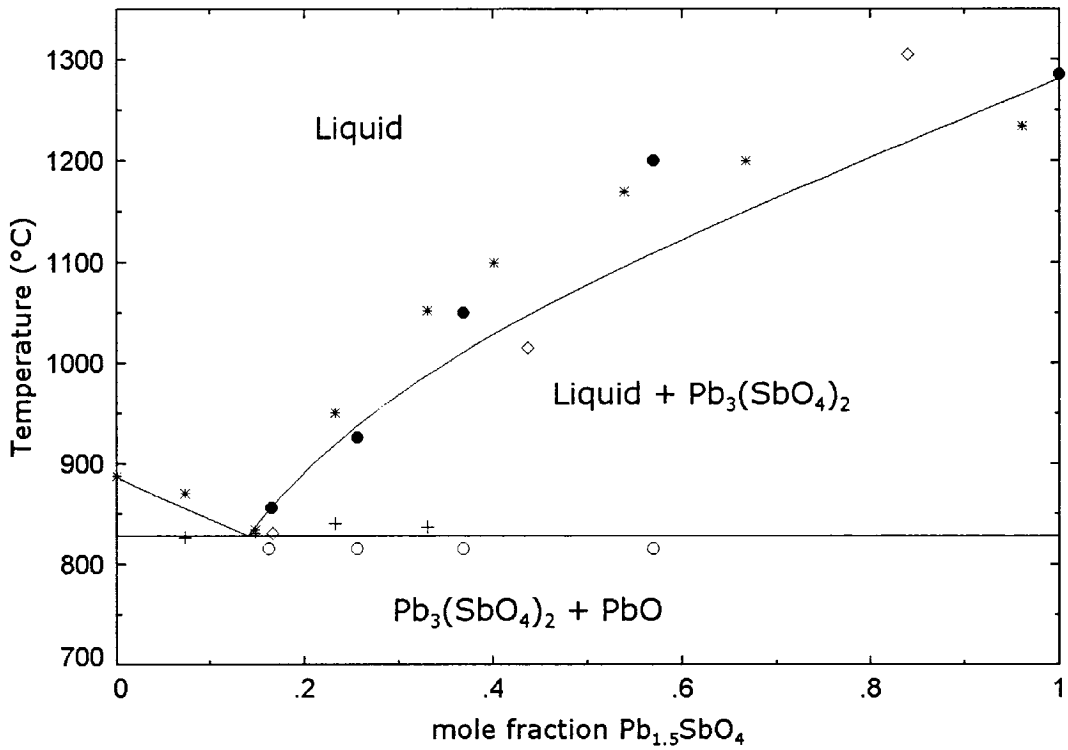

Figure 47 – Phase diagram for $PbO\text{-}Pb_{1.5}SbO_4$ calculated from the thermodynamic model. • liquidus and ○ eutectic temperatures from Hennig and Kohlmeyer [43]; ✱ liquidus and + eutectic temperatures from Bush and Venevtsev [49], ◇ from Gerlach et al. [35] (figure generated with FACT*Sage*™ [31]).

6.2.1 Discussion of the Present $PbO\text{-}Sb_2O_5$ Model

The calculated $PbO\text{-}Pb_{1.5}SbO_4$ pseudo-binary phase diagram, which is in the PbO rich region of the $PbO\text{-}Sb_2O_5$ system, shows good agreement with the measured liquidus and eutectic temperatures. Slight deviation can be observed for the $Pb_{1.5}SbO_4$ liquidus curve. It is likely that the two reported solids that were not included in the model (i.e. $Pb_6Sb_2O_{11}$ and $Pb_4Sb_2O_9$), affected the liquidus curves and therefore caused the observed deviation.

It was found that only one excess energy parameter with a small value was necessary to fit the model to the experimental values. In fact, the assumption of ideal behavior, i.e. no excess term, showed reasonable agreement between the model calculations and the experiment results (figure not shown). Consequently, it was concluded that the assumed

ideal interaction and random distribution of the O^{2-} and $(SbO_4)^{3-}$ ions were close to reality, meaning that the assumed ionic structure of the liquid oxide with the Pb^{2+} cation and O^{2-} and $(SbO_4)^{3-}$ anions was reasonable to represent the system.

Similar to the $PbO\text{-}As_2O_5$ system, the structure of the oxide phase is more complex than the presence of only Pb^{2+}, O^{2-} and $(SbO_4)^{3-}$ ions in the solution and there is a possibility of polymerization of the $(SbO_4)^{3-}$ even in the ultra rich PbO region of the solution. However in the current model the presence of any other species was ignored.

The standard Gibbs energy of solid $Pb_3(SbO_4)_2$ was estimated using the empirical equations mentioned above. Since the standard Gibbs energy of $Pb_{1.5}SbO_4$ in the solution was derived from the summation of the empirical value and the calculated heat of melting, an unreported and hence unknown degree of uncertainty is associated with the values for this component. However, it should be noted that because $Pb_3(SbO_4)_2$ is an essential component of this system, other thermodynamic models, e.g. the quasichemical model, would also suffer because of the uncertainty in the properties of this compound.

6.3 PbO-Sb_2O_3 System

Thermodynamic properties of the pure compounds:

In the PbO rich region, several reports have shown the existence of a $Pb_5Sb_2O_8$ compound with a congruent melting point at about 640 °C (Figure 12) [35, 44, 122]. The presence of $Pb_3(SbO_3)_2$, which was an end member of the present solution model, was reported by Barthel [44], and Freidman and Mustaev [123]. Figure 12 shows incongruent melting for this compound at about 580 °C. The $PbSb_2O_4$ compound is reported in many articles [41, 43-45] with a melting temperature ranging from 564 °C to 650 °C. However, no thermodynamic properties were reported for any of these compounds.

Initially, Equations 73 to 75 with $\Delta G^0 = 0$ were used to estimate an initial value for the Gibbs energies of these compounds. Subsequently, the standard heats of formation of these compounds were changed during the optimization (see the following section) to match melting temperatures of the predicted to the measured. The thermodynamic

properties for the solid compounds that were estimated by this method are presented in Table 12.

$$5PbO_{(s)} + Sb_2O_{3\,(s)} = Pb_5Sb_2O_{8\,(s)} \quad (73)$$

$$3PbO_{(s)} + Sb_2O_{3\,(s)} = Pb_3Sb_2O_{6\,(s)} \quad (74)$$

$$PbO_{(s)} + Sb_2O_{3\,(s)} = PbSb_2O_{4\,(s)} \quad (75)$$

Liquid solution:

The ionic model for the $PbO\text{-}Sb_2O_3$ system was introduced in Section 3.4. Similar to the $PbO\text{-}Sb_2O_5$ system, the PbO liquidus temperatures measured in the $PbO\text{-}Sb_2O_3$ pseudo-binary [37, 41, 44] were used to calculate the excess Gibbs energy parameter in the $PbO\text{-}Pb_{1.5}SbO_3$ pseudo-binary. Similar equations were used for both the $PbO\text{-}Pb_{1.5}SbO_4$ system (Equations 67 to 71) and this system, with Sb_2O_3 replacing Sb_2O_5 and $Pb_{1.5}SbO_3$ replacing $Pb_{1.5}SbO_4$. With the same method that was used for the $PbO\text{-}Sb_2O_5$ system, the excess Gibbs energy parameter for $PbO\text{-}Pb_{1.5}SbO_3$ was estimated to be -2430 J/mol[i].

Equation 76 was used to calculate the standard Gibbs energy of $Pb_{1.5}SbO_3$ (l).

$$1.5\ PbO_{(l)} + \tfrac{1}{2}\ Sb_2O_{3\,(l)} = Pb_{1.5}SbO_{3\,(l)} \quad (76)$$

$$K_{eq} = \frac{a_{Pb_{1.5}SbO_3}}{a_{PbO}^{1.5}\ a_{Sb_2O_3}^{0.5}} \quad (77)$$

In order to calculate the equilibrium constant, Equation 77, the published activities of PbO and Sb_2O_3 between 650 ° and 950 °C were used [37, 46, 47]. The activity of $Pb_{1.5}SbO_3$ (l) was derived from the optimized excess Gibbs energy as described in Section 3.4. Thereafter, with the known standard Gibbs energies of PbO and Sb_2O_3, the temperature dependant standard Gibbs energy for $Pb_{1.5}SbO_3$ was determined (Table 13). The heat capacity for this component was estimated via the relationship:

$$C_p\ (Pb_3(SbO_3)_2) = 3C_P\ (PbO(l)) + C_P\ (Sb_2O_3(l)) \quad (78)$$

[i] From experience this was considered to be a small value [119].

The defined model was not sufficiently accurate to calculate the antimony distribution between the metal and oxide phases over the range of interest because, at the limit of the range, the activity of PbO in the PbO-$Pb_{1.5}SbO_3$ system becomes zero. This means that metal/oxide equilibrium calculations were not possible. To overcome this deficiency, the model was expanded by the addition of another species. To this end, Maier and Hincke [41] suggested the presence of $PbSb_2O_4$ (or $PbO{\cdot}Sb_2O_3$) species in the liquid oxide, based on their vapor pressure measurements (see Section 2.4). This compound corresponds to the $(SbO_2)^{1-}$ group. As a result, the $PbSb_2O_4$ compound was introduced into the model. Since the properties of this compound were not measured previously, Reaction 79 was used to estimate its properties.

$$PbO_{(l)} + Sb_2O_{3\,(l)} = PbSb_2O_{4\,(l)} \tag{79}$$

$$K_{eq} = \frac{a_{PbSb_2O_4}}{a_{PbO} \cdot a_{Sb_2O_3}} \tag{80}$$

Similar to the treatment of $Pb_{1.5}SbO_3$, the equilibrium constant, Equation 80, was calculated from the published activities of PbO and Sb_2O_3 [37, 46, 47]. The activity of $PbSb_2O_4$ was set equal to its mole fraction. In order to minimize the error caused by this assumption of ideal behavior, only compositions close to pure $PbSb_2O_4$ were considered. Subsequently, with the known standard Gibbs energies of PbO and Sb_2O_3, the temperature dependant standard Gibbs energy for $PbSb_2O_4$ was determined (Table 13).

Finally, the heats of formation of the solid compounds (i.e., $Pb_5Sb_2O_8$, $Pb_3(SbO_3)_2$ and $PbSb_2O_4$) that were initially estimated from Equations 73 to 75 were modified to match the predicted melting temperatures with their measured melting temperatures. The calculated pseudo-binary phase diagram for PbO-$Pb_{1.5}SbO_3$, where the model was optimized in this range, is shown in Figure 48. The PbO-Sb_2O_3, pseudo-binary up to 0.5 mol fraction Sb_2O_3 that was constructed with the expanded model, is shown in Figure 49. The calculated distribution of the antimony between the metal and the oxide phases is presented in the next Section in which the PbO rich region of the ternary system PbO-Sb_2O_3-Sb_2O_5 is described.

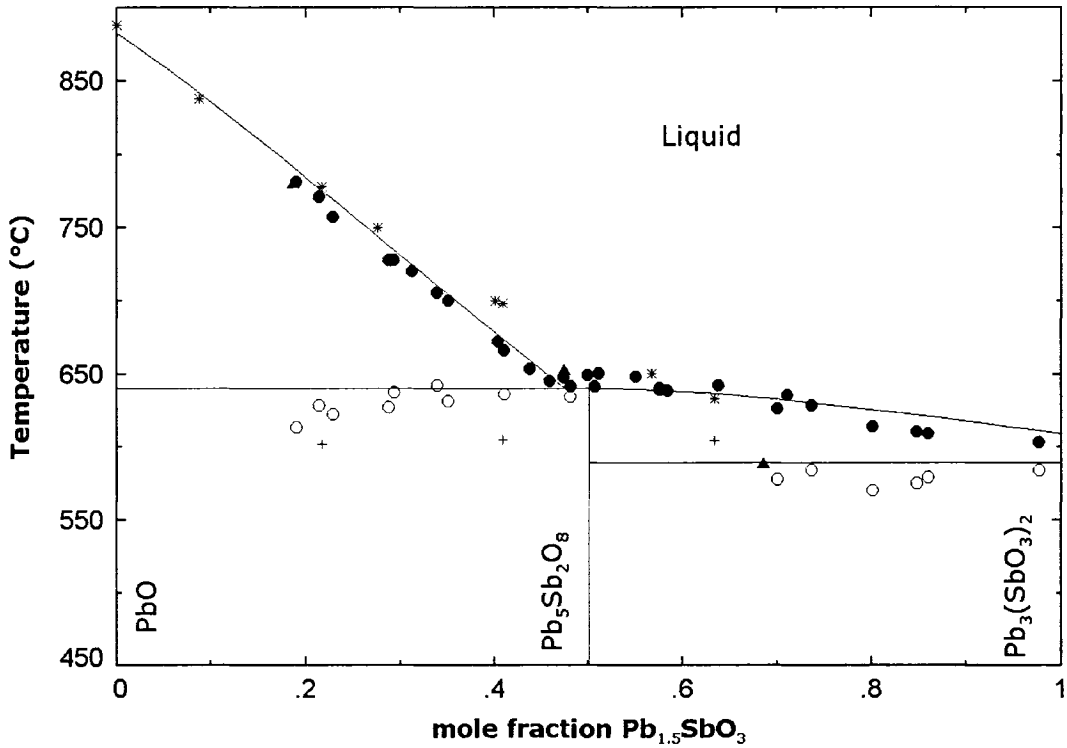

Figure 48 – Phase diagram of PbO-$Pb_{1.5}SbO_3$ calculated from the thermodynamic model. • liquidus and ○ eutectic temperatures from Barthel [44]; ✱ liquidus and + eutectic temperatures from Zunkel and Larson [37] and ▲ from Maier and Hincke [41] (figure generated with FACT*Sage*™ [31]).

Table 12 – Thermodynamic properties for one mole of the pure compounds estimated in this work).

	ΔH^0_{298} (J)	S^0_{298} (J/K)	*C*p (J/K)	Temperature range (K)
$Pb_3(SbO_4)_2$	-1859172	328.7	$207.45 + 0.17T$	298-1573
$Pb_3(SbO_3)_2$	-1397650	340.6	$234.97 + 0.1028T - 1.36e8T^{-3} - 197T^{-0.5}$	298-880
$Pb_5Sb_2O_8$	-1854600	464.2	$330.2 + 0.12738T - 2.28e8T^{-3} - 328T^{-0.5}$	298-910
$PbSb_2O_4$	-937865	198.95	$179.29 + 0.0594T - 681T^{-0.5}$	298-845

Table 13 – Standard molar Gibbs energy of the component that were used in the liquid solution model.

i	g_i^0 (J/mol)
$Pb_3(SbO_4)_2$(l)	$-1837966 + 1060.2T - 8.961\text{e-}2\,T^2 - 207.4\,T\ln(T)$
$Pb_3(SbO_3)_2$(l)	$-1369672 + 1603.6T - 1.84\text{e-}2T^2 + 2.3\text{e}7T^{-2} - 789T^{0.5} - 299.8T\ln(T)$
$PbSb_2O_4$(l)	$-934126 + 1123.3T - 6.13\text{e-}3T^2 + 7.60\text{e}6T^{-2} - 263T^{0.5} - 204.5T\ln(T)$

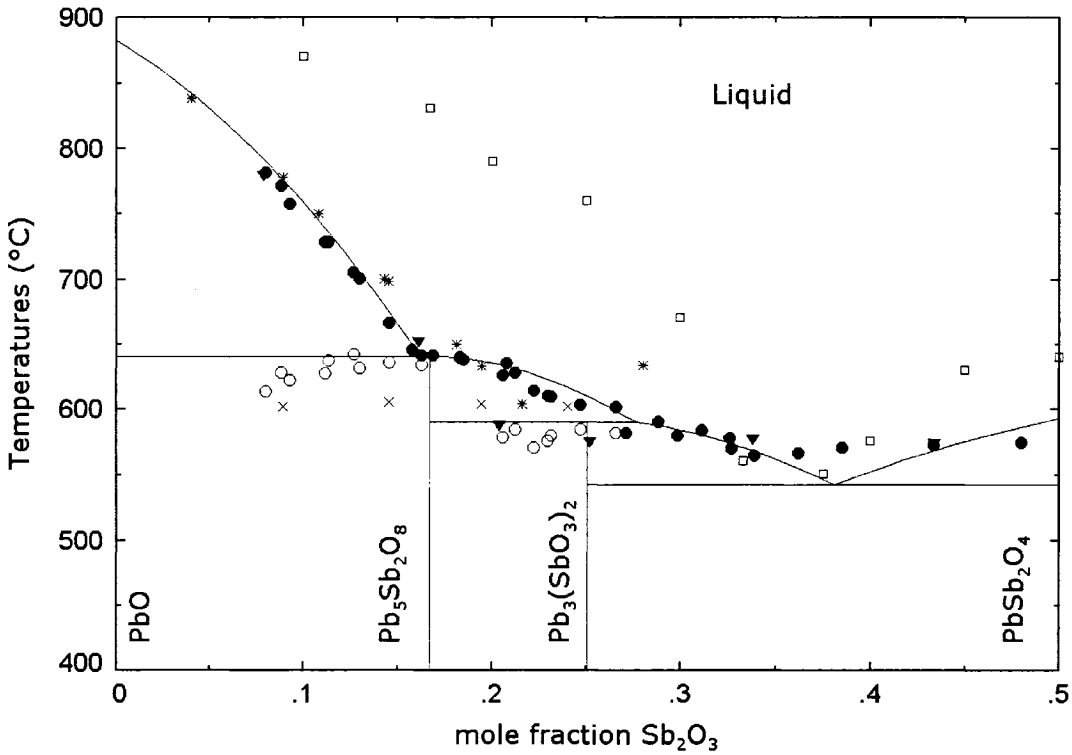

Figure 49 – Phase diagram of PbO-Sb_2O_3 calculated from the thermodynamic model. • liquidus and ○ eutectic temperatures from Barthel [44]; ✱ liquidus and × eutectic temperatures from Zunkel and Larson [37], ▼ liquidus from Maier and Hincke [41] and □ liquidus from Hennig and Kohlmeyer [43].

6.3.1 Discussion of the Present PbO-Sb_2O_3 Model

The calculated phase diagram PbO-$Pb_{1.5}SbO_3$ (Figure 48) pseudo-binary showed good agreement with the experimental values of Barthel [44], Maier and Hincke [41] and Zunkel and Larson [37]. Results from Hennig and Kohlmeyer [43] showed substantial

deviation from all the other experimental results (Figure 12) and were thus not considered in the optimization. Because only a single excess Gibbs parameter with a small value was necessary to fit the model to the experimental values, similar to the $PbO\text{-}Pb_{1.5}SbO_4$ system, it was concluded that in the basic region of the $PbO\text{-}Sb_2O_3$ pseudo-binary, the assumed Pb^{2+}, O^{2-} and $(SbO_3)^{3-}$ ionic structure was reasonable.

It was necessary to expand the $PbO\text{-}Sb_2O_3$ pseudo-binary because the initial model was not accurate for equilibrium calculations between the metal and oxide phase in the region of interest for softening. The expansion could have been accommodated using the assumption of the formation of oxygen sharing dimers of $(SbO_3)^{3-}$ in the form of $(Sb_2O_5)^{4-}$ ions. However, no report was found to suggest the presence of this type of structure in either liquid or solid form and because Maier and Hincke [41] suggested that the $PbSb_2O_4$ compound existed in the liquid $PbO\text{-}Sb_2O_3$ system, the $(SbO_2)^{1-}$ group that corresponded to the composition of $PbSb_2O_4$, seemed to be a better choice.

The assumption of ideal activity for $PbSb_2O_4$ and no interaction between $PbSb_2O_4$ and $Pb_3(SbO_3)_2$ in the solution was simplistic. In order to consider polymerization that would allow an extension of the range of composition, a more advanced model e.g. a modified quasichemical model, [121] would be a better choice (see Section 5.3.1.1 for a brief description of the use of the quasichemical model). The calculated phase diagram of $PbO\text{-}Sb_2O_3$ (Figure 49) deviated from the experimental values above 0.4 mol fraction of Sb_2O_3. In general, the present model is not suggested for use near the 0.5 mole fraction Sb_2O_3 limit.

6.4 $PbO\text{-}Sb_2O_5\text{-}Sb_2O_3$ System and Its Application

For interpolation of the binary systems to ternaries, the Kohler symmetric approximation [96] was used without ternary parameters. Figure 50 shows the calculated liquidus projection of $PbO\text{-}Pb_{1.5}SbO_3\text{-}Pb_{1.5}SbO_4$ along with the experimental values from Hennig and Kohlmeyer [43]. The primary regions for PbO, $Pb_3(SbO_4)_2$ and $Pb_5Sb_2O_8$ are shown in the graph. The univariant lines are shown with thicker lines.

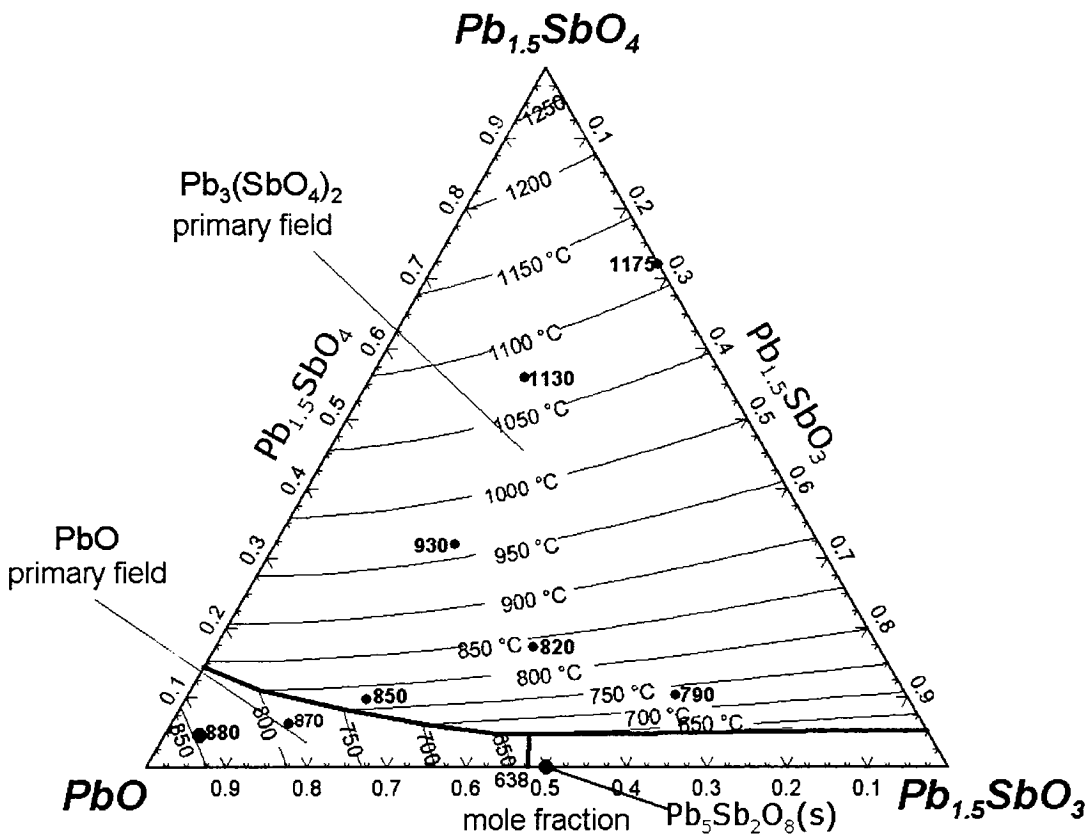

Figure 50 – Calculated projection of liquidus surfaces of the PbO-$Pb_{1.5}SbO_4$-$Pb_{1.5}SbO_3$ ternary system, experimental values from Henning and Kohlmeyer [43] (figure generated with FACT*Sage*™ [31]).

Equilibrium antimony distributions between the molten metal and the oxide phases were calculated using the Gibbs energy minimization module of the FACT*Sage*™ [31] thermochemical program. The databases that were used for equilibrium calculations were the present Pb-Sb-O oxide solution, the pure oxide compounds in Table 12, and the liquid Pb solution database which is part of the FACT*Sage*™ [31] solution databases. Figure 51 shows the calculated distribution of antimony between the metal and oxide phases at 750 °C in comparison with the measured values from different published studies [33, 37, 44, 47]. It should be noted that in Figure 51 all the antimony in the oxide phase was considered to be Sb_2O_3 regardless of its oxidation state in order to make the comparison between the measurements and model predictions possible. This assumption was not problematic because the equilibrium calculations found that antimony existed in the oxide

phase mainly as trivalent oxides over the range of compositions and temperature considered.

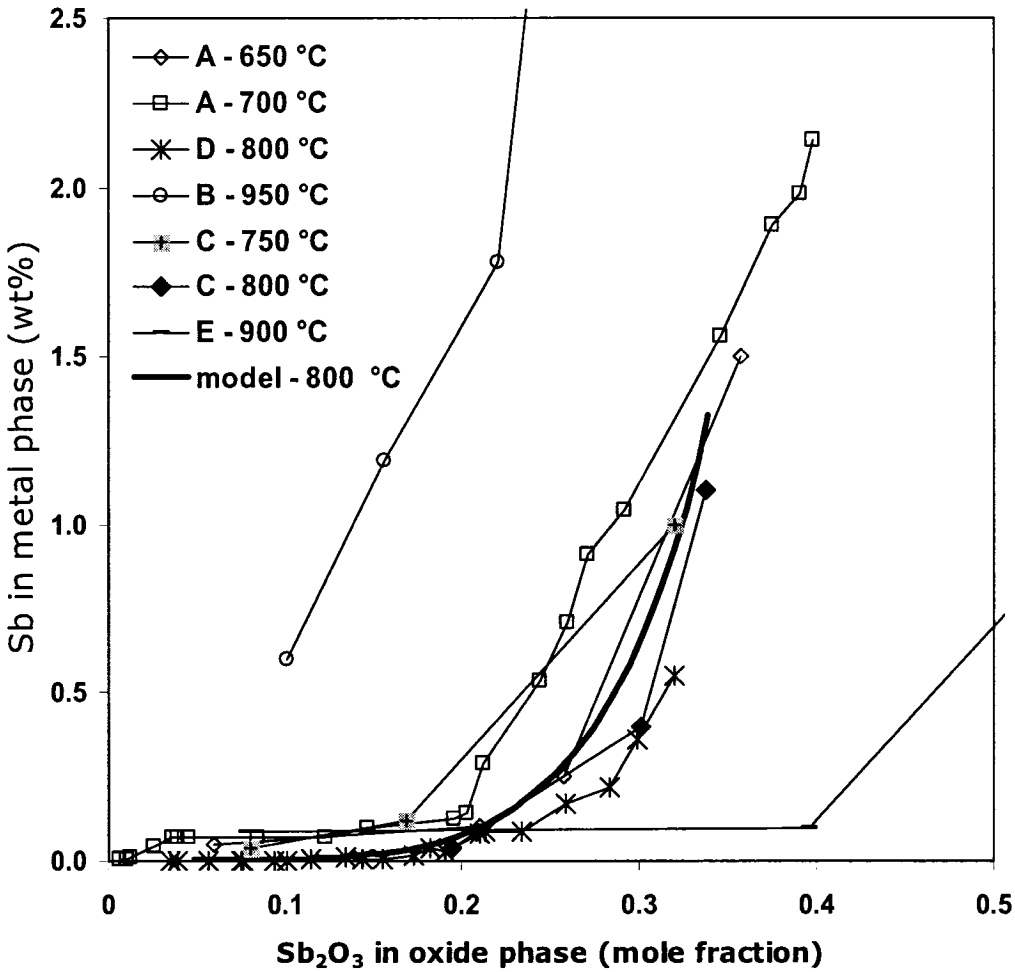

Figure 51 – Calculated antimony distribution between metal and oxide phases at 800 °C in comparison with the measured experimental values. A from Zunkel and Larson [37], B from Itoh et al. [47] C from Pelzel [33], D from Barthel [44] and E from Wang et al. [48].

Figure 52 shows the predicted antimony distribution between the oxide and metal phases at 3 temperatures between 650 and 850 °C. In this temperature range, and over the single-phase liquid oxide region, the model predicted lower antimony content in the metal phase, at a constant antimony content in the oxide phase, as the temperature decreased. The lower limit of antimony oxidation occurred after the formation of a PbO solid phase.

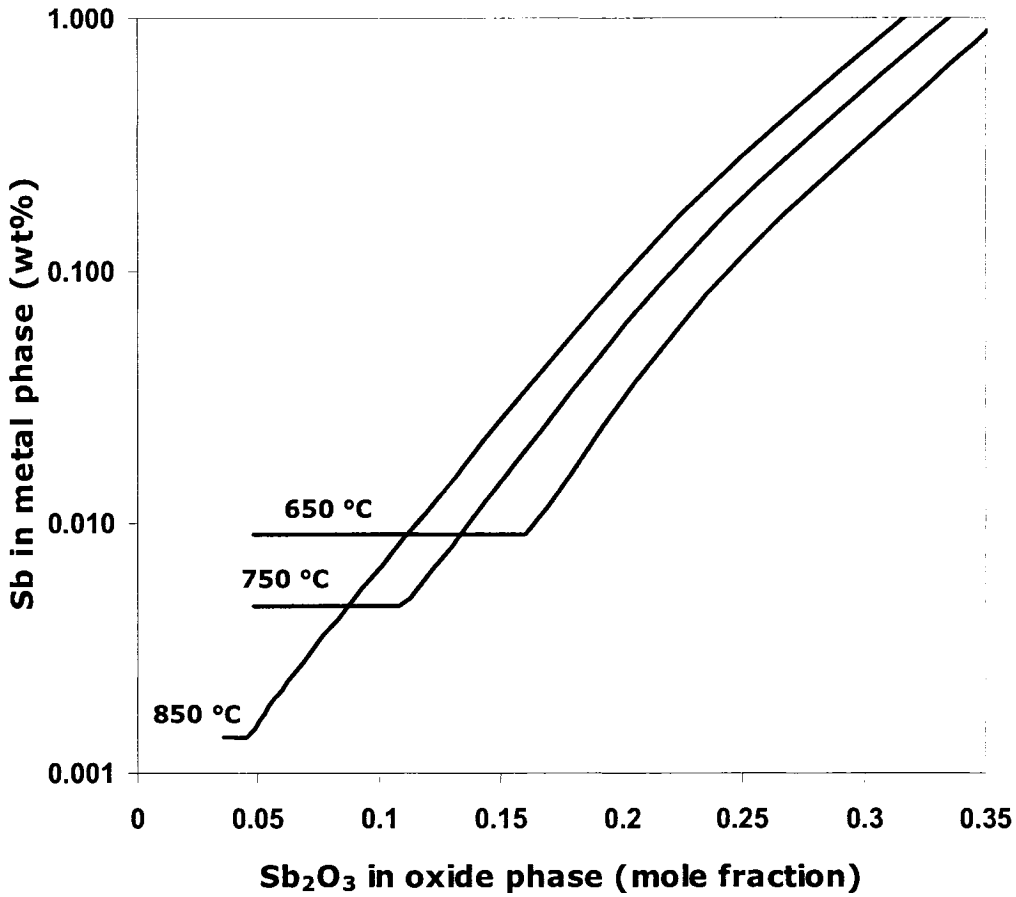

Figure 52 – Calculated antimony distribution between metal and oxide phases between 650 and 850 °C.

Interpolation of the Pb-As-O and Pb-Sb-O systems into quaternary Pb-As-Sb-O system:

The optimized solution models of the Pb-As-O and Pb-Sb-O systems were interpolated to produce a Pb-As-Sb-O solution model without the use of any additional excess Gibbs energy terms (i.e. ideal mixing was assumed), and it was assumed that no new As and/or Sb species were formed. This model was not optimized, although it was used to calculate the equilibrium conditions in a simulated Teck Cominco softening operation using 100 g lead bullion with 1.6 g Sb and 0.6 g As at 620 °C and a stepwise addition of a total 0.3 g oxygen. The final calculated equilibrium composition was comprised of lead bullion with 0.7 wt% Sb and 0.5 wt% As and a liquid slag phase with 60 wt% Pb, 25 wt% Sb and 4 wt% As. The result of the calculation was not in good agreement with the reported Teck

Cominco slag composition (Table 1) and showed that further study of the quaternary system is required.

6.4.1 Discussion of the Present Ternary Model

Experimental values from Hennig and Kohlmeyer [43] were the only set available for comparison with the interpolated[i] ternary phase diagram for PbO-$Pb_{1.5}SbO_3$-$Pb_{1.5}SbO_4$. On the PbO liquidus, the predicted phase diagram did not correlate to the experimental measurements of Hennig and Kohlmeyer. However, their results showed substantially higher liquidus temperatures than all other reported values for the PbO-Sb_2O_3 pseudo-binary [37, 41, 44], and the observed lower liquidus temperatures were to be expected.

On the $Pb_{1.5}SbO_4$ liquidus surface, the predicted isotherms showed reasonable agreement with the measurements of Hennig and Kohlmeyer. Nevertheless, because it was speculated that the measurements of Hennig and Kohlmeyer on the PbO-Sb_2O_3 binary were not reliable (Section 2.4), parameters in the model were not changed to fit the model to these values. Undoubtedly, if the model were to be fitted to the experimental values of Hennig and Kohlmeyer, then it ceases to fit the other [37, 41, 44] experimental values. No other experimental values were available to compare with the model prediction and thus experiments are required to evaluate this phase diagram and if necessary to adjust the parameters of the model to reproduce the ternary system.

The calculated antimony distribution between the oxide and metal phase, Figure 51, showed reasonable agreement with the results of Barthel [44], Zunkel and Larson [37], and Pelzel [33] up to 0.35 mol% Sb_2O_3. The model at 800 °C and these sets of results between 650 and 800 °C showed relatively low antimony content in the metal phase up to ~ 20 mol% Sb_2O_3 (Figure 51). Beyond this composition, a rapid increase in the antimony content of the metal phase was observed both from the model and these sets of experimental results.

The results from Itoh et al. [47] showed considerably higher antimony distributions to the metal phase as compared to the other workers measurements and the ternary model

[i] Kohler symmetric interpolation [96] without any ternary parameters.

predictions. Results from Wang et al. [48] showed similar behavior to the results of Barthel [44], Zunkel and Larson [37], and Pelzel [33] and the predicted model calculations up to 0.2 mol fraction Sb_2O_3 (Figure 51), however the sharp increase in Sb in the metal phase occurred at only ~ 40 mol% Sb_2O_3 in the oxide phase. The reason for this discrepancy is not obvious.

Comparing the three lines on Figure 52, the model showed at greater than 14 mol% Sb_2O_3, and with an increase in the temperature, the antimony content of the metal phase was increased and was in good agreement with the findings of Zunkel and Larson who studied the effect of temperature. The reason for such a behavior was that with the onset of the formation of solid PbO, the oxidation of antimony stopped, thereby fixing the limit of further antimony oxidation. Since at higher temperatures the formation of solid PbO occurred at lower Sb_2O_3 concentrations, the minimum antimony that could be achieved was lower.

Observations by Vineberg [1] of the oxidation of a Pb 2 wt% Sb molten alloy, by oxygen, found the formation of a solid oxide at the surface of the melt at 500 °C. The two full circles at the end of the dotted tie line in Figure 53 show the composition of the liquid lead alloy and the solid oxides that are in equilibrium with it. From the present model, the solid oxides, PbO, $Pb_5Sb_2O_8$ and $Pb_3(SbO_3)_2$ would be present at equilibrium with this molten metallic lead alloy at 500°C. No liquid oxide formed at 500 °C in Vineberg's experiments, and Figure 53 is in agreement with Vineberg's experiments showing no liquid oxide being formed.

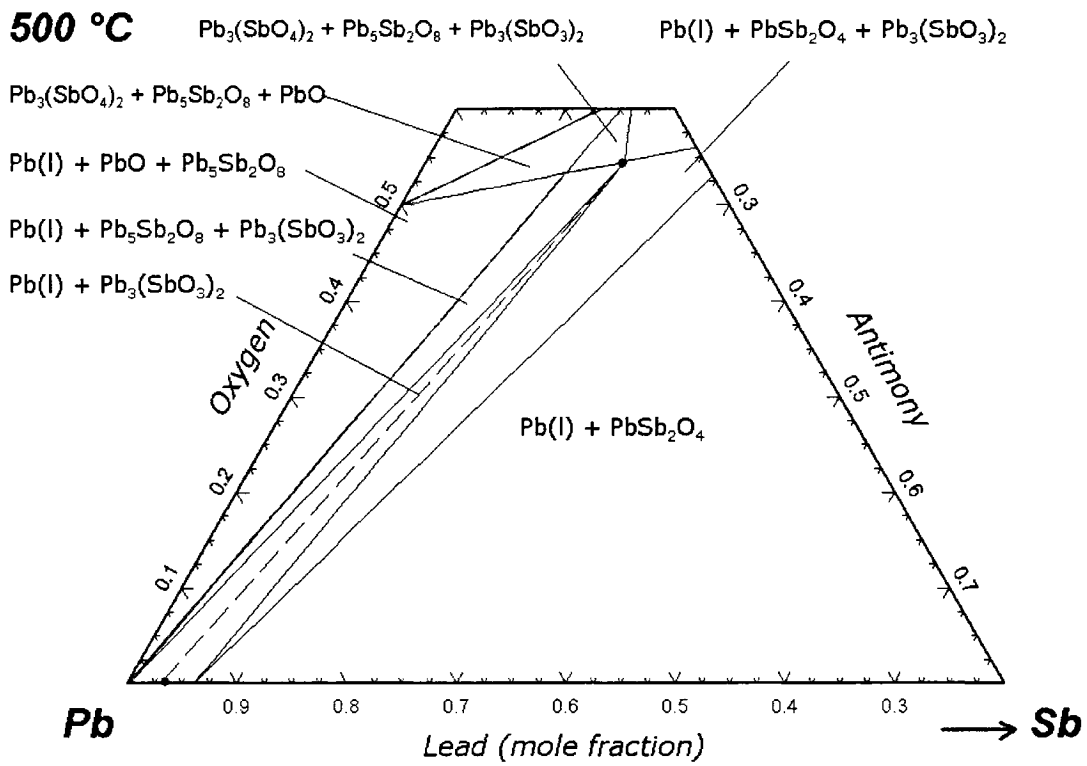

Figure 53 – Isothermal section of the Pb-Sb-O ternary system at 500 °C. Two dots at the end of tie line show the starting composition of Vineberg experiment [1]. (graph generated by FACT*Sage*™ [31]).

Vineberg performed the same experiment at 600 °C and observed that once the liquid lead had been kept under a low oxygen partial pressure for some extended period of time, a liquid oxide was formed on the surface of the melt. This liquid oxide remained even after pure oxygen was introduced onto the surface of the melt, but with time and the progression of oxidation, a solid oxide started to form which eventually completely covered the surface of the melt. The XRD spectrum of the accumulated oxides from that test (Figure 70 in Appendix 3)[i] showed the presence of PbO, $Pb_5Sb_2O_8$ and was in agreement with the predictions of the present model. $Pb_4Sb_2O_9$ was also observed. Paulin et al. [52] reported that during the softening of lead antimony alloy with oxygen enriched air at temperatures below 640 °C, a solid skim was formed and the XRD analysis showed this skim consisted mainly of $Pb_5Sb_2O_8$ and PbO. The presence of the $Pb_4Sb_2O_9$ that was observed only in Vineberg's experiments might have occurred because of a local equilibrium being established between the top surface of the solid oxide layer

[i] The XRD analysis was conducted by the current author on materials obtained from Vineberg.

and the oxygen gas ($P_{O2} \approx 1$ atm). This could have happened as the sample was kept under the oxygen gas for an extended period of time (~ 60 minutes). Paulin et al. used subsurface injection of oxygen enriched air in which the oxidizing air sees fresh lead alloy compared with static experiments of Vineberg in which oxygen had to diffuse through a solid oxide layer. As a result, it can be assumed that the oxide phase in the experiments by Paulin et al. was more likely to be at equilibrium with the metallic lead.

Figure 54 is the prediction of the model of the phases formed at equilibrium between the metal and oxide at 620 °C. The two full circles at the end of dotted tie line show the composition of the molten lead alloy and the fully liquid oxide phase at equilibrium with the molten lead.

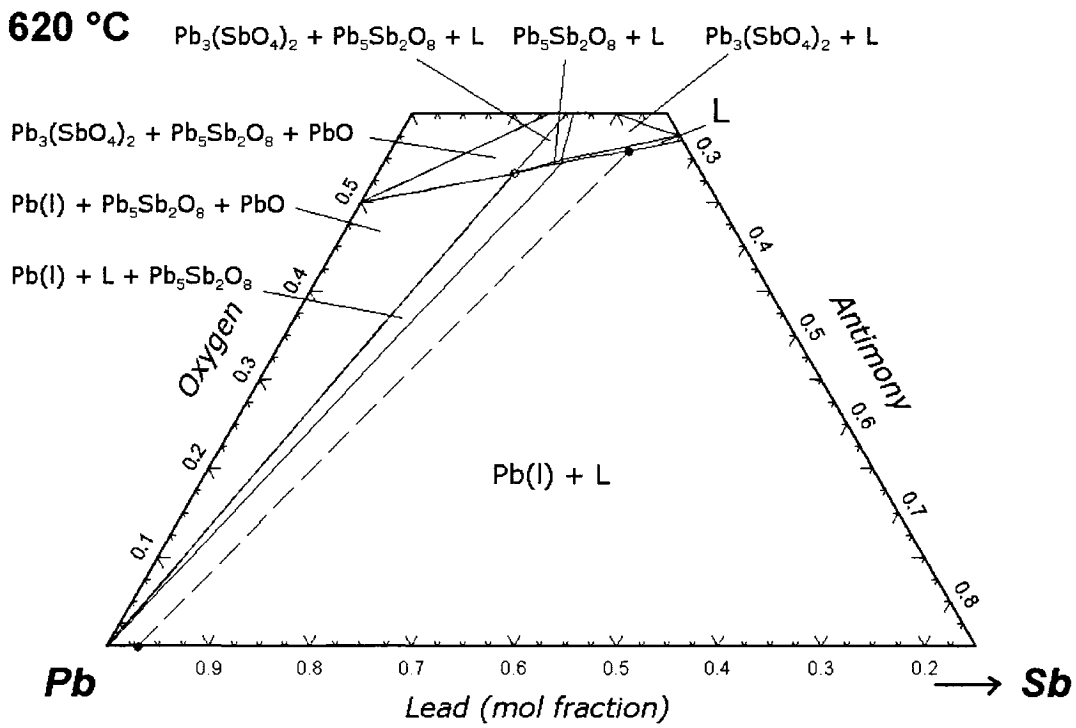

Figure 54 – Isothermal section of the Pb-Sb-O ternary system at 620 °C. Two dots at the end of tie line show the starting composition of Vineberg experiment [1]. (graph generated by FACT*Sage*™ [31])

With time, and the progress of oxidation, the system shifted toward lower antimony concentrations where the $Pb_5Sb_2O_8$ started to form. The open circle in the middle of graph shows the position of the $Pb_5Sb_2O_8$(s) compound. At slag concentrations with PbO

greater than 74 mol% in this ternary system, the liquid oxide phase disappeared and only solid PbO and $Pb_5Sb_2O_8$ existed in equilibrium with the metallic lead, resembling Paulin et al.'s work, and end part of the Vineberg experiment.

6.5 Conclusions

The suggested ionic structure of a liquid oxide phase containing only Pb^{2+}, O^{2-}, $(SbO_4)^{3-}$ $(SbO_3)^{3-}$ ions was successfully used to reproduce the reported pseudo-binary phase diagrams in the PbO-Sb_2O_3-Sb_2O_5 system. The small magnitude of excess Gibbs energy terms that were needed to fit the model to the experimental values were an indication that the assumption that antimony forms $(SbO_4)^{3-}$ $(SbO_3)^{3-}$ ions for basic melts was reasonable.

The model was expanded in the PbO-Sb_2O_3 system to predict antimony distribution in the range of interest. The predictions of the model were reasonably good up to ~ 30 mol% Sb_2O_3. The expansion of the model was simplistic and the use of a more powerful model such as quasichemical model is suggested as a means to further improve the range of agreement. The model was able to explain some of the reported observations for the softening of Pb-Sb alloys.

CHAPTER 7. CONCLUSIONS, ORIGINAL CONTRIBUTIONS AND FUTURE WORK

7.1 Scope

Conclusions and key findings for each part of this study have been presented at the end of each of the previous chapters[i] and in Appendix 1. Here, the overall conclusions and findings are summarized in view of the entire work. Following these, the original contributions to knowledge are articulated. Finally, recommendations for continuation of this study are offered.

7.2 Conclusions

Previous visual observations and kinetic measurements of the oxidation of static lead bullion melts by Vineberg [1] showed that the formation of solid phases in the gas/melt interface acted as a barrier for the oxygen transfer to the melt and resulted in a very slow rate of oxygen uptake.

- In agreement with this previous study, and based on the present experimental visual observations of the gas/melt interface in the top jetting of oxygen onto the lead bullion, and experimental mass change and temperature change measurements in subsurface injection of oxygen into the lead bullion, it was hypothesized that the ignition of the softening reactions was controlled by the physical form of the oxide formed at the bubble/melt interface.

- The review of the known literature found insufficient, and at times inconsistent, thermodynamic data for Pb-As-O and Pb-Sb-O systems. The inconsistency and scarcity of useful data was more acute in the Pb-As-O system and made it necessary to conduct experimental measurements in this system in order to develop and validate a thermodynamic solution model of the liquid slag.

---

[i] For Chapter 5 and Chapter 6, in addition to the end of each chapter, key findings are presented at the end of each Section.

- Based on the previous studies of lead oxide combined with oxides of arsenic and antimony, and on previous studies of the structure of arsenic and antimony in basic (PbO rich) and acidic (As_2O_3 or Sb_2O_3 rich) melts, and also on previous solution modeling of arsenic and antimony in metallurgical slags with a matrix phase other than lead oxide, it was concluded that the structure of PbO rich melts in the Pb-As-O and Pb-Sb-O systems was ionic and an ionic solution model could describe these two oxide systems in the PbO rich region.

- The resulting thermodynamic model with Pb^{2+}, O^{2-}, AsO_4^{3-} and AsO_3^{3-} ions for the Pb-As-O system and Pb^{2+}, O^{2-}, SbO_4^{3-} and SbO_3^{3-} ions for the Pb-Sb-O systems was optimized using all available thermodynamic data (phase diagrams, activity measurements and metal/slag equilibrium measurements). The optimized thermodynamic model was able to well reproduce the available thermodynamic data. The subsystems in the PbO-As_2O_3-As_2O_5 and PbO-Sb_2O_3-Sb_2O_5 systems showed small deviation from the ideal ionic solution model with the species that were defined in this study. In this regard small magnitude excess parameters were sufficient to fit the predicted liquidus curves to the experimental measurements. This work validated the hypothesis that the ionic solution model would be able to represent the basic PbO rich Pb-As-O and Pb-Sb-O systems.

- The variation in the measured arsenic distribution between metal and oxide phases and the ratio of trivalent to the total arsenic in the oxide phase showed a strong interaction between Pb-As-O atoms in the 3:1 molar ratio of PbO:As_2O_3. Such interaction suggests a short range ordering corresponding to the formation of AsO_3^{3-} groupings. It was concluded that the suggested $Pb_3(AsO_3)_2(l)$ species in the PbO rich region of the Pb-As-O system is possible.

- Empirical methods were used to estimate the properties of the $Pb_3(SbO_4)_2(s)$, which is an essential component of the current PbO-Sb_2O_5 model. As a result, an unknown error is associated with PbO-Sb_2O_5 model and the PbO-Sb_2O_5-Sb_2O_3 model that used the PbO-Sb_2O_5 model. Although the thermodynamic model was

able to reproduce the present experimental data, reliability of this model relies on the accuracy of the empirical value and not an experimental value.

- The measured arsenic distribution between the slag and metal in the Pb-As-O system at ~ 620 °C showed that in order to have the maximum concentration of arsenic in the slag phase, the slag should be in equilibrium with bullion containing more than 0.2 wt% As. A practical upper limit for the slag arsenic content is about 18 wt% As because of the substantial increase of arsenic in the bullion with greater than 18 wt% arsenic in the slag phase. This finding suggests that a counter-current slag/bullion contacting scenario, in which the output slag would be in equilibrium with the input lead with the higher arsenic contents, would increase the ratio of the As to Pb in the slag.

- The thermodynamic model explained both the current and previous [1, 52] laboratory studies and some industrial studies of Pb-As-O and Pb-Sb-O systems. However, the multi-component Pb-As-Sb-Sn-O system in industrial practice is more complex than the controlled laboratory experiments and the current thermodynamic model is still unable to fully explain the different situations in industrial practice that result in difficulties in ignition or maintaining the softening operation. Because of the success of the current model in explaining the laboratory experiments in Pb-As-O and Pb-Sb-O systems, it is believed that an optimized thermodynamic model of the complete Pb-Sb-As-Sn-O system would allow Teck Cominco to extend their knowledge based optimization of the refining technology beyond the contribution of the present work.

7.3 Original Contributions to Knowledge

In this study, the complexity of the softening reactions, equilibrium states between lead bullion and oxide phases, and the role of different phases in the rates of softening was a back drop for the beginning of the study. Different disciplines of metallurgical science, kinetic studies, experimental thermodynamics and thermodynamic modeling were combined to provide a new interpretation of an old process. For each of these disciplines relatively simple approaches were pursued and provided useful information to understand

the thermodynamics and mechanisms of lead softening. With the successful application of this combined effort to describe the laboratory observations and experiments, this study provided a significant step toward a knowledge based understanding of the industrial practice. The following points describe the original contributions to knowledge that each, in its way, helped to provide a better understanding of the softening process.

1. This project was the first to use the thermal analysis and equilibration technique coupled with EPMA to determine the phase boundaries in the PbO rich region of the PbO-As_2O_3-As_2O_5 ternary system. In this respect, these measurements contribute original knowledge to the thermodynamics of the Pb-As-O system by identifying the phase relations in this ternary system.

2. EPMA was successfully used to quantitatively determine the ratio of arsenic at different valances in a PbO rich Pb-As-O liquid solution. The comparison between the results for the fully-liquid oxide samples performed by the conventional wet analytical methods and EMPA showed good agreement. In this respect, it was an original method to quantify arsenic in different oxidation states in three-element Pb-As-O system.

3. Two new compounds ($Pb_3(AsO_3)_2$(s), Pb_2AsO_4(s)) were identified in the Pb-PbO-As_2O_3 quenched samples via wavelength-dispersive spectrometry using the electron microprobe.

4. For the first time, $Pb_2As_2O_5$(s) was synthetically prepared via synthesis of 2:1 molar ratio of PbO:As_2O_3 in sealed silver capsules at 390 °C. The formation of the compound was confirmed with XRD analysis and matched against the standard diffraction pattern of the rare natural mineral Paulmooreite with chemical formula $Pb_2As_2O_5$.

5. Arsenic in different oxidation states was quantitatively measured in the PbO rich region of the Pb-As-O liquid solution in the temperature range of 420 °C to 875 °C. The measured changes of the ratio of trivalent arsenic to the total arsenic, as well as changing behavior of arsenic distribution between metal and oxide phases

with increase of arsenic in the oxide phases, showed a strong interaction between Pb-As-O atoms at the 3:1 molar ratio of $PbO:As_2O_3$. Such a finding contributed to an original conception the liquid oxide structure and short range ordering in the PbO rich region.

6. The previously reported redox reactions that oxidized the trivalent arsenic to pentavalent oxide in the presence of PbO were found not to be in agreement with experimental results. The XRD analysis of the synthesized $PbO-As_2O_3$ mixtures as well as the phase equilibrium measurements in the fully liquid oxide phases were used to propose and validate new redox reactions (Reactions 49, 50, 61) for oxidation of trivalent arsenic oxide in the presence of PbO.

7. An original ionic solution model for the Pb-As-O and Pb-Sb-O systems using Pb^{2+}, O^{2-}, AsO_4^{3-} and AsO_3^{3-} ions in Pb-As-O system and Pb^{2+}, O^{2-}, SbO_4^{3-} and SbO_3^{3-} ions in Pb-Sb-O system was optimized and successfully used to reproduce the phase diagrams in the PbO rich region of the Pb-As-O and Pb-Sb-O system as well as providing a new database to predict the equilibrium conditions relevant to softening operation and providing a new tool for knowledge based optimization of the operation.

7.4 Recommendations for Future Work

This laboratory study and thermodynamic modeling exercise has provided some of the necessary thermodynamic knowledge of the Pb-As-O and Pb-Sb-O systems needed to understand the complex industrial and laboratory observations. Future work to further this goal is presented below:

1. Thermodynamic data for lead-tin-oxygen (Pb-Sn-O) systems should be reviewed and a solution model should be developed based on the properties of the Pb-Sn-O liquid solution. The need for any experimental work should be determined after the survey of the available data.

2. The phase diagram of the PbO-$Pb_3(SbO_3)_2$-$Pb_3(SbO_4)_2$ system, which is in the PbO rich region of the Pb-Sb-O system, was not evaluated because of the lack of reliable data inside the ternary region. It is suggested that experimental studies (e.g. thermal analysis or equilibrium studies) in the ternary region be conducted to evaluate and, if necessary modify the ternary solution model that was generated by interpolation of the optimized pseudo-binaries.

3. Reworking the present analysis using the modified quasichemical model for the Pb-As-O and Pb-Sb-O slag systems is recommended. The quasichemical model simplifies the expansion of the model range and does not require the definition of new species into the system as was necessary in the current ionic model. The proposed structure of the solution that was established in the current modeling study facilitates the optimization of the new quasichemical solution model.

4. Further study and new experimental measurements (e.g. equilibrium measurements) for the Pb-As-Sb-O system to obtain thermodynamic data for the optimization of the quaternary system is suggested. This would permit the optimization of the more complex Pb-As-Sb-O system using optimized ionic or quasichemical solution models of the Pb-As-O and Pb-Sb-O systems.

5. Further experimental work is recommended to characterize the compounds (i.e. $Pb_3(AsO_3)_2$ and Pb_2AsO_4) that were detected in this study for the first time. This information is valuable for the refinement of the present solution model, and/or optimization of a new solution model. This goal requires the preparation of the pure form of these compounds.

The current project began with a kinetic study of the oxygen uptake by lead bullion. The subsequent thermodynamic study was designed to understand some of the phenomena that was observed in that study. Continuation of the kinetic study would help solve some of the industrial challenges and facilitate a knowledge-based optimization of the current process. The following actions are recommended:

6. Weight change measurements using a modified design with controlled inlet gas flow, monitored gas outlet, and with larger sample size container to facilitate the oxygen injection is recommended for quantitative rate measurements coupled with temperature measurements. This would allow physical testing of the hypothesis relating to the softening initiation and extinction. Continuation of this experiment with a better control strategy for the sample and furnace temperature may be useful in conjunction with the rate measurements to complete the study of the softening kinetics.

7. Evaluation of different reactor configurations is suggested to determine the feasibility and potential of the counter-current process for increasing the As/Pb ratio of the slag.

Appendix 1. Study of Softening Mechanisms

A.1.1 Scope

To move toward an understanding the mechanism of softening reactions with a particular focus on the ignition phenomenon, required kinetic studies of the oxidation of lead bullion were undertaken. Prior to the current study, D. Vineberg[i] [1] performed Thermo-Gravimetric (TG) experiments and visual observations of the melt/gas interface to obtain information on the rate of oxygen uptake in static melts of pure lead, Pb-Sb-As-Sn alloys and lead softener feed. His study showed a pronounced effect of these impurities on the rate of oxygen uptake.

In order to better understand of the mechanisms of softening in agitated melts, preliminary observations and kinetic studies of the oxidation of pure and impure lead melts agitated by submerged injection or surface jetting of oxygen were conducted by the present author. The similarity between the static melt oxidation and the oxidation of melts agitated by gas bubbling was the focus of the current activity.

Kinetic studies were conducted using a specially designed thermo-gravimetric apparatus to measure the rate of oxygen uptake during submerged injection of oxygen into the melt. Visual observations were made in the same apparatus in separate experiments without quantitative mass change measurements during the experiment.

In this appendix, the experimental methodology that was used is explained and the observations and results are presented. The visual observations and results are discussed and a hypothesis for the mechanism of ignition in softening is suggested. Finally, the appendix concludes with remarks on the value of the findings and suggested future work.

A.1.2 Experimental

Commercial thermo-gravimetric instruments do not have the capability of submerged gas injection into the melt and, because of the need to have a sample large enough to

[i] M. Eng., former graduate student in R. Harris research group.

accommodate an injection lance, a specially designed TG device with large sample capacity was built using Vineberg's [1] setup as a starting point.

Apparatus:

First design: Vineberg [1] constructed the first version of this large sample thermo-gravimetric apparatus to measure the rate of oxygen transfer into stagnant lead bullion. In Vineberg's apparatus, oxygen was introduced into the furnace in the region above the melt. Sealed quartz windows were placed on the walls and top of the electric resistance furnace for observation and video recording of the melt/gas interface. The present author used this setup with some minor changes for observations of the lead-arsenic melt/oxygen interface. For observation purposes, oxygen was impinged onto the surface of the melts instead of submerged injection, because the opacity of the metals makes it impossible to observe the bubble/melt interface in submerged gas injection.

Modified design: Because of the limitation of the first design for sub-surface injection, a modified setup was designed and constructed. The modified TG equipment was comprised of three main components (Figure 55):

1. A sealed cylindrical furnace: A 450 watt Watlow cylindrical ceramic fiber radiant heater, 10 cm long and 5 cm ID was placed inside a stainless steel sealed cylinder. The control system for the furnace comprised a Watlow 935A temperature controller, a solid-state relay and type K thermocouple. A separate K type thermocouple was positioned inside the melt to measure the melt temperature.

2. An analytical balance: A Mettler AT200 analytical balance with 0.1 mg precision that produced 160-weight readings per minute was connected to a PC for data acquisition. The capacity of the balance was 0.2 kg, which made it capable of holding a much larger crucible and sample than a conventional TG instrument. The balance was sealed in a Plexiglas cover and placed on a steel shelf above the furnace. A suspension wire, hooked underneath the balance, connected the balance to a crucible, which was hanging in the hot zone of the furnace. The space between the balance and furnace box was sealed with flange connections.

3. A gas injection system: Stainless steel tubes (type 316) with two different diameters were used for injection of oxygen into the melt: a capillary tube with 0.76 mm ID, 1.5 mm OD and another tube with 2.2 mm ID, 2.9 mm OD. Oxygen flow was controlled using a 0.8 cm^3/s scale rotameter. A separate gas delivery system was used for the argon that was used to flush air from the apparatus. For observation experiments using the first design, a copper tube with a 1.5 mm ID was placed 1 cm above the melt surface. This tube was connected to a three-way valve that could be switched between oxygen and argon.

1 - plexiglass sealed box
2 - Thermocouple
3 - Off-gas to Scrubber
4 - Sealed furnace box
5 - Ceramic heater
6 - Oxygen lance
7 - Suspended Crucible
8 - Thermocouple (to furnace controller)
9 - Rising Stand
10 - Suspension wire
11 - Balance connection to PC

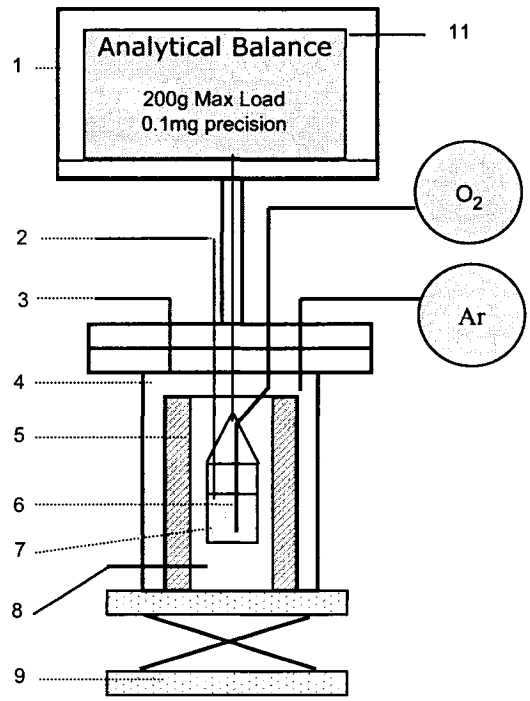

Figure 55 – Schematic view of Thermo-Gravimetric apparatus.

Procedure:

Visual observation experiments:

The lead alloy was melted in a steel crucible of 4 cm OD, and 3 cm in height, under an argon atmosphere. An oxide free surface was observed to form on the molten Pb-As alloy under the argon atmosphere before oxygen gas was introduced. Oxygen gas was then impinged vertically on to the melt surface at about 7.5 cm^3/s (STP). Once the melt was completely covered with an oxide layer, the oxygen gas was switched to argon.

Thermo-gravimetry and temperature measurement tests:

Pb-As alloys were prepared by melting the appropriate amounts of pure lead and lead-arsenic master alloys in an alumina crucible under an argon atmosphere. Because of the 200 g maximum capacity of the balance, the mass of the samples in each test was chosen to be 100 g. Each test alloy charge was placed inside a cylindrical high-alumina crucible, 4 cm long and 2.5 cm ID, which was attached to the suspension wire. The suspension wire was then raised to connect with a hook underneath the balance and the furnace was adjusted so that the suspended crucible was in the hot zone of the furnace. After sealing the setup by lifting the adjustable laboratory stand, argon gas was introduced into the system at 30 cm^3/s for 20 minutes to purge the furnace of oxygen. Subsequently, the furnace was powered and the sample heated. The sample was kept at the desired temperature for 30 minutes under a mixture of argon containing ~ 2 vol% hydrogen to remove the residual oxygen in the furnace, and to assure temperature and composition homogeneity in the melt. During this period, the oxygen lance was positioned above the melt. Hydrogen gas was stopped at the end of the 30 minute period, but the argon flow was maintained throughout the experiment. An alumina lid, with a central opening for the lance, covered the crucible throughout the experiment to prevent possible splashing of melt out of the crucible.

After the homogenization period, an oxygen flow was started at 0.33 cm^3/s before being lowered into the melt to a depth 1.4 cm below the melt surface. The mass change was constantly monitored and recorded until the end of the injection period. The injection time set at 20 or 60 minutes. In some cases, the submerged tip of the tube clogged because of formation of a solid oxide and the test was ended before the pre-determined time.

Physical contact between the lance and the inside of the opening in the crucible cover could exert a force to the crucible and cause instability in the measurements. Because of the small opening on the crucible cover, placing both the oxygen lance and thermocouple into the melt without making physical contact with the opening was difficult; hence, temperature measurements during gas injection were performed for only some samples.

At the end of the injection period, the lance was raised out of the melt and the oxygen flow was stopped. The sample was cooled to below the melting point of lead inside the furnace under an argon atmosphere before being removed from the furnace.

A.1.3 Results

Visual observations:

Figure 56 shows the formation of solid and/or liquid/solid oxides on the surface of a Pb-0.9 wt% As melt when oxygen was impinged in the surface of the melt at about 600 °C. In this test, the lead alloy was melted in a steel crucible, 4 cm OD, 3 cm height, under an argon atmosphere. An oxide free surface was observed before oxygen gas was introduced. Oxygen gas was then impinged vertically from a 1.5 mm ID stainless steel tube at about 7.5 cm^3/s (STP).

The left picture shows the formation of small globular shaped oxides that formed at the impingement point and quickly moved toward the edges of the crucible due to the shear force of the gas stream on the surface of the melt. The oxides accumulated on the crucible wall and started to cover the surface of the melt (middle picture). Finally, with the continuation of the impingement, the surface was completely covered (right picture) by what appeared to be a solid oxide phase and the dimple that was originally formed in the middle of the melt under the jet (left and middle pictures), was no longer evident.

Figure 57 shows the disappearance of the solid oxide phase once the oxygen gas flow was terminated and the argon gas was restarted. A low argon flow rate (< 5 cm^3/s) was used to preserve the oxide layer. The oxide layer appeared to melt and then move toward the crucible walls (left and middle pictures) rather than being physically pushed to the crucible wall by the force the argon stream. In the right-side picture, the surface of the lead alloy was almost oxide free and all the oxides formed had accumulated in what appeared to be a liquid ring around the crucible wall. The switching between oxygen and argon was repeated and the same behavior was observed on each occasion.

Figure 56 – Formation of an apparently solid oxide on Pb-0.9 wt% As molten alloy surface by impingement of oxygen gas.

Figure 57 – Disappearance (melting) of the solid oxide layer on the surface of Pb-0.9 wt% As molten alloy by the flow of the argon gas on the surface of the melt.

Thermo-gravimetry:

Samples of pure Pb, Pb containing 0.9 to 1.2 wt% As, and a sample of Teck Cominco softener feed were studied with the modified thermo-gravimetric device. Table 14 gives the chemical composition and test conditions samples representative of the range behaviors encountered. For each sample, the weight change was plotted against time (Figure 58 to Figure 61).

Figure 58 shows the change in weight and temperature of the pure lead sample with an initial temperature of 615 °C. It can be seen that the temperature remained almost constant at 614 ± 2 °C during the oxygen injection. Sample weight decreased during the first 10 minutes of the test, and then increased almost linearly with the cumulative injected oxygen weight, as calculated from the volumetric flow of the oxygen. The TG curve showed a vibrating behavior believed to be due to the bubbling of the oxygen, this noise was observed in all of the submerged gas injection experiments.

Table 14 – Sample composition and experimental conditions for the representative thermo-gravimetric tests.

Sample	Composition (Pb-wt% As)	Initial Temperature (°C)	Oxygen flow rate (cm^3/s)	Injection Tube ID (mm)
1	Pure Pb	615	0.3	0.8
2	Pure Pb	~ 615	0.4	0.8
3	Pb - 1.2 As	~ 600	0.3	2.1
4	Pb - 1.2 As	~ 600	0.3	2.1
5	Pb - 1.12 Sb - 0.22 As - 0.10 Sn	~ 600	0.2	0.8

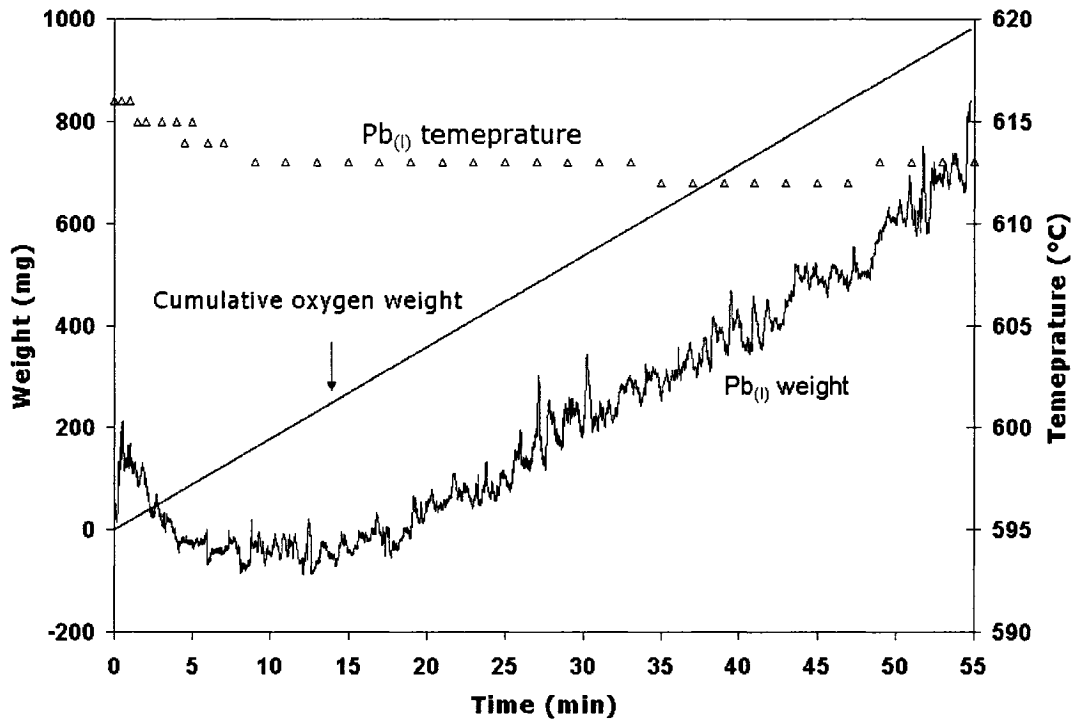

Figure 58 – Weight change (TG) and temperature of the pure Pb, Sample 1 during oxygen injection.

Sample 2, Figure 59, shows the TG curve for a pure Pb sample similar to Sample 1 but at a higher oxygen injection rate. The weight increase was seen to be higher than the weight of oxygen injected inside the melt and was more pronounced after 20 minutes of injection. The magnitude of noise in the weight measurements was higher than for Sample 1.

Figure 60 shows the TG curves for two, almost identical tests (Samples 3 and 4) of Pb 1.2 wt% As samples at initial temperatures of about 600 °C. The upper curve in Figure 60 shows the first derivative of mass gain for Sample 3. Both samples showed two distinctive mass gain behaviors. The first period, which lasted for about 6 minutes, showed low or no mass increase (TG curve) and intense vibrations (DTG curve). The second period, which lasted until the end of the test, had a calmer bath and lower vibration intensity. The rate of weight increase was higher than the first period and had an almost linear relationship with accumulative oxygen weight.

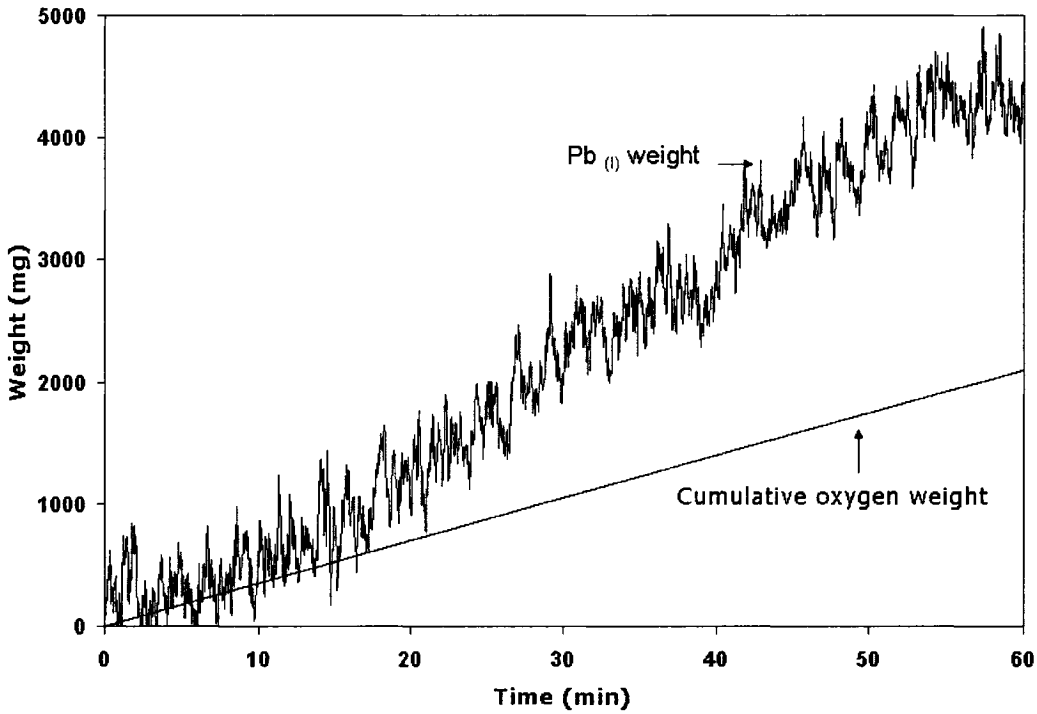

Figure 59 – Weight change (TG) of the pure Pb, Sample 2, during oxygen injection.

Figure 61 (Sample 5) shows the TG curve for a sample of Teck Cominco softener feed. Similar to Samples 3 and 4, it has two distinct region of an initial period with a slight decrease in sample weight, followed by a period of higher weight gain.

It is important to note that for Samples 3 to 5, the tests were stopped because the tube tip clogged. This was confirmed by visual observation of the tubes, which were taken out of melt after the gas flow stopped or became unstable.

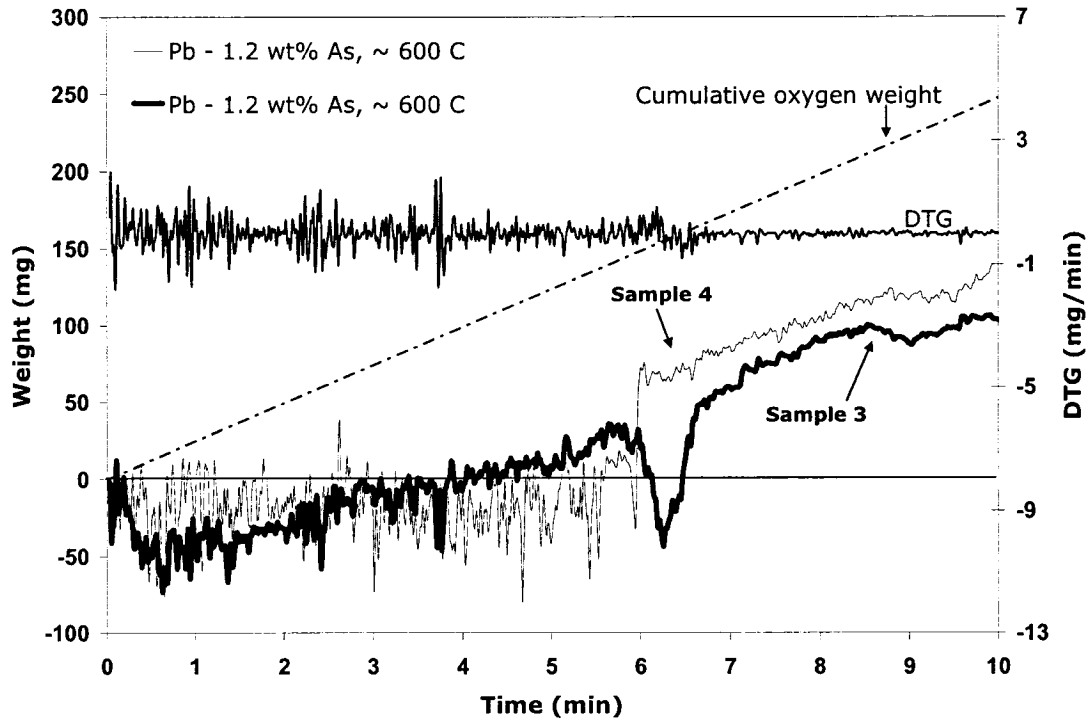

Figure 60 – (Lower curves) weight change of the Pb-1.2 As, Samples 3 and 4, during oxygen injection. (Upper curve, Sample 3), first derivative of weight change (DTG).

Temperature change:

Figure 62 shows the temperature change during the oxygen injection into a sample of pure Pb and the two Pb - 1.2 wt% As melts at similar test conditions but at different initial temperatures. The temperature of the pure lead showed almost no change during the injection period. The alloyed lead at an initial temperature of 578 °C showed the previously mentioned two-stage behavior. The first stage lasted about 12 minutes during which a gradual temperature increase was observed. The second stage began with a rapid temperature increase to ~ 600 °C, with subsequent temperature stabilization for the remainder of the test. Test was stopped because of oxygen tube clogged at 34 minutes. The second Pb – 1.2 wt% As sample, with $T_{initial}$ = 605 °C also showed two stage behavior, but the difference was that the first stage lasted only two minutes. Temperature increased rapidly to ~ 630 °C and oxygen injection stopped after 14 minutes because of clogging of the oxygen tube. In both tests, once the oxygen flow stopped, temperature decreased to the initial set temperature.

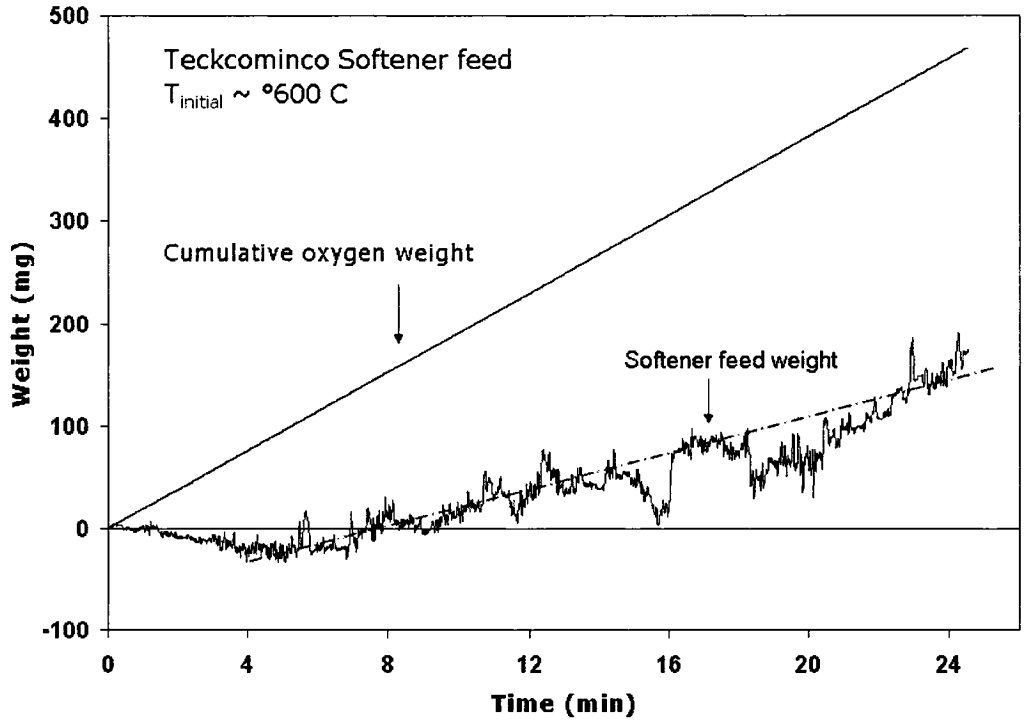

Figure 61 – Weight change of the softener feed sample, Sample 5, during oxygen injection.

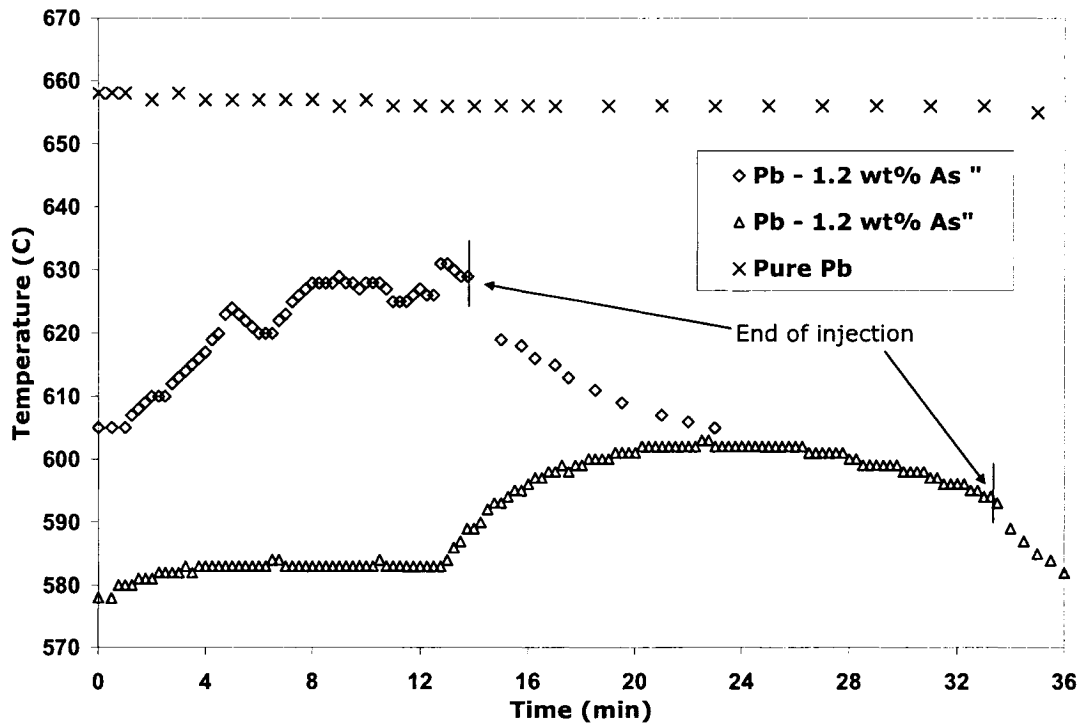

Figure 62 – Temperature change during injection of oxygen into the pure Pb and Pb – 1.2 wt% As alloy.

A.1.4 Discussion:

Visual observations:

Visual observations of the melt/gas interface saw the effect of oxygen partial pressure on the physical form of the oxides formed at the surface of Pb-0.9 wt% As alloy at 600 °C.

It was hypothesized that the rate of softening was controlled by the physical form of the oxides covering the oxygen bubbles inside the melt, i.e., the solid oxide layer provided a physical barrier to the oxygen transfer into the melt. A logical consequence of such a picture of the reaction mechanism was that once the rate of oxygen supply was greater than the rate of oxygen consumption, the oxide phase would be at local equilibrium with the oxygen in the gas phase, and arsenic in the +5 valency state would have been predominant in the oxide phase. The phase diagram of $PbO\text{-}As_2O_5$ (Figure 10) showed that at 600 °C, the oxide phase was in solid form throughout the entire range of As compositions. On the other hand, if the rate of oxygen supply was lower than the oxygen consumption, the oxide that was formed would be at local equilibrium with the metallic lead, and arsenic in both +3 and +5 oxidation valances would have existed in the oxide layer.

The optimized thermodynamic model of $PbO\text{-}As_2O_3\text{-}As_2O_5$ and the experimental results on the Pb-As-O system that were presented in 5.3.3 showed that, the oxide phase at equilibrium with the Pb-0.9 wt% As at 600 °C is completely liquid.

Certain similarities were observed between the proposed mechanism of softening reaction and the proposed mechanism for the removal of sodium and magnesium impurities from aluminum by chlorine gas as studied by Kulunk and Guthrie [124]. Kulunk and Guthrie stated that chlorine gas first reacted with aluminum to form aluminum chloride gas. The aluminum chloride gas then reacted with sodium and magnesium to form chlorides of these elements. Depending on the composition and temperature, the intermediate reaction products formed either a solid or a liquid film on the surface of bubbles and depending on the physical properties and adhesion characteristics of this film, they either covered the bubble during its passage through the liquid, or they were continuously stripped from the

bubbles, by the hydrodynamic shear. Fu et al. also [125] studied the kinetics of magnesium removal from aluminum by chlorine gas. They observed chlorine emissions below the melting temperature of $MgCl_2$, indicating that formation of solid $MgCl_2$ interfered with the progress of chlorination. Above this temperature there was no chlorine emitted when the magnesium content was above a critical value, this likely corresponded to the equilibrium value of the Mg content in the Al.

Thermo-gravimetric results:

The thermo-gravimetric results showed some similarities between the laboratory model and Teck Cominco's actual softening practice. The initial period in which the rate of weight increase was very low or even negative was similar to an initial commercial softening stage during which oxygen is injected into the lead bullion and a very low rate of softening is observed. This is demonstrated by the breaking of oxygen bubbles at the surface of the industrial softening vessel. Once the softening reaction "ignited" in the laboratory tests, the rate of weight increases at a rate almost equal to the cumulative weight of the injected oxygen. This type of behavior was interpreted as a fast rate of softening and was similar to the observed normal commercial softening practice, during which a fast rate of reaction is observed when no bubbles (or very few bubbles) break at the surface of the melt. When no bubbles break at the surface of the melt, it implies a very fast rate of oxygen consumption.

Unfortunately, the thermo-gravimetric results were in the most part unreliable and failed to provide quantitative values for the rates of softening. In fact, several problems were encountered during the experiments and despite best efforts that were invested to solve them, persisted throughout the tests. Eventually it was concluded that the current method was unable to provide meaningful and repeatable data of PhD value. A description of the problems follows.

The first problem arose because of the vibration of the crucible, which created noise in the weight signal. The magnitude of the noise was sometimes greater than the measured weight change, making the results meaningless.

The second problem was the clogging of the oxygen tube during the tests. The only practical way to overcome this problem was to increase the oxygen flow rate, which in turn increased the vibration of the crucible and therefore increased the noise in the weight signal.

A third problem was the accretion of solid oxide on the oxygen tube. Assuming the solid oxide was pure PbO, this could cause a weight reading up to 3.2 times the actual weight of the PbO that was produced (explained below). This apparent measured weight increase was greater than the weight of oxygen injected into the melt for some of the pure Pb samples (Figure 59), which tended to form a sticky solid PbO oxide.

The analysis of this phenomenon presented below balances the forces acting on the scale, exerted by the mass of lead and crucible and the reaction to the buoyancy force by the fixed oxygen tube (Equation 81 to 83 - Figure 63).

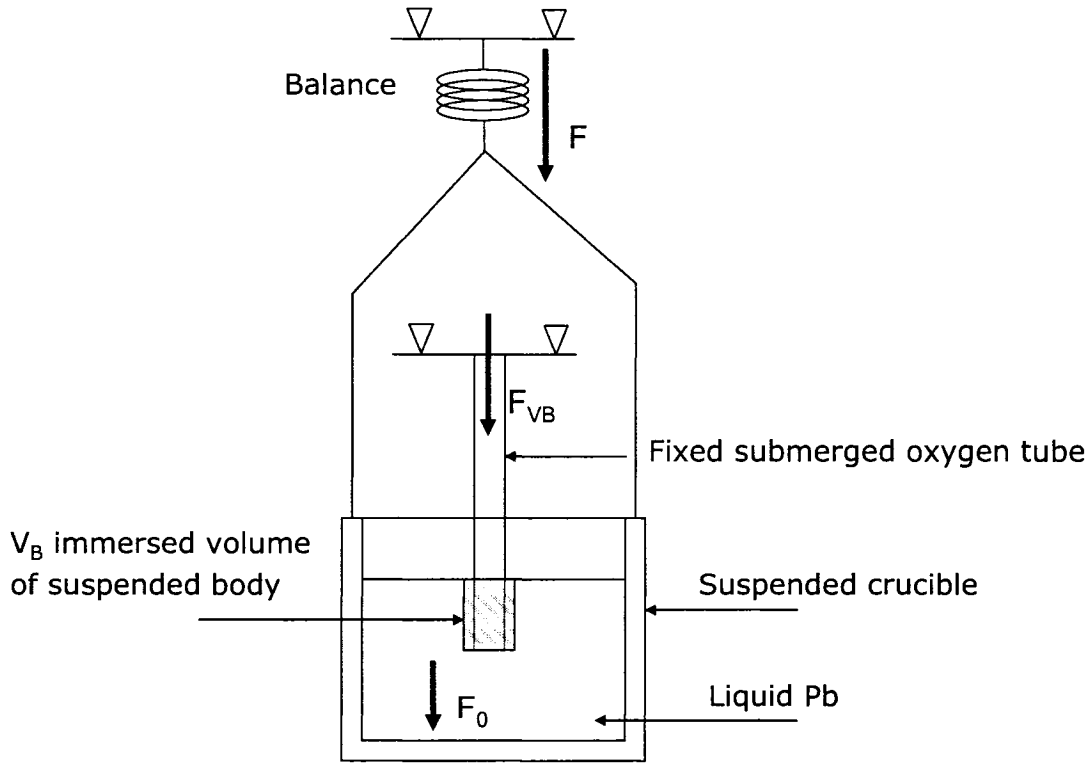

Figure 63 – Force balance on the fixed oxygen tube and the crucible containing liquid lead.

$$F = F_0 + F_{VB} \tag{81}$$

$$F_0 = (m_L + m_{crucible}).g \tag{82}$$

$$F_{VB} = V_B \rho_L g \tag{83}$$

Here F is the force acting on the balance, F_0 is the force due to the mass of liquid lead (m_L) and the crucible ($m_{crucible}$), F_{VB} is the reaction to buoyancy force caused by the immersed volume of the suspended body (V_B) in the liquid lead, ρ_L is the density of liquid lead, and g is the acceleration of gravity.

In the force balance of the system, the buoyancy force acts upwards, and the reaction to that force is downward, thus has a positive sign because it is the opposite of the buoyancy force. It thus adds to the force exerted on the balance.

Assuming the addition of a mass of gas, m_G, consumes a mass of liquid, m_R, for a mono-stoichiometric reaction, the mass of the product is $m_R + m_G$. Attachment of the reaction product to V_B, physically removes the mass $m_R + m_G$ from the liquid system. This has two effects:

1. The mass of liquid (m_L) is reduced by an amount of m_R and reduces the weight of liquid by an amount of $m_R \cdot g$.

2. The attachment of product increased the immersed volume by $(m_R + m_G)/\rho_R$ and the buoyancy force by an amount $(m_R + m_G) / \rho_R \cdot \rho_L \cdot g$, where ρ_R is the density of the reaction product.

Adding these two terms to Equation 81 yields:

$$F = (F_o - m_R.g) + \left(F_{VB} + \frac{m_R + m_G}{\rho_R}.\rho_L.g \right) \tag{84}$$

Equation 85 relates the mass of the product to the mass of the gas:

$$m_R = m_G \cdot \frac{A_L}{A_G} \tag{85}$$

where A_L is the atomic weight of the lead and A_G is the atomic weight of oxygen gas.

Rearranging Equation 84 and substituting for m_R yields:

$$F = F_o + F_{VB} + m_G \cdot g \cdot \left[\left(1 + \frac{A_R}{A_G} \right) \cdot \frac{\rho_L}{\rho_R} - \frac{A_R}{A_G} \right] \tag{86}$$

Setting ρ_L = 10.4 g/cm^3 at 600 °C, $\rho_R \approx$ 9.3 g/cm^3 (estimate), A_R = 207.2 and A_G = 16, Equation 86, simplifies to:

$$F = F_o + F_{VB} + 3.2 m_G \cdot g \tag{87}$$

The rate of weight change is thus calculated as:

$$\frac{dF}{dt} = 3.2 \frac{dm_G \cdot g}{dt} \tag{88}$$

According to Equation 88, if the entire reaction product attached to the tube, the measured weight would be 3.2 times higher than the weight of the oxygen injected into the lead. However, if only a portion of the reaction product attached to the tube, the measured weight was indeterminate and somewhere between 1 to 3.2 times that of the weight of the injected oxygen.

Temperature measurements:

Temperature measurements showed a two-stage behavior for the Pb – 1.2 wt% As samples at ~ 600 °C similar to the thermo-gravimetric results. The initial slow increase in the temperature was explained by a slow rate of softening and the sharp increase in the temperature was explained as the "ignition" of softening and the higher rate of softening thereafter. The main difference between temperature measurements and weight gain measurements was for the pure lead samples. The melt temperature did not increase during the oxygen injection for pure lead melts at the temperature of 660 °C. This

observation was explained by the insignificant rate of oxidation of pure lead by injection of oxygen. This was not evident in the weight gain experiments because the attachment of reaction product to the tube could cause the weight measurements to be up to 3.2 times higher than the mass of injected oxygen.

The lack of any temperature increase also provided evidence that if the reaction products were in solid form, they created a physical barrier for the transfer of oxygen into the melt.

A.1.5 Conclusions and Recommendations:

Based on the visual observations of the melt/gas interface and the temperature change during the injection of oxygen into both the pure and impure lead, it was hypothesized that the ignition of the softening reactions was controlled by the physical form and characteristics of the oxide formed at the bubble/melt interface. The kinetic study performed by a specially designed thermo-gravimetry apparatus was unsuccessful in providing meaningful and repeatable results for the rate of softening.

The author believes that once the thermodynamics of the softening are understood, experiments continuing the temperature change measurements under more controlled conditions would be capable of determining the effect of the process variables on the ignition of the softening. A modified experimental method would be required to provide quantitative data on the rate of oxygen uptake during the oxygen injection into the lead bullion.

Appendix 2. Calculating Liquidus Composition from Experiments of Zunkel & Larson

Experimental values from Zunkel and Larson [34] were used to calculate the composition of their liquidus points but where as Zunkel and Larson assumed a solid solubility region, while here it was assumed that there was no solid solubility because the present results showed that there was no solid solubility of As_2O_3 in PbO (see Section 5.2.3). Zunkel and Larson [34] represented the equilibrium between lead alloy and oxide phase via Equation 89.

$$As_{(1\ wt\%\ in\ Pb,\ l)} + 3\ PbO_{(l)} = As_2O_{3\ (l)} + 3Pb_{(l)} \quad (89)$$

$$\text{Log}\ K_{eq} = 2860/T - 0.778\ \text{(from [34])} \quad (90)$$

Using the equilibrium constant for this reaction and the known activity of arsenic in lead [31] and based on the arsenic distribution measured by Zunkel and Larson, the ratio of $a_{As_2O_3} / a_{PbO}^3$ was calculated. Thereafter, $\gamma_{As_2O_3} / \gamma_{PbO}^3$ versus $X_{As_2O_3} / X_{PbO}^3$ was plotted and independent straight lines were fitted between data points in two separate regions, the solid/liquid oxide region, and the liquid oxide region (Figure 64). The three compositions of the liquidus points that were calculated in this way had in average of ~ 2 mol% more As_2O_3 than what was calculated by Zunkel and Larson. These new values were used in this research for optimization of the Pb-As-O solution model.

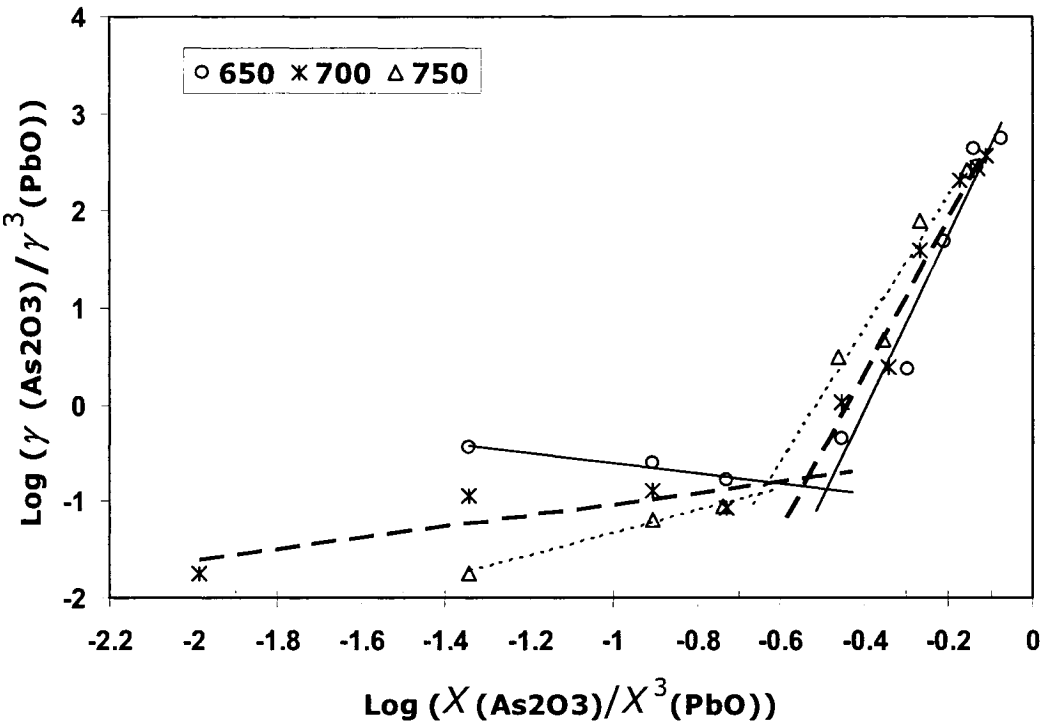

Figure 64 – Log $\gamma_{As_2O_3} / \gamma^3_{PbO}$ vs. $X_{As_2O_3} / X^3_{PbO}$ for Pb-PbO-As_2O_3 system between 650 °C and 750 °C. Experimental data extracted from Zunkel and Larson [34].

Appendix 3. Complementary Experimental Results

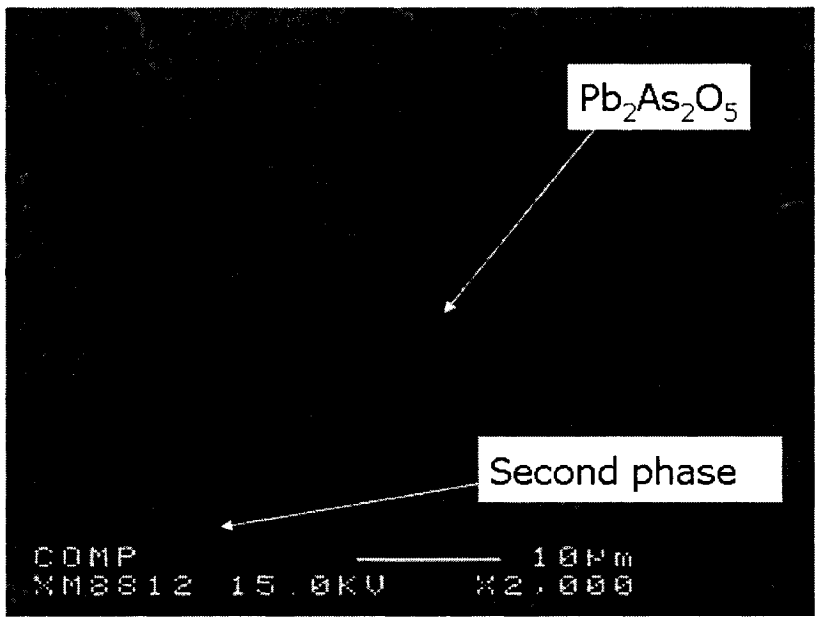

Figure 65 – Back-scattered electron image of the prepared $Pb_2As_2O_5$ standard showing mainly the presence of a $Pb_2As_2O_5$ compound with a small amount of a second phase.

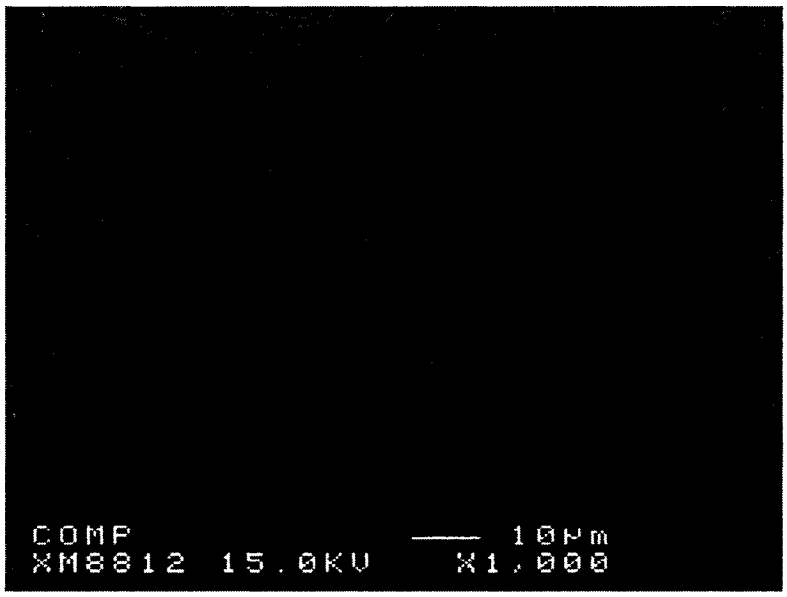

Figure 66 – Back-scattered electron image of the quenched liquid in sample I. Thin flakes of PbO formed during the quenching.

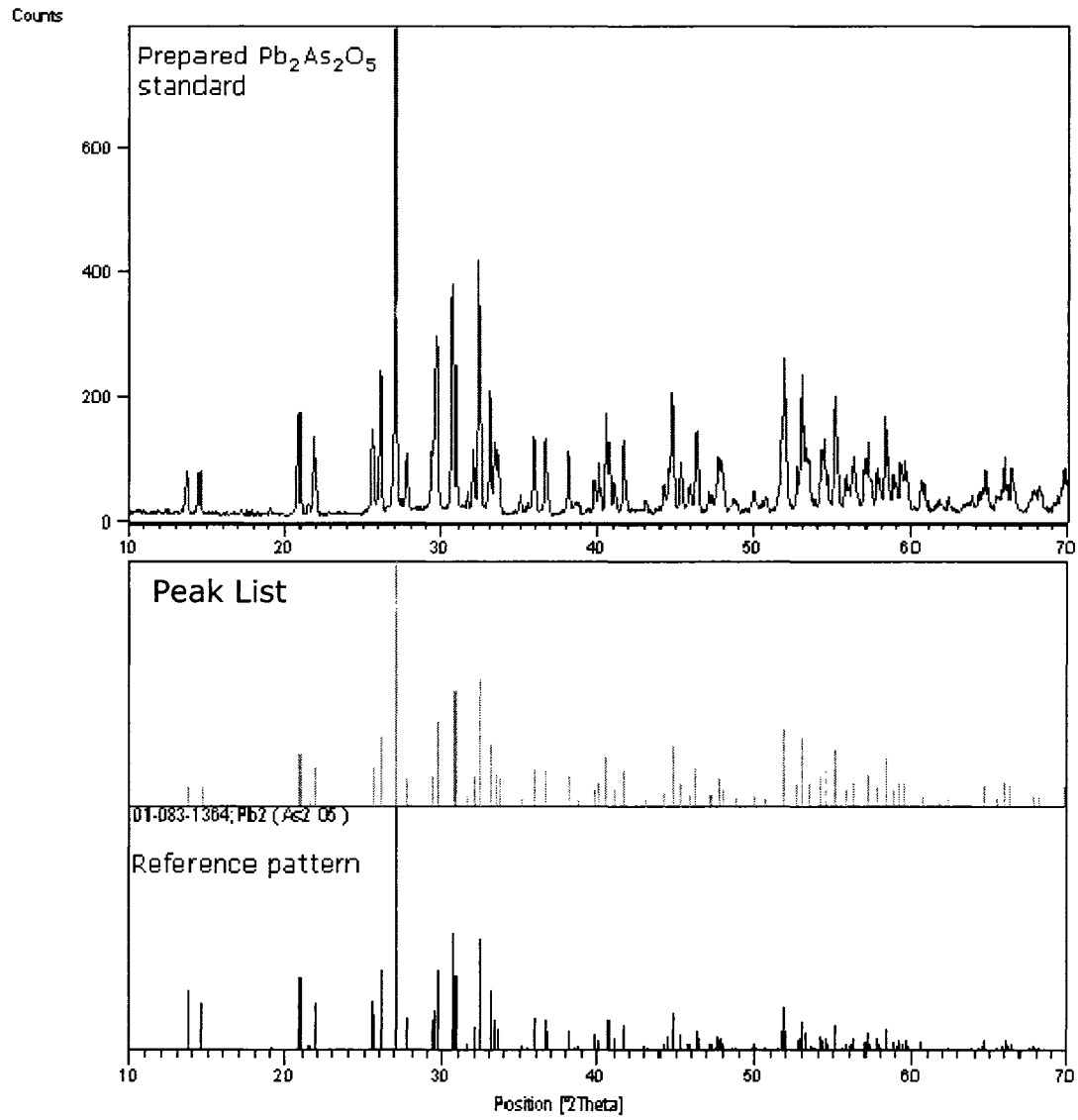

Figure 67 – XRD pattern of the prepared $Pb_2As_2O_5$ standard. No shift of the major peaks was observed.

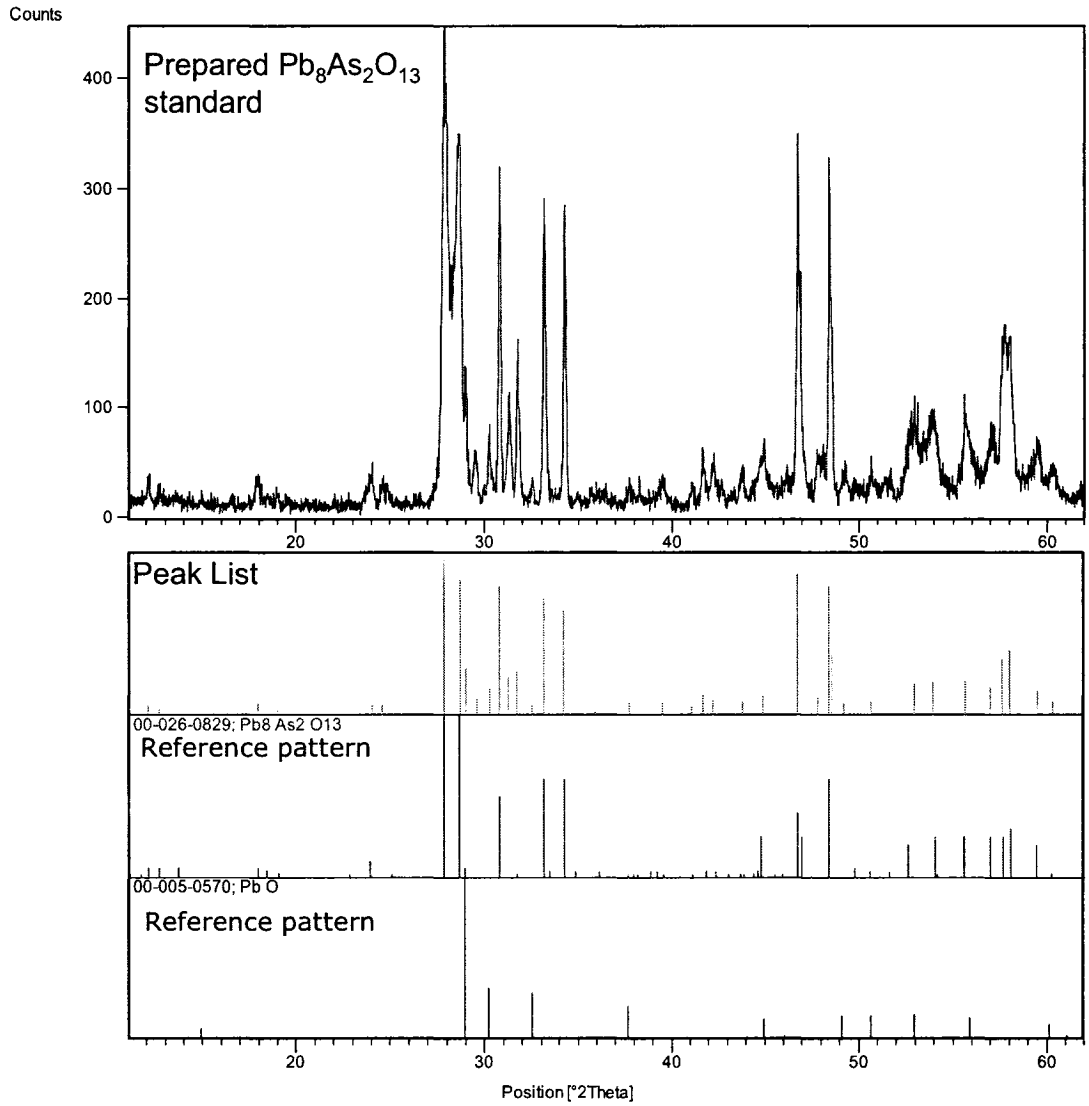

Figure 68 – XRD pattern of the prepared $Pb_8As_2O_{13}$ standard. No shift of the major peaks were observed

Table 15 – Comparison of the composition of the quenched liquid oxides in DTA experiments determined by wet chemical analytical methods and EPMA.

	Initial As_2O_3 Content (wt%)	Quenched liquid oxide composition (wet chemical analysis)			Quenched liquid oxide composition (EMPA)		
		X_{PbO}	X_{As2O5}	X_{As2O3}	X_{PbO}	X_{As2O5}	X_{As2O3}
H	15.3	0.815	0.053	0.132	0.814	0.043	0.143
I	18.1	0.782	0.035	0.184	0.779	0.043	0.178
J	22.8	0.750	0.008	0.243	0.746	0.016	0.237
K	30.7	0.675	0.004	0.321	0.684	0.001	0.315

Table 16 – Composition of the quenched liquid oxide that was used to represent the solidifying liquid oxide in DTA experiments. Compositions represented are based on the mole fraction of the elements and also based on their mole fraction in the defined ternary system.

	Initial As_2O_3 Content (wt%)	Quenched liquid oxide composition (elements)			Quenched liquid oxide composition (PbO-$Pb_{1.5}AsO_4$-$Pb_{1.5}AsO_3$ ternary)		
		X_O	X_{As}	X_{Pb}	X_{PbO}	$X_{Pb1.5AsO4}$	$X_{Pb1.5AsO3}$
A	2.9	51.77	3.15	45.08	0.928	0.045	0.027
B	4.2	52.79	4.68	42.53	0.884	0.081	0.036
C	6.9	53.70	6.53	39.77	0.821	0.113	0.066
D	8.1	54.78	8.06	37.16	0.757	0.167	0.076
E	10.0	55.23	9.44	35.33	0.691	0.188	0.121
F	11.2	54.1	9.2	36.7	0.713	0.114	0.173
G	12.9	55.40	12.20	32.40	0.536	0.179	0.285
H	15.3	55.46	13.78	30.75	0.422	0.169	0.409
I	18.1	55.3	16.0	28.7	0.224	0.123	0.652
J	22.8	54.9	18.1	27.1	0.001	0.038	0.961
K	30.7	55.6	21.8	22.6	-	-	-

Table 17 – Composition of the quenched liquid oxide that were prepared in platinum and silver capsules.

	Initial As_2O_3 Content (wt%)	Quenched liquid oxide composition (wet analysis)			Quenched liquid oxide composition (EMPA)		
		X_{PbO}	X_{As2O5}	X_{As2O3}	X_{PbO}	X_{As2O5}	X_{As2O3}
A	2.9	0.965	0.029	0.006	-	-	-
B	4.2	0.947	0.043	0.010	-	-	-
C	6.9	0.919	0.070	0.011	-	-	-
D	8.1	0.902	0.092	0.007	-	-	-
E	10.0	0.886	0.081	0.033	-	-	-
F	11.2	0.875	0.099	0.026	-	-	-
G	12.9	0.838	0.096	0.065	-	-	-
I	18.1	0.777	0.046	0.177	0.775	0.078	0.147
J	22.8	0.749	0.018	0.233	0.737	0.041	0.221
K	30.7	0.657	0.002	0.340	0.649	0.006	0.345

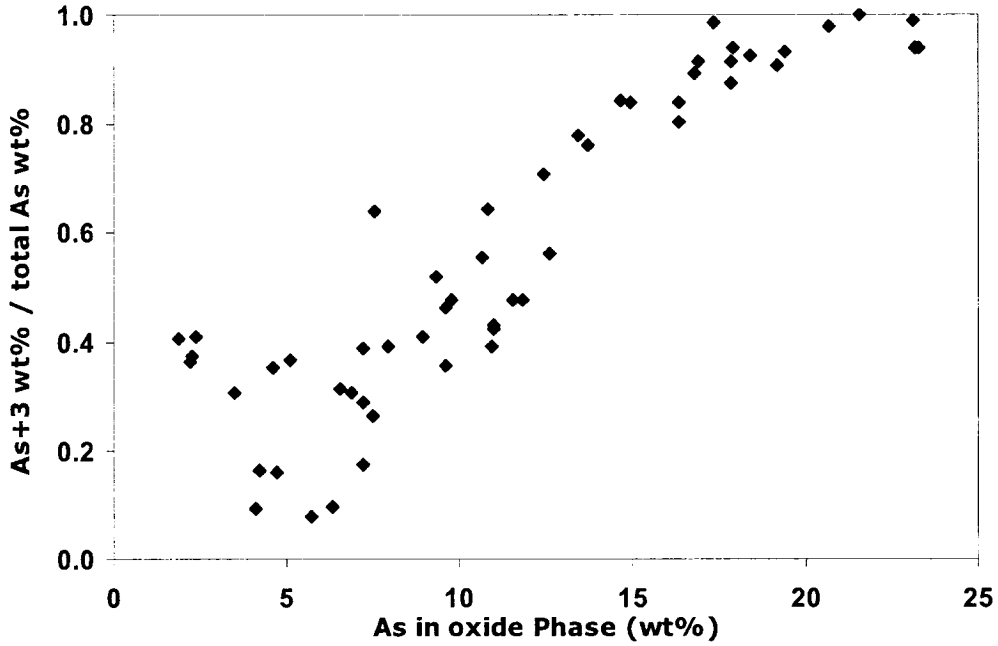

Figure 69 – mass fraction of As^{3+} as a function of total arsenic in the oxide phase, for liquid and solid/liquid slag at temperatures between 410-870 °C.

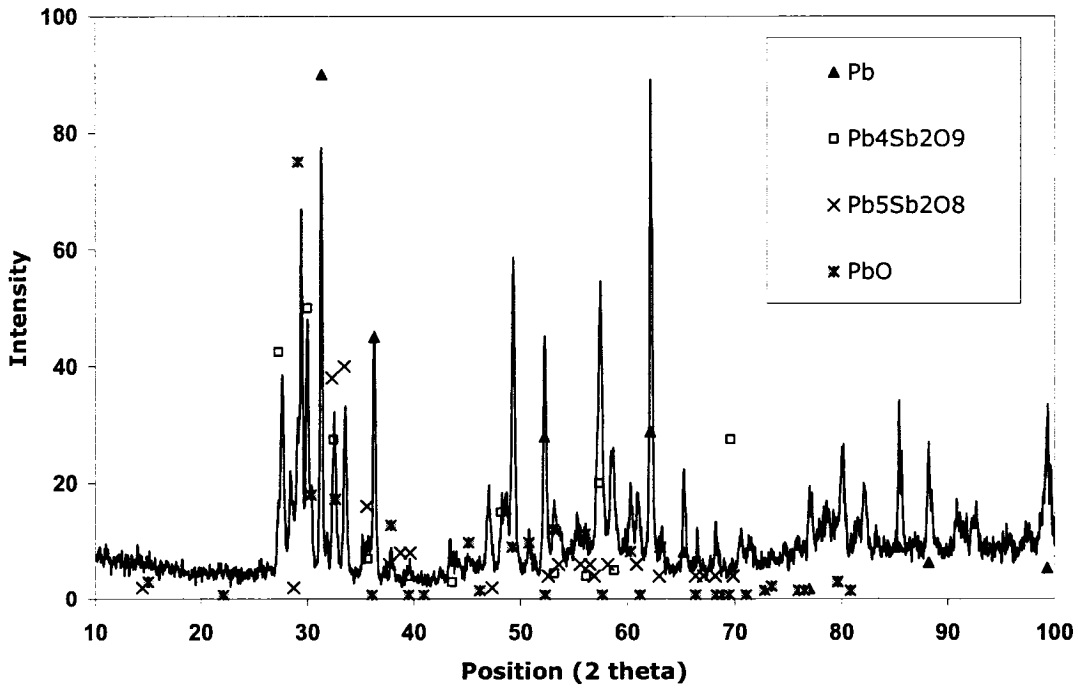

Figure 70 – XRD spectrum of the oxide layer formed at 600 °C during the softening of a Pb-2 wt% Sb alloy.

Appendix 4. Compilation of the Thermodynamic Data

Tables 18 to 20 compile the thermodynamic properties of the pure compounds, equations for Gibbs energy of the components in the liquid solution model and the excess Gibbs energy equations of the liquid solution model that were used in this study.

Table 18 – Thermodynamic properties for one mole of the pure compounds in the PbO rich region of the Pb-As-O and Pb-Sb-O systems that was used in this study (PbO from [31] and $Pb_3(AsO_4)_2$ from [115] and the rest estimated in this work).

	ΔH^0_{298} (J)	S^0_{298} (J/K)	Cp (J/K)	Temperature range (K)
PbO (s)	-218062	68.7	$47.63 + 0.0122T - 4.554e7T^{-3} - 65.75T^{-0.5}$	298-1159
			65.00	1159-2000
PbO (l)	-192540	90.7	= Cp (PbO(s))	298-2000
$Pb_8As_2O_{13}$	-2915492	669.1	$520 + 0.103T - 328.8T^{-0.5} - 3.43e6\,T^{-2} + 1.77e\text{-}5\,T^2 -$	298-1159
			$598 + 0.067T - 3.08e6\,T^{-2}$	1159-1315
$Pb_4As_2O_9$	-2040295	357.3	$487 + 0.021T - 2726.8T^{-0.5} - 3.213e6T^{-2}$	298-1048
$Pb_3(AsO_4)_2$	-1785208	324.6	$208 + 0.0417T - 1.773e\text{-}5T^2 - 3.43e6\,T^{-2}$	298 – 600
			$273 + 0.066T - 6.03e\text{-}5T^2 - 3.08e6\,T^{-2}$	600-1315
$Pb_3(AsO_3)_2$	-1344081	312.0	$355 + 0.038T - 2045T^{-0.5} - 1.26e6\,T^{-2}$	298-607
			$388 - 0.020T - 2045T^{-0.5}$	607-866
$Pb_2As_2O_5$	-1117000	244.1	$158 + 0.137T - 131.5T^{-0.5} - 9.11e7T^{-3}$	298-663
$PbAs_2O_4$	-886278	179.7	$180 + 0.052T - 682T^{-0.5} - 1.26e6\,T^{-2}$	298-607
			$213 - 0.007T - 682T^{-0.5}$	607-866
$Pb_3(SbO_4)_2$	-1859172	328.7	$207.45 + 0.17T$	298-1573
$Pb_3(SbO_3)_2$	-1397650	340.6	$234.97 + 0.1028T - 1.36e8T^{-3} - 197T^{-0.5}$	298-880
$Pb_5Sb_2O_8$	-1854600	464.2	$330.2 + 0.12738T - 2.28e8T^{-3} - 328T^{-0.5}$	298-910
$PbSb_2O_4$	-937865	198.9	$179.29 + 0.0594T - 681T^{-0.5}$	298-845

Table 19 – Standard molar Gibbs energies of the components that were used in the liquid solution model.

i	g_i^0 (J/mol)
$Pb_3(AsO_4)_2$(l)	-1813532 + 1491 T -0.0327 T^2 + 1.5e6 T^{-1} -273 T ln T
$Pb_3(AsO_3)_2$(l)	-1340776 + 1615 T -0.01838 T^2 + 2.3e7 T^{-2} -789 $T^{-0.5}$ -295 T ln T
$PbAs_2O_4$(l)	-908230 + 1135 T -0.00613 T^2 + 7.6e6 T^{-2} -263 $T^{-0.5}$ -200 T ln T
$Pb_3(SbO_4)_2$(l)	-1837966 + 1060 T – 8.961e-2 T^2 – 207.4 T ln$T$
$Pb_3(SbO_3)_2$(l)	-1369672 + 1604 T – 1.84e-2 T^2 + 2.3e7 T^{-2} – 789 $T^{0.5}$ – 299 T ln$T$
$PbSb_2O_4$(l)	-934126 + 1123 T – 6.13e-3 T^2 + 7.60e6 T^{-2} – 263 $T^{0.5}$ – 205 T ln$T$

Table 20 – Excess Gibbs energy of the pseudo-binary systems of the Pb-As-O and Pb-Sb-O systems in the region that defined in current study.

	g^E (J/mol)
PbO-$Pb_{1.5}AsO_4$	$-4950\, X_{PbO}^2 \cdot X_{Pb_{1.5}AsO_4}$
PbO-$Pb_{1.5}AsO_3$	$1620\, X_{PbO}\, X_{Pb_{1.5}AsO_3}$
PbO-$Pb_{1.5}SbO_4$	$2350\, X_{PbO} \cdot X_{Pb_{1.5}SbO_4}$
PbO-$Pb_{1.5}SbO_3$	$-2430\, X_{PbO}\, X_{Pb_{1.5}SbO_3}$

REFERENCES:

[1] D. G. Vineberg, "A Study of Lead Softening," *M. Eng. Thesis*, McGill University, Montreal, QC, Canada, 2003.

[2] A. H.-J. Siegmund, "Primary Lead Production – a Survey of Existing Smelters and Refineries," *Lead-Zinc 2000*, J. E. Dutrizac, J. A. Gonzalez, D. M. Henke, S. E. James, and A. H.-J. Siegmund, Eds., TMS (Minerals, Metals & Materials Society), Warrendale, Pa, USA, 2000, pp. 55-116.

[3] T. R. A. Davey, "The Physical Chemistry of Lead Refining," *Lead-Zinc-Tin '80*, J. M. Cigan, T. S. Mackey, and T. J. O'Keefe, Eds., The Metallurgical Society of AIME, New York, 1980, pp. 477-507.

[4] C. A. Sutherland and E. F. Milner, "Lead," in *Ullmann's Encyclopedia of Industrial Chemistry*. Verlag GmbH & Co KGaA: Wiley-VCH, 2005.

[5] D. R. Blaskett and D. Boxall, *Lead and It's Alloys*, New York: Ellis Horwood, 1990.

[6] J. P. Kapusta, "Sensing and Modeling for Oxygen Lead Softening," *PhD Thesis*, University of British Columbia, Vancouver, British Columbia, Canada, 1995.

[7] J. P. Kapusta and G. G. Richards, "A Process Control System for Oxygen Lead Softening," *2nd International Symposium on Quality in Non-Ferrous Pyrometallurgy*, M. A. Kozlowski, R. W. McBean, and S. A. Argyropoulos, Eds., Canadian Institute of Mining, Metallurgy and Petroleum, Vancouver, B.C., 1995, pp. 173-83.

[8] H. Perez, R. Leclair, P. Hancock, and J. G. Lenz, "Recent Process Intensification Efforts at the Brunswick Lead Smelter," *International Symposium on Challenges in Process Intensification*, C. A. Pickles, P. J. Hancock, and J. R. Wynnyckyj, Eds., Canadian Institute of Mining, Metallurgy and Petroleum, Montreal, Quebec, Canada, 1996, pp. 247-266.

[9] A. Paulin, "Application of Oxygen in Refining Lead - Thermodynamic Fundamentals," *Rudarsko-Metalurski Zbornik*, 1989, 36, pp. 15-27.

[10] Z. He, B. Yang, and Y. Dai, "Arsenic, Tin and Antimony Removal by Blowing Oxygen during Crude Lead Refining," *Youse Jinshu*, 1988, 40, pp. 49-53.

[11] G. W. Toop, "Pyrometallurgical Operations of the Cominco Lead-Zinc Smelter," *CIM Bulletin*, 1994, 87, pp. 89-92.

[12] E. T. deGroot, M. T. Martin, and G. W. Toop, "Partial Softening of Lead Bullion with Oxygen," *Non-ferrous Smelting Symposium*, September 1989, pp. 61-63.

[13] E. F. G. Milner and E. T. deGroot, "Method for Softening Lead Bullion," *Canadian Patent 1,333,664*, 1994.

[14] J. P. Kapusta, T. R. Meadowcroft, and G. G. Richards, "Oxygen Softening of Lead: On-line Measurement of Bullion Quality," *Canadian Metallurgical Quarterly*, 2002, 41, pp. 451-464.

[15] Y. Omediran, Teck Cominco Trail Operations, Personal Communications, 2003-2005.

[16] G. G. Richards, Teck Cominco Trail Operations, Personal Communications, 2005.

[17] R. Harris, "Mechanism and Kinetics of Lead Softening," NSERC Collaborative Research and Development Grant Proposal, McGill University, 2001/01/25.

[18] G. C. Quigley and J. V. Happ, "Kinetics of Arsenic Removal from Bullion," *Research and Development in Extractive Metallurgy*, 1987, pp. 187-195.

[19] R. J. Mcclincy and A. H. Larson, "Activity of Arsenic in Dilute Arsenic-Lead Alloys at 703 Degrees C," *Transactions of the Metallurgical Society of AIME*, 1969, 245, pp. 173.

[20] K. Itagaki, T. Shimizu, and M. Hino, "Thermodynamic Studies of the Liquid Lead-Arsenic System," *Tohoku Daigaku Senko Seiren Kenkyusho Iho*, 1978, 34, pp. 45-52.

[21] N. A. Gokcen, "The As-Pb (Arsenic-Lead) System," *Bulletin of Alloy Phase Diagrams*, 1990, 11, pp. 120-124.

[22] H. Rannikko, S. Sundstrom, and P. Taskinen, "An Optimized Equilibrium Phase-Diagram and Solution Thermodynamics of Arsenic Lead Alloys," *Thermochimica Acta*, 1993, 216, pp. 1-14.

[23] Roland-Gosselin, *Bull. SOC. encour. ind. nut.*, 1896, 1, pp. 1301.

[24] H. Seltz and B. J. Dewitt, "A thermodynamic Study of the Lead-Antimony System," *Journal of American Chemical Society*, 1939, 61, pp. 2594-2597.

[25] Z. Moser, K. L. Komarek, and A. Mikula, "Thermodynamics and Phase-Diagram of Lead-Antimony System," *Zeitschrift Fur Metallkunde*, 1976, 67, pp. 303-306.

[26] P. Taskinen and O. Teppo, "Critical-Assessment of the Thermodynamic Properties of Antimony-Lead Alloys," *Scandinavian Journal of Metallurgy*, 1992, 21, pp. 98-103.

[27] A. Taskinen, "Oxygen-Metal (Ag, Au, Bi, Cu, in, Ni, Sb, Sn, Te) Interactions in Dilute Molten Lead Alloys," *Acta Polytechnica Scandinavica-Chemical Technology Series*, 1981, pp. 2-44.

[28] A. Taskinen and K. Jylha, "Influence of Arsenic on the Activity-Coefficient of Oxygen in Liquid Lead," *Scandinavian Journal of Metallurgy*, 1982, 11, pp. 158-160.

[29] A. Taskinen, "Activity-Coefficient of Oxygen in Pb-Bi and Pb-Sb Melts," *Zeitschrift Fur Metallkunde*, 1982, 73, pp. 163-168.

[30] Y. Dessureault and A. D. Pelton, "An Optimized Thermodynamic Database for Matte, Slag, Speiss and Metal Phases in Lead Smelting," *International Symposium on Computer Software in Chemical Extractive Metallurgy (The Met. Soc. of CIM)*, C. W. Bale and G. A. Irons, Eds., 1993, pp. 143-151.

[31] C. W. Bale, P. Chartrand, S. A. Degterov, G. Eriksson, K. Hack, R. B. Mafoud, J. Melançon, A. D. Pelton, and S. Petersen, "FactSage Thermochemical Software and Databases," *Calphad*, 2002, pp. 189-228, (http://www.crct.polymtl.ca).

[32] J. Gerlach, U. Hennig, and F. Pawlek, "Contribution to Studies of System Lead-Arsenic-Oxygen," *Metall.*, 1968, 22, pp. 812-816.

[33] E. Pelzel, "Reaction Equilibrium between Liquid Pb and Metal Oxides. III. Significance of the Oxidation Maximum of Antimony in Lead Refining," *Zeitschrift fuer Erzbergbau und Metallhuettenwesen*, 1959, 12, pp. 558-561.

[34] A. D. Zunkel and A. H. Larson, "Slag-Metal Equilibria in the Pb-PbO-As_2O_3 System," *Transactions of the Metallurgical Society of AIME*, 1967, 239, pp. 1771-1775.

[35] J. Gerlach, U. Hennig, R. Kurz, and F. Pawlek, "Contribution to Studies of System Lead-Antimony-Oxygen," *Metall*, 1968, 22, pp. 15-24.

[36] M. Amadori, "Anhydrous Phosphates, Arsenates and Vanadates of Lead," *Atti reale ist. Veneto*, 1917, 76, pp. 419-433.

[37] A. D. Zunkel and A. H. Larson, "Slag-Metal Equilibria in the Pb-PbO-Sb_2O_3 System," *Transactions of the Metallurgical Society of AIME*, 1967, 239, pp. 473-477.

[38] E. Pelzel, "Reaction Equilibriums between Liquid Lead and Metal Oxides. I.," *Zeitschrift fuer Erzbergbau und Metallhuettenwesen*, 1958, 11, pp. 56-63.

[39] B. K. Kasenov, R. B. Shashchanova, A. Z. Beilina, and V. B. Malyshev, "Phase Equilibria in the As_2O_5-PbO System," *Inorganic Materials*, 1991, 27, pp. 1236-1240.

[40] B. K. Kasenov and R. B. Shashchanova, "Calculation of the Liquidus Curves and Thermodynamic Characteristics of Melts in the Lead Arsenate-Lead Oxide System," *Kompleksnoe Ispol'zovanie Mineral'nogo Syr'ya*, 1991, 5, pp. 87-89.

[41] C. G. Maier and W. B. Hincke, "The System PbO-Sb_2O_3 and Its Relation to Lead Softening," *Transactions of the American Institute of Mining and Metallurgical Engineers*, 1932, 102, pp. 97-106.

[42] G. Tammann and H. Kalsing, "Chemical Reactions in Powdered Mixtures of Two Kinds of Crystals. IV. The Behavior of V_2O_5, SiO_2, TiO_2, ZrO_2, Sb_2O_3 and As_2O_3 with Basic Oxides," *Z. Anorg. Allgem. Chem*, 1925, 149, pp. 68-89.

[43] H. Hennig and E. J. Kohlmeyer, "The Mutual Behavior of Lead-Antimony Oxides in the Molten Condition," *Zeitschrift fuer Erzbergbau und Metallhuettenwesen*, 1957, 10, pp. 8-15 & 64-71.

[44] J. Barthel, "The Oxidation Maximum of Antimony during Dry Lead Refining," *Freiberger Forschungshefte A*, 1958, B29, pp. 5-66.

[45] R. J. Mcclincy and A. H. Larson, "Activity of Sb_2O_3 in PbO-Sb_2O_3 and PbO-SiO_2-Sb_2O_3 Slags," *Transactions of the Metallurgical Society of AIME*, 1969, 245, pp. 23-27.

[46] E. Sugimoto, S. Kuwata, and Z. Kozuka, "Activity Measurements in the Lead-Bismuth and Lead-Silver Alloys by EMF Method with Yttrium Oxide Doped Stabilized Zirconia at Low Temperatures," *Nippon Kogyo Kaishi*, 1981, 97, pp. 1199-1203.

[47] S. Itoh, A. Kikuchi, and M. Hino, "Thermodynamic Study on Recovery of Lead and Antimony from a Used Lead-Battery," *Metallurgical and Materials Processing: Principles and Technologies, Yazawa International Symposium*, San Diego, CA, United States, 2003, pp. 709-720.

[48] M. Wang, S. Anik, and M. G. Frohberg, "Thermodynamics of Oxygen in the Lead-Antimony System at 1173 K," *Erzmetall*, 1987, 40, pp. 316-319.

[49] A. A. Bush and Y. N. Venevtsev, "Phase Diagram of the Lead Oxide-Antimony Oxide (PbO-Sb_2O_3) System in the Presence of Atmospheric Oxygen," *Russian Journal of Inorganic Chemistry*, 1978, 23, pp. 1207-1211.

[50] G. G. Urazov and E. I. Speranskaya, "Interaction of Lead Oxide with Antimony Oxides," *Journal of Inorganic Chemistry-USSR*, 1956, 1, pp. 312-325.

[51] A. Paulin, " Use of Oxygen in Lead Refining - Oxygen Injection into the Melt," *Rudarsko-Metalurski Zbornik*, 1989, 36, pp. 479-491.

[52] A. Paulin, S. Polajner, and D. Dretnik, "On Lead softening with Oxygen-Enriched Air," *Rudarsko-Metalurski Zbornik*, 1996, 43, pp. 77-89.

[53] B. Friedrich, A. Arnold, and A. Lossin, "Equilibria in Pb-As-Sb-O Melts," *European Metallurgical Conference - EMC 2003*, Dresden, Germany, 2003, pp. 589-609.

[54] A. D. Pelton, "Thermodynamics and Phase Diagrams of Materials," in *Phase Transformation in Materials*, G. Kostorz, Ed. Weinheim: Wiley-VCH, 2001.

[55] R. D. Agrawal, V. N. S. Mathur, and M. L. Kapoor, "Thermodynamics of Binary Lead-Bearing Substitutional Solutions," *Transactions of the Indian Institute of Metals*, 1980, 33, pp. 237-240.

[56] S. K. Das and A. Ghosh, "Thermodynamic Measurements in Molten Pb-Sn Alloys," *Metallurgical Transactions*, 1972, 3, pp. 803-806.

[57] B. Onderka and J. Wypartowicz, "Thermodynamic Activities in the Liquid and the Liquidus Line in the Pb-As-System," *Zeitschrift Fur Metallkunde*, 1990, 81, pp. 345-348.

[58] K. Osamura, "The Pb-Sb-Sn (Lead-Antimony-Tin) System," *Bulletin of Alloy Phase Diagram*, 1985, 6, pp. 372-379.

[59] S. Otsuka, Y. Kurose, and Z. Kozuka, "Activity of Oxygen in Liquid Pb-Sb Alloys Determined by a Modified Coulometric Titration Method," *Zeitschrift Fur Metallkunde*, 1984, 75, pp. 46-52.

[60] J. Sebkova and M. Beranek, "Thermodynamic Properties of Pb-Sb-Sn Alloys Measured by the Emf Method," *Kovove Materialy-Metallic Materials*, 1980, 18, pp. 660-668.

[61] H. Seltz and B. J. DeWitt, "A Thermodynamic Study of the Lead-Antimony System," *Journal of the American Chemical Society*, 1939, 61, pp. 2594-2597.

[62] K. Nitsch, M. Matyas, and J. Bok, "Validity of the Anionic Model of Rare-Earth Iron-Garnet Solubility in $PbO-B_2O_3$ Flux," *Physica Status Solidi A-Applied Research*, 1986, 98, pp. 465-469.

[63] A. Vertes, "Structure of $PbO-B_2O_3-Fe_2O_3$ Melts," *Acta Physica Academiae Scientiarum Hungaricae*, 1979, 47, pp. 209-217.

[64] G. Ottonelloa and R. Moretti, "Lux-Flood Basicity of Binary Silicate Melts," *Journal of Physics and Chemistry of Solids*, 2004, 65, pp. 1609–1614.

[65] K. Nassau, D. L. Chadwick, and A. E. Miller, "Arsenic-Containing Heavy-Metal Oxide Glasses," *Journal of Non-Crystalline Solids*, 1987, 93, pp. 115-124.

[66] G. Srinivasarao and N. Veeraiah, "The Role of Iron Ion on the Structure and Certain Physical Properties of $PbO-As_2O_3$ Glasses," *Journal of Physics and Chemistry of Solids*, 2002, 63, pp. 705-717.

[67] H. M. Heaton and H. Moore, "Glasses Consisting Mainly of the Oxides of Elements of High Atomic Weight. I," *Journal of the Society of Glass Technology*, 1957, 41, pp. 3-27T.

[68] A. J. G. Ellison and S. Sen, "Role of Sb^{3+} as a Network-Forming Cation in Oxide Glasses," *Physical Review B*, 2003, 67, pp. 1-4.

[69] B. V. Raghavaiah and Veeraiah, "The Role of As_2O_3 on the Stability and Some Physical Properties of $PbO-Sb_2O_3$ Glasses," *Journal of Physics and Chemistry of Solids*, 2004, 65, pp. 1153-1164.

[70] G. Srinivasarao and N. Veeraiah, "Characterization and physical Properties of $PbO-As_2O_3$ Glasses Containing Molybdenum Ions," *Journal of Solid State Chemistry*, 2002, 166, pp. 104-117.

[71] W. L. Konijnendijk and J. H. J. M. Buster, "Raman-Scattering Measurements of Arsenic-Containing Oxide Glasses," *Journal of Non-Crystalline Solids*, 1975, 17, pp. 293-297.

[72] K. Masayasu, D. Tomoyuki, M. Ken-Ji, and Y. Tsutomu, "The Behavior of Arsenic in Slag Melts," *Nippon Kogyo Kaishi*, 1979, 95, pp. 877-882.

[73] R. Pyare, S. P. Singh, A. Singh, and P. Nath, "The As^{+3}-As^{+5} Equilibrium in Borate and Silicate Glasses," *Physics and Chemistry of Glasses*, 1982, 23, pp. 158-168.

[74] V. Sudarsan and S. K. Kulshreshtha, "Study of Structural Aspects of PbO-P_2O_5-Sb_2O_3 Glasses," *Journal of Non-Crystalline Solids*, 2001, 286, pp. 99-107.

[75] P. Buhler, "Thermodynamics of Redox Reactions between Oxides of Glass Melts and Oxygen: IV Equilibrium of Antimony, Arsenic and Tin Oxides with Oxygen," *Glass Physics and Chemistry*, 1998, 24, pp. 521-524.

[76] T. Hayashi and W. G. Dorfeld, "Electrochemical Study of As^{+3} /As^{+5} Equilibrium in a Barium Borosilicate Glass Melt," *Journal of Non-Crystalline Solids*, 1994, 177, pp. 331-339.

[77] I. V. Kojo, P. Taskinen, and K. Lilius, "The Thermodynamics of Antimony, Arsenic and Copper in Na_2CO_3-Slags at 1473 K," *Erzmetall*, 1984, 37, pp. 21-26.

[78] W. L. Konijnendijk and J. H. J. M. Buster, "Raman-Scattering Measurements on Silicate-Glasses Containing AsO_4^{3-} Ions," *Journal of Non-Crystalline Solids*, 1976, 22, pp. 379-389.

[79] H. Verweij, "Raman-Study of Arsenic in Potassium Silicate-Glasses," *Journal of Non-Crystalline Solids*, 1980, 38-9, pp. 885-890.

[80] J. M. Font and R. G. Reddy, "Arsenate Capacities of Copper Slags," *Arsenic Metallurgy, TMS 2005*, R. G. Reddy and V. Ramachandran, Eds., San Francisco, California, USA, 2005, pp. 51-60.

[81] R. G. Reddy and J. M. Font, "Arsenate Capacities of Copper Smelting Slags," *Metallurgical and Materials Transactions B*, 2003, 34B, pp. 565-571.

[82] P. Coursol, "Experimental Study and Thermodynamic Modeling of the Ca^{2+}, Na^{+}// SO_4^{2-}, O^{2-}, AsO_4^{3-}, SbO_4^{3-} Reciprocal System and Its Applications in Copper Fire-

refining," *PhD Thesis*, École Polytechnique de Montreal, Montreal, Quebec, Canada, 2004.

[83] P. Coursol, A. D. Pelton, P. Chartrand, and M. Zamalloa, "The $CaSO_4$-CaO-$Ca_3(AsO_4)_2$ Phase Diagram", submitted to Canadian Metallurgy Quarterly, Personal Communications, 2004.

[84] T. Honma, R. Sato, Y. Benino, T. Komatsu, and V. Dimitrov, "Electronic Polarizability, Optical Basicity and XPS Spectra of Sb_2O_3-B_2O_3 Glasses," *Journal of Non-Crystalline Solids*, 2000, 272, pp. 1-13.

[85] J. Bitskei, "Oxidimetric Titrations in Alkaline Solutions," *Acta Chimica Academiae Scientiarum Hungaricae*, 1957, 10, pp. 313-326.

[86] S. P. Singh, R. Pyare, G. Prasad, and P. Nath, "Rapid Spectrophotometric Method for the Determination of Arsenic(III) in Borate Glasses," *The Analyst*, 1979, 104, pp. 1094-1097.

[87] E. V. Kantsler, V. M. Rudoi, M. S. Khadyev, and A. I. Levin, "Structure of Antimony Obtained by Electrodeposition from Aqueous Solutions," *Elektrokhimiya*, 1969, 5, pp. 1312-1315.

[88] M. Pettine, L. Campanella, and F. J. Millero, "Arsenite Oxidation by H_2O_2 in Aqueous Solutions," *Geochimica et Cosmochimica Acta*, 1999, 63, pp. 2727–2735.

[89] T. Araki, P. B. Moore, and G. D. Burton, "The Crystal Structure of Paulmooreite, $Pb_2As_2O_5$: Dimeric Arsenic Groups," *American Mineralogist*, 1980, 65, pp. 340-345.

[90] S. K. Sharma, H. S. Yoder, and D. W. Matson, "Raman-Study of Some Melilites in Crystalline and Glassy States," *Geochimica Et Cosmochimica Acta*, 1988, 52, pp. 1961-1967.

[91] F. Dinterer, H. Effenberger, A. Kugler, F. Pertlik, P. Spindler, and M. Wildner, "Structure of Lead(II) Arsenate(III)," *Acta Crystallographica Section C-Crystal Structure Communications*, 1988, 44, pp. 2043-2045.

[92] M. Z. Makhmetov, "Theoretical Principles of Precipitation of Arsenic and Antimony from Acidic and Alkaline Solutions by Iron (II) Salts," *Kompleksnoe Ispolzovanie Mineralnogo Syria*, 2003, 1, pp. 50-56.

[93] L. Bencivenni and K. A. Gingerich, "The Characterization of Alkali Arsenites and Antimonites - the Ir-Spectra of Matrix-Isolated $MAsO_2$ and $MSbO_2$ Molecules," *Journal of Molecular Structure*, 1983, 99, pp. 23-29.

[94] M. Temkin, "Mixtures of Fused Salts as Ionic Solutions," *Acta Physicochimica URSS*, 1945, 20, pp. 411-420.

[95] H. A. ØYE, "The Power of Thermodynamic Modeling; Examples from Molten Halide Mixtures," *Metallurgical and Materials Transactions B*, 2000, 31B, pp. 641-650.

[96] A. D. Pelton, "A General "Geometric" Thermodynamic Model for Multicomponent Solutions," *Calphad-Computer Coupling of Phase Diagrams and Thermochemistry*, 2001, 25, pp. 319-328.

[97] P. J. Haines, *Thermal Methods of Analysis: Principles, Applications and Problems*, London; New York: Blackie Academic & Professional, 1995.

[98] T. Hatakeyama and Z. Liu, *Handbook of Thermal Analysis*: John Wiley & Sons, 1998.

[99] A. D. Pelton, "Phase Diagrams," in *Physical Metallurgy*, Vol. 1, R. W. Cahn and P. Haasen, Eds., 4th ed. Amsterdam: North Holland, 1996.

[100] O. A. Gokçen, J. V. Styve, J. K. Meen, and D. Elthon, "Phase Equilibria of the $1/2Bi_2O_3$-CaO System in Oxygen at 1 atm Pressure," *Journal of American Ceramic Society*, 1999, 82, pp. 1908-1914.

[101] Y. Umetsu, T. Nishimura, K. Tozawa, and K. Sasaki, "Liquidus Surfaces in a Part of the Systems ZnO-PbO-SiO_n and ZnO-FeO-SiO_2," *Australia Japan Extractive Metallurgy Symposium*Eds., Sydney, Australia, 1980, pp. 95-106.

[102] S. Chen, B. Zhao, P. C. Hayes, and E. Jak, "Experimental Study of Phase Equilibria in the PbO-Al_2O_3-SiO_2 System," *Metallurgical and Materials Transactions B*, Dec. 2001, 32B, pp. 997-1005.

[103] P. Coursol, A. D. Pelton, and M. Zamalloa, "Phase Equilibria and Thermodynamic Properties of the Cu_2O-CaO-Na_2O System in Equilibrium with Copper," *Metallurgical and Materials Transactions B*, 2003, 34, pp. 631-638.

[104] E. Jak, B. J. Zhao, N. G. Liu, and P. C. Hayes, "Experimental Study of Phase Equilibria in the System PbO-ZnO-SiO_2," *Metallurgical and Materials Transactions B*, 1999, 30, pp. 21-27.

[105] W. B. Nobbins and P. Ridge, "Arsenic Determination by Hydride Generation," Varian Inc. March 1982, http://www.varianinc.com/image/vimage/docs/products/spectr/aa/atworks/aa022.pdf

[106] A. I. Vogel, *A Text-book of Quantitative Inorganic Analysis Including Elementary Instrumental Analysis*, London: Longman, 1962.

[107] O. Lafroukhi, J. Hertz, J. P. Hilger, and G. Cornier, "Electrochemical Measurement of Oxygen Activity in Lead Glass by Means of a Stabilized ZrO_2 Sensor. 2. Determination of the Equilibrium-Constants in the Redox Systems Arsenic and Antimony," *Glastechnische Berichte-Glass Science and Technology*, 1991, 64, pp. 281-290.

[108] "Fundamentals of Electron Microprobe Analysis (EMPA)," Accessed May 2005, http://www.geo.ucalgary.ca/UCLEMA/EMPA1.html

[109] L. Helsen, E. V. d. Bulck, M. K. V. Bael, G. Vanhoyland, and J. Mullens, "Thermal Behaviour of Arsenic Oxides (As_2O_5 and As_2O_3) and the Influence of Reducing Agents," *Thermochimica Acta*, 2004, 414, pp. 145-153.

[110] K. Schwerdtfeger, "Activity Measurements in Pt-Pb and Pd-Pb Melts in Temperature Range 800 ° to 1200 ° C," *Transactions of the Metallurgical Society of AIME*, 1966, 236, pp. 32-35.

[111] I. Barin, *Thermochemical Data of Pure Substances*, Weinheim: VCH, 1989.

[112] I. Barin, O. Knacke, and O. Kubaschewski, *Thermochemical Properties of Inorganic Substances*, Berlin: Springer-Verlag, 1977.

[113] V. N. Nekrasov, N. Barbin, D. Terent'ev, and G. K. Moiseev, "Thermodynamic Modeling of Oxidative Refining of Lead," *Rasplavy*, 2001, 6, pp. 51-61.

[114] R. B. Shashchanova, B. K. Kasenov, and V. F. Malyshev, "Thermodynamics of the Thermal Dissociation of Lead Orthoarsenate," *Izvestiya Akademii Nauk Kazakhskoi SSR, Seriya Khimicheskaya*, 1991, 3, pp. 90-92.

[115] I. Barin, *Thermochemical Data of Pure Substances*, Weinheim: VCH, 1993.

[116] G. K. Moiseev and J. Sestak, "Some Calculations Methods for Estimation of Thermodynamical and Thermochemical Properties of Inorganic-Compounds," *Progress in Crystal Growth and Characterization of Materials*, 1995, 30, pp. 23-81.

[117] S. V. Krivovichev, T. Armbruster, and W. Depmeier, "Crystal Structures of $Pb_8O_5(AsO_4)_{(2)}$ and $Pb_5O_4(CrO_4)$, and Review of PbO-Related Structural Units in Inorganic Compounds," *Journal of Solid State Chemistry*, 2004, 177, pp. 1321-1332.

[118] W. D. Zhuang, J. K. Liang, Z. Y. Qiao, J. Y. Shen, Y. Shi, and G. H. Rao, "Estimation of the Standard Enthalpy of Formation of Double Oxide," *Journal of Alloys and Compounds*, 1998, 267, pp. 6-10.

[119] P. Coursol, Falconbridge, Sudbury, Personal Communications, 2005.

[120] H. Verweij, "Raman-Study of Arsenic-Containing Potassium Silicate-Glasses," *Journal of the American Ceramic Society*, 1981, 64, pp. 493-498.

[121] A. D. Pelton, S. A. Degterov, G. Eriksson, C. Robelin, and Y. Dessureault, "The Modified Quasichemical Model I - Binary Solutions," *Metallurgical and Materials Transactions B*, 2000, 31, pp. 651-659.

[122] V. V. Zyryanov, "Structure of Mechanochemical Reaction Products in the Systems PbO-Sb_2O_5 and PbO-Sb_2O_3," *Inorganic Materials*, 2001, 37, pp. 1278-1284.

[123] Y. D. Fridman and A. K. Mustaev, "Displacement Reaction of Metals from Vapors of Their Compounds," *Trudy Inst. Khim., Akad. Nauk Kirgiz. S.S.R.*, 1955, pp. 23-39.

[124] B. Kulunk and R. Guthrie, "On the Kinetics of Removal of Sodium from Aluminum-Magnesium Alloys," *Light Metals 1992*, E. R. Cutshall, Eds., The Minerals, Metals & Materials Society, Warrendale, PA, United States, 1992, pp. 963-975.

[125] Q. Fu, D. Xu, and J. W. Evans, "Chlorine Fluxing for Removal of Magnesium from Molten Aluminum: Part II. Mathematical Model," *Metallurgical and Materials Transactions B*, 1998, 29B, pp. 979-986.